Development of LDL based nanodelivery system for drugs and a role of PKCα and PKCδ in the cell death induced by photoactivated hypericin

Jaroslava Joniova

PAVOL JOZEF SAFARIK UNIVERSITY IN KOSICE
AND UNIVERSITÉ PIERRE ET MARIE CURIE PARIS VI

DEVELOPMENT OF LDL BASED NANODELIVERY SYSTEM FOR DRUGS AND A ROLE OF PKCα AND PKCδ IN THE CELL DEATH INDUCED BY PHOTOACTIVATED HYPERICIN

PARIS 2014 **RNDr. Jaroslava Joniová**

Dissertation thesis

Doctoral school « Chimie Physique & Chimie Analytique de Paris Centre » ED 388

and

Doctoral School of Biophysics 4.1.12

Presented by

Ms. Jaroslava Joniová

to obtain the degree of

Docteur de l'Université Pierre et Marie Curie

and

Philosophiae doctor of Pavol Jozef Safarik University

Title of the thesis

Development of LDL based nanodelivery system for drugs and a role of PKCα and PKCδ in the cell death induced by photoactivated hypericin.

Defended on the 30th of October 2014

Doctoral committee:

Prof. Germain Trugnan	President of the committee, examiner (UPMC, Paris, France)
Dr. Alexandra Zahradníková	Referee (SAS, Bratislava, Slovak Republic)
Dr. Patrice Xavier Petit	Referee (Université Paris Descartes, France)
Dr. Santiago Sanchez Cortez	Examiner (CSIC, Madrid, Spain)
Prof. Pavol Miškovský	Supervisor (UPJS, Kosice, Slovak Republic)
Dr. Franck Sureau	Supervisor (UPMC, Paris, France)

PAVOL JOZEF ŠAFÁRIK UNIVERSITY IN KOŠICE
FACULTY OF SCIENCE
AND UNIVERSITÉ PIERRE ET MARIE CURIE PARIS VI
LABORATOIRE JEAN PERRIN

DEVELOPMENT OF LDL BASED NANODELIVERY SYSTEM FOR DRUGS AND A ROLE OF PKCα AND PKCδ IN THE CELL DEATH INDUCED BY PHOTOACTIVATED HYPERICIN

DISERTATION THESIS

All the data regarding D_{Ch} are confidential because of patent application

Study program:	Biophysics, ED 388
Department:	Department of Biophysics (UPJS), Laboratoire Jean Perrin (UPMC)
Supervisors:	prof. RNDr. Pavol Miškovský, DrSc. Franck Sureau, PhD. RNDr. Zuzana Naďová, PhD.

Košice, Paris 2014

RNDr. Jaroslava Joniová

ANALYTICAL LIST

Author:	RNDr. Jaroslava Joniová
Title of the thesis:	Development of LDL based nanodelivery system for drugs and a role of PKCα and PKCδ in the cell death induced by photoactivated hypericin
Language of the thesis:	English
Type of the thesis:	Dissertation thesis
Number of pages:	159
University:	Pavol Jozef Safarik University in Kosice and Universite Pierre et Marie Curie in Paris
Faculty:	Faculty of Science (UPJS), ED 388 (UPMC)
Department:	Department of Biophysics (UPJS), Laboratoire Jean Perrin (UPMC)
Study program:	Biophysics
Town:	Košice, Paris
Supervisor:	prof. RNDr. Pavol Miškovský, DrSc. Franck Sureau, PhD. RNDr. Zuzana Naďová, PhD.
Key words:	Low density protein, hypericin, photo dynamic therapy, PKC

ACKNOWLEDGEMENT

I would like to thank:

Prof. Pavol Miskovsky for making my PhD study unique by giving me the opportunity to be a part of co-tutelle and to have a chance to work in Paris. For his guidance, consultations and help during my study.

Dr. Franck Sureau for the fact that anytime I could come for consultation, for his help, suggestions, guidance, advices, patience and taking care of me during my stays in Paris. Merci, Franck!

Dr. Zuzana Nadova, supervisor specialist, for her guidance, support and friendly help, during my study and her suggestions during writing this thesis.

Dr. Alexandra Zahradnikova and Dr. Patrice Petit for their comments and suggestions which enriched this thesis.

My thanks belong as well to Dr. Daniel Jancura for his help and consultations.

Dr. Veronika Huntosova for her friendship, help, sharing her experiences and knowledge, her visits in Paris, great time at the conferences in Brixen and Cordoba and long conversations until morning.

Jana “Kuba” Kubackova for her friendship and “craziness” which made me laugh anytime we talked together. Even when we were chatting and I was smiling at the screen of my computer and trying not to laugh out loud in the office.

Barbora Profantova, my fellow in Paris, for her friendship, making the stays in Paris more pleasant and our exploring the beauties of Paris together (and of course introducing me to the geocaching).

Of course, I want to thank to all members of Department of Biophysics in Kosice (especially to Marienka, the soul of the Department of Biophysics) and Laboratoire Jean Perrin in Paris for making very comfortable working atmosphere.

My big thank you belongs to Stanko for his support and patience during my study and to my mom, FOR EVERYTHING…

ABSTRACT

Photodynamic therapy (PDT), non-invasive method for cancer treatment requires three necessary components: photosensitizer (pts), light of wavelength equal to the wavelength of pts excitation and oxygen. Activation of pts by irradiation results in a formation of reactive oxygen species at the place of light application and starts destructive mechanism. Low density lipoproteins (LDL) are considered as suitable natural *in vivo* delivery system for hydrophobic pts such as Hypericin (Hyp) and it was shown that over expression of LDL-receptors in tumor cells can be used for specific targeting. However, in spite of extensive tumor accumulation observed *in vivo*, Hyp, loaded in LDL, can be redistributed towards others biological macromolecules from plasma before cell delivery process. In using cholesterol modified dextran (D_{ch}) coating of LDL-Hyp complexes we succeed to decrease such redistribution process. We show that this D_{Ch} coating has negligible impact on the cellular uptake of Hyp from [LDL-Hyp]/D_{Ch} complexes. Like LDL, high density lipoproteins (HDL) are able to deliver Hyp to cancer cells as well and their interaction was studied. Because isolation of LDL or HDL is difficult and isolated lipoproteins vary in size and composition, synthetic lipid-based nano-particles (sLNP) were prepared and their interaction with Hyp was analysed by fluorescence spectroscopy. These synthetized sLNP are suitable carriers of Hyp and can enter cells by endocytosis. The main aim of our transport system is to selectively accumulate Hyp in the cancer cells. Subsequently, after Hyp accumulation and irradiation, cell death will occur. In the present work we have focused our attention on some regulation processes involved in Hyp photo-induced cell death pathway. In using specific siRNA, the consequence of gene silencing of protein kinase C PKCα or PKCδ was examined. Post-transcriptional silencing of *pkcα* gene expression did not significantly modify cell death level but the balance between apoptosis and necrosis id seeply sffected. Our results show that Hyp photo-induced ROS production is significantly increased in $PKC\alpha^-$ cells. Such increase of intracellular ROS has been related to the decrease of Bcl-2 phosphorylation and the level of mitochondrial GSH binding. Post-transcriptional silencing of *pkcδ* gene expression did not affect type of the cell death when we compared it with the effect of *pkcα* gene silencing, reduced ROS production and effected Bak and Bax translocation in the cells.

RESUME

La photo thérapie dynamique (PDT) est une méthode non invasive de traitement de certains cancers qui requiert la combinaison de trois éléments: un photosensibilisateur (pts), une source lumineuse de longueur d'onde adaptée à l'excitation du pts et la présence d'oxygène. La photo activation du pts induit la production locale d'espèces réactives de l'oxygène (ROS) à l'origine des mécanismes cytotoxiques. Les lipoprotéines de faible densité (LDL) sont considérées comme des vecteurs naturels adaptés au transport des pts hydrophobes tel que l'hypéricine (Hyp) et il a été montré que la surexpression des récepteurs aux LDL dans les cellules tumorales peut être utilisée pour un ciblage spécifique. Cependant, malgré l'accumulation du pts, observée *in vivo*, dans les cellules tumorales, celle-ci reste limitée du fait de la redistribution de l'Hyp incorporée dans les LDL vers d'autres macromolécules du plasma avant d'atteindre sa cible. Nous avons pu réduire ce processus de redistribution en associant au complexe LDL-Hyp des molécules de Dextran sur lesquelles ont été greffées du cholestérol (DCh). Nous avons pu montrer que l'interaction de ces DCh avait un impact négligeable sur les processus de reconnaissance du complexe [LDL-Hyp]/DCh par les récepteurs au LDL et sur son incorporation cellulaire. Du fait de la grande variabilité de taille et de composition des lipoprotéines et de la complexité d'isolation de fractions pures de LDL ou de HDL, l'utilisation alternative de nanoparticules lipidiques synthétiques (sLNP) pour le transport de l'Hyp a également été étudiée. Nos résultats indiquent que ces sLNP sont des vecteurs appropriés de l'Hyp susceptibles de pénétrer dans les cellules par voie d'endocytose. Dans la perspective d'utilisation de ce type de vecteurs pour une application en PDT, nous nous sommes ensuite intéressés au processus de régulation des voies de mort cellulaire photo-induite par l'Hyp. En utilisant des si-RNA spécifiques, les conséquences de l'extinction de l'expression des gènes de la protéine kinase C α ou δ ont été étudié. Nous avons pu montrer que l'inhibition post-transcriptionelle de ces protéines ne modifie pas significativement le taux global de mort cellulaire mais que cela affecte profondément l'équilibre nécrose/apoptose des voies photo-induites. Nos résultats indiquent, entre autre, une importante augmentation de la production de ROS. Cette augmentation des ROS a pu être corrélée à une réduction de la phosphorylation de Bcl-2 ainsi qu'à une baisse du taux de fixation de la glutathion S-transférase (GSH) au niveau des

mitochondries. L'ensemble des ces résultats suggèrent que l'inhibition post-transcriptionelle du gène de la PKCα et la réduction consécutive de la concentration intracellulaire en PKCα affecte considérablement les propriétés anti-apoptotiques et notamment la fonction anti-oxydante de Bcl-2. Cela signifie que la PKCα, en tant que kinase de Bcl-2, protège indirectement les cellules U-87 MG contre le stress oxydatif et la mort cellulaire photo-induite par l'Hyp.

ABSTRAKT

Fotodynamická terapia (PDT) je neinvazívny spôsob liečenia rakoviny, pri ktorom sú potrebné tri veci: fotosenzitívna látka (pts), svetlo excitačnej vlnovej dĺžky pts a kyslík. Po aktivácii pts sa v mieste ožiarenia vytvárajú reaktívne formy kyslíka. Nízkohustotné lipoproteíny (LDL) sú považované za vhodné *in vivo* transportné systémy pre hydrofóbne pts akým je hypericín (Hyp). Bolo preukázané, že LDL môžu byť používané pre cielenú terapiu vďaka zvýšenej expresii LDL-receptorov v nádorových bunkách,. Aj keď napriek pozorovanej zvýšenej akumulácii Hyp *in vivo*, Hyp nachádzajúci sa v LDL môže byť redistribuovaný k ďalším voľným biologickým makromolekulám nachádzajúcich sa v plazme. Pomocou cholesterol-modifikovaného dextránu (D_{ch}) sa nám podarilo znížiť proces redistribúcie. Ukázali sme, že pokrytie LDL-Hyp komplexu pomocou D_{ch} nemá nežiaduci účinok na vychytávanie [LDL-Hyp]/D_{Ch} bunkami. Tak ako LDL, aj vysokohustotné lipoproteíny (HDL) sú schopné transportovať Hyp k nádorovým bunkám a ich interakcia s Hyp bola študovaná. Proces izolácie LDL aj HDL je veľmi zložitý pričom izolované lipoproteíny sa odlišujú veľkosťou a zložením. Preto boli vytvorené syntetické nano-častice na báze lipidov (sLNP) a pomocou fluorescenčnej spektroskopie bola študovaná ich interakcia s Hyp. Hlavným cieľom nášho transportného systému je selektívna akumulácia Hyp v nádorových bunkách. Následne, po nahromadení a ožiarení Hyp nastáva bunková smrť.

V druhej časti tejto práce sme sa zamerali na študovanie procesu regulácie bunkovej smrti vyvolanej fotoaktivovaným Hyp. Použitím siRNA sme študovali vplyv vyblokovanej proteín kinázy C (PKC) α a δ. Post-transkripčná úprava expresie *pkcα* génu neovplyvnila stupeň bunkovej smrti, ale mala výrazný vplyv na dráhu bunkovej smrti (rovnováha medzi apoptózou/nekroózou). Z našich výsledkov vyplýva, ze pri vyblokovaných PKCα$^-$ bunkách, produkcia ROS je po ožiarení Hyp značne zvýšená. Toto zvýšenie vnútrobunkových ROS súvisí s poklesom fosforylácie Bcl-2 ako aj s nižším stupňom mitochondriálneho GSH. Pri porovnaní post-transkripčnej úpravy expresie *pkcδ* génu s post-transkripčnou úpravou *pkcα* génu, vlpyv na druh bunkovej smrti, produkciu ROS nebol vyrazný, ale ovplyvnil translokáciu Bak a Bax v bunkách s vyblokovanou PKCδ$^-$.

TABLE OF CONTENTS

LIST OF FIGURES

LIST OF TABLES

LIST OF ABBREVIATIONS

$^1O_2$	singlet oxygen
Ab	**a**nti**b**ody
ALA	**a**mino**l**evulinic **a**cid
apoB	**apo**lipoprotein **B**-100
BHT	**b**utylated **h**ydroxy**t**oulene
BSA	**b**ovine **s**erum **a**lbumin
CO	**c**holesteryl **o**leate
cryo-EM	**cryo**-**e**lectron **m**icroscopy
CSLM	confocal scanning laser microscopy
DAG	**d**i**a**cyl**g**lycerol
D_{Ch}	**ch**olesterol modified **d**extran
$DiOC_{18}(3)$	3,3′-**dio**ctadecyloxa**c**arbocyanine perchlorate
DLS	**d**ynamic **l**ight **s**cattering
D-MEM	**D**ulbecco's **m**odified **E**agle **m**edium
DMSO	**d**i**m**ethyl **s**ulf**o**xide
DOPC	1,2-**d**iole**o**yl-sn-glycero-3-**p**hospho**c**holine
DOPE	1,2-**d**iole**o**yl-sn-glycero-3-**p**hospho**e**thanolamin
DOPE-Rhod B	1,2-**d**i**o**leoyl-*sn*-glycero-3-**p**hospho**e**thanolamine-N - lissamine **rhod**amine **B** sulfonyl
FBS	**f**etal **b**ovine **s**erum
FRET	**F**örster **R**esonant **E**nergy **T**ransfer
GSH	glutathione
HDL	**h**igh **d**ensity **l**ipoprotein
HIV	immunodeficiency virus
Hyp	**hyp**ericin
LDL	**l**ow **d**ensity **l**ipoprotein
LDLR	**LDL r**eceptor
LUV	**l**arge **u**nilamellar **v**esicles
LUV-Chol	**l**arge **u**nilamellar **v**esicles with cholesterol
LUV-Rhod B	**l**arge **u**nilamellar **v**esicles stained with **Rhod**amine **B**
M_E	modulations of the excitation
M_F	modulations of the emission
MTT	3-[4, 5-dimethylthiazol-2-yl]-2, 5 diphenyltetrazolium bromide
OMM	**o**uter **m**itochondrial **m**embrane
pBcl-2	**p**hosphorylation of **Bcl-2**
PBS	**p**hosphate **s**aline **b**uffer
PC	egg yolk **p**hosphatidyl **c**holine
PCD	**p**rogrammed **c**ell **d**eath
PDT	**p**hoto**d**ynamic **t**herapy
PI	**p**ropidium **i**odide
PKC	**p**rotein **k**inase **C**
PKCα	**p**rotein **k**inase **C alpha**
PKCδ	**p**rotein **k**inase **C delta**
PMA	**p**horbol **m**yristate **a**cetate
PMT	**p**hoto-**m**ul**t**iplyer (detector)
PS	phosphatydylserine
pts	**p**ho**t**o**s**ensitizer
R_H	hydrodynamic radius
ROS	**r**eactive **o**xygen **s**pecies
sLDL	**s**ynthetic **l**ow **d**ensity **l**ipoprotein
sLNP	**s**ynthetic **l**ipid-based **n**ano-**p**articles
TAG	**t**ri**a**cyl**g**lycerol
TNF	**t**umor **n**ecrosis **f**actor
TO	**t**ri**o**lein
UG	**u**ltroser **G**
VLDL	**v**ery **l**ow **d**ensity **l**ipoprotein
τ_M	modulation lifetime
τ_P	phase lifetime

1 INTRODUCTION

1.1 CANCER AND CANCER TREATMENT

Cancer has been a huge problem for mankind for centuries. The earliest written record regarding cancer is from 3000 BC in the Egyptian Edwin Smith Papyrus and describes cancer of the breast. Hippocrates (ca. 460 BC–ca. 370 BC) described several kinds of cancer, referring to them with the Greek word carcinos (crab or crayfish). The Greek, Celsus (25 BC–50 AD) translated carcinos into the Latin cancer, also meaning crab and recommended surgery as treatment [1].

Cancer is the world's major public health problem. One in 4 deaths in the United States is due to the cancer. In 2013, total predicted number of cancer deaths in the European Union was 1 314 236 and according to American Cancer Society a total of 1 660 290 new cancer cases and 580,350 cancer deaths were projected to occur in the United States in 2013 [2], [3].

As understanding of the cancer biological processes has increased the treatment of the cancer has undergone evolutional changes. Tumor removal surgeries have been documented in ancient Egypt, hormone therapy was developed in 1896, and radiation therapy was developed in 1899. Chemotherapy, immunotherapy, and newer targeted therapies are the products of the 20th century. As new information about the biology of cancer emerges, treatments will be developed and modified to increase effectiveness, precision, survivability, and quality of life. Depending on the location, type and stage of cancer as well as the general state of the patient the proper treatment is proposed. There are several types of treatment:

Surgery: in theory, non-hematological cancers can be cured if entirely removed by surgery, but this is not always possible. When the cancer has metastasized to other sites in the body prior to surgery, complete surgical excision is usually impossible.

Radiation therapy: use of ionizing radiation to kill cancer cells and shrink tumors. Radiation therapy injures or destroys cells in the area being treated by damaging their genetic material. Although radiation damages both cancer cells and normal cells, most normal cells can recover from the effects of radiation and function properly. The goal of

radiation therapy is to damage as many cancer cells as possible, while limiting harm to nearby healthy tissue. Radiation therapy may be used to treat almost every type of solid tumor or soft tissue sarcomas.

Chemotherapy: traditional chemotherapeutic agents act by killing cells. This means that chemotherapy also harms cells that divide rapidly under normal circumstances: cells in the bone marrow, digestive tract, and hair follicles. This results in the most common side-effects of chemotherapy: myelosuppression (decreased production of blood cells, hence also immunosuppression), mucositis (inflammation of the lining of the digestive tract), and alopecia (hair loss). Because some drugs work better together than alone, two or more drugs are often given at the same time. This is called "combination chemotherapy"; most chemotherapy regimens are given in a combination [4].

Targeted therapy: uses drugs or other substances to more precisely identify and attack cancer cells. These drugs tend to have different (and often less severe) side effects than standard chemotherapy drugs [5]. In this category one of the treatments is photodynamic therapy (see Chapter 1.2)

Immunotherapy: uses immune system to reject cancer. The main premise is stimulating the patient's immune system to attack the malignant tumor cells that are responsible for the disease. This can be either through immunization of the patient (e.g., by administering a cancer vaccine), in which case the patient's own immune system is trained to recognize tumor cells as targets to be destroyed, or through the administration of therapeutic antibodies as drugs, in which case the patient's immune system is recruited to destroy tumor cells by the therapeutic antibodies [6].

Hormonal therapy: involves the manipulation of the endocrine system through exogenous administration of specific hormones, particularly steroid hormones, or drugs which inhibit the production or activity of such hormones (hormone antagonists). Because steroid hormones are powerful drivers of gene expression in certain cancer cells, changing the levels or activity of certain hormones can cause certain cancers to cease growing, or even undergo cell death [7].

The goal of the treatment is complete removal of the cancer without damage to the rest of the body. Sometimes this can be accomplished by surgery, but the fact that cancers can invade tissue or to spread to distant sites by microscopic metastasis often

limits its effectiveness; chemotherapy and radiotherapy can unfortunately have a negative effect on normal cells [8]. To enhance the effect and to get rid of the cancer two or three types of therapy are often used simultaneously.

1.2 PHOTODYNAMIC THERAPY

Photodynamic therapy is an entirely new treatment modality and its development can be likened to that of the discovery of antibiotics. This is just beginning, and its possible uses are only limited by the imagination.

(McCaughan J. S. Drugs & Aging 1999; 15:49–68.)

For more than three thousand years light has been used as therapy. Ancient Egyptian, Indian and Chinese civilizations used light to treat various diseases, including psoriasis, rickets, vitiligo and skin cancer [9]. At the end of the nineteenth century in Denmark, Niels Finsen further developed 'phototherapy' or the use of light to treat diseases. He found that red-light exposure prevents the formation and discharge of smallpox pustules and can be used to treat this disease. He also used ultraviolet light from the sun to treat cutaneous tuberculosis. This was the beginning of the modern light therapy. More than 100 years ago researchers also observed that a combination of light and certain chemicals could induce cell death. In 1900 German medical student Oscar Raab reported that certain wavelengths were lethal to infusoria including a species of *Paramecium* in the presence of acridine. In the same year a neurologist in France named J. Prime found that epilepsy patients who were treated with oral eosin developed dermatitis in sun exposed areas. Later, Herman Von Tappeiner and A. Jesionek treated skin tumors with topically applied eosin and white light. In 1903 they described this phenomenon as 'photodynamic action' [10].

Photodynamic therapy (PDT) can be defined as the administration of a nontoxic drug or even dye known as photosensitizer (pts) to a patient's lesion followed after some time by the illumination of the lesion with visible light, which, in the presence of oxygen, leads to generation of cytotoxic species-reactive oxygen species (ROS) and consequently to cell death and tissue destruction.

Concept of dual selectivity is one of the main attractions of PDT as a therapy. By increasing the selective accumulation of pts in the tumor or other diseased tissue and by delivering the light in a spatially confines and focused manner collateral damage to normal tissue can be minimized. Another advantages of PDT are minimal toxicity, high efficiency, it can be proceeded as diagnostic and therapeutic procedure at the same time, shorter recovery after PDT treatment-typically hours or days when compared to other methods of treatments. Nevertheless PDT can have also side effects including long-lasting skin photosensitivity and excessive tissue destruction at the treated site. It is hoped that advances in mechanistic understanding of PDT will minimize these side effects [11].

1.2.1 PHOTOPHYSICS AND PHOTOCHEMISTRY OF PDT

As mentioned above, the effect of PDT consists in combination of three non-toxic agents.

Photosensitizers

A large number of photosensitizing drugs have been tested *in vitro* and *in vivo* during last 20 years. Table 1 presents most commonly used pts and precursors in PDT. The physico-chemical properties of the pts are very important for the efficacy of photosensitization. Chemical purity, capability to localize specifically in neoplastic tissue, short time interval between the administration of the drug and its maximal accumulation in hyper proliferating tissue, rapid clearance from normal tissues, activation at wavelength with optimal tissue penetration, high quantum yields for the generation of singlet oxygen, and lack of dark toxicity are desirable features of ideal pts. The fundamental prerequisite for optimal response to photosensitization is a sufficient amount of drug localized in the target tissue. Initially, pts are taken up by most normal and hyper proliferating cells, but are retained longer in the hyper proliferating cells. The mechanisms of this selective prolonged retention are not understood in detail yet. Increased blood vessel permeability as well as poor lymphatic drainage in neoplastic tissues may contribute to the retention of the drug in neoplastic lesions [12].

Porphyrins	Hematoporphyrin derivative Dihematoporphyrin ether/ester Porfimer sodium Tetrasodium-meso-tetraphenylporphyrin-sulphonate Metallotetra-azaporphyrin
Porphyrin precursors	d-Aminolevulinic acid (ALA) d-Aminolevulinic acid (ALA)-methyl-, propyl-, hexyl-esters
Phthalocyanines	Chloroaluminum tetra-sulfonated phthalocyanine Zinc(II)phthalocyanine Silicone naphthalocyanine Aluminum sulfonated phthalocyanine
Porphycenes	9-Acetoxy-2,7,12,17-tetra-N-propylporphycene 2-Hydroxyethyl-7,12,17-tris(methoxyethyl)por- phycene 23-carboxy-24-methoxycarbonylbenzo(2, 3)-7,12, 17-tri(methoxyethyl)-porphycene
Chlorines	Monoaspartyl chlorine e_6, diaspartyl chlorine e_6 Chlorine e_6 sodium, bacteriochlorin a Benzoporphyrin derivative monoacid ring A
Pheophorbides	Pheophorbide a, bacteriopheophorbide
Others	Fluoresceins (fluorescein sodium, tetrabromofluo- rescein-eosin) Anthracenes (anthraquinone, acridine orange, yel- low) Hypericin Furocoumarin (5-methooxypsoralen, 8-methoxyp- soralen) Chlorophyll derivatives Purpurins (metallopurpurin, tin etiopurpurin Sn ET2) Phenothiazines Methylene blue, violet green Azure C, thionine, Nile blue A Hypocrellin Rose Bengal Rhodamine 123 Lutetium texaphyrin

Table 1: Photosensitizers and their precursors used in experimental and clinical PDT applications

[source: [12]]

The pts can be categorized by chemical structure and by origin of broad families. The porphyrins are generally called first generation pts. Sometimes first generation labels pts developed in the 1970s and early 1980s. Second generation pts refer more to porphyrin derivatives or synthetics made from the late 1980s on. Third generation pts

takes available drugs and then modify them with antibody conjugates, biologic conjugates, etc.

Light source

The first light sources used in PDT were conventional lamps where the output wavelengths were defined by the use of filters. A drawback with this was that there was often a significant thermal component, and also calculating the dose of delivered light dose was difficult. These non-coherent light sources are attractive because they are easy to use and relatively cheap. The introduction of lasers equipped with optical fibers revolutionized photosensitization and expanded its applicability in medicine, enabling the endoscopic delivery of light to almost every site of the human body [13]. They are useful because they produce monochromatic light, and the light dosimetry is relatively easy. The used laser system can be chosen according to the pts used. The most commonly used lasers in PDT are pumped dye lasers and semiconductor lasers.

Oxygen

Numerous investigations supported the idea that the efficacy of photosensitization is directly related to the yield of singlet oxygen ($^1O_2$) in the tumor environment and the yield of $^1O_2$ depends on the concentration of oxygen in the tissue. $^1O_2$ can be produced by cellular metabolism, redox reactions, photosensitization, etc. Since $^1O_2$ acts as a strong oxidation reagent, there are various intracellular enzymes and antioxidant mechanisms to deactivate $^1O_2$. Thus, in normal cells, the naturally produced $^1O_2$ as well as other ROS do not cause significant damage for the intracellular organelles because of the cell antioxidant defence mechanisms. In PDT $^1O_2$ originated from molecular oxygen (O_2) created via an energy transfer from triplet state of pts.

The initiating step of the photosensitizing mechanism is the absorption of a light by pts, the unstable excited singlet state with a half life in range of 10^{-6} to 10^{-9} seconds. The singlet excited pts either decays back to the ground state, resulting in the fluorescence or undergoes intersystem crossover to the longer lived tripled excited state (10^{-3} second). The interaction of the triplet state of the pts with surrounding molecules results in two types of photo-oxidative reaction (Figure 1).

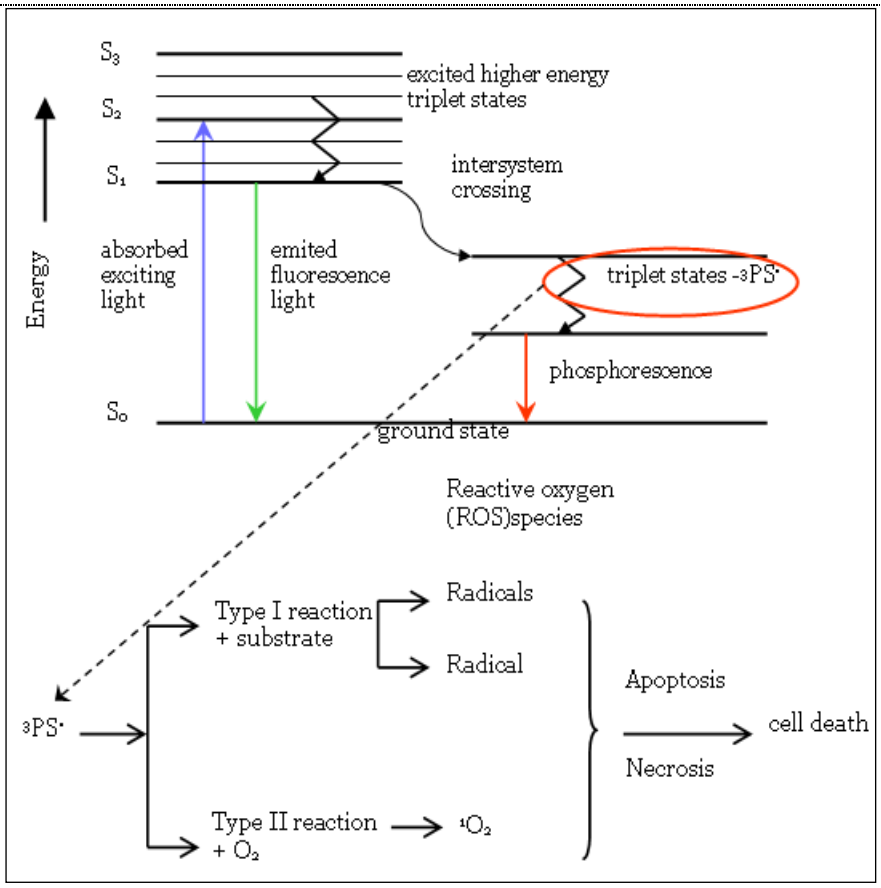

Figure 1: Jablonski diagram and Scheme of Type I and Type II mechanism of PDT.

[source [12]]

Type I pathway involves electron or hydrogen atom transfer, producing radical forms of the pts or the substrate. These intermediates may react with oxygen to form peroxides, superoxide ions, and hydroxyl radicals, which initiate free radical chain reactions. Type II mechanism is mediated by the energy transfer process from the triplet state of the pts to the oxygen ($^1O_2$) ground state. The *in situ* generation of singlet oxygen via type II pathway appears to play the central role in photodynamic cytotoxicity because of the highly efficient interaction of the singlet oxygen species with different biomolecules [12], [14].

1.3 HYPERICIN AS THE MODEL MOLECULE OF PTS FOR PDT

Hypericin (Hyp, Figure 2) is naturally occurring perylene quinone pigment that has stimulated great interest because of its broad spectrum of light induced biological activities. It can be extracted from the plants of *Hypericum* widely distributed around the world, most common of which is *Hypericum perforatum*. It is known that Hyp exhibits antiviral, anticancer and antiangiogenic activities against infectious, neoplastic and ophtalmologic diseases [15]. Hyp possesses powerful phototoxicity on different cell lines [16], displays light induced virucidal activity *in vitro* against several types of viruses [(herpes, murine cytomegalovirus, sindbis, hepatitis B, equine anemia including the human immunodeficiency virus (HIV)]. Hyp was also used in clinical treatment of AIDS patients [17].

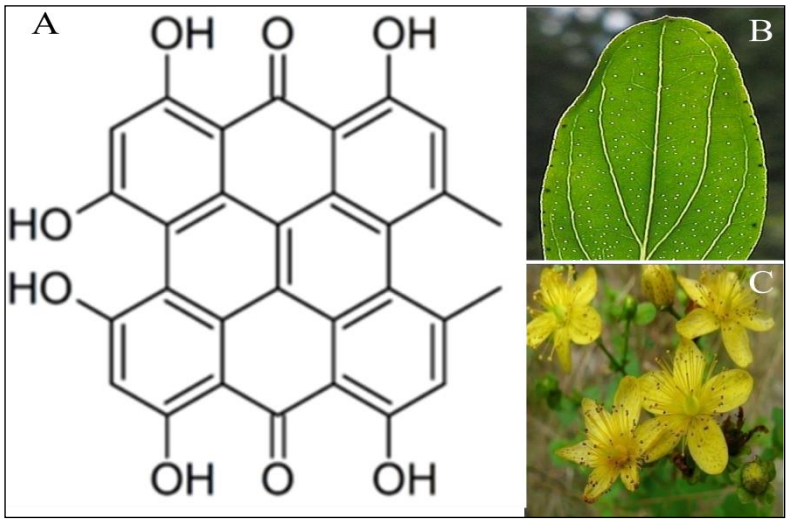

Figure 2: A-Hypericum perforatum (blossom), B-chemical structure of Hyp, C-Hypericum perforatum (blatt).

[source [18]]

1.3.1 PHYSICO-CHEMICAL AND PHOTODYNAMIC PROPERTIES OF HYP

Hyp ($C_{30}H_{16}O_8$)- 1,3,4,6,8,13-hexahydroxy-10,11-dimethylphenanthro[1,10,9,8-opqra]perylene-7,14-dione (Figure 2A) is hydrophobic molecule insoluble in water, oil, methylene chloride and most other nonpolar solvents. It is soluble in alkaline aqueous

solutions, organic bases such as pyridine, and polar organic substances including acetone, ethanol, dimethyl sulfoxide (DMSO), methanol, ethyl acetate, ethyl methyl ketone and other solvents. In most organic solvents Hyp forms a red solution and green solution in basic media. Hyp can be soluble in biological media by formation of complex with biological macromolecules (e.g. human serum albumin and other plasma proteins, membrane fragments and cellular compounds) [17]. Fluorescence emission maximum of Hyp is about 600 nm (Figure 3). Depending on different factors like solvent, aggregation, production process, moisture etc, the molar extinction coefficient of Hyp vary from 27 000 to 52 000 at 590 nm. In water insoluble aggregates pellets of Hyp are formed. These aggregates are non-fluorescent, and show very weak visible absorption spectra in the same region as free Hyp (Figure 3), but have much lower extinction coefficients [19]. Hyp monomer is the only biologically active form [17].

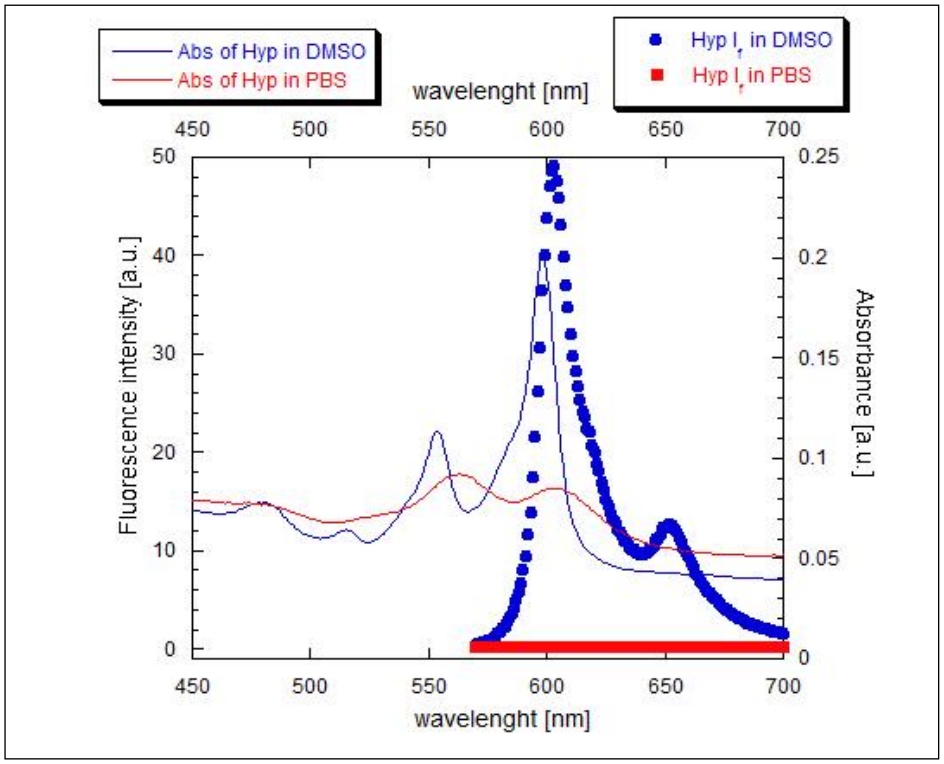

Figure 3: Absorbance and fluorescence spectrum of Hyp in PBS and DMSO

With minimal dark toxicity, high quantum yield of singlet oxygen, differential uptake in normal and tumor cells resulting in high tumor selectivity and rapid clearance from the body, Hyp is a suitable choice for PDT application [17]. After photoactivation, Hyp can inhibit protein kinase C (PKC) and other growth factor stimulated protein

kinases, it induces peroxidation of membrane lipids, increases the activity of superoxide dismutase and decreases levels of cellular gluthatione as well as other enzymes such as monoamine oxidase and mitochondrial succinoxidase, possibly via generation of singlet oxygen [20], [21].

The standard for photodynamic activity is the 'quantum yield' [Φ_Δ] of $^1O_2$ production. Quantum yield depends on the reaction media, temperature, pH-value and various other physical and chemical influences. Hyp bound to liposomes shows a singlet oxygen quantum yield of: $\Phi\Delta = 0,4$ [22]. Several mechanisms have been proposed for the photodynamic activity of Hyp, but the type II mechanism (singlet OXY generation is a predominant one) [20], [23].

1.4 CELL DEATH

Cell death plays a key role during the physiological processes especially during embryogenesis and metamorphosis. The homeostatic control of cell number is the result of the dynamic balance between cell proliferation and cell death. The death of a cell can be defined as an irreversible loss of plasma membrane integrity. In mammalian cells, three types of cell death have been distinguished by morphological criteria. Autophagy is characterized by a massive accumulation of two-membrane autophagic vacuoles in the cytoplasm [24]. Apoptosis is defined by characteristic changes in the nuclear morphology. All of the changes occur before plasma membrane integrity is lost [25]. Necrosis is often defined in a negative manner as death lacking the characteristics of the apoptosis and autophagy processes. The distinction between cell death types is important [26][27].

PDT can activate many of the cell signaling pathways in order to activate the cell death. Concentration, physico-chemical properties of pts, concentration of oxygen, wavelength or the cell type can have important influence at the cell survival and extensity of the cell death [28].

1.4.1 AUTOPHAGIC CELL DEATH

Macroautophagy (also referred to as autophagy) is a homeostatic and evolutionarily conserved dynamic muti-step process that can be modulated at several steps both positively and negatively [24]. Autophagy is a catabolic cellular mechanism that allows the cell to maintain a balance between the synthesis, degradation, and recycling of cellular products [29]. A variety of autophagic processes exist, all of which involve the lysosomal degradation of the cellular organelles and proteins. The most well-known mechanism proceeds in the following manner: A double membrane structure called autophagosome surrounds the target region, creating a vesicle that separates its contents from the rest of the cytoplasm. This vesicle is then transported and fused to the lysosome, forming a structure called the autophagolysosome, the contents of which are subsequently degraded by lysosomal hydrolases [30]. Besides facilitating the disposal of unwanted proteins, organelles, and invading microorganisms, autophagy also allows a cell to reallocate its nutrients from unnecessary processes to life-essential ones in times of starvation or stress. Autophagy is important in all cells for the removal of damaged or long-lived proteins and organelles. Although autophagy is a mechanism of tumor suppression, it also confers stress tolerance that enables tumor cells to survive under adverse conditions. Autophagy is induced in tumor cells within hypoxic tumor regions. Stress-induced autophagy in tumor cells can lead to treatment resistance and tumor dormancy, with eventual tumor regrowth and progression. Understanding the role of autophagy in cancer treatment is critical, because many anticancer therapies have been shown to activate autophagy [33]. Autophagy and apoptosis often occur in the same cell, mostly in a sequence in which autophagy precedes apoptosis [34]. It often happens that stress stimulates an autophagic response, especially if the level of stress is not lethal. Apoptotic and non-apoptotic lethal programmes are activated when stress exceeds a critical duration or an intensity threshold. In many cases, autophagy constitutes a strategy to adapt to and cope with stress [35]. Recently Hyp became the first PDT paradigm characterized to be capable of inducing the cell death through formation of autophagy. It should be noted, however, that other pts might also be capable of inducing autophagic cell death but their properties need to be thoroughly and more comprehensively tested [36]. The complex role of autophagy in cancer continues

to emerge, and it is important to elucidate the mechanisms by which autophagy influences tumorigenesis as well as treatment response. Analysis of autophagic signaling may identify novel therapeutic targets for modulation and therapeutic advantage [33].

1.4.2 APOPTOSIS

Programmed cell death (PCD), also termed apoptosis, is the necessary mechanism complementary to the proliferation that ensures homeostasis of all tissues. It is used to describe the type of cell death that possesses two major morphological features: cell shrinkage and nuclear condensation [37]. It has been estimated that 50 to 70 billion cells perish each day in the average adult because of PCD a process by which, in a year, each individual will produce and eradicate a mass of cells equal to its entire body weight. This process needs to be highly regulated since defects in the apoptotic machinery will lead to extended cell survival and may contribute to neoplastic cell expansion. Extended cell survival also creates a permissive environment for genetic instability and accumulation of mutations. Furthermore, defects in apoptotic pathways confer resistance to chemotherapy, radiation, and immune-mediated cell destruction [31]. Although understanding of the detailed signaling pathways that trigger apoptosis is incomplete, this process is controlled by a number of complex proteins, which are activated by various triggers and arranged in sequential signaling modules. Apoptosis occurs through two main pathways. The first, referred to as the extrinsic or cytoplasmic pathway, is triggered through the Fas death receptor, a member of the tumor necrosis factor (TNF) receptor superfamily. The second pathway is the intrinsic or mitochondrial pathway which leads to the release of cytochrome *c* from the mitochondria and activation of the death signal, when stimulated. Both pathways converge to a final common pathway involving the activation of a cascade of proteases called caspases that cleave regulatory and structural molecules, culminating in the death of the cell (Figure 4) [32].

1.4.2.1 The Extrinsic Pathway: Fas

This pathway comprises several protein members including the death receptors, the membrane-bound Fas ligand, the Fas complexes, the Fas-associated death domain, and caspases 8 and 10, which ultimately activate the rest of the downstream caspases leading to apoptosis. Activation of the extrinsic pathway is initiated with the ligation of cell surface receptors called death receptors. Fas is a member of the tumor necrosis factor receptor superfamily and is also called Apo-1 or CD95. When a death stimulus triggers the pathway, the membrane-bound Fas interacts with the inactive Fas complexes and forms the death-inducing signaling complex. The Fas death-inducing signaling complex contains the adaptor protein Fas-associated death domain protein and caspases 8 and 10 and leads to activation of caspase 8, which in turn can activate the rest of the downstream caspases. In some cells, the activation of caspase 8 may be the only requirement to execute death, while in other cell types, caspase 8 interacts with the intrinsic apoptotic pathway by cleaving Bid (a pro-apoptotic member of the Bcl-2 family), leading to the subsequent release of cytochrome *c*. Several pathways and proteins regulate the activation of the extrinsic pathway. Dysregulation of these modulators may also lead to malignant transformation, as mutations or deletions of the Fas gene have been found in some hematologic malignancies [32].

1.4.2.2 The Intrinsic Pathway

One of the most important regulators of this pathway is the Bcl-2 family of proteins. Members of the Bcl-2 family are key regulators of apoptosis and are over expressed in many malignancies. Increased expression of Bcl-2 causes resistance to chemotherapeutic drugs and radiation therapy, while decreasing Bcl-2 expression may promote apoptotic responses to anticancer drugs. In addition, over expression of Bcl-2 may result in accumulation of cells in the G_0 phase of cell cycle division and contribute to chemo résistance. The Bcl-2 family includes pro-apoptotic members such as Bax, Bak, Bad, Bcl-Xs, Bid, Bik, Bim, and Hrk, and anti-apoptotic members such Bcl-2, Bcl-X_L, Bcl-W, Bfl-1, and Mcl-1. Anti-apoptotic Bcl-2 members act as repressors of

apoptosis by blocking the release of cytochrome *c*, whereas pro-apoptotic members act as promoters. These effects are more dependent on the balance between Bcl-2 and Bax than on Bcl-2 quantity alone. Following a death signal, pro-apoptotic proteins undergo posttranslational modifications that include dephosphorylation and cleavage resulting in their activation and translocation to the mitochondria leading to apoptosis. All BH3-only molecules require multidomain BH3 proteins (Bax, Bak) to exert their intrinsic pro-apoptotic activity. In response to apoptotic stimuli, the outer mitochondrial membrane becomes permeable, leading to the release of cytochrome *c* and second mitochondria-derived activator of caspase. Cytochrome *c*, once released in the cytosol, interacts with Apaf-1, leading to the activation of caspase-9 proenzymes. Active caspase-9 then activates caspase-3, which subsequently activates the rest of the caspase cascade and leads to apoptosis. Activated caspases lead to the cleavage of nuclear lamina and breakdown of the nucleus through caspase-3 Figure 4 [32].

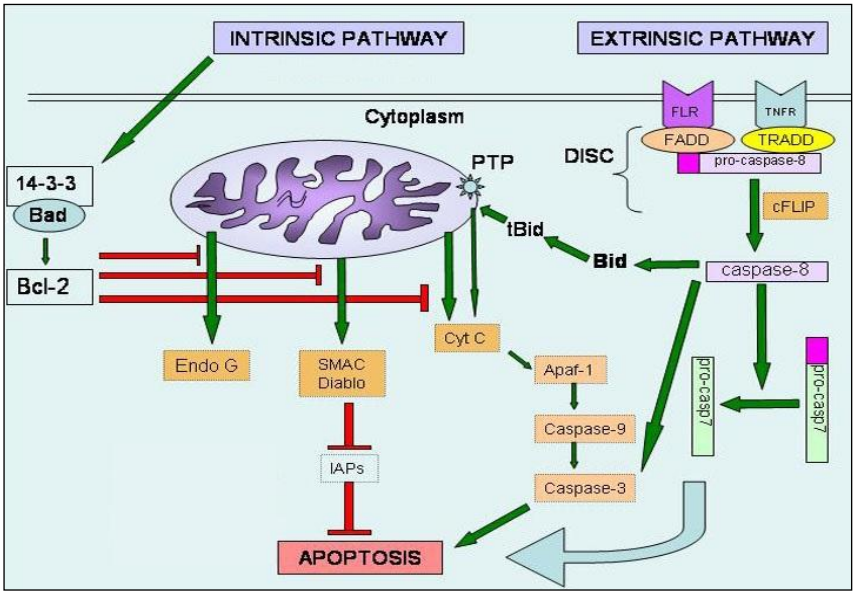

Figure 4: Extrinsic and intrinsic pathway of apoptosis

[source [32]]

1.4.2.3 The Final Pathway: Caspases

The final pathway that leads to execution of the death signal is the activation of a series of proteases termed caspases. Not all caspases are involved in apoptosis. The caspases

that have been well described are caspases-3, -6, -7, -8, and -9. The intrinsic and extrinsic apoptotic pathways converge to caspase-3, which cleaves the inhibitor of the caspase-activated deoxyribonuclease, and the caspase-activated deoxyribonuclease becomes active leading to nuclear apoptosis. The upstream caspases that converge to caspase-3 are caspases-9 and -8 in the intrinsic and extrinsic pathways, respectively. The downstream caspases induce cleavage of protein kinases, cytoskeletal proteins, DNA repair proteins, inhibitory subunits of endonucleaes (CIDE family), and finally, destruction of "housekeeping" cellular functions. Caspases also affect cytoskeletal structure, cell cycle regulation, and signaling pathways, ultimately leading to the morphologic manifestations of apoptosis, such as DNA condensation and fragmentation, and membrane blebbing [32].

1.4.3 CROSS TALK BETWEEN AUTPHAGY AND APOPTOSIS

The turnover of organelles and proteins within cells, and of cells within organisms, respectively are controlled by autophagy and apoptosis. Many stress pathways sequentially elicit autophagy, and apoptosis within the same cell. Generally autophagy blocks the induction of apoptosis, and apoptosis-associated caspase activation shuts off the autophagic process. However, in special cases, autophagy or autophagy-relevant proteins may help to induce apoptosis or necrosis, and autophagy has been shown to degrade the cytoplasm excessively, leading to ‘autophagic cell death’. The normal clearance of dying cells, as well as immune recognition of the dead cell antigens is influenced by the dialogue between autophagy and cell death pathways. Therefore, the disruption of the relationship between autophagy and apoptosis has important pathophysiological consequences. The stimuli which cause cell death trigger also autophagy. In these cases, autophagy usually manifests well before apoptosis dismantles the cell [38].

If apoptosis is suppressed, autophagy induction is exacerbated. for instance, by removing pro-apoptotic proteins such as Bcl-2-associated X protein (BAX) and Bcl-2 antagonist or killer (BAK) or by adding caspase inhibitors, including those encoded by viruses [39][40]. By induction of autophagy the cell reflects the instinct to adapt to stress. This is followed by the activation of the cell death pathways in response to

multiple external signals such as ionizing radiation, chemotherapeutic anticancer agents, the inhibition of growth factor receptors or a scarcity of essential nutrients [40][41]. The fact that many signal transduction pathways that are elicited by cell-intrinsic stress regulate both autophagy and apoptosis might explain the sequential activation of both processes [38].

Although autophagy and apoptosis are under the control of multiple common upstream signals, these processes also cross-regulate each other, mostly in an inhibitory manner. Thus, autophagy reduces the propensity of cells to undergo apoptosis, and activation of the apoptotic programme is coupled to the suppression of autophagy. The mutual relationship between autophagy and apoptosis is highly context-dependent. Beyond rare cases of autophagy cell death, in which autophagy truly mediates cell death, there are a few examples in which autophagy or elements of the autophagic machinery may favour the activation of apoptotic or necrotic cell death programmes. However, in the majority of cases, it seems that apoptosis and autophagy are mutually inhibitory. In most instances, autophagy suppresses apoptosis (or at least raises the threshold of stress required to induce it), which means that autophagy tends to be anti-apoptotic rather than pro-apoptotic. The mutually negative regulation of autophagy and apoptosis can be expected to increase the contrast between both processes, hence generating a steeper gradient that differentiates nonlethal from lethal stress levels [38].

1.4.4 NECROSIS

Necrosis is signaled by irreversible changes in the nucleus and in the cytoplasm (condensation and intense eosinophilia, loss of structure, and fragmentation). In contrast to apoptosis, necrosis is accompanied by swelling of the entire cytoplasm (oncosis) and of the mitochondrial matrix, which occur shortly before the cell membrane ruptures [42], [43].

Until recently, apoptosis was considered as the only form of regulated cell death and for a longtime necrosis generated limited interest within the scientific community.[45]. Conversely, necrosis was viewed as a merely accidental subroutine of cell death, mostly resulting from very harsh stimuli including steep changes in

temperature, osmotic pressure or pH [27]. Nowdays necrosis is no longer considered as a purely accidental, and hence completely uncontrollable, cell death subroutine [44]. The possibility that necrosis (similar to apoptosis) might also occur in a regulated fashion continued to gather momentum through out the 1990s [44][46], and was definitively confirmed in 2005, when the team of Junying Yuan discovered a groups of molecules that inhibit several instances of necrotic cell death, namely, necrostatins [47][48].

Regulated necrosis plays a major role in both physiologal scenarios (*e.g*., embryonic development) and pathological settings (*e.g*., ischemic disorders), consistend efforts have been made throughout the last decade toward the characterization of the molecular mechanisms that underline this cell death modality. Nowdays, various types of the regulated necrosis have been characterized, including (but not limited) necroptosis, mitochondrial permeability transition and parthanatos. The inhibition of onlu one of these modules generally exerts limited cytoprotective effects *in vivo*, underscoring the degree og interconnectivity that characterized regulated necrosis [45].

1.4.5 CELL DEATH PATHWAYS IN PDT OF CANCER

After PDT treatment there is an acute stress response that leads to changes in calcium and lipid metabolism and causes the production of cytokines and stress response mediators in the cells. Enzymes (particularly protein kinases) are activated and transcription factors are expressed. Many of the cellular responses center on mitochondria and frequently lead to induction of apoptosis by the mitochondrial pathway involving caspase activation and release of cytochrome *c*. Certain specific proteins (such as Bcl-2) are damaged by PDT-induced oxidation thereby increasing apoptosis, and a build-up of oxidized proteins leads to an ER-stress response that may be increased by proteasome inhibition. Autophagy plays a role in either inhibiting or enhancing cell death after PDT [49].

1.4.5.1 PDT and autophagy

It is still unclear exactly how autophagy affects the outcome of PDT [50][51]. In general, mammalian cells use autophagy as a defense against ROS mediated damage by clearing the cell of damaged organelles [52]. Depending on the type of ROS and degree of oxidative injury, PDT may stimulate autophagy [53] that either acts in a cytoprotective manner or induces autophagic cell death [54]. Autophagy may play a role in PDT induced apoptosis, but the two processes can also occur independently of one another [55]. A study done on murine leukemia L1210 cells found that a wave of autophagy occurs right before apoptosis [56]. It was also found that prevention of autophagy by silencing the Agt7 gene allowed photo-killing to occur at lower light doses. This observation is consistent with the theory that autophagy is a defense mechanism against PDT induced ROS [57]. In general, the induction of autophagy in PDT treated cells occurs independently of an apoptotic outcome. While autophagy seems to play a pro-survival role in tumor cells that are capable of apoptosis, it has been shown to promote death in cells that are apoptosis-deficient. In order to understand how PDT affects autophagy it is important to take note of the PDT affected proteins that are involved in this mechanism. Many proteins, some directly involved in the autophagic process, are damaged by PDT induced ROS [49]. Although many proteins involved in the autophagic process are photodamaged by PDT, it appears that those involved in the formation of autophagosomes remain active [55]. PDT can also affect autophagy by damaging organelles that are directly involved in the process. Several photosensitizers target autophagy-related organelles such as lysosomes and endosomes. In this type of PDT, lysosomal enzymes are inactivated before the membrane ruptures, which allows for specific targeting of this organelle without causing damage to the rest of the cell. This treatment can be used to selectively enrich autophagosomes [58].

It can be concluded that the effect of PDT on the autophagy of a tumor cell depends on the type of photosensitizer used. Based on studies with various cancer lines and photosensitizers it can be concluded that PDT directly induces autophagy. This is independent of photosensitizer target, as autophagy was observed with photosensitizers that localize in the ER, mitochondria, lysosomes, and endosomes. A second conclusion that can be drawn is that apoptosis often occurs in cells that are already undergoing

autophagy and is also a result of PDT. The rates of autophagy and apoptosis depend on the cancer cell type, photosensitizer, and light dosage. Depending on cell type, autophagy will either promote or prevent cell death from PDT. In cells that are able to undergo apoptosis autophagy alleviates the destructive effects of PDT by recycling damaged organelles [59]. This opens up a possibility that PDT of these cancer cells can be enhanced by suppressing pro-autophagic proteins. Autophagy has the opposite effect on cells that are apoptosis-deficient, promoting cell death through necrosis. The last conclusion that can be made is that autophagic processes are compromised, but not prevented, in PDT protocols that employ lysosome targeting photosensitizers. In these procedures, autophagy is initiated by formation of autophagosomes but cannot be completed by fusing with the lysosome. This is because the proteins involved in autophagosome formation are not photodamaged by PDT [49].

1.4.5.2 PDT and apoptosis: involvement of Bcl-2 family in the PDT response

In mammals the Bcl-2 family has at least 20 relatives, all of which share at least one conserved Bcl-2 homology domain. The family includes four other anti-apoptotic proteins: BclXL, Bcl-w, A1 and Mcll, and two groups of proteins that promote apoptosis: the Bax and the BH3-only families [60][61]. Bcl-2 and other members of the family potently inhibit apoptosis in response to many, but not all cytotoxic insults. Bcl-2 and several other pro-survival molecules associate with the mitochondria outer membrane and the endoplasmic reticulum/nuclear membrane and maintain their integrity [62]. They probably regulate the activation of several other caspases, independently of mitochondrial damage **Erreur ! Source du renvoi introuvable.**. PDT is thought to induce photodamage of Bcl-2 and related antiapoptotic proteins and activate the proapoptotic members of the family [63]. Alteration in expression of members of Bcl-2 family proteins following PDT has been reported in various cell lines and tumors [64]-[66]. Hyp mediated PDT in human breast adenocarcinoma cell line involved downregulation of Bcl-xl and upregulation of Bax [67]. This study indicated a possible involvement of the antiapoptotic Bcl-2 family members in PDT induced

apoptotic cell death, but a more definite role for Bcl-2 comes from studies involving antisense treatment and overexpression approaches.

Bcl-2 family members seem to spend most of their time simply trying to block each other's next move. Many family members can homodimerize, but more importantly, pro- and anti-apoptotic members can form heterodimers [68][69].

1.4.5.3 PDT and necrosis

Studying the factors and parameters that cause cellular necrosis after PDT is not as easy as studying those factors which lead to apoptosis. The crucial factors in determining the type of cell death, *e.g.*, apoptosis or necrosis following PDT are: the cell type, the presence of an intact set of apoptosis machinery, the subcellular localization of the pts, the light dose applied to activate it locally, and the oxygen partial pressure [70]. The high dose PDT (either a high photosensitizer concentration or a high light fluence or both) tends to cause cell death by necrosis, while PDT administered at lower doses tend to predispose cells towards apoptotic cell death [49]. A common feature of the apoptotic program initiated by PDT is the rapid release of mitochondrial cytochrome *c* into the cytosol followed by activation of the apoptosome and procaspase-3. With pts localized in the plasma membrane the photosensitization process can rapidly switch the balance towards necrotic cell death likely due to loss of plasma membrane integrity and rapid depletion of intracellular ATP [71]. It is also possible that high doses of PDT can photochemically inactivate essential enzymes and other components of the apoptotic cascade such as caspases [49].

1.5 FAMILY OF PROTEIN KINASE C

Protein kinase C also known as PKC is a family of protein kinase enzymes that are involved in controlling the function of other proteins through the phosphorylation of hydroxyl groups of serine and threonine amino acid residues on these proteins. PKC was one of the very first protein kinases to be identified [73].

In humans the PKC family consists of fifteen isozymes [73]. They are divided into three subfamilies, based on their second messenger requirements:

a.) conventional (or classical)

b.) novel

c.) atypical

Conventional contain the isoforms α, β_I, β_{II}, and γ. These require Ca^{2+}, diacylglycerol (DAG), and a phospholipid such as phosphatidylserine for activation. Novel PKC include the δ, ε, η, and θ isoforms, and require DAG, but do not require Ca^{2+} for activation. Thus, conventional and novel PKC are activated through the same signal transduction pathway as phospholipase C. On the other hand, atypical PKC (including protein kinase Mζ and ι / λ isoforms) require neither Ca^{2+} nor DAG for activation. The term "protein kinase C" usually refers to the entire family of isoforms [74].

PKC plays a fundamental signaling role in many physiological processes, including modulating membrane structure, mediating the immune response, and regulating the cell proliferation and differentiation via phosphorylation of various transcription factors. Generally, inactive PKC are considered to be primarily cytoplasmic. However, upon activation by different signals, PKC translocate to the plasma membrane, other membrane organelles and to the nucleus. PKC activity has been reported to be increased in gliomas and glioma cell lines as compared with astrocytes, and PKC inhibitors markedly reduced glioma cell proliferation. Moreover, differential expression of specific PKC isoforms has been reported in gliomas and other malignant cells [75].

1.5.1 PKCα: ANTI-APOPTOTIC PROTEIN

Protein kinase C alpha (PKCα) is a specific member of the protein kinase family. These enzymes are characterized by their ability to add a phosphate group to other proteins, thus changing their function. PKCα (Figure 5) has been widely studied in the tissues of many organisms including drosophila, xenopus, cow, dog, chicken, human, monkey, mouse, pig, and rabbit [75].

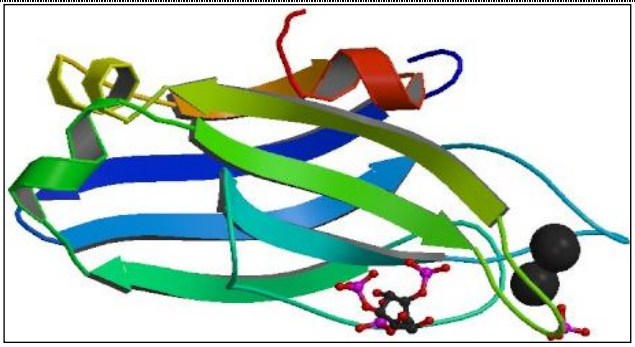

Figure 5: Crystal Structure Analysis of PKC (alpha)-C2 domain complexed with Ca2+ and PtdIns(4,5)P2

Protein chains are colored from the N-terminal to the C-terminal using a rainbow (spectral) color gradient [source [77]]

There is an extensive literature relating to the role of PKC in suppressing or stimulating apoptosis in various cell types [76], [79]. At the mitochondrial level, key players are members of Bcl-2 family proteins [81]. One of the PKCα roles is phosphorylation of Bcl-2 proteins in several cancerous cell lines including U-87 MG. Members of the family of Bcl-2 proteins are key regulators of apoptosis by acting either as promoters or as suppressors of the cell death process. Recent studies have shown that phosphorylation of Bcl-2 is required for the anti-apoptotic function of Bcl-2 and that PKCα activates Bcl-2 phosphorylation [80]. Pro-apoptotic proteins of the Bcl-2 family (e.g. Bax, Bak) can translocate from cytosol to mitochondria and participate in outer membrane destabilization. Anti-apoptotic family members (e.g. Bcl-2) protect the integrity of the outer mitochondrial membrane via inhibitory interactions with pro-apoptotic Bax and Bak [82][83]. In this context, Bcl-2 contains at least three sites that have been identified as phosphorylation sites in a flexible loop region (Thr69, Ser70 and Ser87). Phosphorylation that occurs at Ser70, the PKC phosphorylation site, is required for full anti-apoptotic function of Bcl-2 [80] and can affect the ability to associate with Bax [84].

Beyond its classical anti-apoptotic role, Bcl-2 is also known to have a critical anti-oxidant like function which has been linked experimentally to the regulation of cellular glutathione (GSH) content [85]. GSH is an endogenous antioxidant and key player averting mitochondrial oxidative stress and evading apoptosis [86][87]. Synthesis of GSH occurs in cytoplasm, and originated GSH must be actively transported into

mitochondria. The results obtained by Wilkins et al. suggest that Bcl-2 plays a central role in the regulation of mitochondrial GSH transport through its interaction with 2-oxoglutarate GSH carrier and maintenance of the mitochondrial glutathione pool [88].

It was shown that Hyp and phorbol 12-myristate-13-acetate (PMA; PKC activator) might competitively bind to the regulatory C1B domain of PKC. Furthermore Hyp influenced intracellular localization of PKC reflecting its activity, and this influence differed from that observed for PMA [162]. It was also demonstrated that the majority of PKCα present in U-87 MG cells is already in a catalytically competent form phosphorylated at Thr638, and that it is a Bcl-2 kinase [75]. In U-87 MG cells, Hyp localizes in subcellular compartments including ER and mitochondria [133]. Photo-activated Hyp affects mitochondrial functions [163] and induces predominantly apoptosis with the participation of Bcl-2 family proteins [75] [133][164].

1.5.2 PKCδ:PRO-APOPTOTIC PROTEIN

Protein kinase C delta (PKCδ) was the first new/novel PKC isoform to be identified by the screening of mammalian cDNA libraries. PKCδ (Figure 6A) is expressed ubiquitously among cells and tissues. PKCδ has catalytic and regulatory domains in the carboxyl- and amino-terminal halves, respectively (Figure 6 B). The catalytic domain contains two conserved regions, C3 and C4, in common with other members of the PKC family [89].

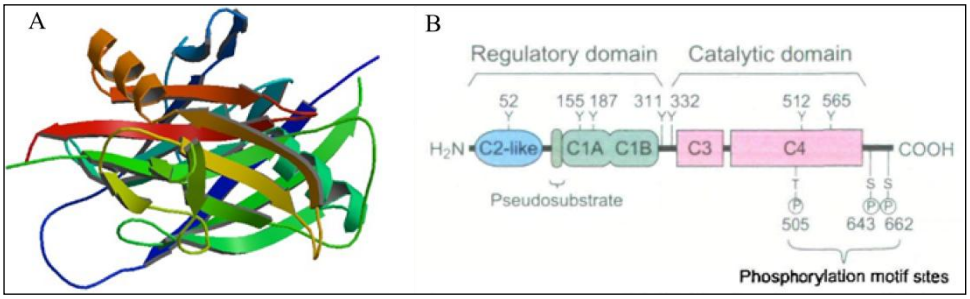

Figure 6: A- C2 domain from protein kinase cδ, B- The structure of PKCδ

A: Protein chains are colored from the N-terminal to the C-terminal using a rainbow (spectral) color gradient; **B:** The domain structure of PKCδ schematically shown, with the phosphorylation sites of serine (S), threonine (T), and tyrosine (Y) residues.
[source [89], [111]]

Over the past 50 years of investigation it was showed that the activity of almost all cellular responses can be regulated by phosphorylation. On the other side, the inverse reaction-dephosphorylation of proteins plays also a crucial role in the regulatory switching. Beside the PS, DAG and phorbol esters, phosphorylation plays an important role in the regulation of PKCδ [90]. PKCδ can be phosphorylated at Ser/Thr residues and tyrosine residues with activation loop, turn, and hydrophobic motif sites at Thr505, Ser643, and Ser662, respectively, and these sites are substantially phosphorylated *in vivo* [89][91]. Ser643 is autophosphorylated but Ser662 is recognized by an upstream kinase [92][93]. Tyrosine phosphorylation can activate or inhibit PKCδ depending on the site of phosphorylation and the stimulus [94]. By phosphorylation, PKC influences the cell functions of targeted proteins and play a key role in the regulation of various cellular processes, such as signal transduction, modulation of gene expression, proliferation, apoptosis, and differentiation [74][95][96].

Different PKC isoforms play important role in apoptosis [97]. It is known that PKCδ promotes apoptosis [113]. The association of tumor growth with the loss of PKCδ and overexpression and/or activation of this isoenzyme leads to the growth arrest at G2/M [98][99]. It has also been suggested that PKCδ may function in the activation of caspase-3 itself creating a positive feedback loop for further PKCδ activation [100]. Abnormalities in the PKC signaling have been associated with several human diseases including cancer [101][102]. By regulation of PKC the invasiveness of the cancer cells can be affected. Degradation of PKCδ causes dephosphorylation prior to ubiquitin-dependent degradation [99]. Apart from the chronic pharmacological activation the degradation of PKCδ occurs as well as response to sustained activation by hormones and growth factors [103][104]. It was showed that relatively selective PKCδ inhibitor rottlerin decreased TN-stimulated glioma invasiveness in a concentration and time-dependent manner [105]. Activation of PKCδ following cerebral ischemia led to the release of cytochrome *c* from the mitochondria via bad pathway [106]. PKCδ plays an important role in osteoclast bone resorption function which thereby opens up new avenues for pharmaceutical intervention in pathological osteolytic conditions [107]. It is known that kinase activity is required for the downregulation and degradation of the kinses [99]. Furthermore, PKCδ may serve as an attractive therapeutic target in Parkinson-related neurological diseases [108]. Several kinase inhibitors are now

approved for the treatment of cancer, and many more are advancing through clinical trials.

It was shown that in human malignant glioma cells Hyp inhibits the cell growth, motility and cell invasion and inhibits the tyrosine kinase activity, the activity of succinoxidase, and selectively inhibits the capability of PKC [109].

1.6 TARGETED DRUG DELIVERY

A holy grail in cancer therapy is to deliver high doses of drug molecules to tumor sites for maximum treatment efficacy while minimizing side effects to normal organs. Drug targeting means an increased accumulation of drug in the required area of the body compared to other tissues and organs mediated by a spontaneous or external force or targeting moiety. For the majority of pharmaceuticals currently in use, the specificity and activity of pharmaceuticals towards disease sites is usually based on the drug's ability to interfere with local pathological processes or with defective biological pathways, but not on its selective accumulation in the specific intracellular compartment or in the target cell, organ or tissue. Usually, pharmaceutical agents are distributed within the body rather evenly, proportionally to the regional blood flow [112]. Moreover, to reach the site of action, the drug has to cross many biological barriers, such as other organs, cells and intracellular compartments, where it can be inactivated or express undesirable effects on organs and tissues that are not involved in the pathological process. As a result, to achieve a required therapeutic concentration of a drug in a certain body compartment or certain tissue, one has to administer the drug in large quantities the great part of which, even in the best case scenario, is just wasted in normal tissues. Drug targeting can bring a solution to all these problems. In a very general sense, drug targeting is the ability of the drug to accumulate in the target organ or tissue selectively and quantitatively, independent of the site and method of its administration. Ideally, under such conditions, the local concentration of the agent at the disease site(s) should be high, while its concentration in other nontarget organs and tissues should be below certain minimal levels to prevent any negative side reactions [113]. The following advantages of drug targeting are evident: drug administration

protocols may be simplified, the drug quantity required to achieve a therapeutic effect may be greatly reduced, as well as the cost of therapy and drug concentration in the required sites can be sharply increased without negative effects on nontarget compartments [114].

To improve the biodistribution of anticancer drugs, nanoparticles have been designed for optimal size and surface characteristics to increase their circulation time in the bloodstream.Various types of nanoparticles are used in biomedical research and drug delivery (Figure 7):

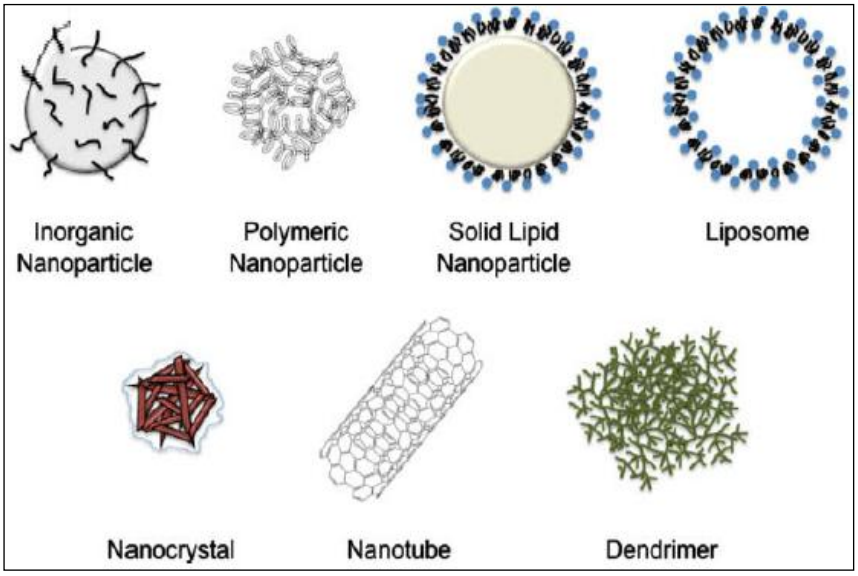

Figure 7: Various types of nanoparticles used in biomedical research and drug delivery

[source [115]]

Inorganic nanoparticles: typically composed of inorganic compounds such as silica or alumina. However, the nanoparticle core is not limited to just these two materials; rather, metals, metal oxides and metal sulfides can be used to produce a myriad of nanostructures with varying size, shape, and porosity [115].

Polymeric nanoparticles: most are biodegradable, biocompatible, and have been adopted as a preferred method for nanomaterial drug delivery. They also exhibit a good potential for surface modification via chemical transformations, provide excellent pharmacokinetic control, and are suitable for the entrapment and delivery of a wide range of therapeutic agents [115].

Solid lipid nanoparticles: lipid-based submicron colloidal carriers. They were initially designed in the early 1990s as a pharmaceutical alternative to liposomes and emulsions. In general, they are more stable than liposomes in biological systems due to their relatively rigid core consisting of hydrophobic lipids that are solid at room and body temperatures, surrounded by a monolayer of phospholipids. These aggregates are further stabilized by the inclusion of high levels of surfactants. Because of their ease of biodegradation, they are less toxic than polymer or ceramic nanoparticles [115].

Liposomes: spherical vesicles of phospholipid bilayer membrane. They are related to micelles which are generally composed of a monolayer of lipids. The amphiphilic nature of liposomes, their ease of surface modification, and a good biocompatibility profile make them an appealing solution for increasing the circulating half-life of proteins and peptides. They may contain hydrophilic compounds, which remain encapsulated in the aqueous interior, or hydrophobic compounds, which may escape encapsulation through diffusion out of the phospholipid membrane. Liposomes can be designed to adhere to cellular membranes to deliver a drug payload or simply transfer drugs following endocytosis [115].

Nanocrystals: aggregates of molecules that can be combined into a crystalline form of the drug surrounded by a thin coating of surfactant. They have extensive uses in materials research, chemical engineering, and as quantum dots for biological imaging, but less so in nanomedicine for drug delivery [115].

Nanotubes: self-assembling sheets of atoms arranged in tubes. They may be organic or inorganic in composition and can be produced as single- or multi-walled structures. A popular version of a nanotube involves the use of soluble fullerene derivatives, such as C_{60}. Nanotubes have large internal volumes and the external surface can be easily functionalized. While they are potentially promising for pharmaceutical applications, human tolerance of these compounds remains unknown, and toxicity reports are conflicting [115].

Dendrimers: polymer-based macromolecules formed from monomeric or oligomeric units, such that each layer of branching units doubles or triples the number of peripheral groups. Dendrimers generally have a symmetrical structure, with the potential to create an isolated ‘active site’ core area through chemical functionalization.

Modification of the degree of branching may allow for encapsulation of a molecule within this structure. [115].

1.7 LIPOPROTEINS

Lipoproteins consist of noncovalently associated lipids and proteins which function in the blood plasma as transport vehicles for triacylglycerols (TAGs) and cholesterol. Lipids, such as phospholipids, TAG, and cholesterol, are sparingly soluble in aqueous solution. Hence, the globular micelle like particles-droplets of TAGs and cholesteryl esters coated with a monolayer of phospholipids, cholesterol, and apolipoproteins transport these lipids by the circulation as components of lipoproteins. Lipoproteins have been classified into five broad categories on the basis of their functional and physical properties (Table 2, Figure 8) [116].

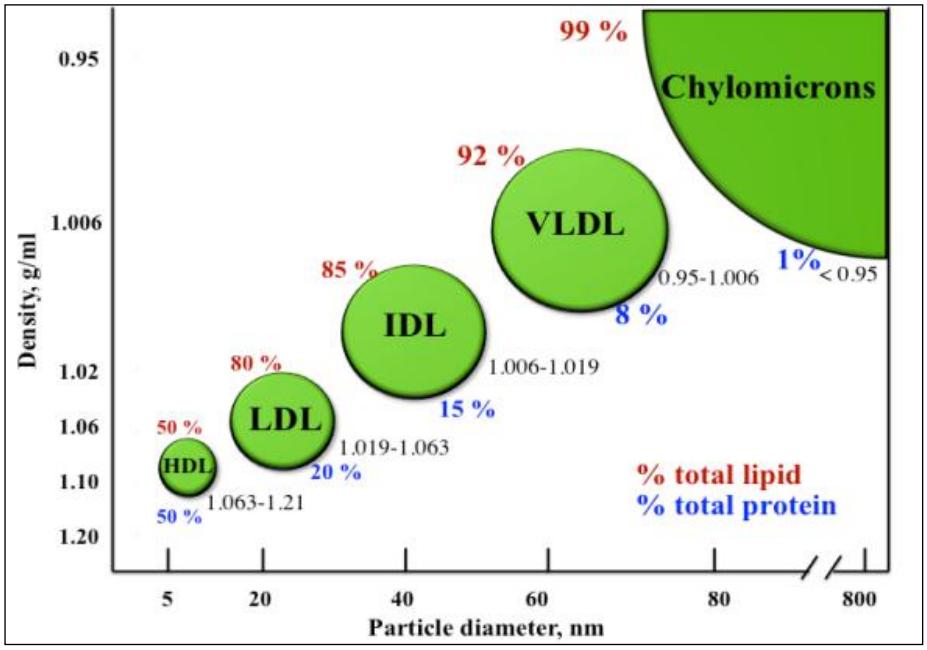

Figure 8: Lipoprotein classes

The classification of the major types of lipoproteins is based on their densities obtained by flotation ultracentrifugation analysis. The density range for each class is shown, in addition to the lipid (red) and protein (blue) content. The diagram is not to scale.

[source [117]]

Chylomicrons: transport exogenous TAGs and cholesterol from the intestines to the tissues.

Very Low Density Lipoproteins (VLDL): are synthesized in the liver and function to export TAGs to peripheral tissues.

Low Density Lipoproteins (LDL): are the major vehicles to transport cholesteryl esters to peripheral cells.

High density lipoproteins (HDL): transport endogenous cholesterol from the tissues to the liver [116].

	Chylomicrons	**VLDL**	**IDL**	**LDL**	**HDL**
Density ($g.cm^{-3}$)	<0,95	<1,006	1,006-1,019	1,019-1,063	1,063-1,210
Particle diameter(Å)	750-12 000	300-800	250-350	180-250	50-120
Particle mass (kD)	400 000	10 000-80 000	5 000-10 000	2300	175-360
% Protein	1,5-2,5	5-10	15-20	20-25	40-55
% Phospholipids	7-9	15-20	22	15-20	20-35
% Free cholesterol	1-3	5-10	8	7-10	3-4
% TAG	84-89	50-65	22	7-10	3-5
% Cholesteryl esters	3-5	10-15	30	35-40	12
Major apolipoprotein	A-I,A-II, B-48, C-I, C-II, C-III, E	B-100, C-I, C-II, C-III, E	B-100, C-I, C-II, C-III, E	B-100	A-I, A-II, C-I, C-II, C-III, D, E

Table 2: Characteristics of the major classes of lipoproteins in human plasma

[source [116]]

1.7.1 HIGH DENSITY LIPOPROTEIN

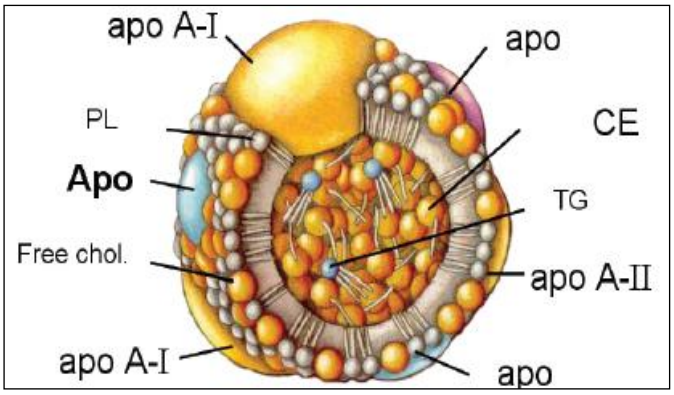

Figure 9: Molecule of HDL

[source [119]]

High density lipoprotein (7-13 nm) is a heterogenous class of plasma lipoproteins that have a density between 1,063 g/ml and 1,21 g/ml. HDL is composed of a hydrophobic core of TAG and cholesterol esters covered in a monolayer of phospholipids into which apolipoprotein A-1 (Apo-I) is embedded (Figure 9) [118]. ApoA-I, which is comprised of 10 amphipathic alpha helices each with a hydrophobic domain and a negatively charged hydrophobic domain, is the main protein component of HDL and defines the structure and physiology of HDL *in vivo*.

HDL is a dynamic serum protective against the development of atherosclerosis and resultant illnesses such as heart disease and stroke [120].

HDL molecules transport cholesterol from the tissues to the liver and have essentially the opposite function of LDL: they remove cholesterol from the tissues. Circulating HDL acquires its cholesterol by extracting it from cell-surface membranes and converts it to cholesteryl esters. HDL therefore functions as a cholesterol scavenger. The life spans in the body of HDL is much longer (5 to 6 days) than other lipoproteins [119].

1.7.2 LOW DENSITY LIPOPROTEIN

This spheroidal particle (~ 22 nm in diameter) consists of 1500 cholesteryl ester molecules surrounded by an amphiphilic coat of 800 phospholipid molecules, 500 cholesterol molecules, and a single 4536-residue molecule of apolipoprotein B-100 (ApoB) that has 550kDa (Figure 10) [116]. The ApoB are highly insoluble in aqueous solutions and, thus, remain with the lipoprotein particle throughout its metabolism [117].

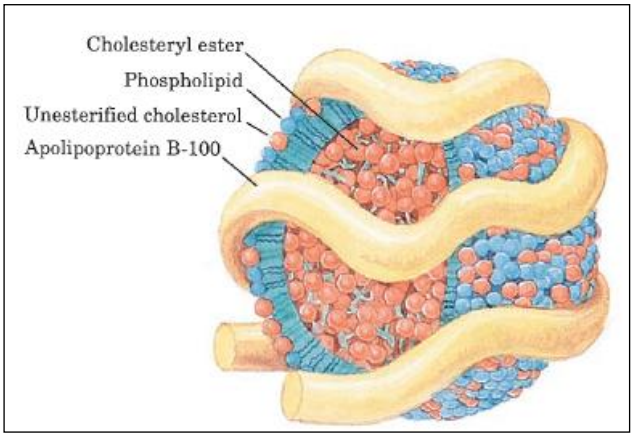

Figure 10: LDL particle-the major cholesterol carrier of the bloodstream

[source [116]]

There are three structurally different regions in LDL particle: the outer surface layer, the core region and an interfacial region between these two [119]. Triglyceride and cholesteryl ester molecules are in the core of LDL molecule and the surface monolayer consists of about phospholipid molecules and a single copy of ApoB-100. In addition, the particles contain molecules of unesterified cholesterol, of which about 1/3 is located in the core and 2/3 in the surface. Toward the surface penetrate a few percent of the triglyceride and cholesteryl ester molecules [121].

Cells take up cholesterol through receptor-mediated endocytosis of LDL. Cells obtain exogenous cholesterol mainly through the endocytosis of LDL in complex with LDL receptor (LDLR), a cell-surface transmembrane glycoprotein that specifically binds ApoB-100. Upon binding to the LDLR, LDL moves into the endosome where a drop of pH causes the receptor to dissociate from LDL. The receptor is recycled back to

the surface of the cell while the LDL is moved to lysosome where the particle is degraded. [116].

1.7.2.1 LDL and HDL for targeted delivery

In the recent years an important attention has been dedicated to the use of lipoproteins for targeted drug delivery [123]. This fact is based on the establishing of a direct relationship between the relative number of lipoprotein receptors in various tumors and the uptake of drugs by malignant cells [124]. Of the lipoproteins the most important in terms of drug delivery are LDL, however, the importance of HDL is also recognized and in many cases seems to be even higher than LDL [124], [125]. The capacity of both types of the lipoproteins, LDL as well as HDL, to bind some drugs and their functionality as drug carriers have been examined in several studies [126][131]. It has been also shown that mixing of anticancer drugs with LDL or HDL before administration led to an increase of the cytotoxic effects of the drugs in the comparison when the drugs are administered alone [125], [127].

LDL are recognized by and internalized into the cells through specific membrane receptors that interact with the ApoB of the LDL particle [128]. Certain tumor cells and tumor vascular endothelial cells express the LDL receptors in higher number due to either their increased proliferation or increased membrane turnover [129]. HDL have been implicated in cholesterol delivery in some malignancies including breast cancer, ovarian cancer, adrenocortical tumors and prostate cancer. The mechanism for HDL mediated delivery appears to be SR-B1 receptor dependent [124]. It is known that this receptor is broadly expressed among a variety of cancer cells. The above mentioned facts make LDL and HDL particles attractive natural occurring vehicles for drug delivery and targeting to cancer tissues.

Both types of the lipoproteins particles assume a globular shape with an average particle diameter 20-25 nm and 7-13 nm for LDL and HDL, respectively. LDL and HDL have important advantages in comparison to other drug nano-delivery systems: i) as natural molecules both lipoproteins escape recognition by mononuclear phagocytic system, which favors their long circulation time in the plasma, ii) they are not

immunogenic, iii) their hydrophobic core and phospholipid shell favor binding of hydrophobic and amphiphilic drugs, respectively [118][124][126]. The importance of the study of the physicochemical properties of complexes of drugs with lipoproteins is confirmed by the fact that the US Food and Drug Administration encouraged the inclusion of lipoprotein-drug interaction studies as part of any investigational new drug application that contains a hydrophobic compound [130].

1.7.3 STATE OF ART AND CONTRIBUTION OF OUR GROUP

PDT is for a long time the main research subject in which our groups (Department of biophysics, UPJS, Kosice and LJP UPMC Paris) collaborate. This subject contains two main scientific problems: The first one is dedicated to the development of a selective nanodelivery system based on LDL molecules and the second one (closely realted to the first one) is dedicated to the study of a physico-chemical mechanism of pts anticancer action. My thesis represents a natural continuation of work in both of them.

State of the art description and objectives of my thesis:

Development of nanodelivery system based of the LDL molecules. It was shown by our group that:

a) LDL particles are capable to bound Hyp molecules as monomers up to the LDL-Hyp ratio = 1:30. Higher concentration of Hyp leads to an aggregation of Hyp molecules which decreases a biological activity of Hyp and protects LDL from oxidation [122][131][133]
b) Hyp loaded in LDL is redistributed towards free lipids [122].
c) Covering of LDL by dextran molecules decreases significantly dynamics of Hyp redistribution to other plasma proteins. This covering does not influence the recognition of LDL molecules by LDL receptors [134].

At this stage of knowledge the **first objective** of my thesis regarding the study of nanodelivery system was defined: to optimize properties of [LDL-Hyp]/DCh delivery system, study the cellular uptake of Hyp delivered by complex [LDL-Hyp]/Dch and its intracellular redistribution which included the development of a synthetic LDL based

delivery system and beside nanodelivery system based on the LDL molecules to study and characterize the interaction of HDL with Hyp as well.

Mechanism of an anticancer action of Hyp: At this field our groups did a lot of different kind of study where different modes of Hyp anticancer action were examined. With regards to the subject of my thesis I will present just results dedicated to the study of PKC role in the induced apoptosis:

a) Interaction of PKC with Hyp in correlation with the influence of Hyp on the PKC localization in U87-MG human malignant glioma cell line was studied. It was shown that PKC intracellular localization in U-87 MG cells is influenced by Hyp and that this influence is different from that observed for the PKC activator PMA [160].

b) Structural models of C1B subdomains of PKCα, PKCγ and PKCδ with Hyp were constructed by molecular simulation. It was shown that Hyp binds to the regulatory of PKC with relatively high affinity, and that after photoactivation, it can induce oxidation of certain amino acid residues which leads to irreversible inactivation of PKC [160].

c) The role of anti-apoptotic PKCα in response to Hyp photodynamic therapy in U-87 MG cells was examined as well. It was shown that the presence of Hyp without irradiation does not affect PKCα distribution but after Hyp photo-activation, PKCα is activated and localized along the plasma membrane and partially in the nuclei. The regulation of PKCα activity may be imporant for increasing cancer cells'sensitivity toward anticancer PDT treatments. In particular, dephosphorylation of PKCα and phosphorylated Bcl-2 may play a role [75].

At this stage of knowledge the **second objective** of my thesis was defined: to study molecular mechanism of the photodynamic induced cell death: understand the impact of PKCα and PKCδ on the cell death after knocking out their expression in U87-MG cells.

2 MATERIAL, METHODS AND PROTOCOLS

2.1 CHEMICALS

Alexa Fluor® 488 F(ab')2 fragment of goat anti-rabbit IgG (H+L), Alexa Fluor® 546 F(ab')2 Fragment of Goat Anti-Rabbit IgG (H+L), Alexa Fluor®, 488 F(ab')2 Fragment of Goat Anti-Mouse IgG, IgM (H+L), Annexin-V-FITC, CellROX® Deep Red Reagent, CellROX Orange Reagent®, MitoTracker® Orange-CMTMRos ThiolTrackerTM, Fetal bovine serum (FBS), Hypericin, Penicillin/streptomycin, Phosphate saline buffer (PBS), Phorbol myristate acetate (PMA), Propidium iodide (PI) and Trypsin, 0.05% (1X) with EDTA 4Na were purchased from Gibco-Invitrogen (France). 3,3′-Dioctadecyloxacarbocyanine perchlorate ($DiOC_{18}(3)$), Acetone, Bovine serum albumin (BSA), Butylated hydroxytoulene (BHT), Chloroform, Cholesterol, Cholesteryl oleate (CO), Ethanol, Formaldehyde, Hoechst 33258, Methanol, MTT (3-[4, 5-dimethylthiazol-2-yl]-2, 5-diphenyltetrazolium bromide), Triolein (TO) and Triton™ X-100 were obtained from Sigma Aldrich (USA). HDL and LDL were purchased from Calbiochem (United Kingdom). Dextran with molecular weight M = 1000 g/mol was obtained from Pharmacosmos A/S (Denmark) and cholesterol modified dextran (D_{Ch}, molecular weight = 1850 g/mol) was synthesized by Dr. Kronek (Polymer Institute, Bratislava, Slovakia). 1,2-dioleoyl-sn-glycero-3-phosphocholine (DOPC), 1,2-dioleoyl-sn-glycero-3-phosphoethanolamin (DOPE), 1,2-dipalmitoyl-sn-glycero-3-phosphoethanolamine-N-lissamine rhodamine B sulfonyl (DOPE-Rhod B) and Egg yolk phosphatidyl choline (PC), were obtained from Avanti Polar Lipids (USA). Synthetic peptide was purchased by Biosynthesis Inc. (USA). Ultroser G (UG) was purchased from Pall Corporation (USA). PKCα siRNA(h), Control siRNA (FITC Conjugate)-A and PKCδ siRNA(h) were obtained from Santa Cruz Biotechnology (USA). Goat polyclonal secondary antibody to rabbit IgG- H&L (FITC) and PKCδ Antibody (ab47473) was purchased from Abcam (United Kingdom). PKCα [p Thr638] Antibody (E195) was obtained from Novus (USA), PKCδ antibody (Phospho-Ser645) was purchased from Acris antibodies (USA), anti-Bak NT was purchased from ψProSci Inc. (USA) and anti Bax 2D2 was obtained from Enzo Life Sciences (Switzerland).

2.2 ABSORPTION SPECTROSCOPY

Absorbance spectroscopy is frequently used to measure concentration. According to the Beer-Lambert law (Eq. (1)), measurements of absorbance for molecules of known ε allow calculation of concentration.

$$A = \varepsilon c l \qquad \textbf{Eq. (1)}$$

ε = molar absorptivity, a constant for a particular species at a particular wavelength, related to the probability of transition,

l = length of cell or cuvette,

c = molar concentration.

Alternatively, if the concentration of the absorbing species is known, the ε can be determined [138].

In this study absorbance spectra were recorded by double beam UV-VIS spectrofotometer Shimadzu UV-2401 PC in the range 400-700 nm which schema is presented on Figure 11.

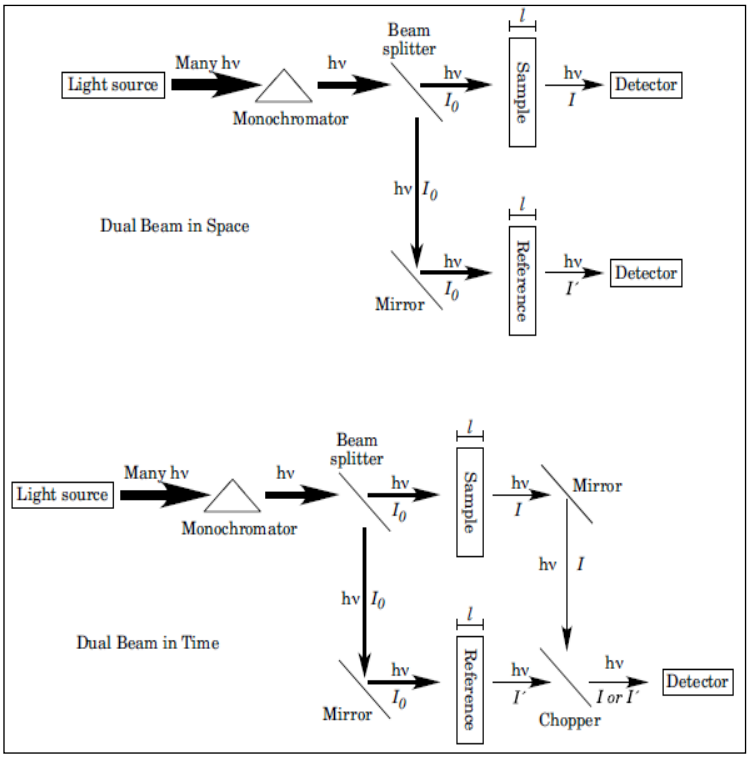

Figure 11: The layout of dual beam spectrofotometer

[source [138]]

2.3 FLUORESCENCE SPECTROSCOPY

Fluorescence is a spectrochemical method of analysis where the molecules of the analyte are excited by irradiation at a certain wavelength and emit radiation of a different wavelength. The emission spectrum provides information for both qualitative and quantitative analysis. As shown on the of the Jablonski diagram (Figure 1), when light of an appropriate wavelength is absorbed by a molecule, the electronic state of the molecule changes from the ground state to one of many vibrational levels in one of the excited electronic states. The excited electronic state is usually the first excited singlet state, S1. Relaxation can occur via several processes once the molecule is in this excited state. Fluorescence is one of these processes and results in the emission of light. Fluorescence corresponds to the relaxation of the molecule from the singlet excited state to the singlet ground state with emission of light. It has short lifetime (usually 10^{-9} to 10^{-8} sec). The wavelength (and thus the energy) of the light emitted is dependent on the energy gap between the ground state and the singlet excited state. Figure 12 shows a schematic diagram of a spectrofluorometer which as a source of exciting light uses a xenon lamp.

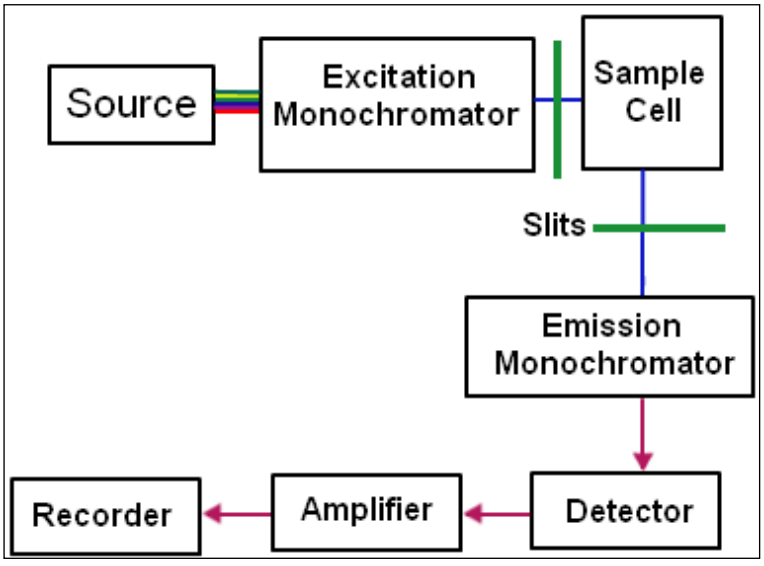

Figure 12: Schematic diagram of spectrofluorimeter

[source [139]]

The instrument is equipped with monochromators to select both the excitation and emission wavelengths. Both monochromators are motorized to allow automatic scanning of wavelength. The fluorescence is detected with photomultiplier tubes and quantified with the appropriate electronic devices [140].

Fluorescence spectra in this work were recorded at room temperature by SHIMADZU RF-5301 spectrofluorimeter (Kyoto, Japan). The excitation wavelength was 560 nm and the emission was collected in the range 570-700 nm for all measurements unless it is written differently.

2.3.1 FRET

Förster Resonant Energy Transfer (or Fluorescent Resonant Energy Transfer), FRET, is the energy transfer mechanism between two fluorescent dyes through long range dipole-dipole interactions. For efficient FRET to occur there must be a substantial overlap between the donor fluorescence emission spectra and acceptor fluorescence excitation (or absorption) spectra. The donor is excited at its specific excitation wavelength and this excited state energy is transferred non-radiatively to the acceptor dye which becomes excited, while the donor returns to the ground state. The acceptor dye rapidly loses some energy through vibrational and rotational modes, and thus the energy match with the donor is lost, meaning that this energy cannot be returned to the donor. The acceptor dye eventually returns to the ground state, this time through a radiative process whereby a photon will be emitted.

FRET can only happen when the two fluorescent dyes are in close proximity usually less than 10 nm. The probability of energy transfer is strongly dependent on the inter-dye distance (Figure 13). Another factor which plays a role in the efficiency of the FRET as well is the orientation of the molecules electric dipoles relative to each other [141].

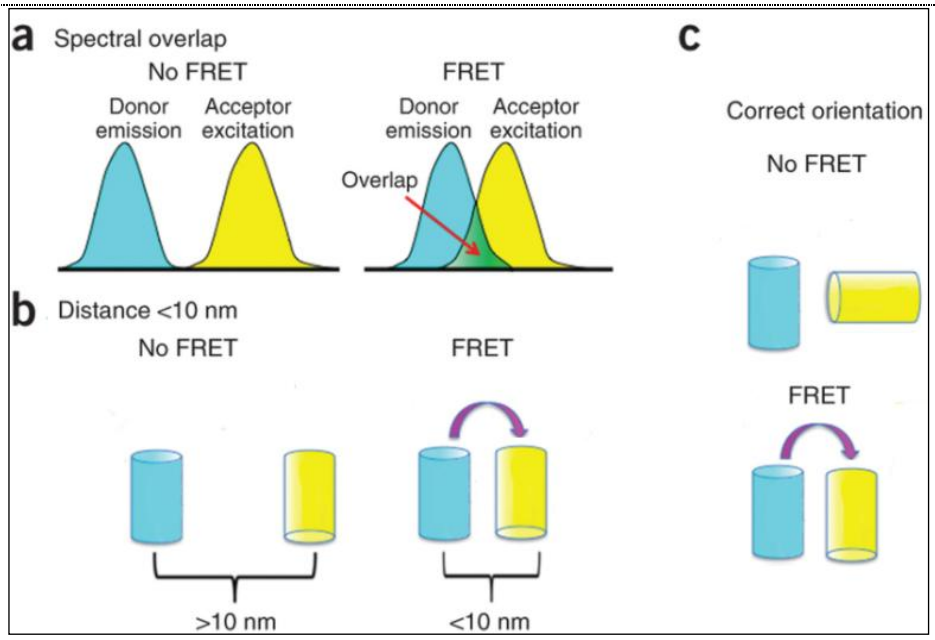

Figure 13: Conditions for FRET

[source [142]]

Förster, demonstrated that the efficiency of the process (E) depends on the inverse sixth-distance between donor and acceptor (Eq. 2).

$$E = \frac{\mathrm{R}o^6}{\mathrm{R}o^6 + r^6} \qquad \textbf{Eq. (2)}$$

Ro = Förster distance at which half the energy is transferred

r = the actual distance between donor and acceptor.

The distance at which energy transfer is 50% efficient is referred to as the Förster radius (Ro). The magnitude of the Ro is dependent on the spectral properties of the donor and the acceptor. Förster distances ranging from 20 to 90 Å are most useful for studies of biological macromolecules. These distances are comparable to the diameters of many proteins, the thickness of biological membranes, and the distances between sites on multisubunit proteins [144].

2.4 FLUORESCENCE LIFETIME

The fluorescence lifetime is a measure of the time a fluorophore spends in the excited state before returning to the ground state by emitting a photon. The lifetimes of fluorophores can range from picoseconds to nanoseconds [140]. In general, the behavior of an excited population of fluorophores is described by a familiar rate equation:

$$\frac{dn^*}{dt} = -n^*\Gamma + f(t) \qquad \text{Eq. (3)}$$

were: n* is the number of excited elements at time t,

Γis the rate constant of emission (dimensions of Γ are sec^{-1}),

f(t) is an arbitrary function of the time, describing the time course of the excitation.

If excitation occurs at t = 0, the equation Eq**. (3**) takes form:

$$\frac{dn^*}{dt} = -n^* \Gamma \qquad \textbf{Eq. (4)}$$

and describes the decrease in excited molecules at all further times. Integration gives:

$$n*(t) = n*(0)e^{(-\Gamma t)} \qquad \textbf{Eq. (5)}$$

The lifetime τ is equal to Γ^{-1}.

The lifetime and quantum yield for a given fluorophore is often dramatically affected by its environment. Examples of this fact would be NADH, which in water has a lifetime of ~0,4 ns but bound to dehydrogenases can be as long as 9 ns [145].

Excited state lifetimes have traditionally been measured using either the impulse response or the harmonic response method. In principle both methods have the same information content. These methods are also referred to as either the "time domain" method or the "frequency domain" method. In the time domain method, the sample is illuminated with a short pulse of light and the intensity of the emission versus time is recorded. As shown in the Figure 14, the fluorescence lifetime t, is equal to the time at which the intensity has decayed to $\frac{1}{e}$ of the original value.

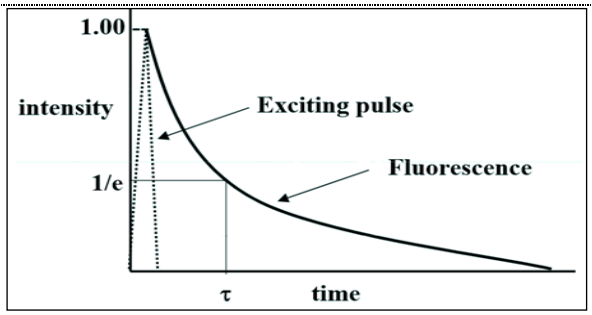

Figure 14: Example of the intensity decay

[source [143]]

The relation for single exponential decay is given:

$$I_t = \alpha e^{\frac{-t}{\tau}} \qquad \textbf{Eq. (6)}$$

were: I_t is the intensity at time t

α is a normalization term (the pre-exponential factor)

τ is the lifetime.

It is more common to plot the fluorescence decay data using a logarithmic scale as shown on Figure 15. If the decay is a single exponential and if the lifetime is long compared to the exciting light then the lifetime can be determined directly from the slope of the curve.

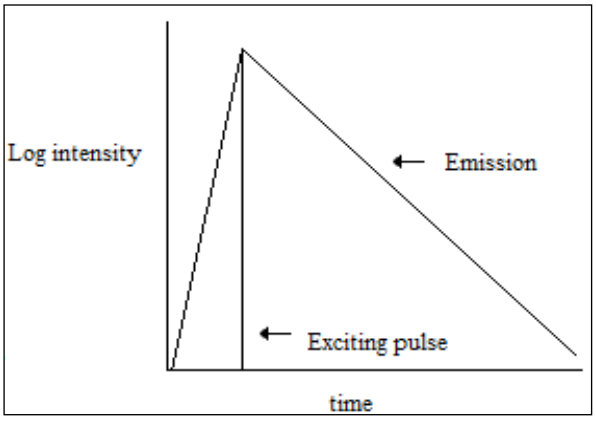

Figure 15: Fluorescence decay data in logarithmic scale

[source [143]]

If the lifetime and the excitation pulse width are comparable, some type of deconvolution method must be used to extract the lifetime. Great effort has been expended on developing mathematical methods to "deconvolve" the effect of the

exciting pulse shape on the observed fluorescence decay. With the advent of very fast laser pulses these deconvolution procedures became less important for most lifetime determinations, although they are still required whenever the lifetime is of comparable duration to the light pulse.

If the decay is multiexponential, the relation between the intensity and time after excitation is given by:

$$I(t) = \sum_i \alpha_i e^{\frac{-t}{\tau_i}} \qquad \textbf{Eq. (7)}$$

In the frequency domain method a continuous light source is utilized, such as a laser or xenon arc, and the intensity of this light source is modulated sinusoidally at high frequency as shown on Figure 16.

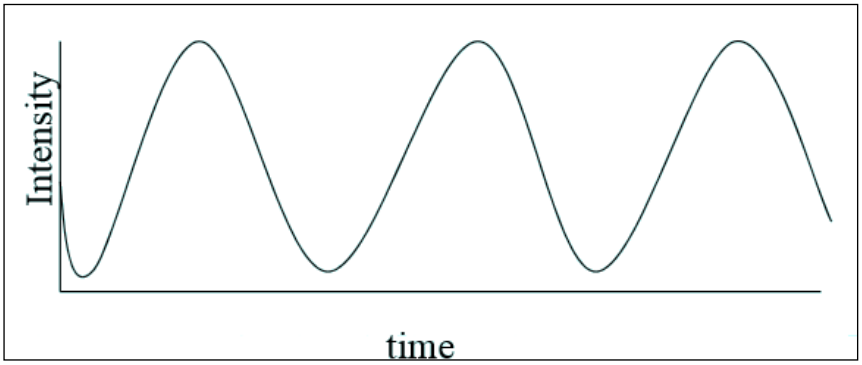

Figure 16: Sinusoidal modulation of the light source

[source [143]]

Typically, an electro-optic device, such as a Pockels cell is used to modulate a continuous light source. Alternatively, LEDs or laser diodes can be directly modulated.

In such a case, the excitation frequency is described by:

$$E(t) = Eo\ [1 + M_E \sin \omega t] \qquad \textbf{Eq. (8)}$$

E(t) and Eo are the intensities at time t and 0,

M_E is the modulation factor which is related to the ratio of the AC and DC parts of the signal,

ω is the angular modulation frequency; $\omega = 2\pi f$ where f is the linear modulation frequency.

Due to the persistence of the excited state, fluorophores subjected to such an excitation will give rise to a modulated emission which is shifted in phase relative to the exciting light as shown on Figure 17 which illustrates the phase delay (φ) between the excitation E(t) and the emission F(t). Also shown are the AC and DC levels associated with the excitation and emission waveforms.

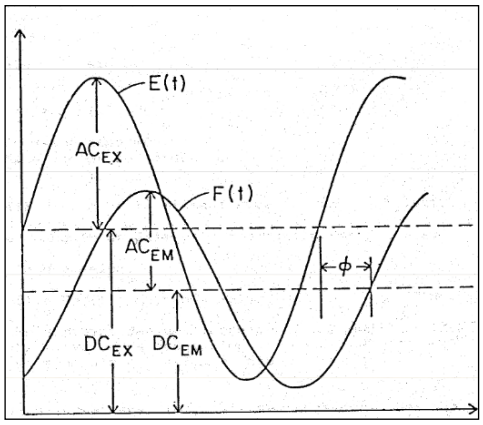

Figure 17: The phase delay between the excitation and emission

[source [143]]

It can be demonstrated that:

$$F(t) = Fo\,[1 + M_F \sin(\omega t + \phi)] \qquad \textbf{Eq. (9)}$$

This relationship signifies that measurement of the phase delay φ forms the basis of one measurement of the lifetime τ. In particular it can be demonstrated as:

$$\tan\phi = \omega t \qquad \textbf{Eq. (10)}$$

The modulations of the excitation (M_E) and the emission (M_F) are given by:

$$M_E = (AC_{Exc}/DC_{Exc}) \text{ and } M_F = (AC_{Em}/DC_{Em}) \qquad \textbf{Eq. (11)}$$

where: AC_{Exc} and AC_{Em} are ratio of amplitude oscillation

DC_{Exc} and DC_{Em} are offsets of AC_{Exc} and AC_{Em}

The relative modulation M of the emission is then:

$$M = \frac{(AC/DC)_F}{(AC/DC)_E} \qquad \textbf{Eq. (12)}$$

τ can also be determined from M to the relation:

$$M = \frac{1}{\sqrt{1 + (\omega\tau)^2}} \qquad \textbf{Eq. (13)}$$

Using the phase shift and relative modulation one can thus determine a phase lifetime (τ_P) and a modulation lifetime (τ_M). If the fluorescence decay is a single exponential, then τ_P and τ_M will be equal at all modulation frequencies. If, however, the fluorescence decay is multiexponential then $\tau_P < \tau_M$ and, moreover, the values of both τ_P and τ_M will depend upon the modulation frequency.

Figure 18 presents multifrequency phase and modulation data [147].

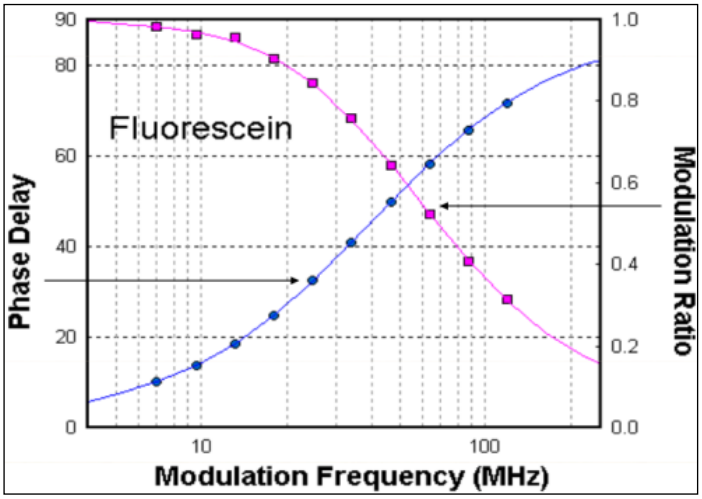

Figure 18: The frequency response curve (phase and modulation

[source [143]

In our experimental set-up samples were excited by a 442 nm laser diode module (Omicron LDM 442.50.A350) with 50 mW output power. Analog intensity modulation of the laser was obtained by direct coupling of the output sine wave of the Master synthesizer (model 2025 from IFR) to the laser diode excitation module. Signal was brought and collected from the sample by confocal epi-fluorescence microscope (Zeiss UMSP-80) through the water immersion 63x objective (Zeiss Neofluar) with 1.2 numerical aperture. Fluorescence signal was focused through the pinhole on the entrance slit of the Jobin-Yvon HR640 spectrograph equipped with a 100 line/mm grating, which enabled to transfer whole 375 nm spectral region on a 25 mm-diameter photocathode of the image intensifier. This high frequency gain modulated (5 to 200 MHz) image intensifier (Lambert Instrument, Netherlands) was optically coupled with CCD detector (1024x1024 pixels). The CCD controller was connected to the detector controler via USB communication interface. For the setup control and data acquisition LIFLIM software was used (Lambert Instruments). A special data conversion program

(PHR) was written by Jiri Bok (from MFF KU in Prague) to calculate the phase shift and the demodulation spectral dependence of the fluorescence signal from the acquired data. Subsequent lifetime determination and spectral decomposition was performed by using a global fitting procedure.

2.5 CONFOCAL FLUORESCENCE MICROSCOPY

In recent years, the confocal scanning laser microscope (CSLM) has become widely established as a research instrument. In a conventional light microscope, object to image transformation takes place simultaneously and parallel for all object points. By contrast, the specimen in a confocal CSLM is irradiated in a pointwise fashion and the physical interaction between the laser light and the specimen detail irradiated is measured point by point as well. To obtain information about the entire specimen, it is necessary to guide the laser beam across the specimen, or to move the specimen relative to the laser beam, a process known as scanning. CSLM uses the confocal aperture (usually called pinhole) arranged in a plane conjugate to the intermediate image plane and, thus, to the object plane of the microscope. As a result, the detector (PMT) can only detect light that has passed the pinhole. The pinhole diameter is variable; ideally, it is infinitely small, and thus the detector looks at a point. The laser beam is focused to a diffraction-limited spot which illuminates only a point of the object at a time; the point illuminated and the point observed lie on conjugate planes. This is called confocal ray path (Figure 19). The pinhole more or less obstructs light coming from object points outside the focal plane and excludes it from detection. Object areas thus obstructed are invisible in the image. Therefore, the confocal microscope is an inherently depth-discriminating optical system. By varying the pinhole diameter, the degree of confocality can be adapted to practical requirements. With the aperture fully open, the image is non-confocal [148].

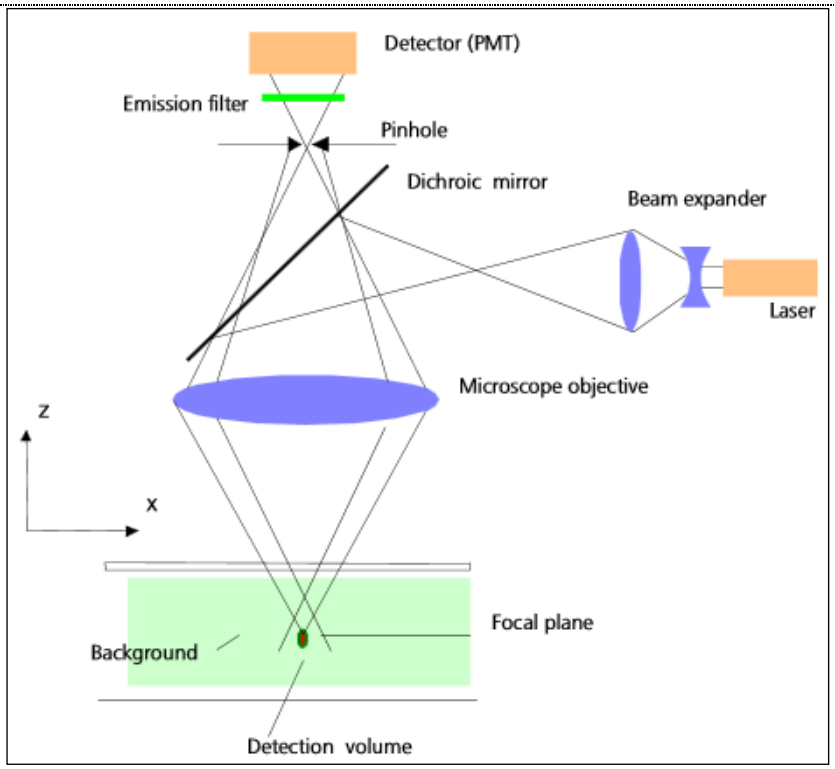

Figure 19: Ray path in a confocal CSLM

[source [148]]

Fluorescence images were obtained by Optiphot-2 epifluorescence microscope equipped with a Nipkow Wheel coaxial–confocal attachment (Technical Instrument, CA, USA). Fluorescence images were taken by using water-immersion objective (Zeiss Neofluar, X63, N.A. 1.2) and TE cooled CCD Micromax camera (Princeton Instruments, NJ, USA). Exposure time was set to 5 s. Image processing was performed by ImageJ software.

Confocal fluorescence images were obtained by CSLM 700 confocal microscope system (CSLM 700, Zeiss Germany) with a 63×oil objective (NA=1.46). The laser line (488 nm) of the solid state laser was used to excite FITC or Alexa 488 fluorophore. Emissions were recorded in single-track configuration with a band-pass filter of 490-555 nm. The laser line (555 nm) of the solid state laser was used to excite Alexa 546 or Hyp. Emissions were recorded in single-track configuration with a long-pass filter of 560 nm. Fluorescence signals were analyzed by the Zen 2011 software (Zeiss, Germany).

2.6 FLOW CYTOMETRY

By flow cytometry the physical and chemical properties of live cells or other biological particles can be measured as they pass in a fluid single-cell stream through a measuring apparatus. In the most common scenario, one or more lasers interrogate each particle and, at a minimum, the system measures the degree and direction of scattered light-indicators of the particle's size, shape and structure. If particles have been stained with one or more fluorescent dyes-known as fluorochromes, the light source excites these dyes to provide additional biological information about each particle, such as metabolic activity, DNA content and the presence of specific surface and intracellular markers. Precise optical and electronic elements collect the fluorescent pulses and scattered light, convert them into digital values and send them to a computer for analysis. The unique power of flow cytometers is that they can rapidly and quantitatively measure multiple simultaneous parameters on individual live cells and then isolate cells of interest [149].

Flow cytometry measurements were performed using a MACSQuant®Analyzer (Miltenyi, GER). The obtained data were analyzed by MACSQuantify™ Software (Miltenyi, GER).

2.7 DYNAMIC LIGHT SCATTERING

Dynamic light scattering (DLS) is an important experimental technique, one of the most popular methods used to determine the size of particles. It measures the fluctuation in the intensity of the scattered light of the sample due to Brownian motion of the particle in the solution. DLS is applicable in range from about 0.001 to several microns, which is difficult to achieve with other techniques. This is because the dimensions are too small for optical spectroscopy and too large for electron microscopy. A typical set-up for the scattering experiment consist of a laser beam illuminating a sample and a detector set up at scattering angle θ measuring the intensity $I(\theta,t)$ of the scattered light. Typically, the incident and scattered beams are shaped by apertures, slits, or by optics such as lenses. Usually, the incident beam is vertically polarized as the

detector moves in a horizontal plane and by this is "catching" the strongest signal. The region of the sample which is illuminated by both incident and outgoing beam, and "seen" by the detector is the "scattering volume". From the collected data the diffusion coefficient of the particle in the sample can be determined, and this can be related to the hydrodynamic radius (R_H) of the particle by the Stokes-Einstein equation:

$$R_H = \frac{k_\beta T}{6\pi\eta D} \qquad \textbf{Eq. (14)}$$

where: k_β is the Boltzmann constant,

T is the temperature in degrees Kelvin,

η is the viscosity of the solution in which particle is diffusing

D is diffusion coefficient [150].

Dynamic light scattering for size characterizations of the samples was performed by Malvern Instruments Zetasizer Nano-ZS instrument (Malvern, Worcs. UK) equipped with a 4mW He–Ne laser (633 nm) operating at 90°angle.

2.8 CRYO-ELECTRON MICROSCOPY

Cryo-electron microscopy (cryo-EM) is a form of transmission electron microscopy where the sample is studied at cryogenic temperature (generally liquid nitrogen temperature). Cryo-EM is developing popularity in structural biology since it allows the observation of specimen that have not been stained or fixed in any way, showing them in their native environment. In this technique, the samples are embedded in amorphous ice and images of fully hydrated macromolecules can be obtained (“frozen-hydrated”). The vitrification process enables the structure of macromolecules to be studied in a frozen-hydrated form near their native state. The method involves ultra-rapid cooling of small samples preventing ice crystal to form or to grow sufficiently large to damage the specimen’s structure. Then, a beam of voltage-accelerated electrons is transmitted in vacuum through an ultra thin specimen, interacting with the specimen as it passes through. An image is formed from the

interaction of the electron transmitted through the specimen; the image is magnified and focused by means of magnetic lenses onto an imaging device, such as a charge-coupled device camera [151].

2.9 PROTOCOLS

2.9.1 SYNTHESIS OF DEXTRAN DERIVATES WITH CHOLESTEROL MOIETY

Synthesis of cholesterol-modified dextran (D_{Ch}) is a two step process. In the first step **cholesterol 3-hemisuccinyl chloride was synthetized** (cholesterol + linker, Figure 20**):** Succinic anhydride (2g) was added to solution of cholesterol (2 g) in 50 ml of pyridine. The mixture was stirred for 3 hours at 70 °C. The crude product was dissolved in a minimum amount of H_2O/ethanol (1:10, v/v), and cholesterol 3-hemisuccinate was crystallized from H_2O/methanol (1:10, v/v), then recrystallized from ethanol.

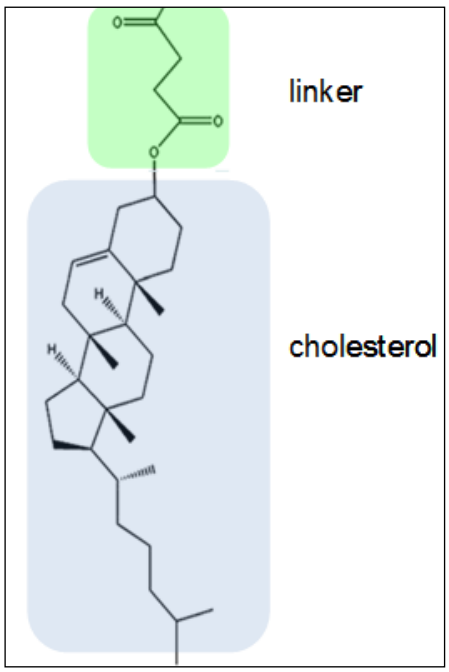

Figure 20: Scheme of cholesterol moiety (cholesterol + linker)

Cholesterol 3-hemisuccinate (2 g) was dissolved in 50 ml anhydrous chloroform, and an excess of $SOCl_2$ (10-fold) in 20 ml anhydrous chloroform was added drop wise under nitrogen protecting. The reaction mixture was stirred vigorously at 30 °C for 14 h,

then the solution was evaporated under vacuum to remove solvent and the remained $SOCl_2$, the residue was used to further steps as a solution in anhydrous chloroform airproofly.

In the second step **cholesterol-modified dextran was synthetised** (dextran + linker + cholesterol, Figure 21): Dextran (T_1 with MW 1000, 100 mg) and 0,1 ml dried triethylamine was dissolved in 10 ml anhydrous DMSO. After the mixture was heated up to 50°C, different amount of Chol-succ-COCl in 5 ml $CHCl_3$ was added drop wise. The reaction was performed for 18 h under argon protecting atmosphere.

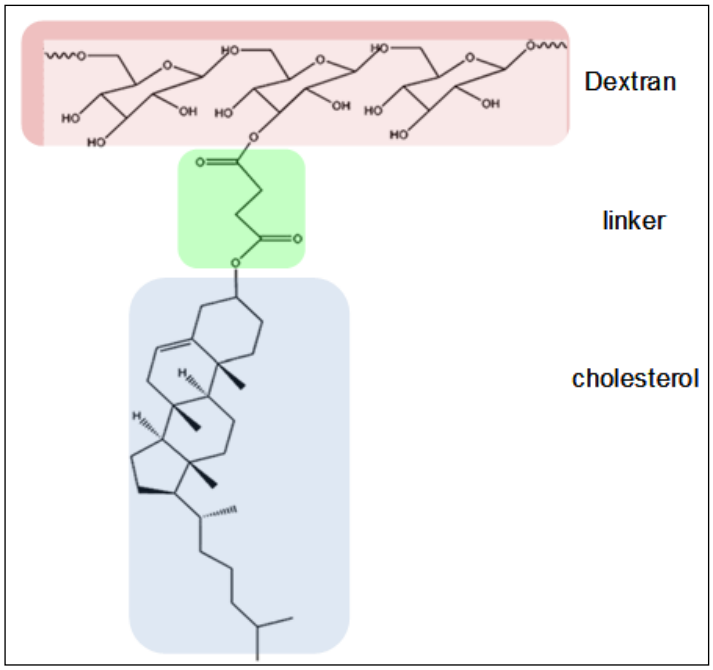

Figure 21: Scheme of dextran derivate with cholesterol moiety

Then D_{Ch} was obtained by dialysis against ultrapure water for 2 days using a permeable membrane with molecular weight cut-off below 1000 Da and subsequently lyophilized. The structure of D_{Ch} was confirmed by ^1H NMR (DMSO-d6, Varian Gemini 300 NMR spectrometer). The substituted degree determined from ^1H NMR spectrum and defined as percent content of cholesterol per glucopyranosidic units, was controlled by varying the amount of cholesterol 3-hemisuccinyl chloride, and the mole ratio of glucopyranosidic units of dextran to cholesterol are listed in

Table 3. Three different substituted degree of D_{Ch} were synthesized.

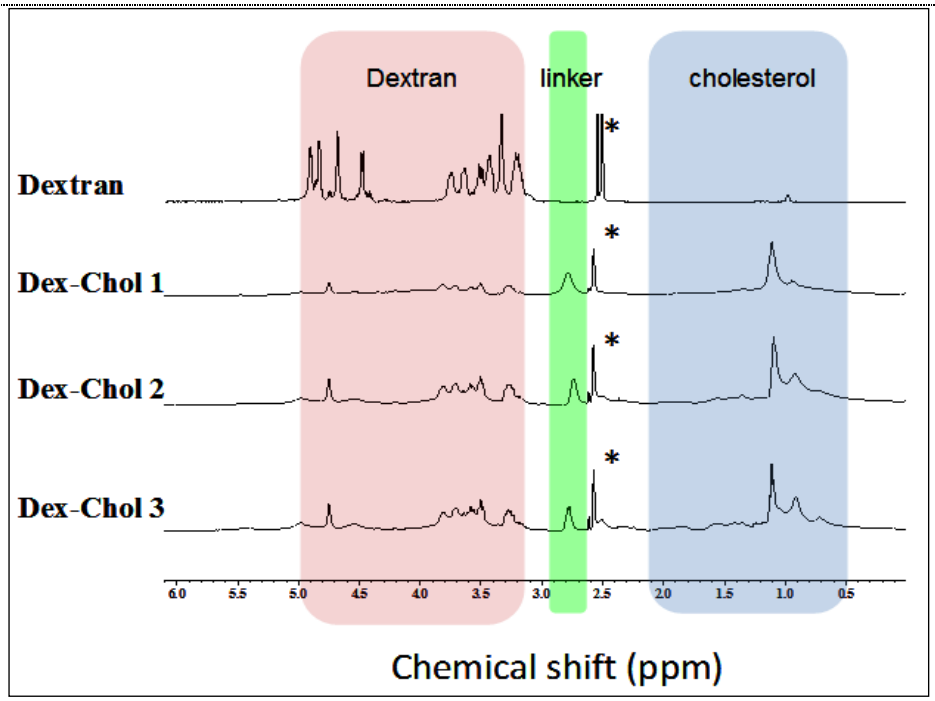

Figure 22: ^{1}H NMR spectra of dextran and different type of modified dextrans

(* solvent)

	% content of cholesterol pred glucopyranosidic units	**number of cholesterol per glucopyranosidic units**
D_{Ch} 1	18,3%	1
D_{Ch} 2	21,5%	mixture 1 and 3
D_{Ch} 3	29,5%	2-2,5

Table 3: Percent and number content of cholesterol per gluocopyranosidic units

All three D_{ch} were used for the redistribution of Hyp from [LDL-Hyp]/D_{ch} complexes (Chapter 3.2). D_{Ch} 3 (Figure 23) was the most effective and because of this it was used for all the other experiments (characterization of interaction of D_{Ch} with LDL and sLNP).

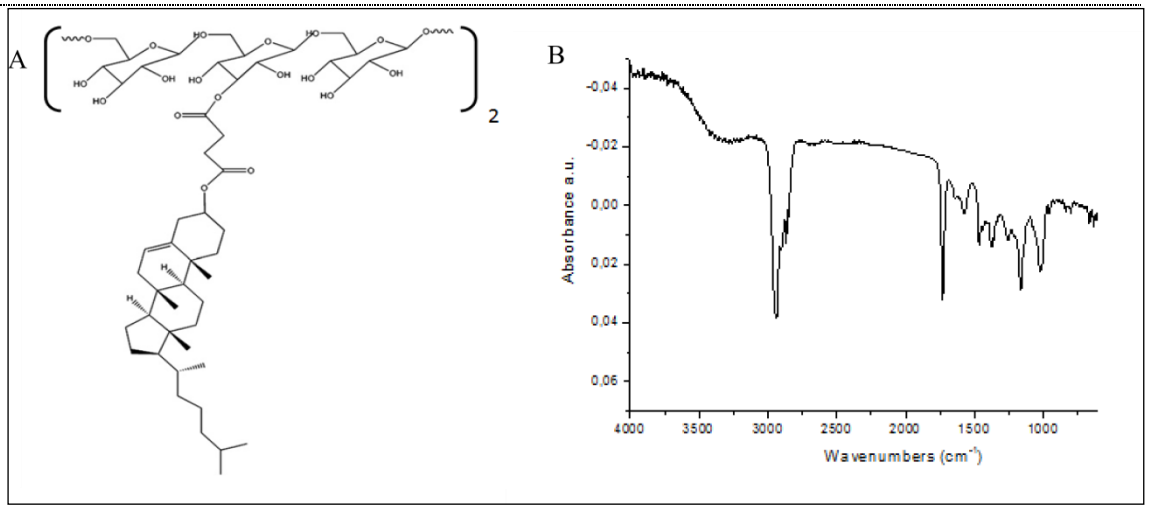

Figure 23: A-Chemical structure of cholesterol-modified dextran-D_{Ch} 3 from GPC measurement, B-FT IR spectra of D_{Ch} 3

2.9.2 PREPARATION OF HDL-HYP AND LDL-HYP COMPLEXES

The stock solution of Hyp was prepared by dissolving Hyp in 100% DMSO. Molar concentration was determined by absorption spectra using Lamber-Beer law and extinction coefficient for Hyp 44 000 cm^{-1} M^{-1} for λ =600 nm. Hyp in DMSO was kept in the dark at 4°C. A stock solution of HDL and LDL was prepared in 150 mM NaCl at pH=7,4 in the presence of 0,1% EDTA. The HDL-Hyp or LDL-Hyp complexes used in experiments were obtained by mixing of appropriate volumes of HDL/LDL and Hyp stock solutions in PBS at pH=7,4. The final quantity of DMSO in all HDL-Hyp and LDL/Hyp solutions was under 0,5%. As revealed by UV-Vis absorption and fluorescence spectroscopy, HDL-Hyp or LDL-Hyp complexes are stable in PBS (pH=7.4) at room temperature (23°C) for several days (5 days in this case).

2.9.3 PREPARATION OF [LDL-HYP]/DEXTRAN COMPLEXES

Unmodified dextran T_1 or D_{Ch} were used for preparation of LDL-Hyp complexes with dextran. Dextran powder T_1 was dissolved in PBS and D_{Ch} in 100% DMSO. Such prepared dextrans were carefully (100 µl by 100 µl) added to LDL-Hyp

complex and solution was gently mixed. Prepared complex was stabilized for 1 hour at the room temperature.

2.9.4 PREPARATION OF LUV, LUV WITH CHOLESTEROL AND LUV STAINED WITH RHODAMINE B

Large unilamellar vesicles (LUV) were prepared as followed: stock solution of DOPC with concentration $5x10^{-2}$M was prepared by dissolving DOPC in chloroform and methanol (1:1m v/v). 100 µl of DOPC was added to the round bottom glass tube and the solution was evaporated under the stream of N_2 forming a thin film of lipids visible at the bottom of the glass tube. 1 ml of PBS was added (making the final concentration of lipids = $5x10^{-3}$ M) to the lipid film, then the solution was vortexed for 1 minute at the highest settings. The emulsion was then extruded using Avanti Polar Lipids extruder with 100 nm filter. The particles were extruded 8-10 times each.

The LUV with cholesterol (LUV-Chol) were prepared the same way as LUV without cholesterol. Three different ratios of LUV-Chol were prepared (8:2, 7:3 and 5:5). The cholesterol powder was dissolved in chloroform (with [cholesterol] = $5x10^{-2}$M) and then according to the ratio of LUV-Chol 80 µl of DOPC and 20 µl of Chol, or 70 µl of DOPC and 30 µl of Chol, or 50 µl of DOPC and 50 µl of cholesterolwere added to the glass bottom tube. All the other preparation of the LUV-Chol was the same as preparation of the SUV without cholesterol.

The preparation of LUV stained with Rhodamine B (LUV-Rhod B) consisted of 1% of DOPE-Rhod B which was introduced with DOPC ([DOPC]= 10^{-3}M). Organic solvent was added to the DOPC and DOPE-Rhod B solutions (chloroform:ethanol = 3:5, v/v). Thin film was obtained by evaporation of 100 µl of the solution. All the other steps were the same as at the preparation of the pure LUV.

2.9.5 PRODUCTION OF SYNTHETIC LDL

Egg yolk phosphatidyl choline (PC) = 11,25 mg, triolein (TO) = 8,73 mg, and cholesteryl oleate (CO) = 3,17 mg were combined in a 3:2:1 molar mixture: in

chloroform and methanol (1:1, v/v) in the volume of 1ml. The solvent was evaporated under the stream of N_2. Tris-saline buffer (6 ml, 20 mM, pH 7,2) was used to reconstitute the lipids, and the solution was then vortexed for 1 min on the high setting. Butylated hydroxytoulene (20 µM) was added to the solution to protect against oxidation during the processing of the particles. The solution was sonificated for 1 hour on ice, under nitrogen, to break up larger lipid complexes. The particles were spun for 20 min at 4000 rpm to remove particulates. The emulsions were then extruded using Avanti Polar Lipids extruder to form smaller particles at 55°C. The particles extruded 4 times each first through a 200 nm, 100 nm filter and then through a 50 nm filter. The final emulsion was filter sterilized using a 0,22 µm filter. Emulsion was combined with the synthetic peptide at 2,15 µMm 10^{-3} M). The mixture was lightly vortexed for 1 min. The solution was allowed to stand at room temperature for 30 min before the start of dialysis to facilitate the binding of peptide to lipid emulsion. Unbound peptide was removed by two days of dialysis against Tris- saline buffer at 4°C with two changes. Ultracentifugation was utilized to separate lipid particles by density in a Beckman Ultracentrifuge using a TL100.2 rotor. Samples were adjusted to d = 1,063 g/ml by addition of sodium bromide and spun for 24 hrs at 40000 rpm (4°C) in 1 ml tubes. At the conclusion of the spin, the top 167 µl of sample (d<1,063 g/ml fraction) was collected by aspiration. An additional 167 µl was collected by aspiration and discarded. Samples were adjusted to d = 1,21 g/ml by addition of 334 µl of sodium bromide solution (d = 1,4744 g/ml) and spun for 48 hrs at 40000 rpm (4°C) in 1 ml tubes. At the conclusion of this spin, the top 167 µl of the sample (d = 1,063 – 1,21 g/ml fraction) was collected by aspiration. An additional 167 µl was collected by aspiration and discarded. The remaining infranatant was retained. All three fractions (d<1,063 g/ml, d = 1,064-1,21 g/ml, d>1,21 g/ml) were dialyzed against Tris-saline buffer with two buffer changes.

Protein concentration of the sLDL was determined according to the Modified Lowry protein kit protocol.

2.9.5.1 Synthesis of synthetic lipid-based nano-particles

sLNP were synthesized similarly to sLDL skipping adding the synthetic peptide and ultracentrifugation process.

2.9.5.2 sLNP stained with DiO_{18}

The green fluorescent lipophilic carbocyanine $DiOC_{18}(3)$ is widely used as a lipophilic tracer. It is weakly fluorescent in water but highly fluorescent and quite photostable when incorporated into membranes. It has an extremely high extinction coefficient and short excited-state lifetimes (~1 ns) in lipid environments. Once applied to cells, the dye diffuses laterally within the plasma membrane [152]. Stock solution of DiO_{18} was prepared in acetone with final concentration of 10^{-3}M. For sLNP staining, 0,1% of DiO_{18} was added to the mixture of PC:TO:CO = 3:2:1 in chloroform:methanol before evaporation under the stream of N_2. Next steps in the preparation of $DiOC_{18}(3)$ stained sLNP were the same as those previously described for synthesis of sLNP.

2.9.6 CELL CULTURE AND HYP PHOTOACTIVATION

U-87 MG human glioma cells (Cell Lines Services, Germany) were routinely maintained in Dulbecco's modified Eagle medium (D-MEM) containing L-glutamine (862 $mg.l^{-1}$), sodium pyruvate (110 $mg.l^{-1}$), glucose (4500 $mg.l^{-1}$), streptomycin (50 $\mu g.ml^{-1}$), penicilin (50 $\mu g.ml^{-1}$) and supplemented with 10% FBS or serum substitute 2% Ultroser G, in the presence of 5% CO_2 humidified atmosphere at 37°C.

Cells were incubated for 1 hour in dark condition in culture medium containing 2% Ultroser G and Hyp. The final concentration of Hyp was either 100 nM or 500 nM. For all experiments final content of DMSO was less than 0,1%. After incubation with Hyp, medium was removed and normal D-MEM containing 10% FBS was added. Cells were irradiated by monochromatic homemade diode illuminator at 590 nm wavelength

and light dose of 4 $J.cm^{-2}$. Cellular response was observed 0, 5 and 24 hours after irradiation.

2.9.7 SI-RNA TRANSFECTION PROTOCOL

Cells were seeded onto 35 mm culture dishes (Corning, USA) at density of $2x10^5$ cells per well in 2 ml antibiotic free D-MEM supplemented with 10% FBS. Then they were incubated at 37°C in CO_2 incubator until they were 60-80% confluent. For each transfection, 5 µl of siRNA duplex (solution A) was diluted in 100 µl siRNA Transfection Medium and 5 µl of siRNA Transfection Reagent (solution B) was also diluted in 100 µl siRNA Transfection Medium. The siRNA duplex solution (solution A) was added to the Transfection Reagent solution (solution B) and mixture was incubated for 45 minutes at room temperature. Meanwhile, cells were once washed with 2 ml of siRNA Transfection Medium. After 45 minutes of mixture incubation 0,8 ml of siRNA Transfection Medium was added to each tube containing the siRNA Transfection Reagent mixture (Solution A + Solution B). Solution was mixed gently and was overlaid to the washed cells and incubated 5 hours in CO_2 incubator. 1 ml of DMEM containing 20% FBS and 2% of antibiotics was added to cells without removing the transfection mixture. Cells were incubated for an additional 18 hours and were treated according to PDT protocol. The effectiveness of transfection was assessed by confocal microscopy after indirect immunofluorescence staining of PKCα and subsequently verified by western blot analysis (all western bloth analysis were performed by M. Misuth). Control siRNA (FITC Conjugate)-A was used as a negative control to avoid false positive results according to manufacturer's recommendation.

2.9.8 IMMUNOCYTOCHEMISTRY PROTOCOL

Cells ($2x10^5$ cells) were seeded onto 35 mm culture dishes with integral No.0 glass cover slip bottoms (MatTek, USA). Cells were incubated with $5x10^{-6}$M CellROX® Green or Orange Reagent for 15 min, Hoechst 33258 for 30 min at room temperature, $4x10^{-7}$ M MitoTracker® Orange [182] and/or with $0.2x10^{-7}$ M ThiolTracker™ Violet

[183] for 10 min at 37°C. For followed indirect immunofluorescence staining the cells were washed three times with 0.2 % BSA/PBS and fixed with 3.7 % formaldehyde for 15 min. Fixed cells were permeabilized with 0.2 % Triton X - 100 for 5 min at room temperature and washed 3 times with 0.2 % BSA/PBS. Cells were incubated for 1 hour in PBS containing 1% BSA, 10% goat serum, 0.4 mM Mg^{2+} and 0.2 mM Ca^{2+} at 37 °C to block unspecific labeling. After 3 washes with 0.2 % BSA/PBS, cells were incubated with specific primary antibodies (Ab) (against PKCα, PKCδ, pBcl-2(Ser70)) overnight at 4°C. Then cells were washed out 3 times with 0.2 % BSA-PBS followed by 1 hour incubation with appropriate secondary Ab AlexaFluor488 or AlexaFluor546at 37°C and washed 3 times with 0.2 % BSA/PBS to remove unbound secondary Ab and were placed in 0.2 % BSA/PBS. Samples were measured by CSLM700 confocal microscope (Zeiss Germany) in using 488nm and 555nm excitations and 63x oil objective (NA=1.46). Fluorescence signals were analyzed by the Zen 2011 software (Zeiss, Germany). Co-localization analysis [75] of fluorescence images was performed by means of the ZEN 2011 image processing.

2.9.9 CO-LOCALIZATION ANALYSIS

Co-localization analysis was performed on fluorescence images obtained above using the ZEN 2011 image processing. Mander's coefficients, defined as follow, were used for co-localization analysis:

$$M = \sum(\mathrm{R_i}.\mathrm{G_i}) / \sqrt{\left[\sum R_i^2 \sum G_i^2\right]} \qquad \textbf{Eq. (15)}$$

$$M_1 = \sum(R_i \,.\, G_i) / \sum R_i^2 \qquad \textbf{Eq. (16)}$$

$$M_2 = \sum(R_i \,.\, G_i) / \sum G_i^2 \qquad \textbf{Eq. (17)}$$

where R_i and G_i are the signal intensity of the pixel number "i"obtained for the red and the green channel, respectively. M-values are thus ranging from 0 to 1. Absolute co-localization corresponds to M = 1. The M_1 correlation coefficient, displays how well the red pixels co-localize with some green ones, and the M_2 correlation coefficient

displays how well the green pixels co-localize with some red ones. Overlap coefficient does not depend on the relative strengths of each channel, but can be affected by the background signal [184].

2.9.10 FLOW CYTOMETRIC ANALYSIS OF APOPTOSIS/NECROSIS AND ROS PRODUCTION

2.9.10.1 Apoptosis/Necrosis analysis

In normal viable cells, phosphatidylserine (PS) is located on the cytoplasmic surface of the cell membrane. However, in the intermediate stages of apoptosis, PS is translocated from the inner to the outer leaflet of the membrane, exposing PS to the external cellular environment where it can be detected. Highly fluorescent annexin V-FITC conjugates provide quick and reliable detection methods for studying the externalization of phosphatidylserine. Propidium iodide (PI) is a red-fluorescent nuclear and chromosome counterstain. Since propidium iodide is not permeant to live cells, it is also commonly used to detect dead cells in a population. Staining protocol: Cells (approximately 0.5 x 10^6 cells per sample) were harvested by low-speed centrifugation, resuspended in 100 µl Annexin-binding buffer and incubated with 5 µl AnnexinV-FITC for 15 min at room temperature. After incubation, 400 µl of Annexin- binding buffer was added to each sample. 2 µl Propidium iodide (PI) was added to each sample just before measurements to distinguish the necrotic cells. 10000 cells were counted and analysis was performed using a MACSQuant®Analyzer (Miltenyi, GER). Fluorescence of AnnexinV-FITC was detected in B1 channel (525 ± 50nm), fluorescence of Hyp was detected in B2 channel (585 ± 40nm) and fluorescence of PI was detected in B3 channel (655-730nm). The data were analyzed by MACSQuantify™ Software.

2.9.10.2 Oxidative Stress Detection

Oxidative stress results from an imbalance between production of reactive oxygen species (ROS) and the ability of cells to scavenge them. ROS play an important

role in the progression of several diseases including inflammation, atherosclerosis, aging, and age-related degenerative disorders as well as in cell death processes. CellROX® Deep Red Reagent is a novel fluorogenic probe for measuring cellular oxidative stress in both live and fixed cell imaging, with absorption/emission maxima at ~644/665 nm. The cell-permeant dye is non-fluorescent while in a reduced state, and exhibits bright fluorescence upon oxidation by reactive oxygen species (ROS).

Staining protocol: cells were harvested by low-speed centrifugation and resuspended in PBS (approximately 0.5 x 10^6 cells pre sample) and 5.10^{-6}M CellROX® Deep Red was added. After 30 min incubation at room temperature samples were measured using a MACSQuant Analyzer. Flouorescence was excited with an Argon laser 488 nm and emission of CellROX® Deep Red was collected in B3 channnel (655nm-730nm). The data were analyzed by MACSQuantify™ Software.

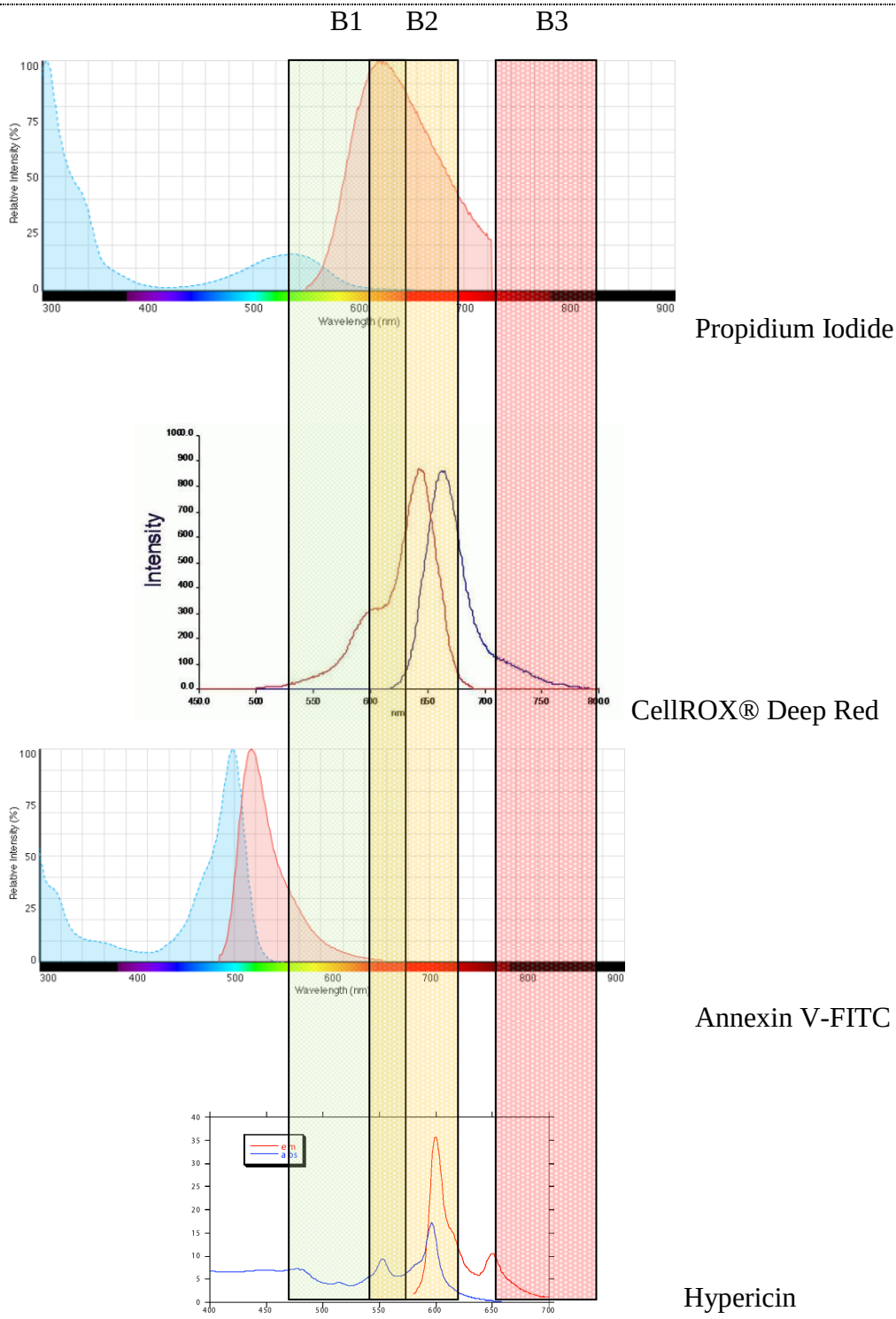

Figure 24: Overlap of the flow cytometry band pass filter of B1, B2 and B3 channels detection with the florescence spectra of PI, CellROX® Deep Red, Annexin V-FITC and Hyp

3 RESULTS AND DISCUSSION

STUDY CONCERNING LDL, HYP AND D_{CH}

3.1 OPTIMALIZATION OF THE PROTOCOL FOR PREPARATION [LDL-HYP]/D_{CH} COMPLEXES

It is crucial for all the experiments to prepare always the same complex [LDL-Hyp]/D_{Ch} which would give reproducible results. Three different approaches of preparation of [LDL-Hyp]/D_{Ch} complexes were done in order to find the best protocol for preparation.

3.1.1 PREPARATION OF COMPLEXES WITHOUT DMSO

As mentioned in Chapter 1.3.1, Hyp is hydrophobic molecule insoluble in nonpolar solvents and soluble in alkaline aqueous solutions, organic bases and polar organic substances including ethanol and DMSO and other solvents.

Complex [LDL-Hyp]/D_{Ch} was prepared without using DMSO. Hyp was solubilized in ethanol (ε = 37 000 $cm^{-1}.M^{-1}$, λ_{abs} = 591 nm, λ_{fl} = 594 nm) and D_{Ch} in propanol. Necessary volume of D_{Ch} was added to the glass round bottom flask and solution was evaporated under the stream of N_2. For rehydration of the dry D_{Ch}, 100 µl of PBS was added and the solution was let 2-3 hours at room temperature. The solution was then again evaporated using the stream of N_2. LDL in PBS was added for 1 hour incubation to the evaporated D_{Ch}. After 1 hour the solution was dialyzed for ~ 17 hours at 4°C. Hyp which was added to the round bottom flask and evaporated under the stream of N_2 was added to the dialyzed [LDL-D_{Ch}] for overnight incubation.

With such prepared complexes numerous experiments were performed. We came to conclusion that after adding of dialyzed [LDL-D_{Ch}] complex to the dried Hyp the whole amount of Hyp was not incorporated to [LDL-D_{Ch}] and some amount of Hyp stayed attached to the glass flask which caused that always different amount of Hyp was incorporated to [LDL-D_{Ch}] complex and the results were not reproducible. Figure 25

represents one of the attempts to monitore the steady state of Hyp inside LDL. According to our previous results with LDL and Hyp, with increasing concentration of Hyp in LDL the fluorescence intensity should increase after reaching the maximum and with additional increasing of Hyp the fluorescence intensity should decrease because of formation of non-fluorescent aggregates of Hyp inside LDL [131]. As it is shown in (Figure 25) the amount of Hyp was in each case different and the proper steady state curve was not obtained.

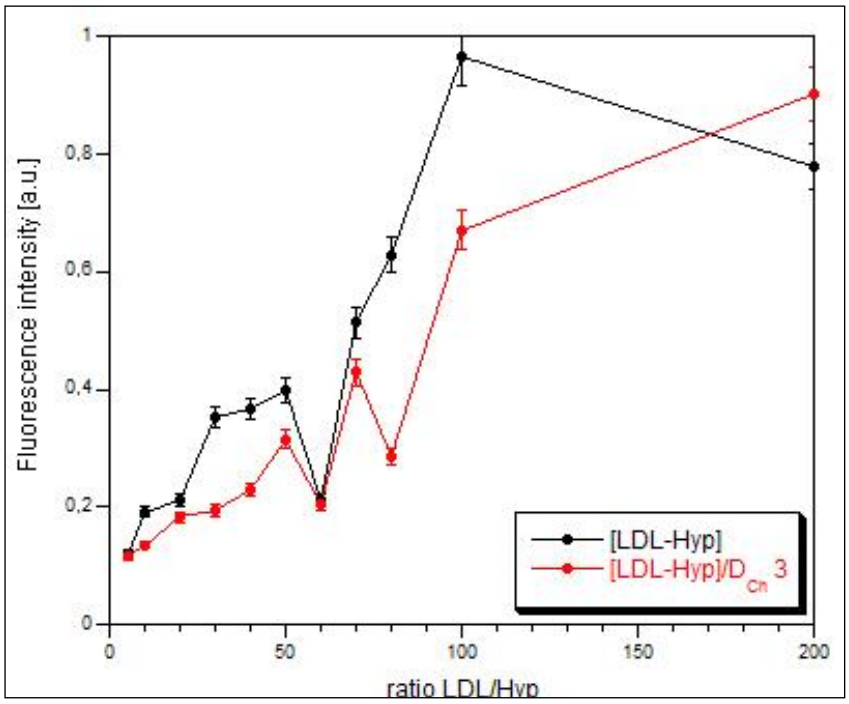

Figure 25: Dependance of the fluorescence intensity of Hyp in different [LDL-Hyp] and [LDL-Hyp]/ D_{Ch} ratios prepared without using DMSO

LDL was added to D_{Ch} dried under the stream of N_2 and solution was incubated for 1 hour following ~17 hours dialysis. Consequently, different amount of Hyp was added to [LDL-D_{Ch}] for overnight incubation.

The attempt for preparing the complexes without using DMSO was not successful resulting in irreproducible results.

3.1.2 PREPARATION OF COMPLEXES WITH DMSO

Because the attempt to exclude DMSO from the preparation process was not successful DMSO was used for solubilization of Hyp and D_{Ch}. The amount of DMSO in all experiments was not higher than 0,5%. Two different ways of preparation were tested:

First protocol:

[LDL-Hyp] was incubated overnight. The next day, D_{Ch} was added for 1 hour and fluorescence intensity was measured. Then the complex was dialyzed for ~ 17 hours at 4°C and fluorescence intensity was measured again and compared with the intensity measured before dialysis.

Figure 26 shows the comparison of fluorescence intensity of Hyp in complex [LDL-Hyp]/D_{Ch} before and after dialysis. The difference of intensity is due to the fact that during 17 hour dialysis Hyp went from LDL through the dialysis membrane to the PBS against which the complex was dialyzed. There is equilibrium between Hyp in LDL and Hyp in PBS. We came to conclusion that dialysis with Hyp cannot be performed when the complex was prepared.

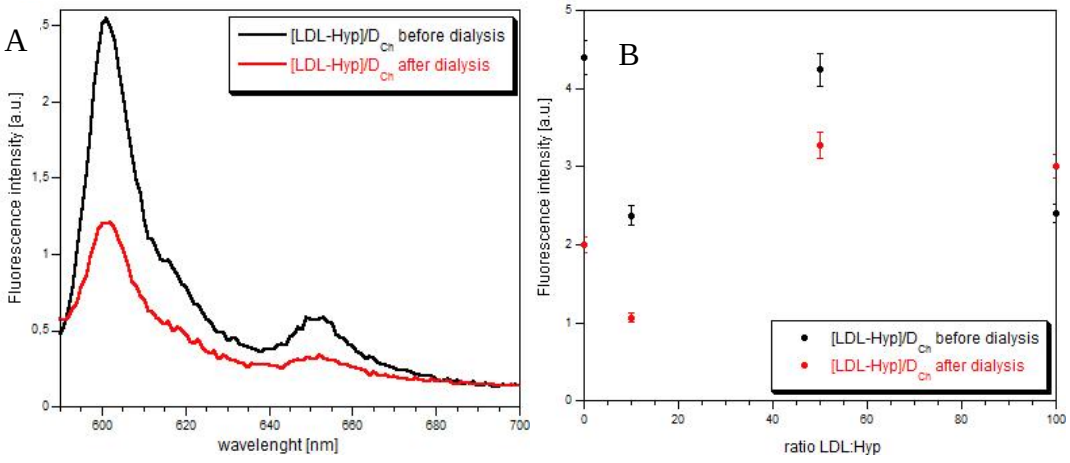

Figure 26: Fluorescence intensity of Hyp before and after dialysis of complex

A: Fluorescence spectrum of Hyp in [LDL-Hyp]/D_{Ch} complex before and after dialysis. **B:** Comparison of the fluorescence intensity of Hyp at the different ratios LDL:Hyp.

Second protocol:

[LDL-D_{Ch}] was incubated for 1 hour at the room temperature and dialyzed for ~ 17 hours at 4°C. After dialysis appropriate amount of Hyp was added to complex.

Numbers of experiments were done which showed that during dialysis there is dilution of the complex and the concentration of [LDL-D_{Ch}] was changed. After dialysis we were not able to find out the changed concentration of the complex and could not determine the final ratio of LDL-Hyp after adding Hyp to [LDL-D_{Ch}].

Third protocol:

The final protocol for preparation of the [LDL-Hyp]/D_{Ch} complexes includes mixing of LDL and Hyp, overnight incubation and adding D_{Ch} for additional 1 hour incubation. The exact method is described in the Chapter 2.9.3.

For future experiments we suggest that complexes should be prepared with ~ 17 hours dialysis of [LDL-D_{Ch}] followed by exact determinination of LDL concentration by protein kit. Appropriate amount of Hyp could then be added to the complex.

In order to find the best protocol for preparation of [LDL-Hyp]/D_{Ch} complexes, three different protocols were tried. Overnight incubation of LDL and Hyp followed by addition of little amounts (100µl) of D_{Ch} and additional 1 hour incubation was selected as the best protocol for complex preparation. Hence, preparation and purification of [LDL-Hyp]/D_{Ch} complexes needs further improvement.

3.2 EXAMINATION OF THREE SYNTHESIZED DEXTRANS

As mentioned in Chapter 2.9.1, three dextrans were synthesized with different cholesterol moiety. All three of them were used for the fluorescence measurements of the redistribution of Hyp to free LDL (Figure 27) and compared to the redistribution of Hyp from complexes that were not covered with D_{Ch}. After incubation of [LDL-Hyp] with D_{Ch}, free LDL was added to the complexes in order to reach the final ratio of three

Hyp per one LDL. At this ratio all molecules of Hyp are in fluorescent monomer form. After addition of free LDL to the [LDL-Hyp]/D_{Ch} complexes, increase of fluorescence intensity of Hyp was observed. This simulates the situation how our transport system would behave in the blood stream. Hyp would be redistributed to other plasma proteins (in our case to free LDL molecules). The redistribution is expressed with the increase of fluorescence intensity of Hyp because some molecules of Hyp which were incorporated in [LDL-Hyp] complex (where it formed aggregates) were relocated to free LDL. This relocation caused increased amount of Hyp in monomer form and consequently, the increase of fluorescence intensity of Hyp. As Figure 27 C, Table 4 shows, D_{Ch} 3 is the most efficient to slow down the Hyp redistribution process and was subsequently used for all further experiments.

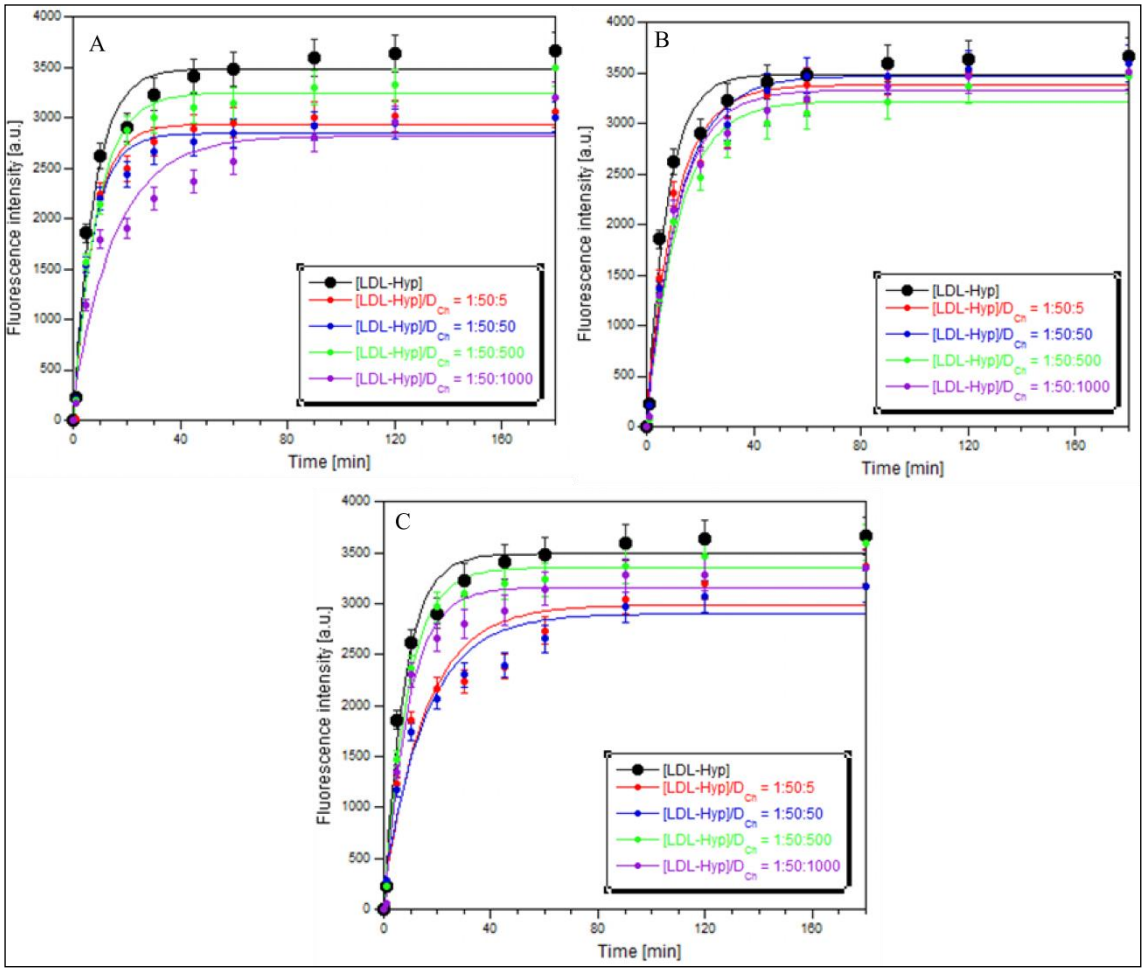

Figure 27: Redistribution of Hyp to free LDL from [LDL-Hyp] complexes covered by D_{Ch} 1 (A), D_{Ch} 2 (B) and D_{Ch} 3 (C) with different ratios of dextrans.

[Hyp] = 2 x 10^{-7}M; initial ratio of complexes were [LDL-Hyp] = 1:50 or [LDL-Hyp]/D_{Ch} = 1:50: different ratios of D_{Ch}, after adding free LDL to complexes final ratios of [LDL-Hyp] was 1:3.

	Efficiency of covering [%]		
ratio [LDL-dextran]	**D_{Ch} 1**	**D_{Ch} 2**	**D_{Ch} 3**
1:5	15,8	3	14,4
1:50	18,5	0,5	21,1
1:500	6,8	7,6	3,9
1:1000	19,2	12,8	12.9

Table 4: Efficiency of covering of dextrans with different cholesterol moiety

D_{Ch} 3 is the most efficient for limitation of Hyp redistribution process.

3.3 CHARACTERIZATION OF THE INTERACTION OF LDL-HYP WITH D_{CH} 3

We already have known that with the increasing concentration of Hyp inside LDL Hyp starts to form aggregates at the ratio ~ 50 molecules of Hyp per one molecule of LDL [131]. But how does Hyp behave in the presence of D_{Ch} 3? Figure 28 shows steady state curve-the fluorescence intensity of Hyp as a function of different [LDL-Hyp] and [LDL-Hyp]/D_{Ch} 3 ratios. It is important to notice that the presence of D_{Ch} 3 does not influence the Hyp aggreggation process inside LDL since for LDL-Hyp ratios > 50 aggregates are forms in both cases.

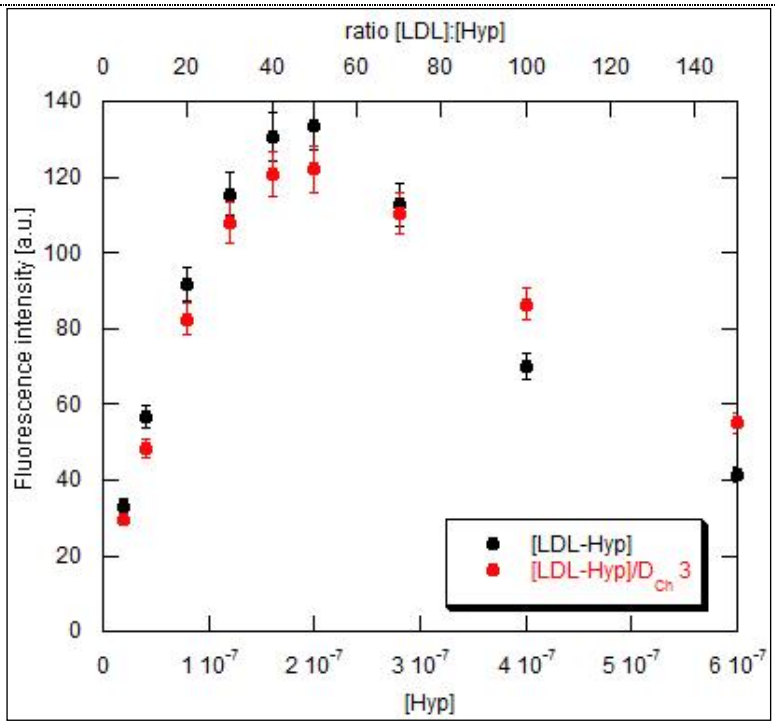

Figure 28: Steady state curve-dependance of the fluorescence intensity of Hyp in different LDL:Hyp ratios with and without D_{Ch} 3

[LDL] was constant = 4 x 10^{-9}M; different amount of Hyp was added to LDL and such prepared complexes were stabilized overnight.

However, the maximum fluorescence intensity is a little bit lower in the presence of D_{Ch} 3. This can be due to the fact, that when D_{Ch} 3 is present on the surface of LDL Hyp molecules might be slightly squeezed inside LDL which leads to a slight decrease of the Hyp fluorescence.

To find out the impact of D_{Ch} 3 on the size of LDL dynamic light scattering experiments were performed. Figure 29 shows DLS of LDL with all three dextrans at the ratio [LDL-D_{Ch}] = 1:75. The average size of LDL is ~ 22 nm. D_{Ch} slightly decreases the size of LDL. Table 5 summarizes the impact of the presence of the different D_{Ch} on the size of LDL. The size of LDL-D_{Ch} 3 was determined to be 17,22 nm.

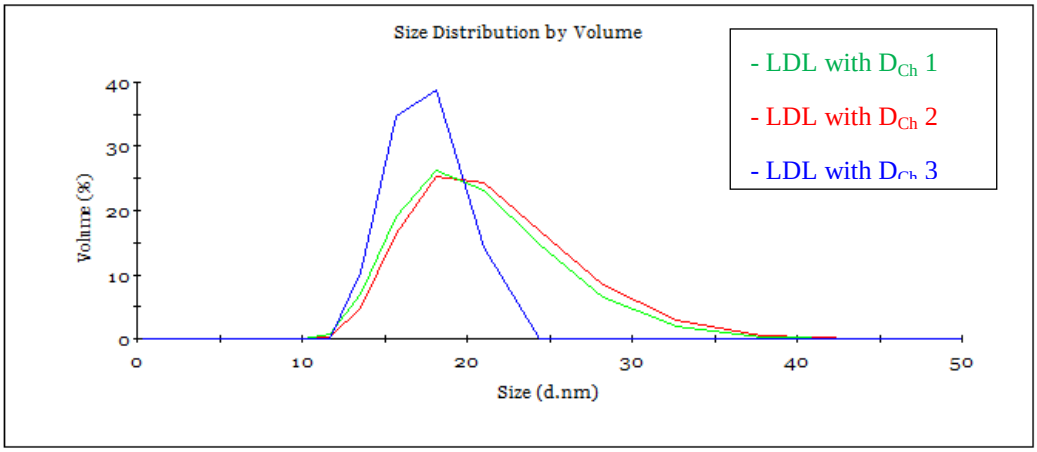

Figure 29: DLS of LDL with D_{Ch} 1, D_{Ch} 2 and D_{Ch} 3 at the ratio [LDL-D_{Ch} 3] = 1:75

([LDL]=10^{-8}M, [LDL was mixed with D_{Ch} and complexes were incubated for 1h at room temperature following by ~17 hour dialysis against PBS at 4°C)

	Size [nm]	Volume
LDL/D_{Ch}1	20,64	99,5%
	191,4	0,5%
LDL/ D_{Ch} 2	11,14	38,7%
	19,89	61,3%
LDL/ D_{Ch} 3	242,2	1,9%
	17,22	98,1 %

Table 5: The size of [LDL-D_{Ch} 1, D_{Ch} 2 and D_{Ch} 3] at the ratio 1:75

Thus, decrease of the maximum intensity of Hyp in [LDL-Hyp]/D_{Ch} 3 previously observed in Figure 28 appears to be related to this size reduction.

Actually, taking into account that DLS measurements have shown that the diameter of D_{Ch} 3 coated LDL were smaller when compared to non coated LDL, FRET process from Hyp monomer to its aggregated form inside LDL might explain such fluorescence decrease. However, as shown in Figure 30, such explanation should be discarded since the measured excited state lifetimes of Hyp are exactly the same for both samples.

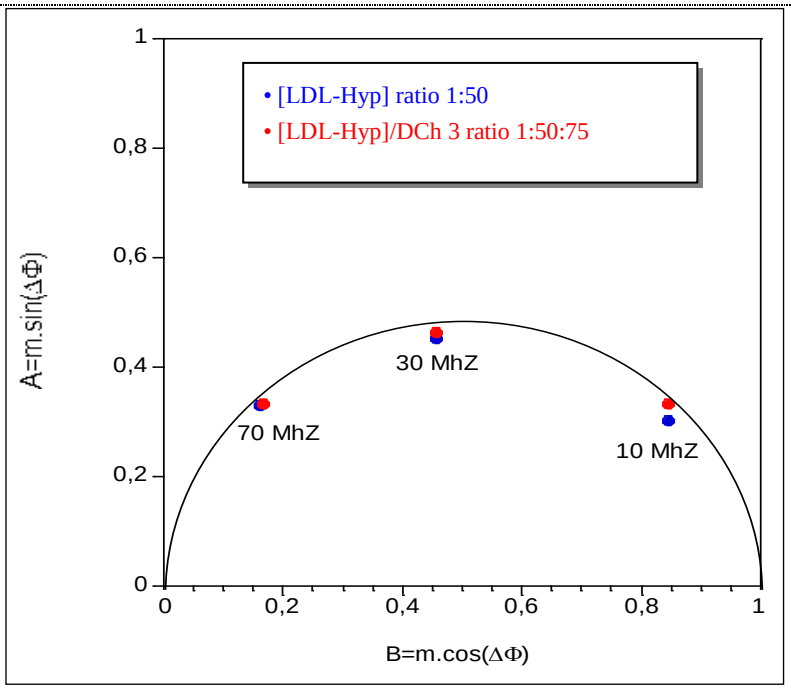

Figure 30: Fluorescence lifetime of complexes [LDL-Hyp] and [LDL-Hyp]/D_{Ch} 3 measured at different intensities

The average calculated lifetime for [LDL-Hyp] and [LDL-Hyp]/D_{Ch} 3 was 5,6 nsec. There are probably two population of Hyp in both samples: about 50% of the fluorescence intensity is characterized by a lifetime of about 8,1 nsec (it corresponds to the lifetime previously observed for Hyp monomer in LDL without any quenching by FRET [133]) and the other 50% of the intensity is characterized by a lifetime of about 3,9 to 4 nsec (it corresponds to some Hyp molecules that are partially quenched by homo-FRET (FRET from monomer toward aggregates). Anyhow, the situation is the same in both samples.

In another experiment, interaction of Hyp in the presence of D_{Ch} 3 was monitored (Figure 31). After adding Hyp to the solution of D_{Ch} 3 in PBS the fluorescence intensity can be observed. This fluorescence was slowly decreased in time after Hyp started to form aggregates inside D_{Ch}3. Thus the higher fluorescence intensity in the Figure 28 at the ratios above 100 Hyp per LDL can be due to the fact that Hyp which was not incorporated in LDL and was in solution was solubilized in D_{Ch} 3. Even though we found out that Hyp is slightly solubilized in D_{Ch} 3 its solubilization is

minimal and does not affect our purpose that is to decrease/reduce the redistribution process of Hyp towards other serum proteins.

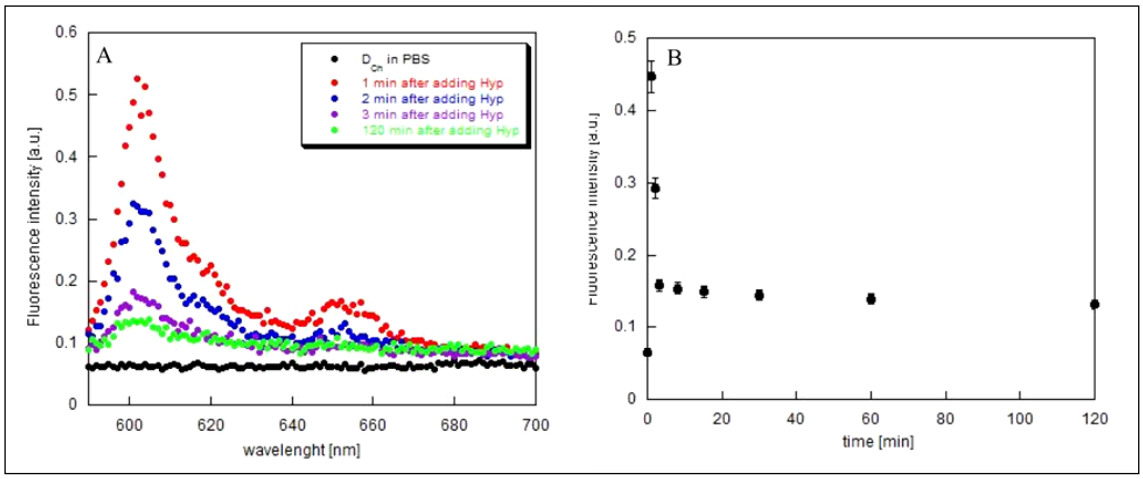

Figure 31: Solubilization of Hyp in D_{Ch} 3

A: Fluorescence intensity spectra of Hyp; **B:** the evolution of fluorescence in time.

The spectra were taken 0-120 min after adding of Hyp to solution of D_{Ch} 3 in PBS;

[Hyp] = $2x10^{-7}$M, [D_{Ch} 3] = $3x10^{-7}$M.

Thus, coating of LDL by D_{Ch} actually leads to some decrease of the amount of Hyp incorporated in LDL as the consequence of reduced available LDL phase volume (Figure 32).

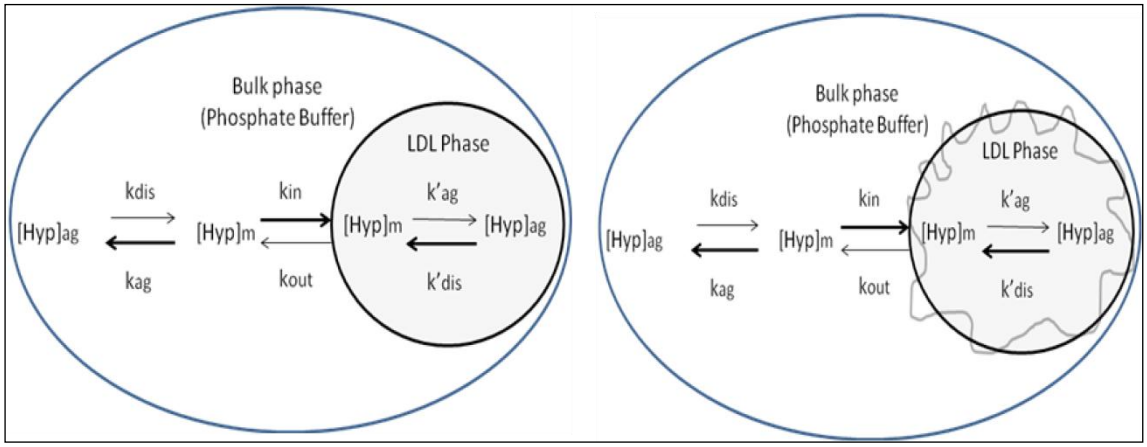

Figure 32: Scheme of two populations of Hyp in the solution without and in the presence of D_{Ch} 3

The presence of D_{Ch} 3 has no impact on the behavior of Hyp inside LDL and slightly reduces the size of LDL.

3.4 DETERMINATION OF THE BEST RATIO BETWEEN [LDL-HYP] COMPLEX AND D_{CH} 3

In order to find the best ratio that would decrease the redistribution process of Hyp the most effectively, fluorescence measurement of the redistribution of Hyp to free LDL from the complex [LDL-Hyp]/D_{Ch} 3 with different ratios of D_{Ch} 3 was performed. The initial ratio of [LDL-Hyp] was 1:50. After adding free LDL the final ratio was [LDL-Hyp] = 1:3. From all the ratios between LDL and D_{Ch} 3, at the ratio [LDL-D_{Ch} 3] = 1:75 the redistribution of Hyp was 27% slower than the redistribution of Hyp toward free LDL from [LDL-Hyp] complex not covered by D_{Ch} (Figure 33). Because of this result along with the result from DLS where at the presence of D_{Ch} 3 with the same ratio the size of LDL was decreased (Figure 29) we used D_{Ch} 3 at the ratio [LDL-D_{Ch} 3] = 1:75 in all the other experiments.

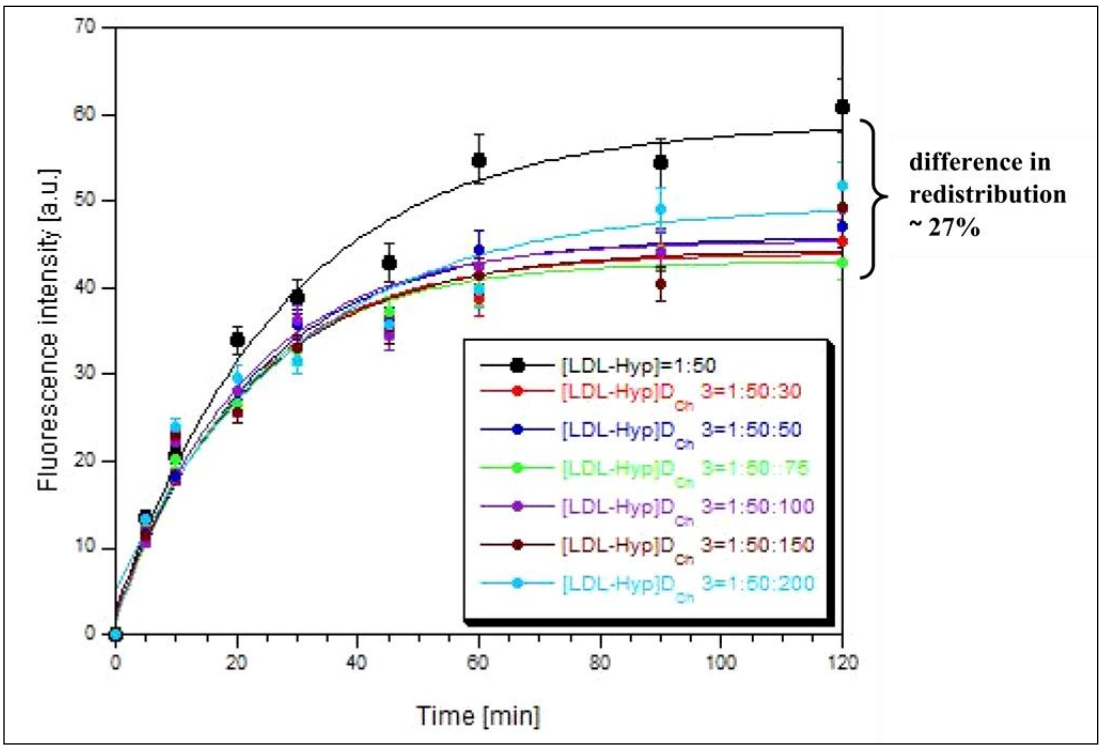

Figure 33: Redistribution of Hyp from complex [LDL-Hyp]/D_{Ch} 3

[Hyp] = $2x10^{-7}$M; initial ratio of complex[LDL-Hyp] was 1:50, after adding free LDL the ratio [LDL-Hyp] was 1:3.

As mentioned in Chapter 1.7.2, LDL particles are recognized by cells through the LDL-receptors on the surface of the cells. This receptor-mediated endocytosis is a general mechanism by which cells take up LDL particles [117]. It was already shown that presence of D_{Ch} 3 decreases/minimizes the redistribution process of Hyp to free LDL particles (Figure 33). However, the modification of the LDL surface could possibly modify and inhibit the recognition of LDL particles through LDLR. In order to find out if LDL molecules covered by D_{Ch} can enter glioma cells the monitoring of cellular uptake of Hyp by U87-MG cells was carried out. Figure 34 shows the uptake of Hyp by U-87 MG cells at 37°C and at 4 °C measured at the FACS MACSQuant®Analyzer where fluorescence of Hyp was detected in B2 channel (Band Pass Filter 585/40nm). The data were analyzed by MACSQuantify™ Software.

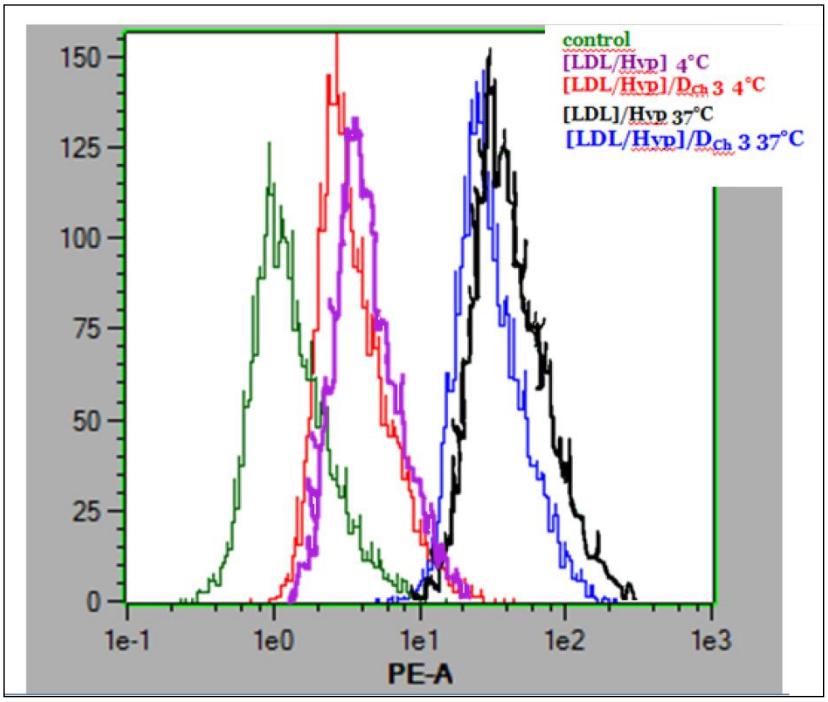

Figure 34: Flow cytometry fluorescence histogram of uptake of Hyp in U-87 MG cells observed at 4°C and at 37°C by flow cytometry.

Cells were incubated with [LDL-Hyp] or [LDL-Hyp]/D_{Ch} 3 for 1 hour either at 37 °C or 4 °C. 10000 cells were counted and fluorescence of Hyp was detected in B2 channel (Band Pass Filter 585 ± 40nm).

For 37°C the process of uptake of LDL by endocytosis is almost identical when D_{Ch} is or is not present. As control uptake of Hyp at 4°C is presented when the endocytosis process is almost completely blocked for both samples (uncoated and D_{Ch}

coated). Thus, D_{Ch} coating of LDL does not preclude the binding of ApoB moiety to the LDL specific receptors for cells.

In order to further study the interaction of [LDL-Hyp]/D_{Ch} 3 transport system with U87-MG cells, fluorescence imaging microscopy was made. [LDL-Hyp] complex with and without D_{Ch} 3 was added to the 10% FBS medium containing U-87 MG cells and was incubated for 1 hour. U-87 MG cells were first grown in 2% UG medium which does not contain any lipids. In this medium the proliferation of the LDLR in cells was increased [132]. It is known that upon administration into the bloodstream Hyp associates with serum proteins [153]. 10% FBS medium contains lipids and therefore after adding Hyp in LDL that was or was not covered by D_{Ch} 3 the redistribution process occurred.

[LDL-Hyp] [LDL-Hyp]/D_{Ch} 3

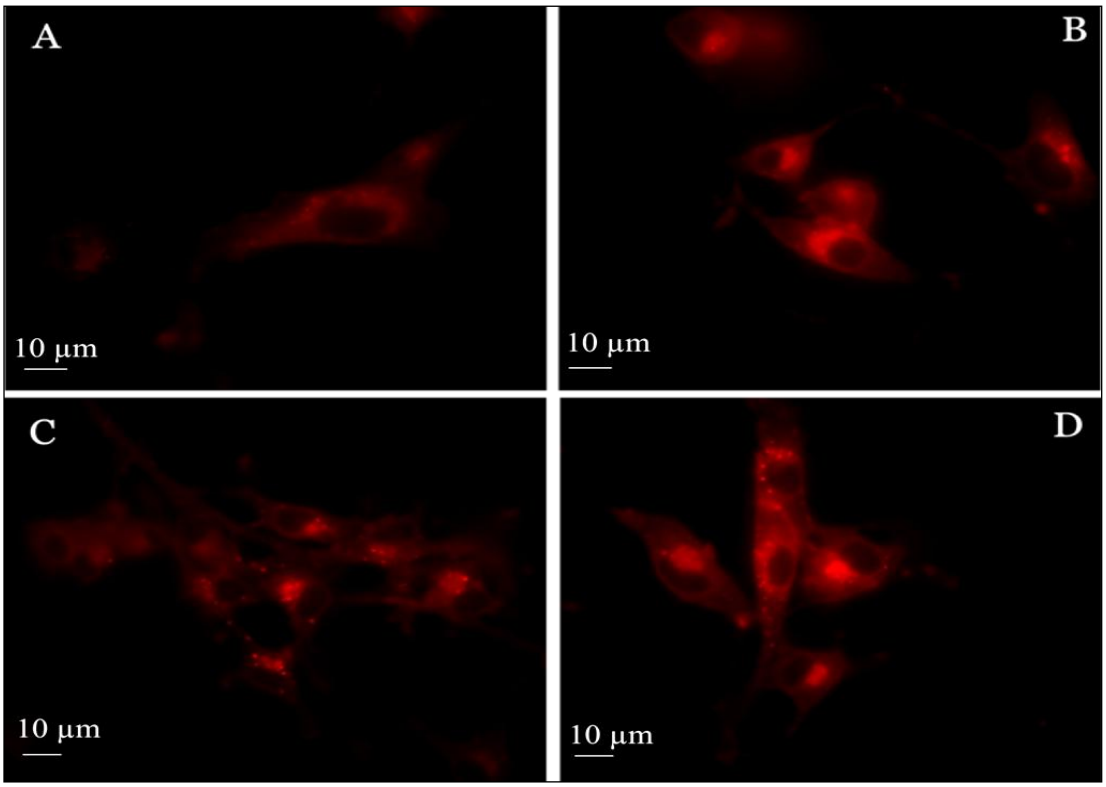

Figure 35: Fluorescence microscopy images of U-87 MG cells incubated with complex [LDL-Hyp] and [LDL-Hyp]/D_{Ch} 3 in 10% FBS

A: U-87 MG cells incubated in the presence of [LDL-Hyp] = 1:50 for 30 min

B: U-87 MG cells incubated in the presence of [LDL-Hyp]/D_{Ch} 3 = 1:50:75 for 30 min

C: U-87 MG cells incubated in the presence of [LDL-Hyp] = 1:50 for 60 min

D: U-87 MG cells incubated in the presence of [LDL-Hyp]/D_{Ch}3 = 1:50 for 60 min

Figure 35 shows fluorescence microscopy images of U-87 MG cells that were incubated for 30 min (A, B) and 60 min (C, D) in the presence of [LDL-Hyp] and [LDL-Hyp]/D_{Ch} 3 complexes. The fluorescence intensity of Hyp in cells that were incubated without presence of D_{Ch} 3 is lower than in cells incubated with D_{Ch} 3. The uptake of complex with D_{Ch} 3 and its subcellular distribution is different as well. 10% FBS containing lipids simulated blood stream in body where as it was already mentioned [122][134][153] Hyp is redistributed to free lipids. Cells incubated with [LDL-Hyp]/D_{Ch} 3 complex have higher fluorescence intensity which means that much less Hyp was redistributed to the cultivating medium containing 10% FBS resulting in the higher accumulation of Hyp inside cells.

In Huntosova et al. the interaction dynamics of Hyp with LDL and U87-MG cells was studied [133]. In this study lower cellular uptake of Hyp in the case of LDL-Hyp compex = 1:20 in comparison with the LDL-Hyp = 1:200 was observed. Hyp can be released from overloaded LDL particles and be incorporated as monomers into cellular membrane. Because of this fact, cells were incubated with [LDL-Hyp] or [LDL-Hyp]/ D_{Ch} 3 for 30 min in 2% UG so no lipids were present in the medium. The ratio between [LDL-Hyp] and [LDL-Hyp]/ D_{Ch} 3 was the same (1:50). Cellular uptake of Hyp and release of Hyp from loaded LDL (covered or uncovered with D_{Ch} 3) was studied.

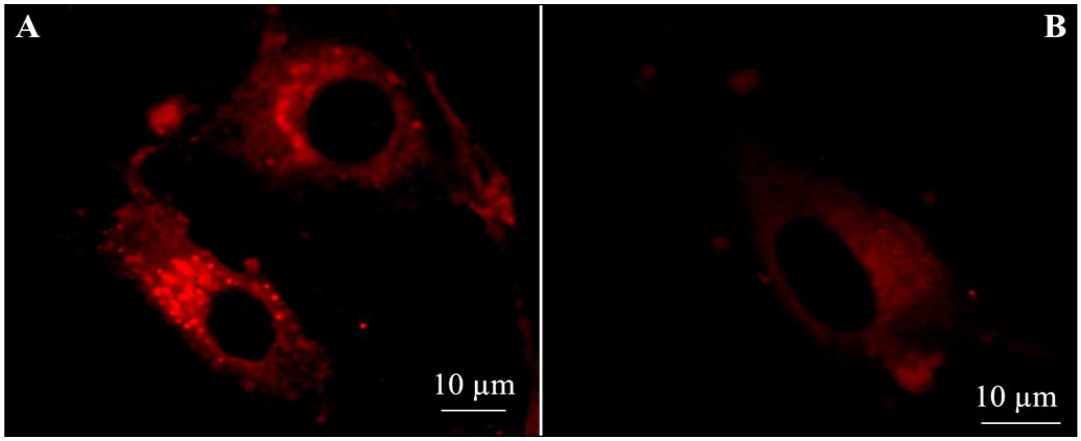

Figure 36: Confocal fluorescence microscopy images of U-87 MG cells incubated with complex [LDL-Hyp] and [LDL-Hyp]/D_{Ch} 3 in 2% UG

A: U-87 MG cells incubated in the presence of [LDL-Hyp] = 1:50 for 30 min

B: U-87 MG cells incubated in the presence of [LDL-Hyp]/D_{Ch} 3 = 1:50:75 for 30 min

Figure 36 shows confocal fluorescence microscopy images of cells incubated with [LDL-Hyp] (A) and [LDL-Hyp]/ D_{Ch} 3 (B) in 2% UG. Fluorescence intensity of Hyp in the cells incubated without D_{Ch} 3 is higher when compared to cells with D_{Ch} 3. This means that more Hyp was released from LDL particles compared to Hyp loaded in LDL covered by D_{Ch} 3. The ability of Hyp to release itself from overloaded LDL and enter cells through diffusion was in the case of [LDL-Hyp]/ D_{Ch} 3 pushed down. This is another result showing the ability of D_{Ch} 3 to protect Hyp from redistribution process and to keep more Hyp inside LDL.

Optimal D_{Ch} 3 coating of LDL allows reaching 27% reduction of Hyp redistribution. It does not preclude interaction with cellular membrane LDL receptors and leads to an increase of the Hyp cellular uptake.

SYNTHETIC LDL

3.5 SYNTHESIS OF SYNTHETIC LDL/sLNP

As it was already described in Chapter 1.7.2.1, LDL are ideal for the delivery of cancer drug and imaging agents since they are able to circulate in the blood stream for a significant amount of time, the hydrophobic core facilitates the incorporation of poorly soluble drugs or imaging agents, and they are highly amenable to bioconjugation [135].

Despite all of this advantages of LDL as carrier for hydrophobic drugs, it is less than ideal as targeting agent since it is difficult to isolate LDL in large quantities. Also, each LDL is variable in composition and size. Another approach used reconstituted LDL consisting of a lipid emulsion containing drugs stabilized by purified ApoB [136]. The ApoB protein, however, is difficult to isolate due to its large size and propensity to aggregate and is therefore not useful for generation of large batches of reconstituted LDL.

A part of my study was to construct synthetic nano-particles with the most possible similarity in composition and properties to natural LDL. We decided to prepare synthetic LDL (sLDL) according to the way Nikanjam et al. have prepared [137]. sLDL particles were constructed by combining a synthetic peptide containing a lipid binding motif and the LDL receptor binding domain of ApoB-100 with a lipid emulsion of phosphatidyl choline, triolein and cholesteryl oleate in a molar ratio 3:2:1. The exact preparation is described in the Chapter 2.9.5. Modified Lowry kit was used for defining the peptide concentration of prepared sLDL particles. In general, the concentration was ~ 10^{-4}M. The size of sLDL was determined by DLS to be 89 nm (Figure 37).

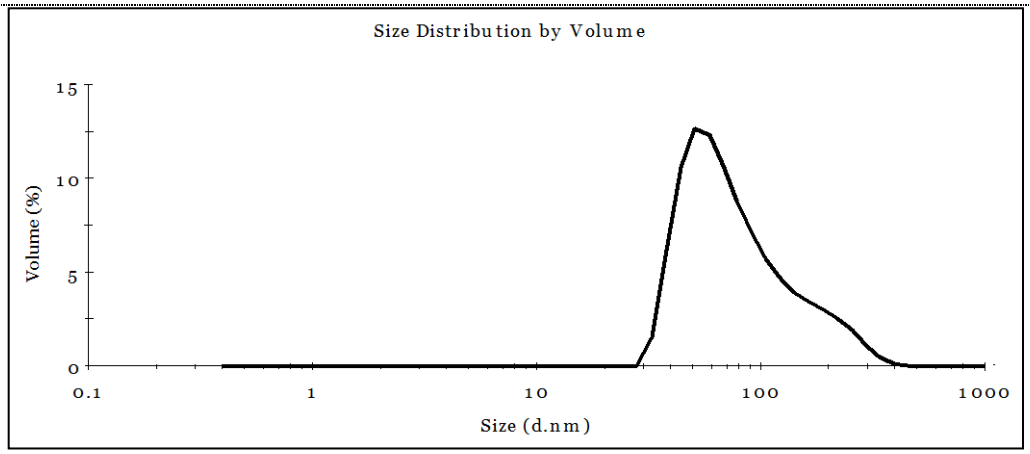

Figure 37: DLS of sLDL

([sLDL] = 10^{-8}M in PBS)

In order to find out if D_{Ch} 3 decreases the size of such prepared sLDL particles as the size of LDL decreases in the presence of D_{Ch} 3 was studied by DLS. The changes in the sizes according to the ratio of [sLDL- D_{Ch} 3] are summarized in Table 6. The ratio 1:1 decreased the size of sLDL from 89 nm to 68,43 nm.

[sLDL-D_{Ch} 3] ratio	**size [nm]**
1:1	68,43
1:3	114,2
1:5	129,7
1:8	126,9
1:10	82,4
1:15	89,5
1:50	128,6
1:100	157,96
1:500	122,5
1:1000	148,5

Table 6: Size of sLDL particles with different [sLDL- D_{Ch} 3] ratios

After studying the interaction of D_{Ch} 3 with sLDL we wanted to define the steady state curve of Hyp in sLDL. We supposed that Hyp would behave inside sLDL

similarly as it does in LDL (Figure 28)-when in excess of sLDL, Hyp would be in monomer form and with increasing concentration of Hyp it would start to form aggregates and the fluorescence intensity would slowly decrease. Different amount of Hyp was mixed with sLDL and the fluorescence intensity was measured (Figure 38).

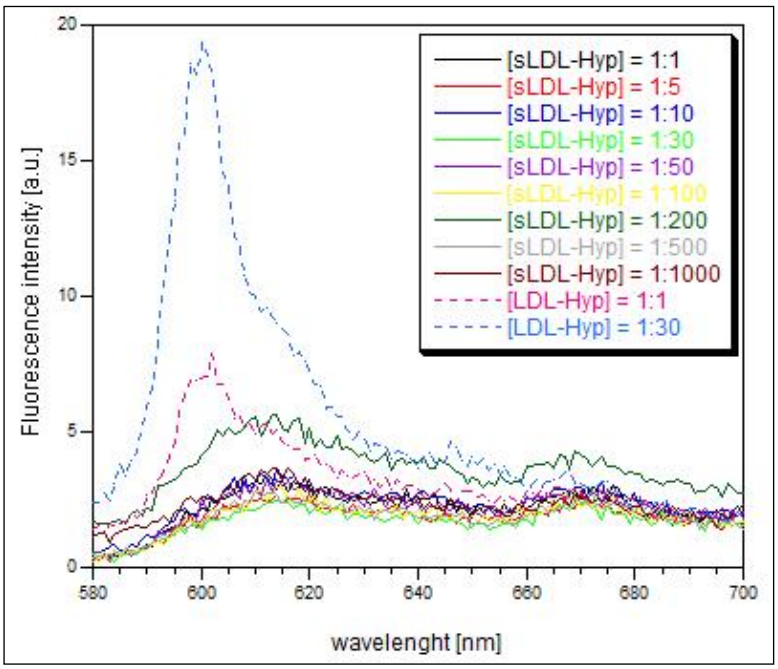

Figure 38: Fluorescence intensity of Hyp in different ratios of [sLDL-Hyp] after 90 min of incubation

[sLDL] was constant and different amount of Hyp was added. Complexes were stabilized for ~12 hours and then fluorescence intensity of Hyp was measured.

We found out that even after 90 min of incubation of Hyp with sLDL in ratios from [sLDL-Hyp] = 1:1 to 1:1000, the fluorescence intensity did not significantly change. For comparison fluorescence intensity of Hyp in LDL in ratio [LDL-Hyp] = 1:1 and 1:30 was measured as well. We came to the conclusion that synthetic peptide which was used for the synthesis of sLDL and was responsible for forming the LDLR binding domain of ApoB-100 caused insolubility of Hyp inside sLDL so when Hyp was mixed with sLDL, Hyp did not enter sLDL and stayed in the solution.

We decided to eliminate synthetic peptide from the protocol of synthesis of sLDL. We are aware of the fact that sLDL particles would not enter cells through the receptor mediated pathway. This fact is not important because in the future plans the Department of Biophysics in Koisce is going to work with DARPins-designed ankyrin

repeat proteins which are genetically engineered antibody mimetic proteins typically exhibiting highly specific and high-affinity target protein binding. These DARPins will be attaches to the surface of sLDL and this way much higher targeting of the nanoparticles which will be loaded with photosensitizer to the desired cancer cells will be reached. For now, we assume that sLDL without the LDLR binding domain of ApoB-100 will enter cells through the endocytosis process. After several different tries of preparing sLDL where we compared the size and characterized the interaction of such prepared particles with Hyp, we came to the conclusion that ultracentrifugation is not necessary for the synthesis either and we skipped this step at the preparation of sLDL. Because there is a difference in the preparation of sLDL according to Nikanjam et al. (no synthetic peptide and centrifugation), name synthetic lipid-based nano-particles (sLNP) is more appropriate.

The size our sLNP was measured by DLS (Figure 39) and cryo-electron microscopy (Figure 40) and was the same as size of sLDL which were prepared according to the protocol by Nikanjam et al. It was determined to be 89 nm.

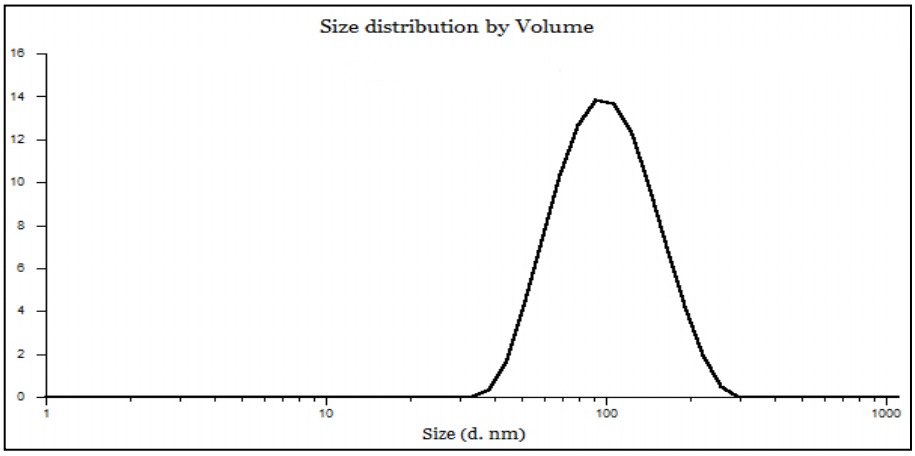

Figure 39: DLS of sLNP without synthetic peptide and ultracentrifugaion

([sLNP] = 10^{-8}M in PBS)

This result was supported by electron-cryo microscopy (Figure 40) and confirmed the size of sLNP particles to be ~ 90 nm in general. Figure 40 B shows cryo-electron microscopy image of LDL. sLNP are bigger than LDL and have different shape (round instead of spheroidical shape of LDL).

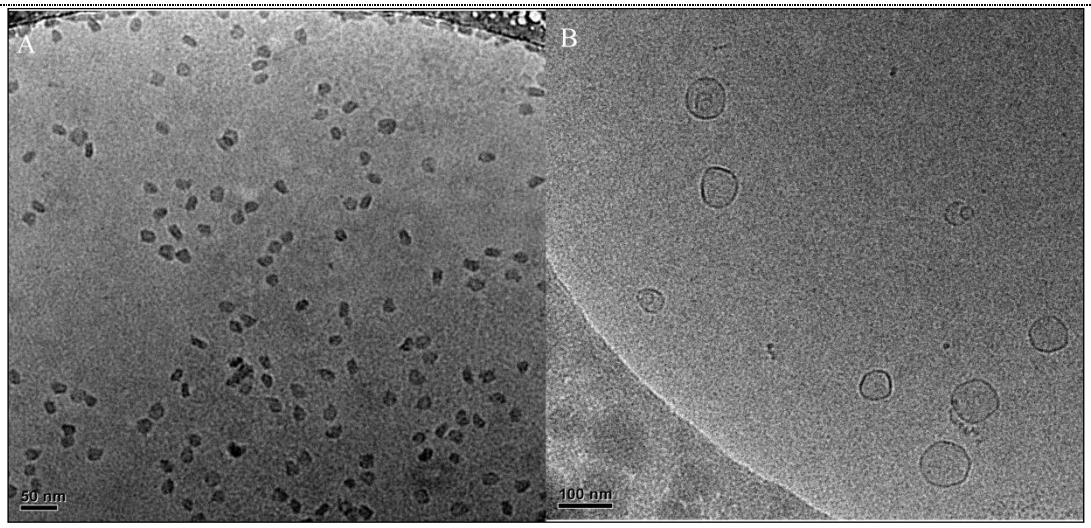

Figure 40: Cryo-electron microscopy of sLNP (A) and LDL (B)

[sLDL-Hyp] complex can not be obtained either because of the unknown problem in the preparation of sLDL or because the synthetic peptide preclude Hyp incorporation in sLDL.

3.6 CHARACTERIZATION OF INTERACTION OF sLNP PARTICLES WITH HYP

We were not able to define the ratio between sLNP and Hyp or sLNP and D_{Ch} 3 anymore since we eliminated synthetic peptide and were not able to determine protein concentration of sLNP. We wanted to know the cholesterol content in sLNP. It was defined through cholesterol kit and was generally ~ 0,58 µg/µl.

To confirm the theory that synthetic peptide was responsible for Hyp insolubility in the presence of sLDL particles, the interaction of Hyp into sLNP was studied. Different concentrations of Hyp were mixed with sLNP and incorporation of Hyp into sLNP was measured in time (Figure 41). As it can be seen on this figure, Hyp is able to incorporate to sLNP.

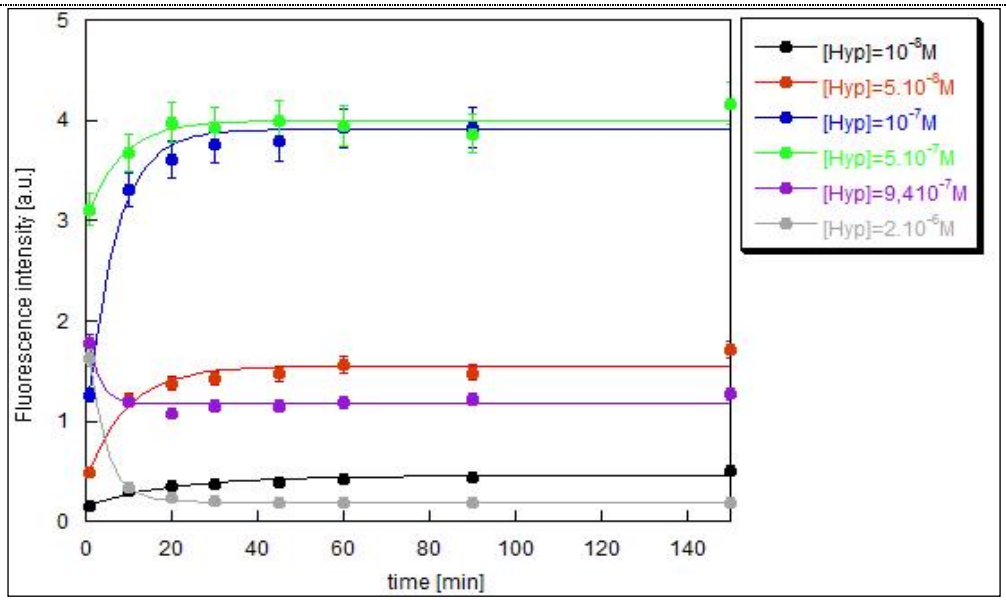

Figure 41: Graph of incorporation of Hyp into sLNP

Different amount of Hyp was added to sLNP and incorporation of Hyp was measured.

This result supports our suggestion that because of synthetic peptide which was present in sLNP, Hyp did not incorporate to sLDL and interacted with these particles very poorly. The fluorescence intensity of different concentration of Hyp after 150 min incubation with sLNP was taken from incorporation graph (Figure 41) and steady state curve was made (Figure 42).

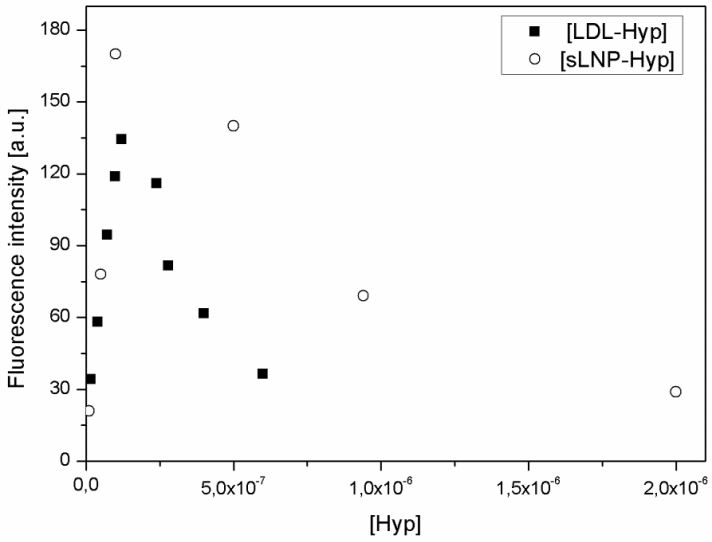

Figure 42: Steady state curve of Hyp in different amount of sLNP and LDL

At the beginning with the rising concentration of Hyp its fluorescence intensity increases. Subsequently, at concentration of Hyp higher that 10^{-7}M Hyp starts to form aggregates and the fluorescence intensity slowly decreases. For comparison, in the Figure 42 is presented the steady state curve of Hyp in natural LDL as well. It is clear, that Hyp behaves similarly in the presence of our synthesized sLNP like it does in the presence of natural LDL particles.

Hyp is able to incorporate into sLNP particles and the steady state curve of Hyp in the presence of sLNP resembles the steady state curve in the presence of natural LDL.

3.7 REDISTRIBUTION OF HYP FROM [SLNP -HYP]/D_{CH} 3 TOWARDS FREE NATURAL LDL

To know if D_{Ch} 3 has similar effect of decreasing/minimalizing of the redistribution of Hyp towards free lipid particles as it does when Hyp is loaded in LDL particles, redistribution of Hyp from sLNP covered by D_{Ch} 3 to free natural LDL was studied.

sLNP were synthesized, incubated with Hyp and covered by D_{Ch} 3. The fluorescence intensity was measured after adding free LDL particles (Figure 43). Three different concentrations of Hyp in sLNP were measured (10^{-7}M, $5x10^{-7}$M and 10^{-6}M) with one concentration of D_{Ch} 3 ($1.5x10^{-7}$M).

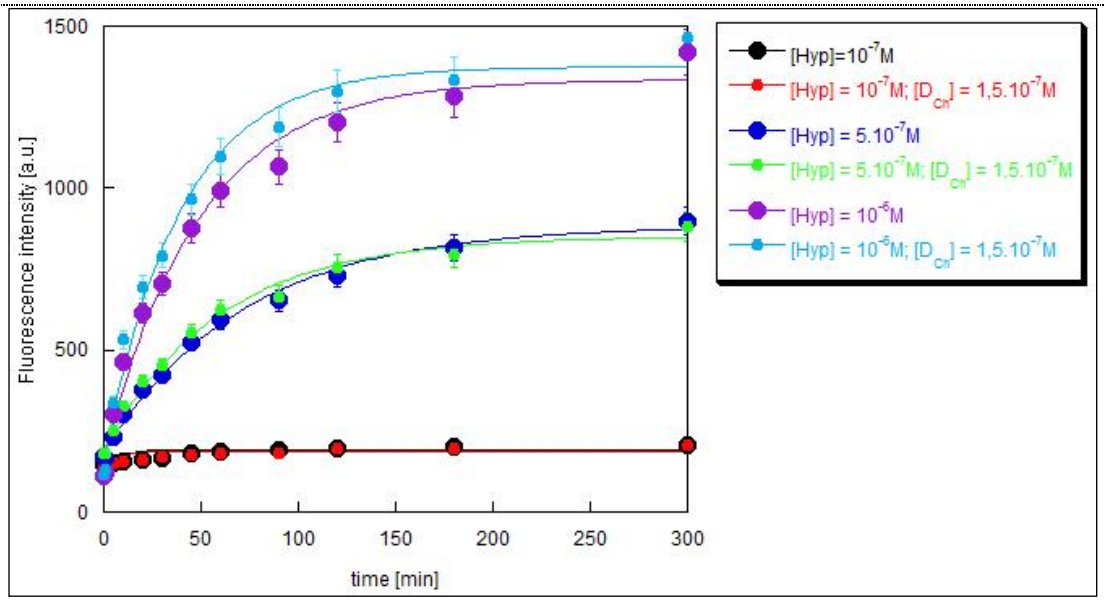

Figure 43: Redistribution of Hyp from [sLNP -Hyp]/D_{Ch} 3 to free LDL

Hyp at different concentrations was added to sLNP. These complexes were stabilized for ~ 3 hours and then D_{Ch} 3 was added. The whole complexes were incubated for 1 hour at the room temperature. Free LDL was added and fluorescence intensity of Hyp was measured.

From the redistribution process on Figure 43, covering of sLNP by D_{Ch} 3 was not as effective as it was in the case when Hyp was in LDL. At the concentration of [Hyp] = $5x10^{-7}$M and [D_{Ch} 3] = $1.5x10^{-7}$M the redistribution was 3,65% decreased. It is hard to find the appropriate ratio so D_{Ch} 3 would be as effective as it is with LDL since we were not able to determine the exact ration between sLNP, Hyp and D_{Ch} 3. In the future measurement it is necessary to find the concentration of D_{Ch} 3 which will be as effective as ratio of [LDL-Hyp]/ D_{Ch} 3 = 1:50:75 is.

The first attempts of decreasing/minimalizing of the Hyp redistribution proces towards free LDL molecules by covering the surface of sLNP with D_{Ch} 3 were performed. Yet, the right concentration of D_{Ch} 3 must be determinted in the future experiments.

3.8 INTERACTION OF sLNP WITH CELLS

sLNP were stained with $DiOC_{18}(3)$ and were incubated with U-87 MG cells to know if they are able to vectorize such hydrophobic compound to glioma cells without LDLR binding domain of ApoB-100.

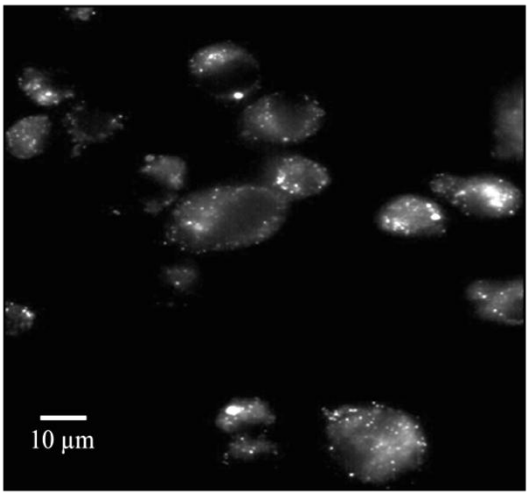

Figure 44: Fluorescence microscopy image of U-87 MG cells incubated with sLNP stained with DiO_{18} (3)

U87-MG cells were incubated with sLNP-$DiOC_{18}(3)$ complex and fluorescence microscopy was used for determining the localization of $DiOC_{18}(3)$ inside the cells. Standard filters system: FITC filter set (λ_{exc} = 450–490 nm, λ_{em} = 520–570 nm) was used for measurement. Exposure time was set to 5 s.

Figure 44 shows that even though there is no Apo-B in sLNP, $DiOC_{18}(3)$ is taken up by cells probably through endocytosis process.

sLNP can be used as transport vesicles form Hyp until above mentioned DARPins will be attached to the surface.

STUDY WITH CHOLESTEROL

Cholesterol is one of the most essential components of natural membranes which can influence the function and structure properties of the membrane as well as the interaction of drugs. The cholesterol molecule (Figure 45) is made up of three groups that have all proven to be essential for their effect on membranes: the fused rigid steroid rings, the hydroxyl group attached to one of the rings and the short flexible hydrocarbon chain [15].

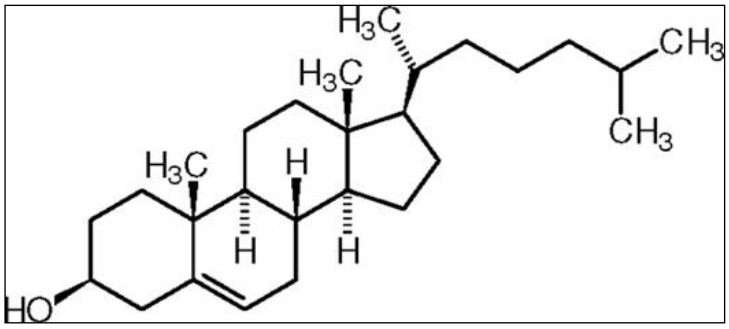

Figure 45: Cholesterol structure

[source [15]]

There are only few studies focused on the behavior of the drug molecules as a function of the presence of cholesterol in lipid membranes. Cholesterol oleate represents in our synthesized sLNP cholesterol. This is the reason why we wanted to examine if Hyp would behave differently in the presence of various amount of cholesterol. According to the studies of Errikson et al. and Ho et al., cholesterol is the major origin of selectivity for Hyp in membrane systems and the presence of cholesterol in membrane affects the permeability of the Hyp molecules [15][154].

3.9 INFLUENCE OF CHOLESTEROL ON HYP

In order to investigate how Hyp behaves in the presence of 20% cholesterol ovelap between Rhod B fluorescence emission spectra and Hyp fluorescence excitation (or absorption) spectra was used for FRET between Hyp and (Rhod B). Firstly LUV

without cholesterol and with 20% cholesterol content were prepared and incubated with Hyp overnight. Subsequently, LUV-Rhod B which preparation is described in the Chapter 2.9.4was added to the solution and fluorescence intensity of Hyp and Rhod B was measured Figure 46.

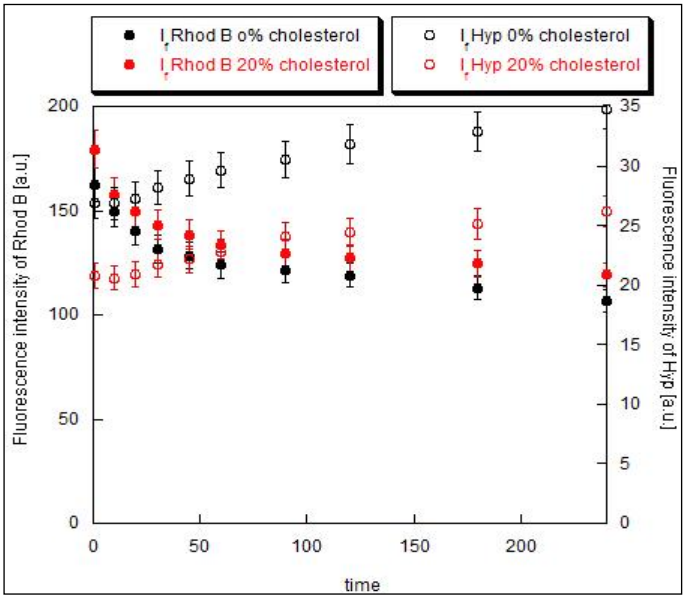

Figure 46: Fluorescence intensity of Hyp and Rhod B in the LUV without cholesterol and with 20% cholesterol

For excitation of Rhod B excitation wavelength of 525nm was used and for Hyp 560 nm. When LUV-Rhod B was added to the solution of LUV± cholesterol the fluorescence intensity of Rhod B became decreasing because of Rhod B quenching due to the Hyp incorporation to the LUV-Rhod B. At the same time the increase of fluorescence intensity of Hyp can be observed as Hyp was redistributed to LUV-Rhod B and was becoming in monomer form. For LUV with 20% cholesterol fluorescence intensity of Rhod B did not decrease as much as it did in the case of LUV with no cholesterol. Likewise, the fluorescence intensity of Hyp redistributed from LUV with 20% of cholesterol was lower than fluorescence of Hyp redistributed from LUV without cholesterol. This means from both points of view that Hyp predominantly accumulates in the particles with cholesterol does not redistribute itself from these particles as it does from LUV with no cholesterol.

The interaction of Hyp with model membranes in the absence or in the presence of cholesterol was studied. Uptakes of Hyp monomer within LUV were measured by

fluorescence intensity. Large unilamellar vesicles (LUV) containing 0%, 20%, 30% and 50% of cholesterol were prepared. The exact protocol of preparation is described in Chapter 2.9.4.

As previously shown (Figure 28), high accumulation of Hyp in vesicles leads to the formation of non fluorescent aggregates. We wanted to find out how would the fluorescence intensity of Hyp differ in the presence of 20%, 30% and 50% cholesterol. Figure 47 shows steady state curve of Hyp in LUV particles in the absence and presence of three different amounts of cholesterol. Similarly as in the case of Hyp interaction with natural LDL or with sLNP, the fluorescence measurements revealed that in the presence of LUV the fluorescence intensity linearly increase until certain Hyp concentration ([Hyp] = $4x10^{-7}$M) and beyond this concentration the quenching of Hyp fluorescence is observed (Figure 47, black line). At high Hyp concentrations > $4x10^{-6}$ M the fluorescence almost disappears. It is obvious that this behavior is common for all known Hyp-lipid structure studies [122][131][133][134]. It means that Hyp can penetrate into lipid structures from aqueous environment and is monomerized in the lipid media. However, an entrance of other Hyp molecules leads to a high local concentration of Hyp resulting in a formation of Hyp aggregates or self-quenching of Hyp fluorescence.

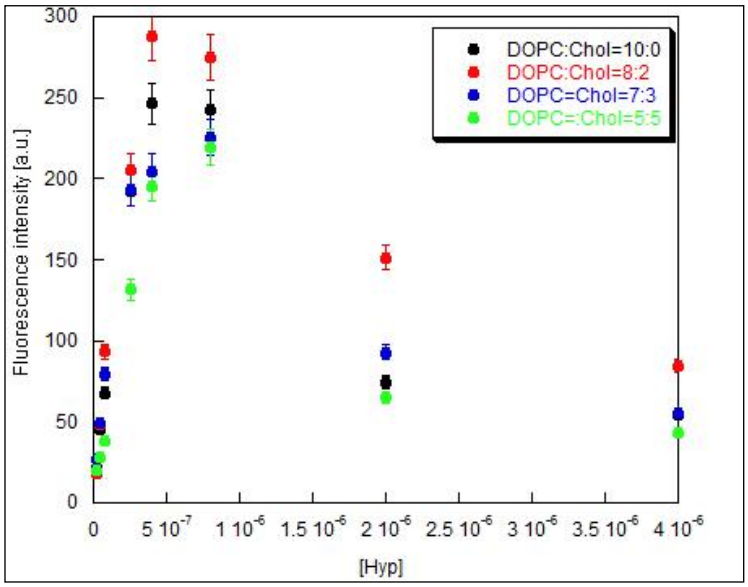

Figure 47: Steady state of Hyp inside LUV with different amount of cholesterol

Hyp was added to LUV with different amount of cholesterol. Solutions were stabilized for ~ 3 hours and fluorescence intensity was measured.

The maximum fluorescence intensity of Hyp monomer observed for LUV with 20% cholesterol is higher than in absence of cholesterol. For LUV with 30% of cholesterol the fluorescence is lower when compared to the fluorescence of Hyp in LUV with 20% of cholesterol but higher than the fluorescence of Hyp in LUV without cholesterol. Fluorescence intensity of Hyp in the presence of 50% of cholesterol is the lowest. It is even lower than in the LUV with no cholesterol. As it was already mentioned the presence of cholesterol influences the membrane permeability, but at the same time Hyp is predominantly accumulated in the cholesterol [15][154]. Ho et al. have proposed that the major element for attracting Hyp in DPPC/cholesterol LUV is cholesterol in other words cholesterol attracts Hyp more effectively than other components of LUV [15]. As a consequence of this fact, Hyp exhibits preferential binding towards cholesterol rich domains in LUV. The lower level of Hyp monomerization in the presence of higher cholesterol concentration in LUV should be explained as follows. The presence of cholesterol in LUV leads to a higher local Hyp concentration around cholesterol rich domains which leads to a formation of non-fluorescent Hyp aggregates around these domains at lower total Hyp concentration than in the case when cholesterol is not present in LUV. However, the role of cholesterol in Hyp, and other hydrophobic drugs, accumulation inside cells lipid structure as well as in lipid-based drug transport system requires further study. A clarification of this topic would substantially contribute to construction of effective transport system for targeted and effective drug delivery.

The presence of cholesterol has an impact on the behavior of Hyp which is predominantly accumulated in the cholesterol rich domains. This accumulation leads to the formation of Hyp aggregates and self-quenching of Hyp fluorescence inside the cholesterol rich domains.

STUDY OF THE INTERACTION OF HDL WITH HYP

As it was mentioned in Chapter 1.7.2.1 in the recent years the use of lipoproetins as transport veicles for drug delivery has been widely studied [123][126]. We have already studied the behavior of Hyp in the presence of LDL [122][131][133]. In this part of the study the emphasis is given on the kinetics of Hyp incorporation into free HDL molecules and the redistribution of Hyp from the complex HDL-Hyp=70:1 to free lipoprotein particles. Similarly to our study of LDL-Hyp complexes [122][131], we have utilized the fluorescence spectroscopy approach and the fact that molecules of Hyp form non-fluorescent aggregates in aqueous solutions and the Hyp aggregates can be formed also in lipoprotein particles at high local Hyp concentrations [131][155]. The differences between characteristics of Hyp association with LDL and HDL are also discussed.

3.10 INCORPORATION OF HYP INTO HDL

The fluorescence emission spectra of Hyp in the presence of HDL resemble those in the presence of LDL (not shown). The spectral maximum is positioned at 599 nm [131] and the intensities are also almost identical in the presence of both types of the lipoproteins (at the same Hyp concentrations and molar ratio Hyp/lipoprotein=1:1). The dependence of Hyp fluorescence intensity at its maximum on the molar ratio HDL-Hyp, 300 minutes after mixing of Hyp with HDL solutions (HDL concentration in the mixtures was 10 nM), is presented in Figure 48.

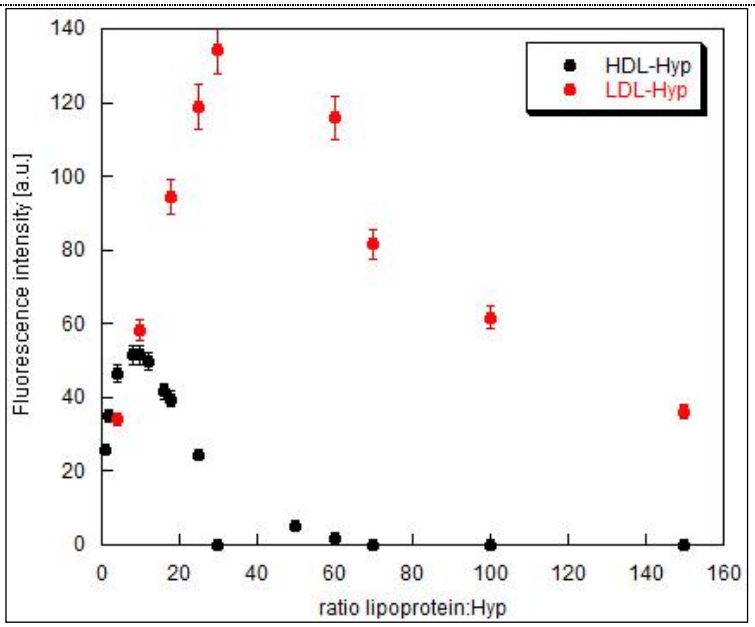

Figure 48: Steady state of incorporation of Hyp into LDL or HDL

Dependence of Hyp fluorescence intensity on concentration ratio HDL-Hyp and LDL-Hyp after 120 min of stabilization of the complexes (fluorescence maximum 599 nm, excitation line 515 nm). Concentration of HDL and LDL was kept constant during the measurements (10nM).

The intensity of Hyp fluorescence increases up to HDL-Hyp molar ratio 1:8 and beyond this value a quenching of Hyp fluorescence is observed. At the molar ratio HDL-Hyp =1:60, the fluorescence of Hyp almost disappears. This behavior can be explained similarly as in the case of Hyp association with LDL [131]. Until HDL-Hyp =8:1 ratio the molecules of Hyp are present inside HDL particles as monomers, and at high HDL-Hyp molar ratios (>1:8), the formation of non-fluorescent Hyp aggregates inside HDL occurs. However, the values of molar ratio at which Hyp still exists in the lipoproteins particles in monomeric state are different, 30:1 for LDL-Hypand 1:8 for HDL-Hyp complex (Figure 48). This difference should be mainly attributed to a smaller size of HDL in comparison with LDL particle (diameter in average of HDL and LDL particles is 11nm and 22 nm, respectively).

The ratio of the values (1:30 and 1:8), which represent thresholds for the existence of the monomeric form of Hyp inside LDL and HDL molecules, respectively, equals approximately to 4. This observation leads to a speculation above the possible localization of the Hyp molecules inside lipoprotein particles. It is apparent that the square of the ratio of the diameters of LDL/HDL is also approximately 4 (22 nm/11

$nm)^2$. It suggests that the molecules of monomeric Hyp are most probably distributed on the "like sphere surface", likely in phospholipid-cholesterol outer layer of LDL and HDL molecules. Further increase of Hyp concentration (above the ratio 1:8 and 1:30 for HDL-Hyp and LDL-Hyp) leads to a Hyp clustering in lipid media which has been previously proposed [131][156] and also theoretically supported [157]. This clustering is mostly due to π-stacking interaction between aromatic cores of Hyp molecules. It was proposed by several groups that Hyp is mainly localized close to the polar headgroups of the outer layer of lipid structure (liposomes, biological membranes) [15][157][158]. This is very probably also the case for the localization of Hyp inside LDL and HDL molecules, however the presence of cholesterol in outer shell of the lipoproteins molecules can move Hyp a more deeply inside the LDL or HDL particles as it was proposed for Hyp localization in cholesterol enriched biological membranes [15].

Hyp is incorporated to HDL molecule in the monomer form until the ratio 1:8. Above this ratio Hyp starts to form non-fluorescent aggregates.

3.11 THE KINETICS OF HYP INTERACTION WITH HDL PARTICLES

The time evolution of the fluorescence intensity of Hyp after mixing of Hyp molecules with free HDL particles is shown in Figure 49. It is evident that there exists two phases of the incorporation of Hyp into HDL molecules. The rapid phase of the incorporation is manifested by a non-zero fluorescence intensity of Hyp immediately (5-10 seconds) after mixing of Hyp and HDL solutions. The second, slow phase of the process lasts several minutes.

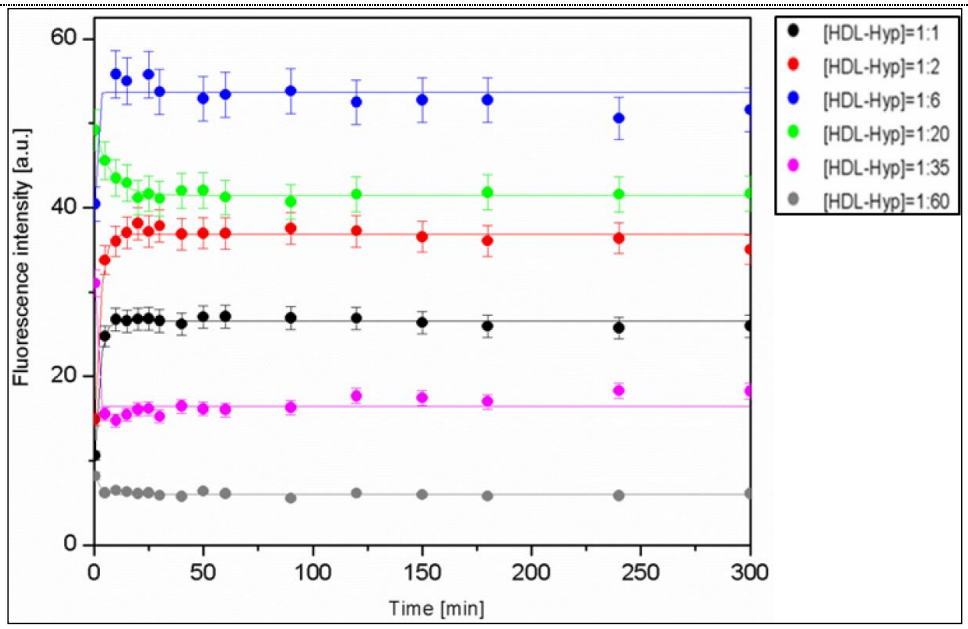

Figure 49: Time dependence of fluorescence intensity

Time dependence of fluorescence intensity of Hyp after mixing of Hyp and HDL solutions. Concentration of HDL was kept constant (10nM). Fluorescence of Hyp was recorded at 599 nm, the excitation line was 515 nm.

The fluorescence intensity of Hyp in HDL-Hyp complexes (until molar ratio 1:8) increases and reaches saturation 10 minutes after mixing. For the complexes with higher HDL-Hyp ratios an increase of Hyp fluorescence observed immediately after mixing is followed by its decrease. This decrease is caused, as it was already mentioned, by the creation of Hyp aggregates and self-quenching of Hyp fluorescence inside HDL particles in situation when continuous flow of Hyp molecules into HDL particles leads to a number of Hyp molecules per one HDL particle above 8. For the HDL-Hyp = 1:1 and 1:2 complexes a major part of Hyp molecules is incorporated into HDL in the slow phase (Table 7). On the other hand, for the complexes with the molar ratios 1:6 and 1:10, the major part of Hyp (about 70%) is incorporated into HDL in the first, rapid, phase (Figure 49,Table 7). This behavior is slightly different than the properties of LDL-Hyp complex, where it was observed that most of Hyp molecules (about 65%) are associated with LDL in the slow phase of the incorporation process until concentration ratio 1:30 [122]. For the determination of the half-times of Hyp incorporation into HDL (until ratio HDL-Hyp =1:8) the experimental data were fitted by mono-exponential function. However, we are aware that the process of Hyp incorporation into lipoproteins

is complicated and mono-exponential fitting is only a rough approximation of the real situation.

HDL-Hyp	τ(min)	I_0 [a.u.]	I_{60} [a.u.]	$I_{0/}$ I_{60}
1	7	10	27	0,39
2	5	15	37	0,48
6	4	32	47	0,68
10	2	40	53	0,75

Table 7: Half-times of the slow phase of Hyp incorporation into free HDL molecules

The obtained half-times for the internalization of Hyp molecules into HDL are summarized in Table 7. The comparison of these values with those for LDL-Hyp complex reveals that the process of internalization of Hyp molecules into lipoproteins is more rapid in the presence of HDL than LDL. The half-times for Hyp incorporation into HDL is 2-7 min depending on the final HDL-Hyp ratio, meanwhile the half-times for Hyp association with LDL is 14-26 min [122]. The reason for this observation should be in a relative higher containing of cholesterol molecules in LDL (11%) in comparison with HDL (7%) [159]. There are similar properties of the kinetics of Hyp incorporation into HDL and LDL molecules, however, incorporation of Hyp into HDL is more rapid than to LDL also the relative contribution of the fast phase *vs* slow phase of Hyp accumulation into HDL particles is higher than into LDL. The concentration of cholesterol molecules in outer shell of the lipoprotein particles is probably the determining factor for the kinetics of Hyp incorporation into lipoproteins.

The major part of Hyp molecules is incorporated into HDL in the slow phase for ratios HDL-Hyp = 1:1 and 1:2. In the ratios 1:6 and 1:10 about 70% of Hyp is incorporated to HDL in the rapid phase.

3.12 KINETICS OF HYP REDISTRIBUTION FROM HDL-HYP COMPLEXES

Similarly as for transport of Hyp molecules from saturated complex LDL-Hyp to free LDL molecules [122], the translocation of Hyp molecules from saturated HDL-Hyp =1:70 complex to free HDL particles was studied. This investigation is possible due to the fact that this translocation leads to a lower number of Hyp molecules per one lipoprotein particle which consequently leads to appearance of Hyp fluorescence. The increase of fluorescence signal corresponds to a monomerization of Hyp molecules which is a consequence of the translocation of these molecules from HDL-Hyp complex on free lipoprotein particles. The kinetics of the redistribution of Hyp molecules from HDL-Hyp =1:70 complex to free HDL particles, represented by the time-evolution of Hyp fluorescence spectra, are presented on the Figure 50.

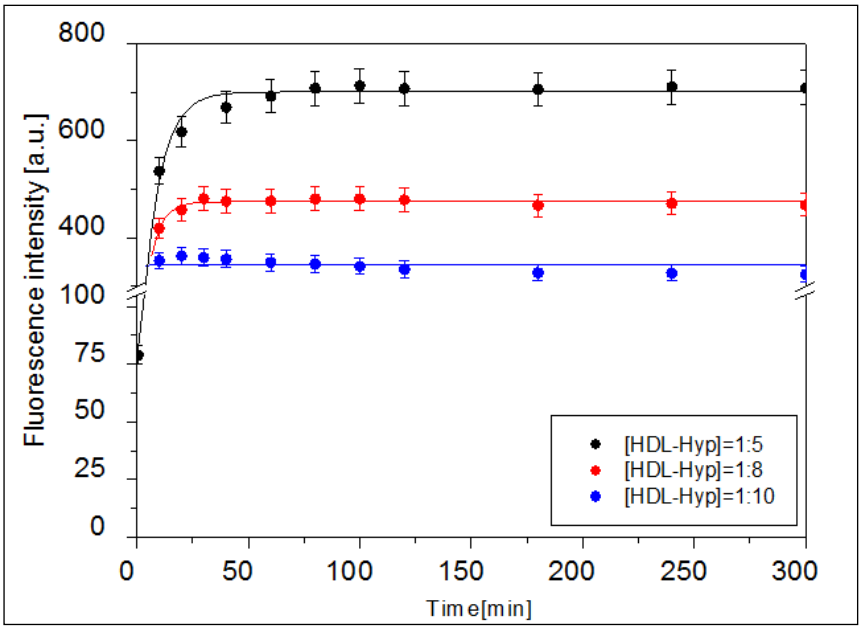

Figure 50: Redistribution of Hyp from complex /HDL-Hyp = 70:1 to free HDL

Time dependence of fluorescence intensity of Hyp after mixing free HDL with HDL-Hyp = 70:1 complex. The initial complex HDL-Hyp = 70:1 was mixed after 2 hours of stabilization with different amount of free HDL to obtain different final HDL-Hyp molar ratios (1:5, 1:8 and 1:10). The concentration of Hyp was kept constant (10μM). Fluorescence of Hyp recorded at 599 nm, excitation line 515 nm.

The appropriate amounts of HDL were added to the stabilized complex HDL-Hyp =1:70 (stabilization for 2 hours at the room temperature) and the evolution of Hyp fluorescence intensity at its maximum (599 nm) was registered. After adding free HDL to the HDL-Hyp =1:70 complex, the increase of Hyp fluorescence for all HDL-Hyp final ratios was observed. The observed redistribution has two phases. First one is represented by the increase of Hyp fluorescence immediately (5-10 sec) after mixing of HDL and HDL-Hyp =1:70 solutions and the second is expressed by the further gradual fluorescence increase (Figure 50). When compared to the redistribution of Hyp from LDL-Hyp to free LDL [122] Hyp translocates from the HDL-Hyp complex towards free HDL faster than it does from LDL-Hyp complexes to free LDL. Lower rates for the Hyp translocation from the complex with LDL to free LDL molecules in comparison with those observed in the presence of HDL again suggests the role of cholesterol in incorporation of Hyp to and releasing from lipoprotein particles. The mechanism of redistribution of Hyp molecules from HDL/LDL-Hyp complex to free HDL/LDL particles is not resolved yet. We think that both direct Hyp translocation from saturated HDL-Hyp complex to free HDL molecules as well as translocation through water phase are possible in this redistribution process. The partition coefficient of Hyp in octanol/water mixture has been determined to be log P=3,43 [160]. This value clearly suggests a strong preference of Hyp to be incorporated in lipid structures in comparison with aqueous phase. As it was previously mentioned, Hyp aggregates formed at high HDL-Hyp ratios can be sticked to the HDL/LDL surface. Under collisions of HDL-Hyp complex with free HDL particles, a part of Hyp molecules can be transferred directly to these free particles. However, certain part of Hyp molecules exists as aggregates in aqueous phase. From this phase, molecules of Hyp can be also incorporated into free HDL molecules. More thorough studies are necessary to be performed to definitely resolve this problem.

When compared to the redistribution of Hyp from LDL, Hyp is translocated from HDL-Hyp complexes to free HDL molecules faster than from LDL-Hyp complexes to free LDL. Molecules of LDL contain more cholesterol than molecules of HDL which can cause the difference in the kinetics of the redistribution.

EFFECT OF PKCα EXPRESSION ON BCL-2 PHOSPHORYLATION AND CELL DEATH BY HYPERICIN

The role of anti-apoptotic PKCα in response to Hyp photodynamic action in U-87 MG cells has been previously investigated [75]. The purpose of study in this part of the thesis was to focus closer on the effect of *pkcα gene* silencing in U-87 MG cell line after Hyp photo-activation and to study the impact and consequence of such silencing on cell survival and cell death.

3.13 TRANSFECTION EFFICIENCY

Control siRNA (FITC Conjugate)-A was used to determine the transfection efficiency. This control contains a scrambled sequence that does not lead to a specific degradation of any known cellular RNA and represents a negative control to avoid false positive results.

Figure 51 A shows confocal fluorescence images of cells transfected with scrambled siRNA. siRNA entered the cells, and green fluorescence originated from Control siRNA(FITC Conjugate)-A was detected in the cytoplasm. Based on nuclear (blue fluorescence originated from Hoechst 33258) and mitochondrial (red fluorescence originated from MitoTracker Orange®) morphology, no significant changes have been detected. The effect of scrambled Control siRNA-A on key investigated parameters (such as cell viability, ROS production and Bcl-2 phosphorylation) is further described within the corresponding paragraphs. Figure 51 B shows histograms of non-transfected control cells (black line) and cells transfected with Control siRNA (FITC Conjugate)-A (red line) obtained by flow cytometry. Flow cytometry clearly demonstrates that after 5 hours the transfection efficiency was about 87%.

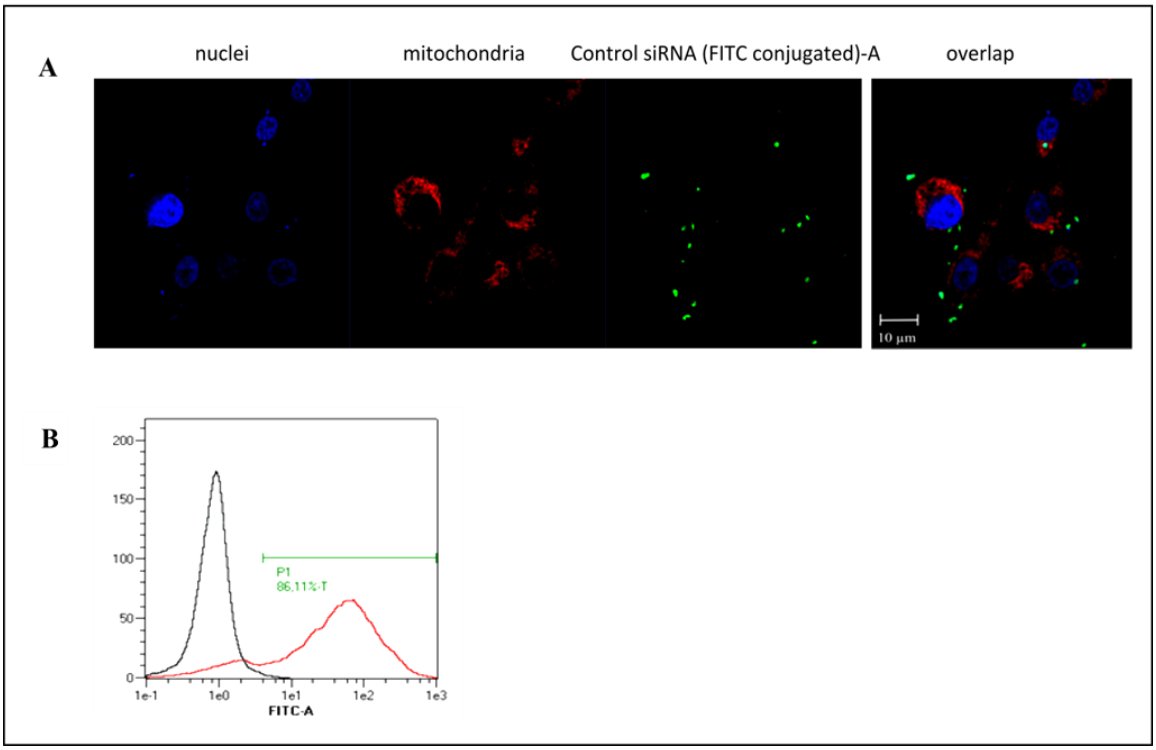

Figure 51: Detection of siRNA transfection efficiency in U87-MG cells

A: Confocal fluorescence image of nuclei (blue) and mitochondria (red) of U87-MG cells entered by FITC-conjugated scrambled siRNA Control-A (green). Scrambled siRNA was transfected into U87-MG cells and nuclei (Hoechst 33258) and mitochondria (MitoTracker Orange) were stained after 5 hours. B: Flow cytometry histograms of control non-transfected cells (black line) and cells entered by FITC-conjugated scrambled siRNA Control-A (red line).

siRNA transfection has no impact on the nuclear and mitochondrial morphology. After 5 hours the transfection efficiency was ~ 90%.

3.14 PKCα GENE SILENCING

To silence *pkcα gene*, U-87 MG cells were treated according to siRNA transfection protocol (Chapter 2.9.7). Confocal fluorescence microscopy along with western blot analysis was used to confirm gene silencing. Figure 52 A shows confocal fluorescence image of non-transfected and transfected cells PKCα$^-$ were fluorescence intensity of cells treated with siRNA is much lower than fluorescence intensity of

control cells. This result was verified by western blot analysis (Figure 52 B) where optical density of transfected PKCα⁻ cells was 6,37% when compared to non-transfected cells with optical density 93,62%. β-actin determined in both samples was used as reference protein. This result proves that *pkcα* gene silencing carried through siRNA efficiently decreased the amount of PKCα protein in transfected U-87 MG cells. The specificity of siRNA PKCα(h) transfection was verified by confocal microscopy (Figure 52 C). Non-transfected and transfected PKCα⁻ cells were stained by indirect immunofluorescence, and PKCδ (as a representative member of PKCs) was visualized. Fluorescence intensity and the outer profile of the measured cells (marked with white line) are comparable (Figure 52 C) and indicate that silencing of *pkcα* gene expression is specific and the expression of PKCδ is not affected. The specificity of pkcα silencing observed in our work was confirmed also by other groups [161].

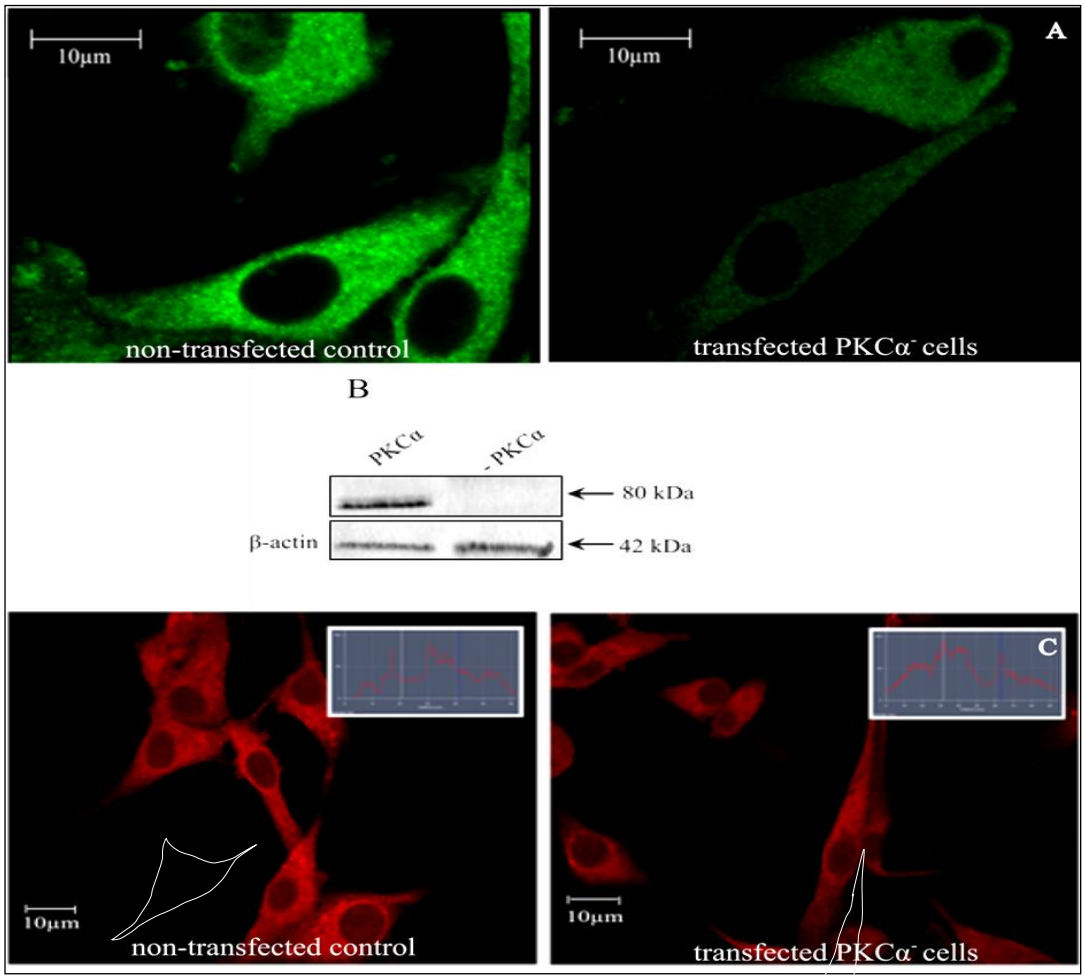

Figure 52: Distribution of PKCα in human U87-MG cells

A: The figure shows confocal fluorescence image ofU87-MG non-transfected control cells (left) and cells transfected with siRNA PKCα(h) (right) both stained with primary Ab against PKCα (E195, Novus,

USA) for visualization of distribution of PKCα. In both cases images were taken with the same measuring parameters (brightness, contrast and laser power). The scale bar represents 10 µm.

B: Western blot analysis of endogenous expression of PKCα in non-transfected and transfected (-PKCα) U87-MG cells. The membranes were probed withAb (E195, Novus, USA), which specifically recognized the catalytically competent form of PKCα phosphorylated at Thr638 (PKC, (pThr638)). As protein reference control anti β-actin antibody (Abcam, GB) was used.

C: Distribution of PKCδ in human U87-MG cells. The figure shows confocal fluorescence image of U87-MG non-transfected control cells (left) and cells transfected with siRNA PKCα(h) (right) both stained with primary Ab against PKCδ (ab47473, Abcam) for visualization of distribution of PKCδ. In all cases images were taken with the same measuring parameters (brightness, contrast and laser power). The scale bar represents 10 µm. *Inserted*: Fluorescence intensity profile of marked cells obtained by using ZEN 2010 software (Zeiss, Germany).

siRNA PKCα(h) specifically blocks the pkcα gene expression without having any impact on the other isoforms of PKC protein family.

3.15 CELL SURVIVAL AFTER HYP PHOTO-ACTIVATION

It was already shown that cells undergo apoptosis after Hyp photo-activation [75][163]. Thus, taking into account that PKCα is an anti-apoptotic protein [75], we can expect that silencing of this protein by using of siRNA would have an effect on Hyp photo-induced cell death. Our predictions were that the level of apoptosis could occur more easily and that this modulation of PKCα expression would result in more effective treatment with lower concentration of Hyp and consequently would reduce amount of survival cells. MTT colorimetric assay showed different cell behavior. Pure silencing of *pkcα gene* did not show noticeable effect on the cell survival with only little changes between control cells and cells with decreased transcription of PKCα. Surprisingly, combination of PKCα silencing and Hyp photo-activation did not result in bigger impact on the cell viability either. MTT tests were assessed with two concentrations of Hyp. It is obvious that $5x10^{-7}$ M Hyp is more effective when compared to $1x10^{-7}$ M concentration, but in both cases cell survival was similar for transfected PKCα^{-} cells and

non-transfected one (Figure 53 A). The colorimetric MTT assay (Figure 53 B) shows that scrambled Control siRNA-A has no influence on cell viability. Figure 53 C shows DNA fragmentation in non-transfected and transfected PKCα$^-$ cells after Hyp photo-activation where the DNA ladder is clearly visible in non-transfected cells, but in transfected PKCα$^-$ cells DNA fragmentation was not observed.

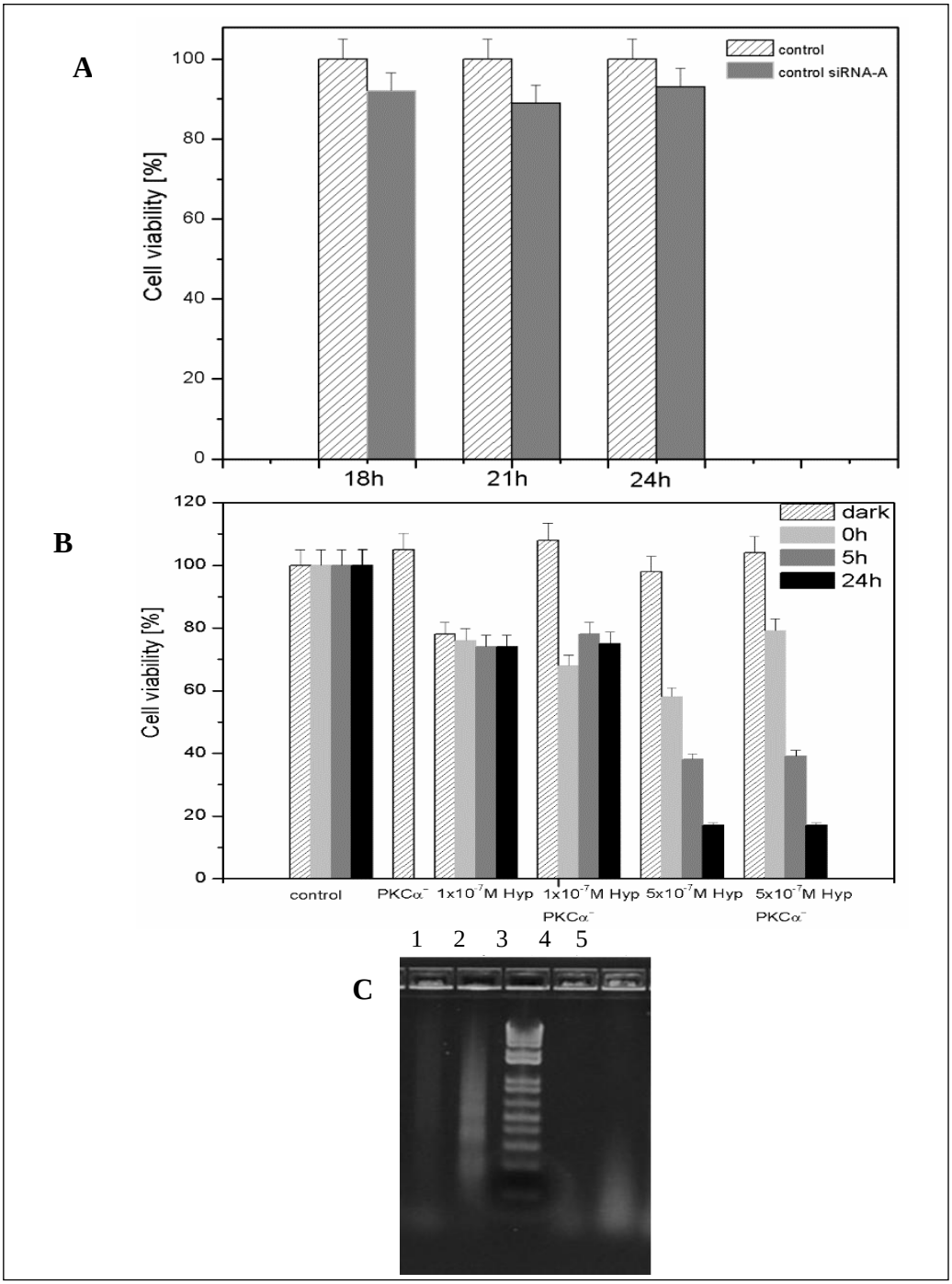

Figure 53: Cell viability test of non-treated and siRNA PKCα(h) treated U87-MG cells before and after Hyp photo-activation.

A: Cell viability test of non-treated and siRNA PKCα(h) treated U87-MG cells before and after Hyp photo-activation. Viability of non-transfected U87-MG cells and cells transfected with siRNAPKCα(h) after Hyp photo-activation was determined by the MTT test. The cells were plated into 96-well tissue culture plates at a density of 10 000 cells per well and were cultivated until an optimal population density was reached. Cells were incubated with Hyp, and Hyp photo-activation protocol was used as described in Material and Methods. Results of adherent cell numbers from three independent experiments are expressed relative to control (100%) and represent mean values. **B:** Cell viability test and the effect of scrambled siRNA Control-A (negative control) on cell survival. **C:** DNA fragmentation after Hyp photo-activation in non-transfected and transfected PKCα$^-$ cells. Non-transfected cells treated with (1) $1x10^{-7}$ Hyp, (2) $5x10^{-7}$ Hyp, (3) DNA Ladder, transfected PKCα$^-$ cells treated with (4) $1x10^{-7}$ Hyp, (5) $5x10^{-7}$ Hyp.

pkcα gene silencing does not affect the cell survival after Hyp photo-activation.

3.16 DETECTION OF APOPTOSIS/NECROSIS AFTER HYP PHOTO-ACTIVATION

Because of cell viability tests showed that decreased amount of PKCα did not have expected influence on the cell survival, the effect of pkcα gene silencing on the type of cell death was further investigated by flow cytometry (Figure 54).

A significant difference between transfected PKCα$^-$ cells was detected when compared with non-transfected cells after Hyp photo-activation. Our results show that cells with blocked *pkcα gene* undergo necrosis prior to apoptosis which was present in the non-transfected cells and in the next steps we were trying to find out the reason. This decrease of apoptosis and increase of necrosis was slightly evident right after photo-activation of Hyp and was more pronounced for 24 hours post-irradiation time (Figure 54).

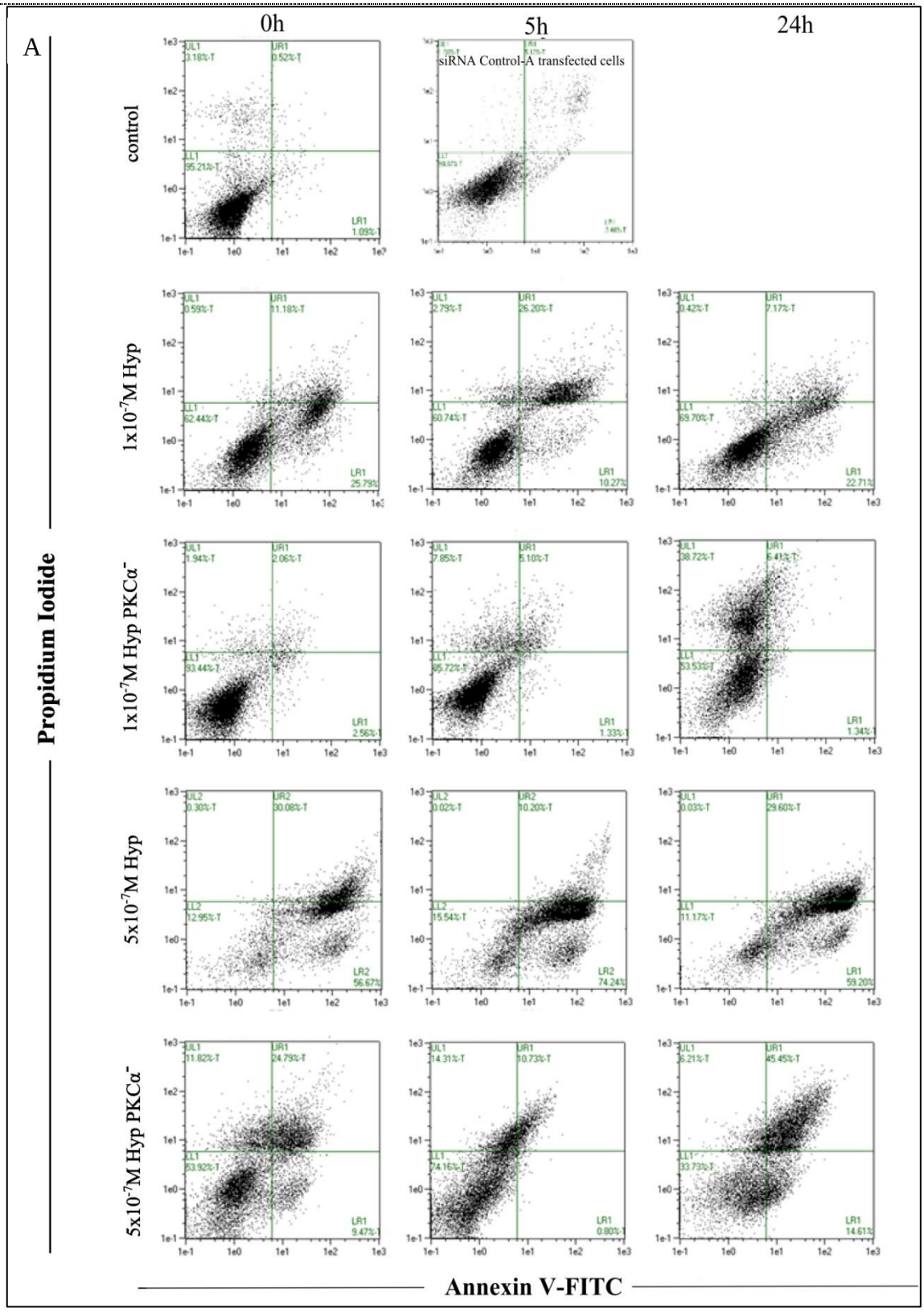
A
0h
5h
24h
siRNA Control-A transfected cells
control
1x10-7M Hyp
1x10-7M Hyp PKCα-
5x10-7M Hyp
5x10-7M Hyp PKCα-
Propidium Iodide
Annexin V-FITC

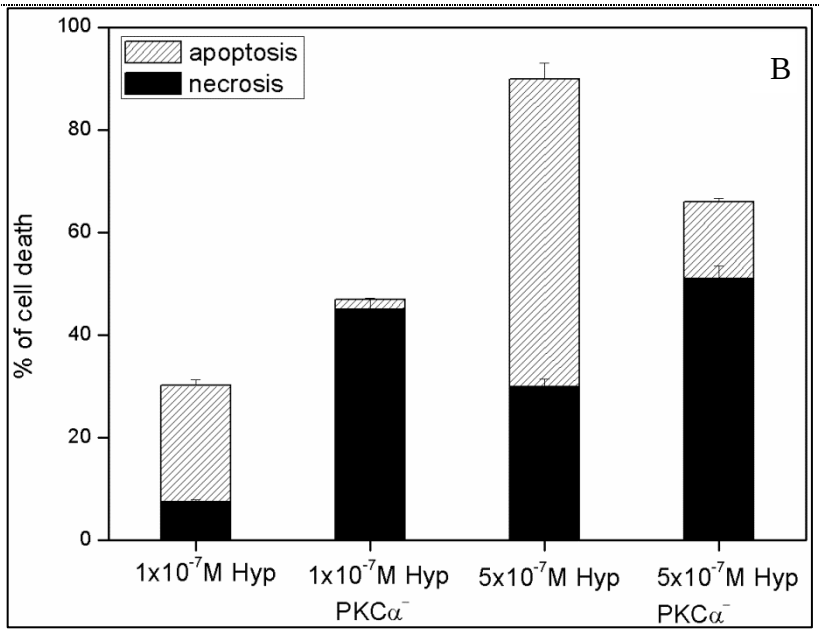

Figure 54: Determination of the cell death (apoptosis/necrosis) induced by photo-activated Hyp

A: Representative flow-cytometric dot plot analysis of apoptosis/necrosis after Annexin V-FITC/PI staining in non-transfected cells and cells transfected with siRNA PKCα(h) obtained 0h, 5h or 24 h after Hyp photo-activation. Three major populations of cells can be observed in the cytotoxicity assay: Annexin V^-/PI^- cells are defined as live cells, Annexin V^+/PI^- cells as apoptotic cells and PI^+ as dead cells (late apoptotic or necrotic). **B:** Histograms showing the comparison ratio of apoptosis and necrosis (live cells are not considered) in the cells non-treated and treated with siRNA PKCα(h)24 hours after Hyp photo-activation. Values are mean ± S.D. of three independent experiments.

pkcα gene silencing shifts Hyp photo-induced cell death from apoptosis towards necrosis.

3.17 REACTIVE OXYGEN SPECIES PRODUCTION

In order to better understand how PKCα silencing can lead to such modification of the cell death pathway, intracellular ROS formation was monitored by confocal fluorescence microscopy and flow cytometry analysis (Figure 55).

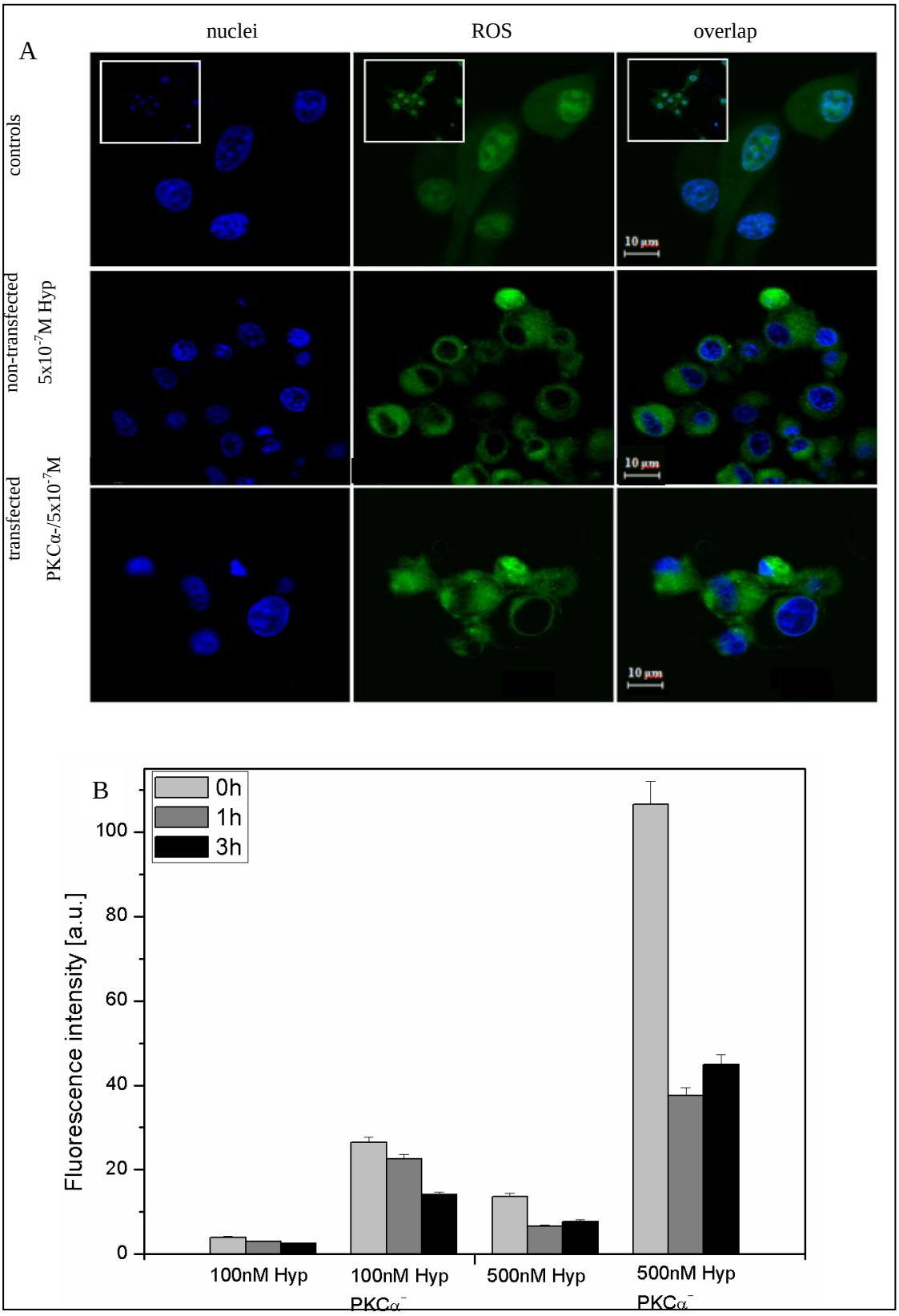

Figure 55: ROS production after Hyp photo-activation

A: CellROX Green™ confocal fluorescence images (green fluorescence) displaying production of ROS in the non-transfected cells (first row) and cells transfected with siRNA PKCα(h) (second row) incubated with Hyp (red fluorescence) measured within one hour after Hyp photo-activation. The scale bar represents 10 µm.

B: Histograms of ROS production obtained by flow cytometry after CellROXDeepRed™ staining in non-transfected cells and cells transfected with siRNA PKCα(h) 1 hour after Hyp photo-activation.

Cells were stained with CellROX reagents (Green, Orange and/or Deep Red), and confocal microscopy and flow cytometry analysis was immediately performed. CellROX reagents are non-fluorescent dyes in a reduced state that exhibit bright fluorescence upon oxidation by ROS. As shown in Figure 55 A, fluorescence related to increased ROS production can be observed after Hyp photo-activation for both transfected PKCα$^-$ cells and non-transfected cells. One can see that Hyp photo-activation leads to an increase of ROS production inside tested cells, and the level of ROS production is more pronounced in transfected PKCα$^-$ cells. To determine the effect of *pkcα* gene silencing and Hyp photo-activation on nuclear morphology, cells were stained with Hoechst 33258, a blue-fluorescent dye used for fluorescence detection of the compacted state of the chromatin. Figure 55 A shows that the nuclear morphology of both controls (non-transfected cells vs. Control siRNA-A transfected cells) is comparable, without observed increase of chromatin condensation. Apoptotic nuclei are more visible after Hyp photo-activation in non-transfected cells. On the contrary, no significant chromatin condensation of nuclei in transfected PKCα$^-$ cells has been observed. However, flow cytometric quantitative analysis of ROS production 5 hours after Hyp photo-activation shows significant differences between transfected PKCα$^-$ and non-transfected cells. In all cases, ROS production appears to be related to the initial concentration of Hyp and slightly decreased as a function of post-irradiation time, but it is also clearly higher in transfected cells when compared to non-transfected ones (Figure 55 B).

As it was already shown, the level of ROS formation plays an important homeostatic role regulating signal transduction involved in proliferation and cell survival [165]. Moreover, when ROS formation is deregulated and surpasses antioxidant defenses, oxidative stress takes place, and when oxidative stress exceeds the capacity of the cell to repair biomolecule oxidation (nucleic acids, lipids and proteins),

irreversible oxidative damage occurs. Thus, predominance of necrosis prior to apotosis in transfected cells can be considered to be related to such ROS increase.

pkcα gene silencing increases the intracellular photo-induced ROS production that seems to be mainly localized at the level of mitochondria.

3.18 BCL-2 PHOSPHORYLATION ON SERINE70 (PBCL-2(SER70))

Taking into account that members of the Bcl-2 family of proteins are important regulators of programmed cell death pathways with individual members that can suppress (e.g. Bcl-2, Bcl-XL) or promote (e.g. Bax, Bad) apoptosis [166], flow cytometry experiments focused on the role of Bcl-2 protein in the cell death were also performed. In this view, phosphorylation of Bcl-2 (pBcl-2) was assessed since such modification is needed in order to protect cells from apoptosis [166]. The results are presented in Figure 56. After Hyp photo-activation we observed a slight decrease of Bcl-2 phosphorylated on Ser70 with much higher decrease of the phosphorylation of Bcl-2 in the transfected PKCα$^-$cells. This result was verified by western blot analysis (Figure 56 B). It proves that *pkcα gene* silencing decreases phosphorylation of Bcl-2 protein at Ser70.

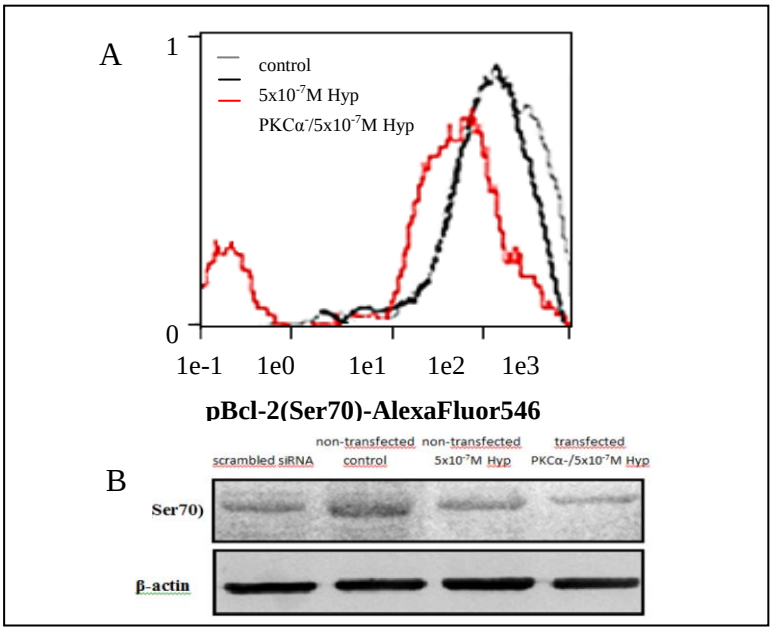

Figure 56: Level of Bcl-2 phosphorylation on Ser70 after Hyp photo-activaion

A: Flow cytometry histogram of Bcl-2 phosphorylation on Ser70 after indirect immuno-fluorescence staining with rabbit mAb (5H2) (Cell Signaling Technology, USA) against human pBcl-2(Ser70). Level of Bcl-2 phosphorylation on Ser70 after Hyp photo-activation is obtained for control cells (grey line), non-transfected cells (black line) and cells transfected with siRNA PKCα(h) (red line). **B:** Western blot analysis of endogenous expression of pBcl-2(Ser70) in non-transfected (PKCα) and transfected (PKCα$^-$) U87-MG cells. Cell lysates were prepared according to the Whole cell lysate preparation protocol described in Material and Methods and were subjected to SDS-PAGE and Western blot analysis. The membranes were probed with Ab (ab47473, Abcam, UK), which specifically recognized Bcl-2αphosphorylated at Ser70. As protein reference control, anti β-actin antibody (Abcam, UK) was used.

Recent studies have shown that agonist-activated phosphorylation of Bcl-2 at Ser70 (single site phosphorylation), a site within the flexible loop domain is required for Bcl-2's full and potent anti-apoptotic function [166]. Thus observed decrease of Bcl-2 phosphorylation after siRNA gene silencing and Hyp photo-activation can explain decreased amount of apoptotic cells. However, question why we observed such important increase of ROS production and subsequent necrosis in transfected PKCα$^-$ cells after Hyp photo-activation remains to be answered.

pkcα gene silencing decreases the level of phosphorylation of Bcl-2.

3.19 FLUORESCENCE IMAGING OF PBCL-2(SER70), MITOCHONDRIA AND GSH

Our hypothesis is that the increased oxidative stress generated during photo-dynamic action of Hyp in transfected cells as well as during cell death development could be a key factor for the observed shift from apoptosis to necrosis. It was reported previously that mitochondria, ROS, gluthation (GSH) and Bcl-2 are closely related things [167]. Indeed, GSH is considered as a key endogenous anti-oxidant to combat ROS produced by the electron transport chain in mitochondria. The role of Bcl-2 in GSH transport into mitochondria is well described in the work of Wilkins et al. [168]. We previously reported changes in the mitochondrial NAD(P)H content and possible alteration in the mitochondrial metabolic state after Hyp photo-activation. Observed rise

of mitochondrial NAD(P)H fluorescence could be explained with relation to enzymatic elimination of mitochondrial oxidative stress with participation of GSH [169].

It was shown that Bcl-2 is an anti-oxidant like protein [170][171] which over expression leads to an increase of cellular contents of GSH [172]. In contrast, Bcl-2 knockout mice had reduced level of GSH in brain tissue and were more sensitive to neuronal cell death induced by mitochondrial oxidative stress [173]. In the context of anti-oxidative protection of mitochondria against oxidative stress we decided to investigate a co-localization of GSH with Bcl-2 and mitochondria. Fluorescence imaging microscopy has been used to assess relative co-localization between mentioned parameters despite the fact that Bcl-2 is localized in outer mitochondrial membrane and GSH within the mitochondrial matrix where its anti-oxidative functions are linked to other enzymatic systems of the mitochondria [169].

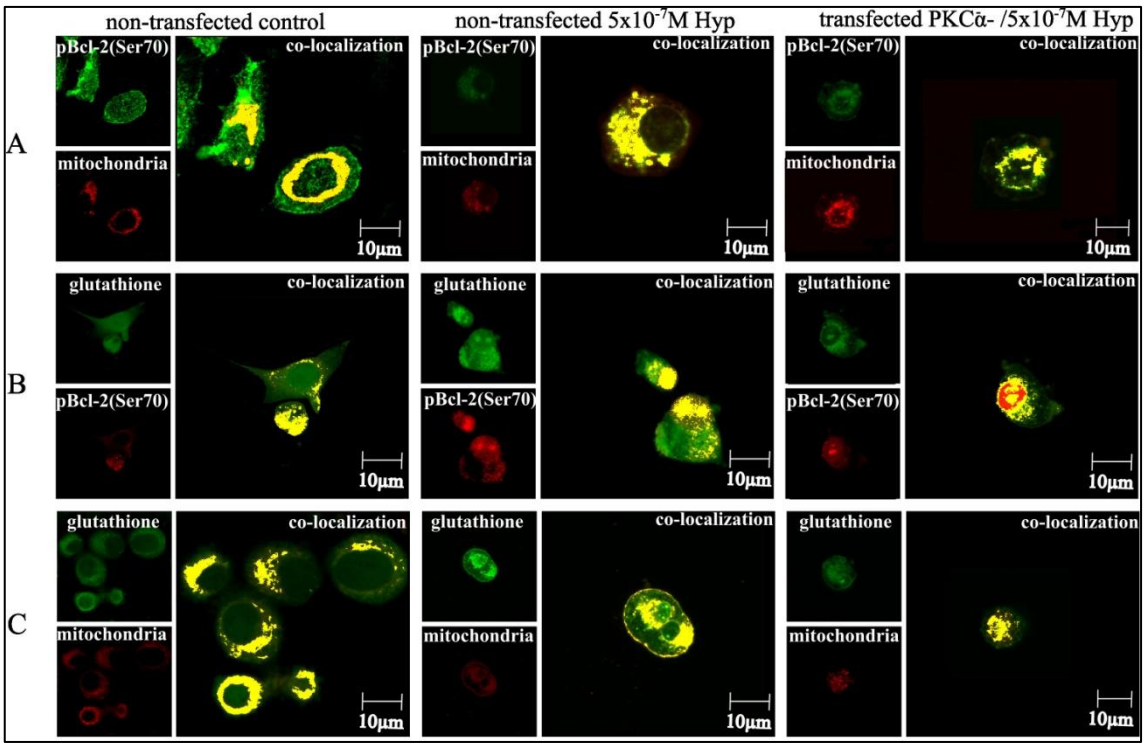

Figure 57: Cellular distribution of pBcl-2(Ser70) and GSH after Hyp photo-activation and its co-localization with mitochondria

A: Cellular distribution of pBcl-2(Ser70) and mitochondria, **B:** cellular distribution of glutathione and pBcl-2(Ser70) and **C:** cellular distribution of glutathione and mitochondria in in control cells (left), non-transfected (middle) and PKCα$^-$ cells transfected with siRNA PKCα after Hyp photo-activation (right). The distribution of pBcl-2(Ser70), glutathione and mitochondria was detected by confocal microscopy

following vital cell staining with ThiolTracker™ Violet and appropriate MitoTracker (Green or Red) and indirect immunofluorescence staining with 5H2 antibody against Bcl-2 phosphorylated on Ser70.

	pBcl-2(Ser70) MitoTracker®Orange			**ThiolTracker™Violet pBcl-2(Ser70)**			**ThiolTracker™Violet_ MitoTracker®Orange**		
	overlap	M_1	M_2	overlap	M_1	M_2	overlap	M_1	M_2
control	0,83	0,62	0,99	0,77	0,17	0,99	0,75	0,37	0,96
$5x10^{-7}$M Hyp	0,77	0,51	**0,91**	0,68	0,65	**0,88**	0,65	0,34	**0,98**
$5x10^{-7}$M Hyp/PKCα$^-$	0,63	0,55	**0,75**	0,65	0,41	**0,73**	0,87	0,65	**0,88**

Table 8: Co-localization analysis of pBcl-2(Ser70) in mitochondria, pBcl-2(Ser70) and GSH, and the presence of GSH in mitochondria.

Co-localization analysis was performed on the obtained fluorescence images using the ZEN 2011 image processing (Zeiss, Germany). Co-localization coefficients M_1; M_2 represents a relative number of co-localized pixels in channel 1 or 2 as compared to the total number of pixels about thresholds (min. value 0: no co-localization, max value 1: all pixels co-localized). Co-localization was calculated only from the cytoplasmic region of measured cells, while fluorescence signal from the nucleus was disregarded.

Mitochondrial localization of pBcl-2(Ser70) and GSH was studied by fluorescence imaging 2 hours after Hyp photo-activation as a function of *pkcα* gene silencing. Figure 57 and corresponding Table 8 represent the results of co-localization analysis. Co-localization analysis was performed on fluorescence images by ZEN2010 Software (Zeiss, Germany) and co-localized pixels are presented as yellow points in the Figure 57. Confocal microscopy showed (Figure 57 A) that the pBcl-2(Ser70) is distributed through whole cells in control conditions. However, after Hyp photo-activation, strong re-localization of pBcl-2(Ser70) to mitochondria occurred in both, non-transfected and transfected PKCα$^-$ cells. There is evidence of co-localization between pBcl-2(Ser70) and mitochondria, but the information from the image is just qualitative. Co-localization coefficients calculated for better understanding and quantification of co-localization are presented in Table 8, where M_1 coefficient displays co-localization of the red pixels with green ones, and the M_2 coefficient displays co-localization of the green pixels with red ones. Quantitative results of the co-localization analysis (Table 8) describe (i) the presence of pBcl-2(Ser70) in mitochondria, (ii) co-localization of pBcl-2(Ser70) and GSH (iii) the presence of GSH in mitochondria. This means that we have observed a slight decrease of co-localization of pBcl-2(Ser70) and mitochondria 2 hours after Hyp photo-activation (M_2 = 0,91) compared with control

cells (M_2 = 0,99). A substantial decrease of co-localization between pBcl-2(Ser70) and mitochondria (M_2 = 0,75) was detected in transfected PKCα$^-$ cells after Hyp photo-activation. Figure 57 B shows confocal images of cells stained with ThiolTracker™ Violet (green fluorescence) and primary antibody against pBcl-2(Ser70) (red fluorescence). Under control conditions GSH (green) is distributed throughout the cells. Co-localization between pBcl-2(Ser70) and GSH was calculated from only the cytoplasmic region of measured cells, while the fluorescence signal from the nucleus was disregarded. Under control conditions, co-localization images show that GSH is co-localized with pBcl-2(Ser70) (M_2 = 0,99). Decreased co-localization was observed after Hyp photo-activation (M_2 = 0,88) in non-transfected cells compared to the control. A considerable decrease of the co-localization was related to *pkcα* gene silencing (M_2= 0,73) in transfected PKCα$^-$cells exposed to photo- activation of Hyp.

Finally, we investigated co-localization between GSH (green fluorescence) and mitochondria (red fluorescence). Figure 57 C shows confocal images of cells stained with ThiolTracker™ Violet and MitoTracker® Red FM. Under control conditions some portion of GSH was strongly associated with mitochondria (M_2= 0,96). After Hyp photo-activation, redistribution of GSH to cellular membranes was detected, and the association of GSH with mitochondria was still evident (M_2= 0,98). In transfected PKCα$^-$ cells co-localization coefficients suggested that photo-activation of Hyp after *pkcα* gene silencing (M_2= 0,88) affects and decreases the presence of GSH in mitochondria.

pkcα gene silencing decreases co-localization of Bcl-2 and GSH with mitochondria and reduces co-localization of GSH with Bcl-2.

Taking all together our observations suggest that the decrease of Bcl-2 phosphorylation due to *pkcα gene* silencing is on the origin of all the following Hyp photo-induced effects. Consecutive decrease of GSH and Bcl-2 binding to mitochondria dramatically reduces cellular antioxidant defense and leads to a higher production level of intracellular ROS at the mitochondrial level.

THE EFFECT OF PKCδ ON HYPERICIN PHOTO-INDUCED CELL DEATH

From the regulation point of view PKCδ has two faces. It is considered to be pro-apoptotic protein and plays a critical role in the regulation of various cellular processes, including cell proliferation, cell death, and tumor promotion but it is also important to recognize that PKCδ not only induces apoptosis, but can also function as an anti-apoptotic protein during receptor-initiated cell death and confer resistance to anticancer drugs. Furthermore, PKCδ is required for the survival of several cancers. The function of PKCδ depends on various factors, including its localization, tyrosine phosphorylation, and the presence of other pro- and anti-apoptoic signaling molecules. [90].

In the next chapter the effect of PKCδ on the cell death pathway after pkcδ gene silencing and Hyp photo-activation was explored.

3.20 *PKCδ* GENE SILENCING

Like in the case of post-transcriptional silencing of *pkcα gene* in U87-MG cells siRNA PKCδ(h) was used for post-transcriptional silencing of pkcδ gene as well. Distribution of PKCδ was monitored by fluorescence microscopy on cells which were not treated with siRNAδ (control cells) and transfected PKCδ$^-$cells. Fluorescence intensity of primary antibody for PKCδ (pSer645) stained with Alexa Fluor® 546 is lower in cells where expression of pkcδ gene was silenced (Figure 58 B) when compared to control cells (A). Silencing of pkcδ gene was confirmed by western blot analysis where optical density of transfected PKCδ$^-$ cells was 31,8% when compared to non-transfected cells with optical density 68,2%. β-actin determined in both samples was used as reference protein. After verification of post-transcriptionally silencing pkcδ gene another set of experiments was performed to find out how decreasing of PKCδ expression in U87-MG cells has effect on the cell survival, cell death pathway and ROS production after Hyp photo-activation.

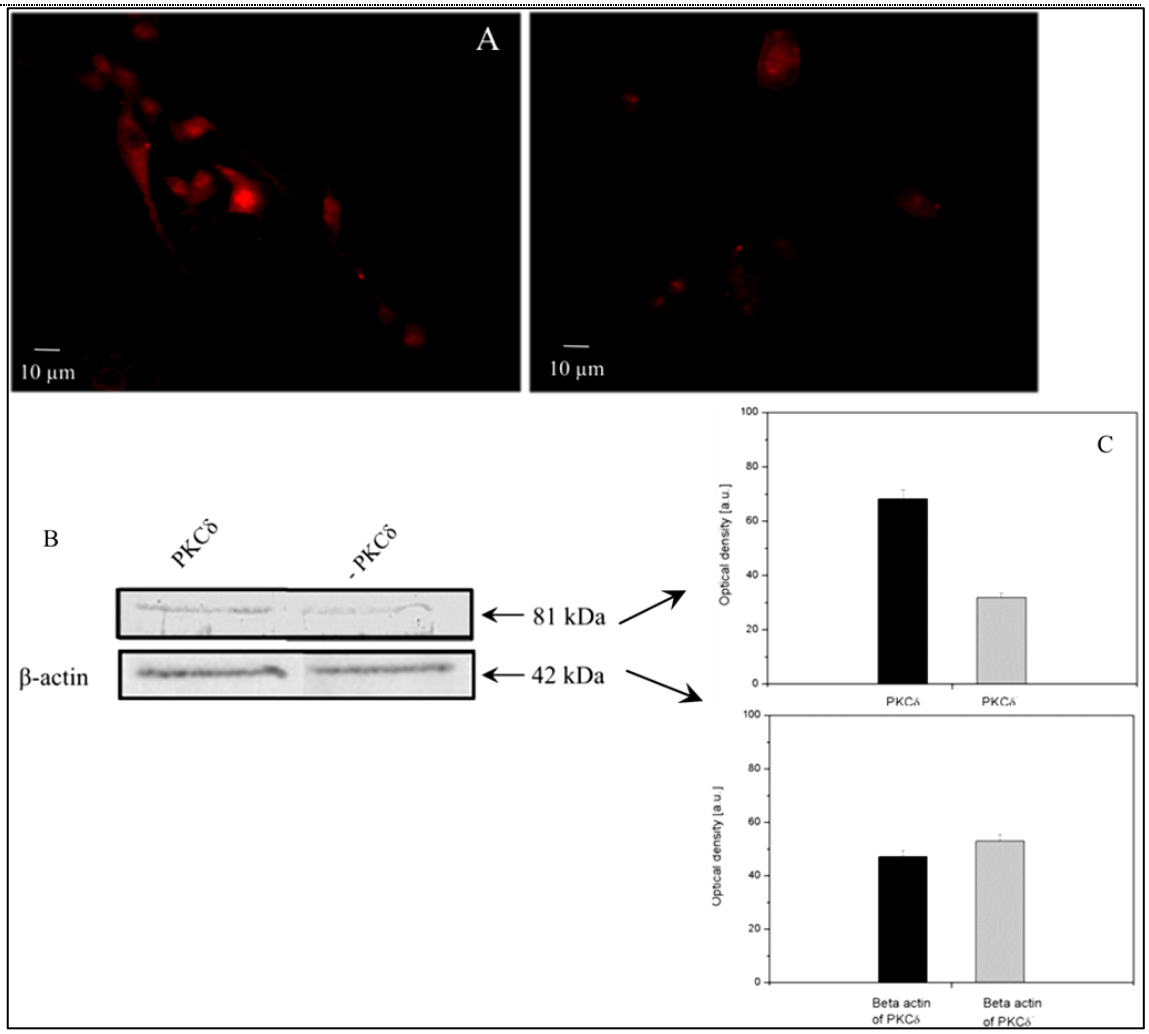

Figure 58: Distribution of PKCδ in the human U87-MG cells

A: The figure shows fluorescence image ofU87-MG non-transfected control cells (left) and cells transfected with siRNA PKCδ(h) (right) both stained with primary Ab against PKCδ (Acris antibodies, USA) for visualization of distribution of PKCδ. In both cases images were taken with the same measuring parameters (brightness, contrast and laser power). The scale bar represents 10 µm.

B: Western blot analysis of endogenous expression of PKCδ in non-transfected and transfected (PKCδ$^-$) U87-MG cells. The membranes were probed with Ab (Acris antibodies, USA). As protein reference control anti β-actin antibody (Abcam, GB) was used.

C: Evaluation of the optical density bands from the western blot analysis by ImageJ software. Values are mean ± S.D. of three independent experiments.

siRNA PKCδ(h) specifically blocks the pkcδ gene expression without having any impact on the other isoforms of PKC protein family.

3.21 CELL SURVIVAL AFTER PKCδ GENE SILENCING AND HYP PHOTO-ACTIVATION

The examining of the effect of pkcδ *gene silencing* on the cell survival after Hyp photo-activation was tested through MTT colorimetric assay (Figure 59). The obtained results were slightly different to those obtained for *pkcα gene* silencing.

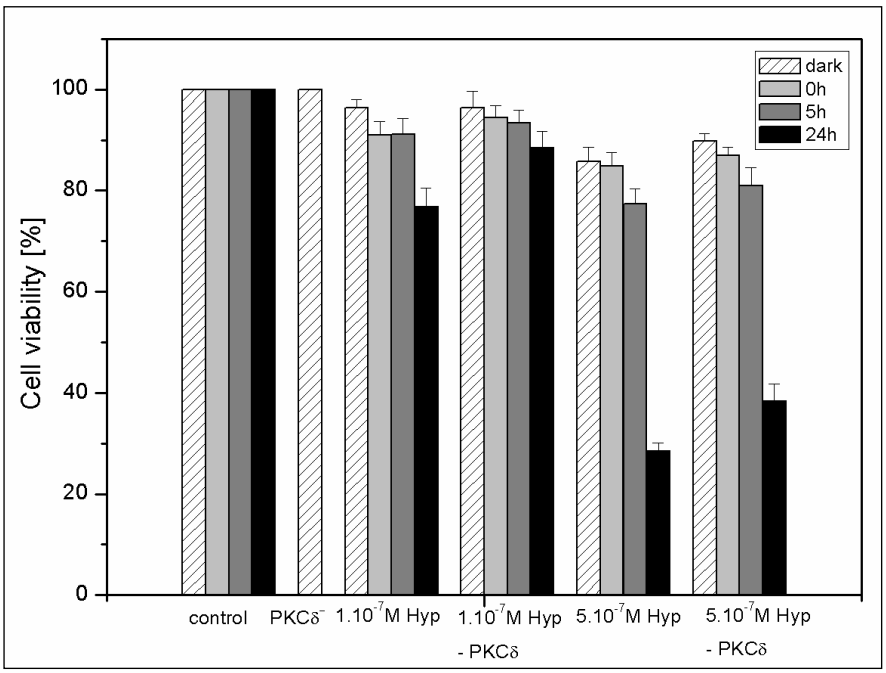

Figure 59: Cell viability test of non-treated and siRNA PKCδ(h) treated U87-MG cells before and after Hyp photo-activation.

Viability of non-transfected U87-MG cells and cells transfected with siRNAPKCδ(h) after Hyp photo-activation was determined by the MTT test. The cells were plated into 96-well tissue culture plates at the density of 10 000 cells per well and were cultivated until an optimal population density was reached. Cells were incubated with Hyp and Hyp photo-activation protocol was used. Results of adherent cell numbers from three independent experiments are expressed relative to control (100%) and represent mean values.

MTT tests were assessed with two concentrations of Hyp where, as expected, $5x10^{-7}$ M Hyp was more effective when compared to $1x10^{-7}$ M concentration. From the amount of cell viability (%) point of view for transfected PKCδ^{-} cells the amount of living cells was a higher compared to non-treated cells even though the difference between non-transfected and transfected PKCδ^{-} cells was little. PKCδ generally

functions as a pro-apoptotic protein during DNA damage–induced apoptosis [90], so silencing of pkcδ gene can cause that transfected PKCδ$^-$ cells were more viable after Hyp photo-activation.

pkcδ gene silencing has a little impact on the cell survival after Hyp photo-activation. Transfected PKCδ$^-$ cells are more viable after Hyp photo-activation.

3.22 DETECTION OF APOPTOSIS/NECROSIS AFTER HYP PHOTO-ACTIVATION

In the next step, determination of the cell death after Hyp photo-activation in the control and transfected PKCδ$^-$cells was performed by flow cytometry. For the detection of apoptosis/necrosis after Hyp photo-activation cells were stained with Annexin V-FITC/PI. Three major populations of cells were observed in the cytotoxicity assay: Annexin V$^-$/PI$^-$ cells were defined as live cells, Annexin V$^+$/PI$^-$ cells as apoptotic, and PI$^+$ as death cells (late apoptotic or necrotic).

As it was already mentioned cells incubated with Hyp undergo apoptosis after Hyp photo-activation [75][163] and our results discussed in the previous chapter (Chapter 3.16) where the cell death after Hyp photo-activation in the cells treated with siRNA PKCα was examined showed that in this case cell death pathway is different and cells undergo necrosis prior to apoptosis after irradiation. Blocking of expression of pro-apoptotic protein PKCδ did not influence the type of cell death (apoptosis/necrosis). Figure 60 shows the percentage of Hyp photo-induced apoptotic and necrotic cells in the control cells and cells treated with siRNAδ 24 after irradiation. Post-transcriptional silencing of pkcδ gene in U87-MG cells after Hyp photo-activation does not have any impact on the way of the cell death pathway. Here again the effect on the cell surviving of the transfected PKCδ$^-$ cells after Hyp photo-activation can be observed where amount of the dead transfected PKCδ$^-$ cells was lower when compared to non-transfected cells. This result is in agreement with MTT test described above (Figure 59).

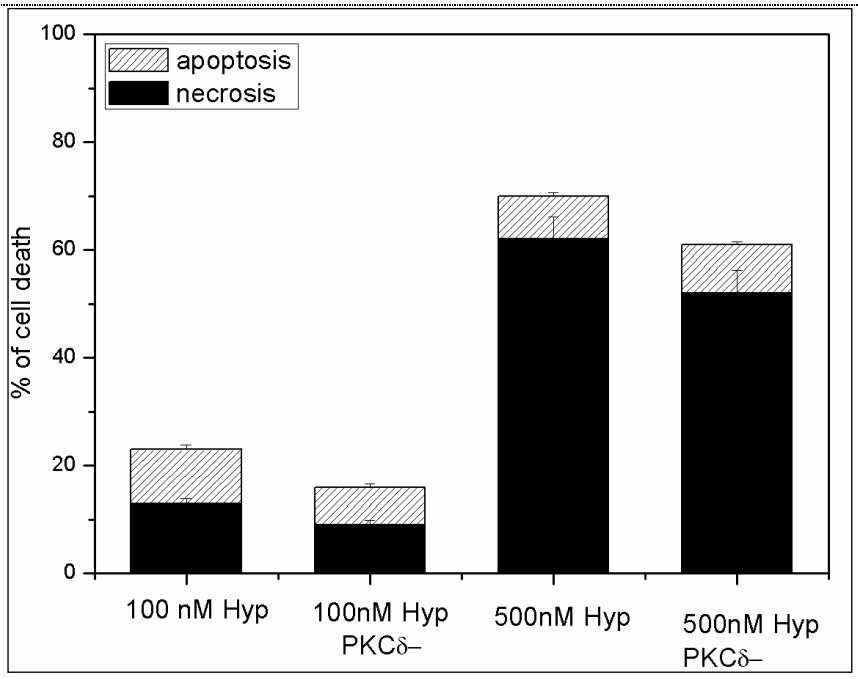

Figure 60: Determination of the cell death (apoptosis/necrosis) induced by photo-activated Hyp within 24 hours after cell irradiation

Histograms showing the comparison ratio of apoptosis and necrosis (live cells are not considered) in the cells non-treated and treated with siRNA PKCδ(h) 24 hours after Hyp photo-activation. Values are mean ± S.D. of three independent experiments.

pkcδ gene silencing does not have any impact on the type of Hyp photo-induced cell death.

3.23 EXAMINATION OF THE ROS PRODUCTION

As it was already mentioned one of the key regulators of the cell survival is level of ROS formation. Because decreasing of PKCδ proliferation in the glioma cells did not have any impact on the cell death pathway, ROS production was investigated in non-transfected and transfected PKCδ$^-$ cells.

For the set of flow cytometry experiments CellROX Deep Red™ was used for ROS production in the non-treated and treated PKCδ$^-$ cells 0, 1 and 3 hours after Hyp photo-activation. A substantial difference between transfected PKCδ$^-$ and non-

transfected cells was observed (Figure 61). When control cells were compared to cells with transfected PKCδ$^-$ cells we found out that the level of the ROS production after Hyp photo-activation in the cells without siRNA treatment was immediately increased. On the other side, in the transfected PKCδ$^-$ cells ROS formation after Hyp photo-activation was significantly decreased. This phenomenon can be observed for both concentrations of Hyp ($1x10^{-7}$M and $5x10^{-7}$M).

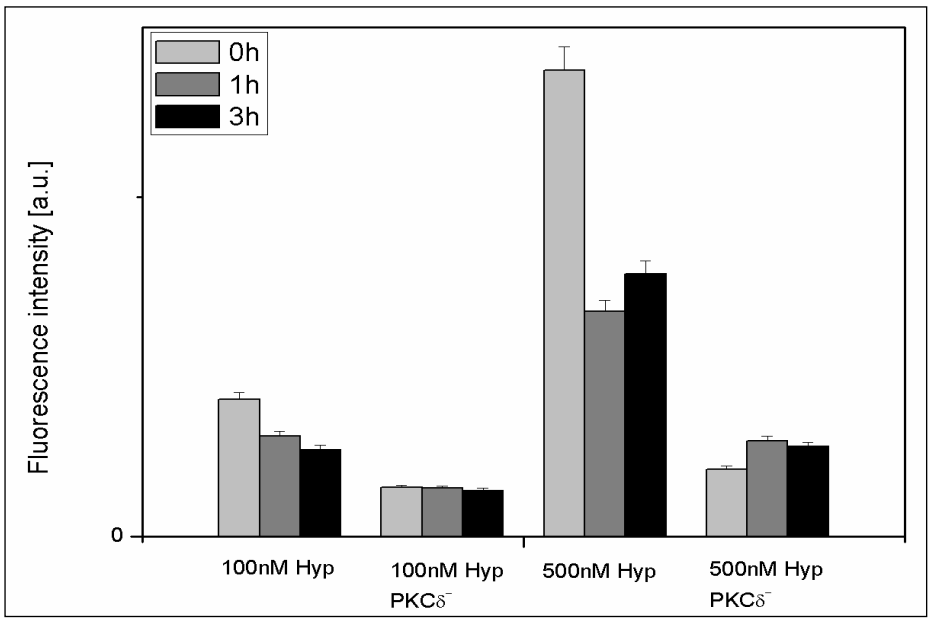

Figure 61: ROS production after Hyp photo-activation

Histograms of ROS production obtained by flow cytometry after CellROXDeepRed™ staining in non-transfected cells and cells transfected with siRNA PKCδ(h) 1 hour after Hyp photo-activation.

This result from flow cytometry can explain why the amount of cell death was slightly lower in the transfected PKCδ$^-$ cells. Transfected PKCδ$^-$ cells did not produce as much ROS as control cells and they were a little bit more viable after Hyp photo-activation. PKCδ is known for its apoptotic properties and is involved in the cellular response to DNA damage and oxidative stress [174]. Our results show that blocking of pkcδ gene blocks the induction of oxidative stress (ROS production) which results in higher cell viability of transfected PKCδ$^-$ cells after Hyp photo-activation compared to control cells.

pkcδ gene silencing decreases the intracellular photo-induced ROS production.

3.24 LOCALIZATION OF BAK AND BAX

From the literature [75][163] as well as from our results (Figure 62) it was observed that apoptosis is the type of cell death pathway which is followed after Hyp photo-activation. In most cases, cells undergo oxidative stress related apoptosis via an intrinsic death pathway, in which the key role play mitochondria and Bcl-2 family of proteins [175]. Bcl-2 proteins can act as pro-apoptotic or anti-apoptotic regulators [176][177] and the outer mitochondrial membrane (OMM) is their main site of action. However, except of mitochondria there have been reports of other cell localization of Bcl-2 proteins such as endoplasmic reticulum and in the nucleus [178]-[179][180]. Most anti-apoptotic Bcl-2 proteins can be constitutively found in the OMM and endoplasmic reticulum in normal healthy cells. Bak, pro-apoptotic protein, is localized on the OMM and on the other side Bax can be predominantly found in the cytosol [181].

In the Balogova et al. study expression patterns of Bak and Bax in U87-MG cells before and after Hyp photo-activation was studied [182]. The occurrence of two distinct mitochondria populations was observed. One contained both proteins simultaneously and the other contained Bax only. By immunocytochemistry we studied the translocation of Bak and Bax in transfected PKCδ$^-$ cells and compared them to the control non-transfected cells. Incubation of cells with siRNAδ without Hyp photo-activation leads to the translocation of both Bak and Bax from cytosol to mitochondria near the plasma membrane (Figure 62 B). It was observed that PKCδ catalytic fragment activated Bax and caused its redistribution and release of cytochrome *c*, activation of the caspase cascade, and loss of inner mitochondrial membrane integrity [185]. It was shown that PKCδ in preeclamptic platentas promotes Bax dissociation from 14-3-3 ζ through the phosphorylation of 14-3-3ζ [186]. Other interaction between PKCδ and Bak/Bax proteins was not described. Taking in to account that similar to other PKCs, activation of PKCδ stimulates its translocation to cellular membrane and increases its serine/threonine kinase activity silencing of pkcδ gene can cause translocation of Bak and Bax to the mitochondria near the plasma membrane as tendency of the Bak and Bax protein to interact and "find" PKCδ throughout the cell.

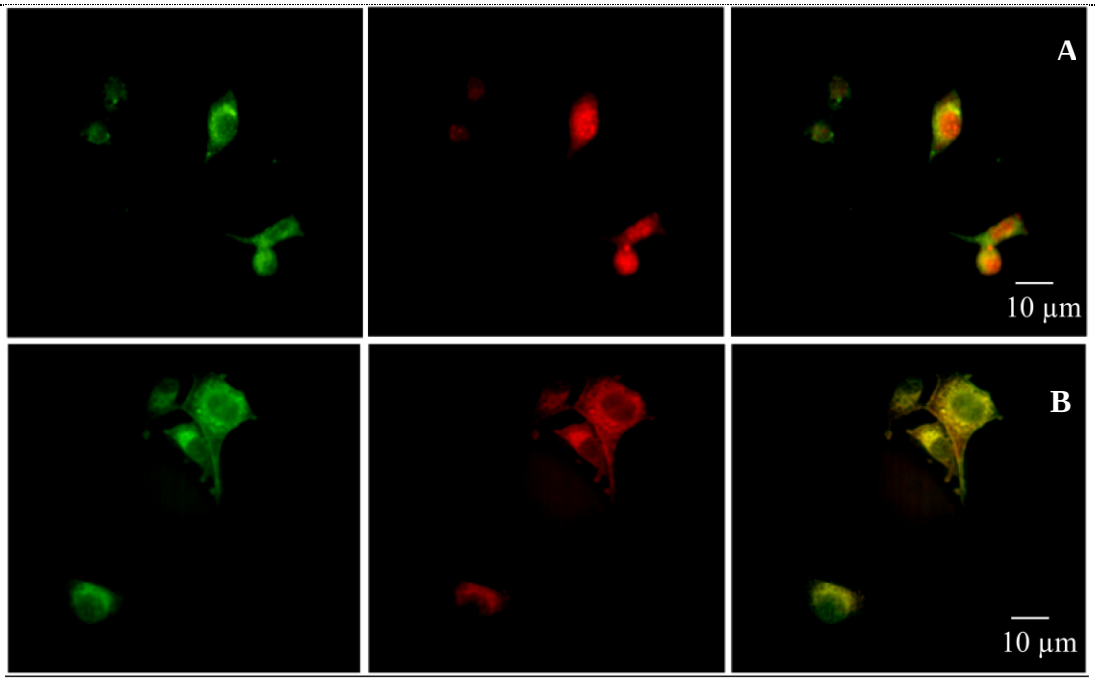

Figure 62: Fluorescence imaging of Bak and Bax localization after Hyp photoactivation.

The figures show fluorescence image of U87-MG non-transfected control cells (first row) andcells transfected with siRNA PKCδ(h) (second row). All the samples were stained with primary Ab against Bak (green fluorescence) and Bax (red fluorescence) for visualization of distribution of Bak and Bax. The scale bar represents 10 µm.

Taking all together, blocking the expression of pro-apoptotic PKCδ has a little impact on the cell survival favoring the cell survival after Hyp photo-activation and has no impact on the type of Hyp photo-induced cell death. Level of ROS production after Hyp photo-activation was significantly decreased compared to non-transfected cells. Pure pkcδ gene silencing translocates Bak and Bax towards mitochondria near the plasma membrane as tendency of the Bak and Bax protein to interact and "find" PKCδ throughout the cell.

4 CONCLUSION AND SUMMARY

Two main problems were studied in this thesis. One was focused on the developing of efficient nano-delivery transport system which would help to keep Hyp inside LDL. In this topic, not only interaction of Hyp with LDL was studied, but other possible lipid particles were examined as well. Incorporation and redistribution of Hyp from HDL was monitored from kinetics point of view and synthetic lipid-based nano-particles able to transport Hyp were produced. Our nano-delivery transport system will be used in the PDT treatment where after Hyp photo-activation cell death will occur. During the cell death PKC isoforms (α and δ) play among other processes important role. In the second part of the study mechanism of the cell death pathway after gene silencing of PKCα and PKCδ was studied. In the beginning of my thesis two main objectives were given and the summarized results are presented in these conclusions:

1.) to optimize properties of [LDL-Hyp]/DCh delivery system, study the cellular uptake of Hyp delivered by complex [LDL-Hyp]/Dch and its intracellular redistribution which included the development of a synthetic LDL based delivery system and beside nanodelivery system based on the LDL molecules to study and characterize the interaction of HDL with Hyp as well.

It was showed that cholesterol-modified dextran is a good solution for Hyp anchoring inside LDL particles. Three cholesterol modified dextrans with different cholesterol moiety were synthetized and the most efficient one was chosen. D_{Ch} 3 was proven to be the most effective. The redistribution of Hyp from [LDL-Hyp] complexes covered by D_{Ch} 3 was reduced by 27% when compared to the redistribution of Hyp from complex not covered by $D_{Ch.}$ Covering of the LDL particles by cholesterol-modified dextran was applied for the patent. Modification of LDL by D_{Ch} could possibly modify and inhibit the recognition of LDL particles through LDLR. By flow cytometry analysis and confocal fluorescence microscopy it was showed that modification of the LDL surface does not influence the cellular uptake of [LDL-Hyp]/ D_{Ch} complexes. Flow cytometry analysis showed that for 37°C the process of uptake of

LDL by endocytosis was almost identical when D_{Ch} was or was not present. By confocal fluorescence microscopy it was shown that [LDL-Hyp]/ D_{Ch} complex is able to deliver higher amount of Hyp to the cells when cells are incubated with [LDL-Hyp]/ D_{Ch} in the lipid containing medium. Preparation of sLDL according to Nikanjam et al. protocol turned out to be not suitable carriers for Hyp since Hyp was not able to incorporate to these particles. sLNP were alternatively synthetized and their ability of Hyp incorporation as well as similar behavior of Hyp inside sLNP like Hyp inside LDL was showed. First attempts to find the right ratio (concentration) between sLNP, Hyp and D_{Ch} in order to minimalize/decrease Hyp redistribution from these particles towards free lipids was done, but further investigation to find the best ratio is required in the future. It was also showed that even if sLNP does not have LDL receptor binding domain of ApoB-100 these particles can enter cells probably through endocytosis. In the future plans DARPins will be attached to the surface of sLNP which will make this delivery system highly tumor targeted. The influence of cholesterol on the Hyp incorporation was studied and it was shown that the presence of cholesterol in LUV leads probably to a higher local Hyp concentration around cholesterol rich domains. As consequence of this fact, a formation of non-fluorescent Hyp aggregates around these domains is reached at lower total Hyp concentration than in the case when cholesterol is not present in LUV. Incorporation of Hyp into HDL particles was studied and it was showed that until molar ratio HDL-Hyp = 1:8 Hyp is incorporated into HDL as monomers. At higher ratios Hyp starts to form non-fluorescent aggregates. The number of Hyp molecules which can exist in the fully monomeric state in the HDL particles is different from that in the case of LDL molecules (8 *vs* 30). This difference is mainly related to the smaller size of HDL molecule in comparison with LDL molecule (11 nm *vs* 22 nm). The kinetics of the association of Hyp molecules with free HDL particles, HDL-Hyp = 1:10 complex as well as the redistribution of Hyp molecules from over-loaded HDL-Hyp = 1:70 complex to free HDL molecules reveal a qualitative similar characteristics of these processes with those obtained for the association of Hyp with LDL. However, some quantitative differences have been detected. In the presence of LDL, the major part of Hyp is incorporated into lipoprotein particles in the slow phase (ca 65 %). On the other hand, in the presence of HDL this statement is valid only for the very low HDL-Hyp ratios (1:1 and 1:2). Higher HDL-Hyp ratios lead to a situation

when most of Hyp molecules is incorporated into lipoprotein in the rapid phase. The lower concentration of cholesterol molecules in outer shell of HDL particles is probably the determining factor for the more rapid kinetics of Hyp incorporation to and redistribution from these molecules when comparing with LDL particles.

2.) to study molecular mechanism of the photodynamic induced cell death: understand the impact of PKCα and PKCδ on the cell death after knocking out their expression in U87-MG cells.

The contribution of PKCα in the cell death induced by photo-activated Hyp was investigated. It was shown that blocking of PKCα expression by siRNA results in significant difference of type of cell death after Hyp photo-activation. The level of necrosis was considerably increased in PKCα- transfected cells as the consequence of higher ROS production. It was shown that the Hyp photo-induced decrease of the phosphorylation level of Bcl-2 protein on Ser70 enhanced after silencing of *pkcα* gene. Such enhancement can explain decreased amount of apoptotic cells and could be considered as another reason of increased necrosis after Hyp photo-activation in transfected PKCα^{-} cells. Moreover, silencing of pkcα gene and subsequent Hyp photo-activation causes significant decrease of co-localization of pBcl-2(Ser70) with mitochondria, pBcl-2(Ser70) with GSH and affects and decreases the presence of GSH in mitochondria. In summary: post-transcriptional silencing of *pkcα* gene significantly increased necrosis as a consequence of acute oxidative stress in relation to the level of Bcl-2 phosphorylation and reduced anti-oxidant protection of mitochondria. Post-transcriptional silencing of *pkcδ* gene did not influence the type of cell death (apoptosis or necrosis), however amount of death cells (%) where PKCδ was not blocked was higher compared to cells with blocked PKCδ. This can be due to the fact that production of ROS was notably decreased in cells treated with siRNAδ. It was shown that inhibition of PKCδ leads to translocation of Bak and Bax from cytosol to mitochondria located near the plasma membrane. This translocation can be explained as effort of cells to target possible PKC after reduction of cytosolic PKCδ in cells.

5 PUBLICATIONS OF JAROSLAVA JONIOVA

Joniova J., Buriankova L., Buzova D., Miskovsky P. and Jancura D. 'Kinetics of incorporation/redistribution of photosensitizer hypericin to/from high-density lipoproteins' *Internation Journal of Pharmaceutics;* 475(1-2): 578-584, (2014)

Joniova J., Misuth M., Sureau F., Miskovsky P. and Nadova Z. 'An importance of PKCα expression on Bcl-2 phosphorylation: Consequence on the cell death induced by photo-activated Hypericin', *Apoptosis,* 10.1007/s10495-014-1043-7

Joniova J., Blascakova L., Jancura D., Nadova Z., Sureau F. and Miskovsky P. 'Incorporation of photosenzitizer hypericin into synthetic lipid-based nano-particles for drug delivery and large unilamellar vesicles with different content of cholesterol', *Proc. SPIE 9166, Biosensing and Nanomedicine VII, 916604,* 2014. (invited to *International Journal of Nanophotonics*)

Buzova D., Huntosova V., Kasak P., Petrovajova D., **Joniova J.**, Dzurova L., Nadova Z., Sureau F., Miskovsky P., and Jancura D. 'Towards Increased Selectivity of Drug Delivery to Cancer Cells: Development of a LDL-Based Nanodelivery System for Hydrophobic Photosensitizers', *Proc. SPIE. 8460, Biosensing and Nanomedicine V, 84600U, 2012.*

6 ORAL AND POSTER PRESENTATIONS

(presented by underlined author)

Jaroslava Joniova, Ludmila Blascakova, Daniel Jancura, Zuzana Danova, Franck Sureau and Pavol Miskovsky: *Incorporation of photosenzitizer hypericin into synthetic lipid-based nano-particles for drug delivery and large unilamellar vesicles with different content of cholesterol*; SPIE Optics+Photonics 2014-San Diego, USA, August 2014 (oral presentation)

Zuzana Nadova, **Jaroslava Joniova**, Matus Misuth, Franck Sureau and Pavol Miskovsky: *The role of PKCα in cell death induced by photo-activated Hypericin*; VI Slovak Biophysical Symposium, Martin, Slovakia, March 2014 (oral presentation)

Jaroslava Joniova, Diana Buzova, Peter Kasak, Daniel Jancura, Franck Sureau and Pavol Miskovsky: *Modified LDL particles: a potential drug delivery systems*; Week of Doctoral Studies - Nový Smokovec, Slovakia, May 2012 (poster presentation)

Diana Buzova, Veronika Huntosova, Peter Kasak, Dana Petrovajova, **Jaroslava Joniova**, Lenka Dzurova, Zuzana Nadova, Franck Sureau, Pavol Miskovsky and Daniel Jancura: *Towards Increased Selectivity of Drug Delivery to Cancer Cells: Development of a LDL-Based Nanodelivery System for Hydrophobic Photosensitizers*I; SPIE Optics+Photonics 2012, San Diego, USA, August 2012 (poster presentation)

Jaroslava Joniova, Diana Buzova, Pavol Miskovsky, Franck Sureau: *Dynamic study of native LDL-based drug nanodelivery system for photodynamic therapy*; ESP Photobiology School, Brixen, Italy, June 2012 (poster presentation)

Jaroslava Joniova, Peter Kasak, Pavol Miskovsky and Franck Sureau*: A new LDL based nano-delivery system for PDT coated with modified dextran*; Journées de Rentrée de l'Ecole Doctorale iViv, Paris, France, November 2012 (poster presentation)

Jaroslava Joniova, Juraj Kronek, Zuzana Nadova, Franck Sureau and Pavol Miskovsky: *Study of native LDL-based drug nanodelivery system for photodynamic therapy*; 9th European Biophysics Congress EBSA, Lisbon, Portugal, July 2013 (poster presentation)

Ludmila Blascakova, **Jaroslava Joniova**, Juraj Kronek, Zuzana Nadova, Franck Sureau, Pavol Miskovsky and Daniel Jancura: *Construction and characterization of physico-chemical properties of drug delivery vehicle based on lipoproteins*; VI Slovak Biophysical Symposium, Martin, Slovakia, March 2014 (poster presentation)

Jaroslava Joniova, Matus Misuth, Franck Sureau, Pavol Miskovsky and Zuzana Nadova: *The effect of PKC δ on hypericin photo-induced cell death*; Regional Biophysical Conference, Smolenice, Slovakia, May 2014 (poster presentation)

Zuzana Nadova, **Jaroslava Joniova**, Matus Misuth, Franck Sureau and Pavol Miskovsky: *Altered expression of PKCs leads to differential response of human glioma cells (U87 MG) on photo-activated Hypericin (Hyp) and switches apoptosis to necrosis*; 37th American Society for Photobiology, San Diego, USA, June 2014 (poster presentation)

Jaroslava Joniova, Luboslava Buriankova, Diana Buzova, Pavol Miskovsky and Daniel Jancura: *Kinetics of incorporation/redistribution of photosensitizer hypericin to/from high - density lipoproteins*; 37th American Society for Photobiology, San Diego, USA, June 2014 (poster presentation)

Jaroslava Joniova, Zuzana Nadova, Pavol Miskovsky and Franck Sureau: Interaction of hypericin with synthetic lipid-based nano-particles for PDT drug delivery and large unilamellar vesicles with different content of cholesterol; 16th International Congress on Photobiology, Cordoba, Argentina, September 2014 (poster presentation)

Jaroslava Joniova, Matus Misuth, Franck Sureau, Pavol Miskovsky and Zuzana Nadova: *The effect of PKC δ on hypericin photo-induced cell death*; 12th Greta Pifat Mrzljak International School of Biophysics, September 2014 (poseter presentation)

7 FINANCIAL SUPPORT

My thesis was realized in co-tutoring program between Pavol Jozef Safarik University in Kosice and Piere et Marie Curie University in Paris (3 times 6 moths stays were supported by French government fellowship) and was supported by:

- Project CELIM funded by 7.FP EU
- International Program for Scientific Cooperation (PICS N°5398) from the French National Center of Scientific Research (CNRS)
- APVV-0242-11
- The Agency of the Ministry of Education of Slovak Republic for the Structural funds of the European Union:
- Operational program Research and Development-Doktorand, ITMS cod: 26110230013
- NanoBioSens ITMS cod: 26220220107
- KVARK
- VVGS PF 32/2011/F
- the European Society for Photobiology (ESP): - fellowship for attending the 16th International Congress on Photobiology, Cordoba, Argentina, September 2014.

8 REFERENCES

[1] JK. Lalla, Sunita Ogale, CV. Achhra, Meena Shah and Deven Parmar. 'Cancer', *IJRPC* , **Vol 3, No 1**, 26-33, 2013.

[2] Malvezzi, M., P. Bertuccio, F. Levi, C. La Vecchia, and E. Negri. 'European Cancer Mortality Predictions for the Year 2013', *Annals of Oncology* **Vol. 24, No. 3**, 792-800, 2013.

[3] Siegel Rebecca, Deepa Naishadham, and Ahmedin Jemal. 'Cancer Statistics, 2013', *Ca-a Cancer Journal for Clinicians* **Vol. 63, No. 1**, 11-30, 2013.

[4] Takimoto CH, Calvo E. 'Principles of Oncologic Pharmacotherapy', Pazdur R, Wagman LD, Camphausen KA, Hoskins WJ. *Cancer Management: A Multidisciplinary Approach* (11 ed.), 2005.

[5] Kratz F. 'Drug Delivery in Oncology: From Basic Research to Cancer Therapy', Germany: Wiley-VCH Verlag GmbH & Co. KGaA, p. 1822. ISBN 978–3–527–32823–9, 2012.

[6] Rosenberg, S. A. 'Progress in Human Tumour Immunology and Immunotherapy', *Nature* **Vol. 411, No. 6835**, 380-384, 2001.

[7] Jones, K. L., and A. U. Buzdar. 'A Review of Adjuvant Hormonal Therapy in Breast Cancer', *Endocrine-Related Cancer* **Vol. 11, No. 3**, 391-406, 2004.

[8] Enger, Eldon et al. 'Concepts in Biology', 2007 Edition. McGraw-Hill., p. 173. ISBN 978-0-07-126042-8, 2007.

[9] Daniell, M. D., and J. S. Hill. 'A History of Photodynamic Therapy', *Australian and New Zealand Journal of Surgery* **Vol. 61, No. 5**, 340-348, 1991.

[10] Dolmans, Dejgj, D. Fukumura, and R. K. Jain. 'Photodynamic Therapy for Cancer', *Nature Reviews Cancer* **Vol. 3, No. 5**, 380-387, 2003.

[11] Castano, Ana P., Tatiana N. Demidova, and Michael R. Hamblin. 'Mechanisms in Photodynamic Therapy: Part One-Photosensitizers, Photochemistry and Cellular Localization', *Photodiagnosis and Photodynamic Therapy* **Vol. 1, No. 4**, 279-293, 2004.

[12] Luksiene Z. 'Photodynamic therapy: mechanism of action and ways to improve the efficiency of treatment'. *Medicina* **Vol. 39 No. 12**, 1137-1150, 2003.

[13] Fisher, A. M. R., A. L. Murphree, and C. J. Gomer. 'Clinical and Preclinical Photodynamic Therapy', *Lasers in Surgery and Medicine* **Vol. 17, No. 1**, 2-31, 1995.

[14] Prasad P. N. 'Introduction to biophotonics', 1st edition, New Jersey, USA: John Wiley & Sons, Inc., p. 593; ISBN 0-471-28770- 9, 2003.

[15] Ho, Yunn-Fang, Ming-Huang Wu, Bor-Hen Cheng, Yar-Wen Chen, and Ming-Chih Shih. 'Lipid-Mediated Preferential Localization of Hypericin in Lipid Membranes', *Biochimica Et Biophysica Acta-Biomembranes* **Vol. 1788, No. 6**, 1287-1295, 2009.

[16] Kamuhabwa, A. R., P. Agostinis, M. A. D'Hallewin, A. Kasran, and P. A. De Witte. 'Photodynamic Activity of Hypericin in Human Urinary Bladder Carcinoma Cells', *Anticancer Research* **Vol. 20, No. 4**, 2579-2584, 2000.

[17] Miskovsky, P. 'Hypericin - a New Antiviral and Antitumor Photosensitizer: Mechanism of Action and Interaction with Biological Macromolecules', *Current Drug Targets***Vol. 3, No. 1**, 55-84, 2002.

[18] http://www.hawk-conservancy.org/Conservation/MeadowMuses/200509.shtml

[19] Kubin, A., F. Wierrani, U. Burner, G. Alth, and W. Grunberger. 'Hypericin - the Facts About a Controversial Agent', *Current Pharmaceutical Design* **Vol. 11, No. 2**, 233-253, 2005.

[20] Agostinis, P., A. Vantieghem, W. Merlevede, and P. A. M. de Witte. 'Hypericin in Cancer Treatment: More Light on the Way', *International Journal of Biochemistry & Cell Biology* **Vol. 34, No. 3**, 221-241, 2002.

[21] Fox, F. E., Z. T. Niu, A. Tobia, and A. H. Rook. 'Photoactivated Hypericin Is an Anti-Proliferative Agent That Induces a High Rate of Apoptotic Death of Normal, Transformed, and Malignant T Lymphocytes: Implications for the Treatment of Cutaneous Lymphoproliferative and Inflammatory Disorders', *Journal of Investigative Dermatology* **Vol. 111, No. 2**, 327-332, 1998.

[22] Ehrenberg, B., J. L. Anderson, and C. S. Foote. 'Kinetics and Yield of Singlet Oxygen Photosensitized by Hypericin in Organic and Biological Media', *Photochemistry and Photobiology* **Vol. 68, No. 2**, 135-140, 1998.

[23] Wynn, J. L., and T. M. Cotton. 'Spectroscopic Properties of Hypericin in Solution and at Surfaces', *Journal of Physical Chemistry* **Vol. 99, No. 12**, 4317-4323, 1995.

[24] Klionsky D.J. et al. 'Guidelines for the Use and Interpretation of Assays for Monitoring Autophagy', *Autophagy* **Vol. 8, No. 4**, 445-544, 2012.

[25] Hengartner, M. O. 'The Biochemistry of Apoptosis', *Nature* **Vol. 407, No. 6805**, 770-776, 2000.

[26] Kroemer G. 'Regulated Necrosis', Semin Cell Dev Biol, 2014.

[27] Golstein, P., and G. Kroemer. 'Cell Death by Necrosis: Towards a Molecular Definition', *Trends in Biochemical Sciences* **Vol. 32, No. 1**, 37-43, 2007.

[28] Robertson, C. A., D. H. Evans, and H. Abraharnse. 'Photodynamic Therapy (Pdt): A Short Review on Cellular Mechanisms and Cancer Research Applications for Pdt', *Journal of Photochemistry and Photobiology B-Biology* **Vol. 96, No. 1**, 1-8, 2009.

[29] Mathew, R.; Karantza-Wadsworth, V.; White, E. 'Role of autophagy in cancer', *Nat. Rev. Cancer*., **Vol 7**, 961-967, 2007.

[30] Kroemer, G.; Jaattela, M. 'Lysosomes and autophagy in cell death control', *Nat. Rev. Cancer*., **Vol 5**, 886-897, 2005.

[31] Robert C. Bast, Donald W. Kufe, Raphael E. Pollock, Ralph R. Weichselbaum, James F. Holland and Emil Frei. 'Holland-Frei Cancer Medicine', 5th edition, Hamilton (ON): BC Decker; ISBN-10: 1-55009-113-1, 2000.

[32] Ghobrial, I. M., T. E. Witzig, and A. A. Adjei. 'Targeting Apoptosis Pathways in Cancer Therapy', *Ca-a Cancer Journal for Clinicians* **Vol. 55, No. 3**, 178-194, 2005.

[33] Yang, Zhineng J., Cheng E. Chee, Shengbing Huang, and Frank A. Sinicrope. 'The Role of Autophagy in Cancer: Therapeutic Implications', *Molecular Cancer Therapeutics* **Vol. 10, No. 9**, 1533-1541, 2011.

[34] Maiuri, M. Chiara, Einat Zalckvar, Adi Kimchi, and Guido Kroemer. 'Self-Eating and Self-Killing: Crosstalk between Autophagy and Apoptosis', *Nature Reviews Molecular Cell Biology* **Vol. 8, No. 9**, 741-752, 2007.

[35] Kroemer, Guido, Guillermo Marino, and Beth Levine. 'Autophagy and the Integrated Stress Response', *Molecular Cell* **Vol. 40, No. 2**, 280-293, 2010.

[36] Garg A. D., Agostinis P. 'ER stress, autophagy and immunogenic cell death in photodynamic therapy-induced anti-cancer immune responses', *Photochem. Photobiol. Sci.* **Vol 13**, 474-487, 2014.

[37] Kroemer, G., P. Petit, N. Zamzami, J. L. Vayssiere, and B. Mignotte. 'The Biochemistry of Programmed Cell-Death', *Faseb Journal* **Vol. 9, No. 13**, 1277-1287, 1995.

[38] Marino, Guillermo, Mireia Niso-Santano, Eric H. Baehrecke, and Guido Kroemer. 'Self-Consumption: The Interplay of Autophagy and Apoptosis', *Nature Reviews Molecular Cell Biology* **Vol. 15, No. 2**, 81-94, 2014.

[39] Shimizu, S., T. Kanaseki, N. Mizushima, T. Mizuta, S. Arakawa-Kobayashi, C. B. Thompson, and Y. Tsujimoto. 'Role of Bcl-2 Family Proteins in a Non-Apoptotic Programmed Cell Death Dependent on Autophagy Genes', *Nature Cell Biology* **Vol. 6, No. 12**, 1221-1228, 2004.

[40] Boya, P., R. A. Gonzalez-Polo, N. Casares, J. L. Perfettini, P. Dessen, N. Larochette, D. Metivier, D. Meley, S. Souquere, T. Yoshimori, G. Pierron, P. Codogno, and G. Kroemer. 'Inhibition of Macroautophagy Triggers Apoptosis', *Molecular and Cellular Biology* **Vol. 25, No. 3**, 1025-1040, 2005.

[41] Shen, Han-Ming, and Patrice Codogno. 'Autophagic Cell Death Loch Ness Monster or Endangered Species?', *Autophagy* **Vol. 7, No. 5**, 457-465, 2011.

[42] Kroemer, G., B. Dallaporta, and M. Resche-Rigon. 'The Mitochondrial Death/Life Regulator in Apoptosis and Necrosis', *Annual Review of Physiology* **Vol. 60**, 619-642, 1998.

[43] Majno, G., and I. Joris. 'Apoptosis, Oncosis, and Necrosis - an Overview of Cell-Death', *American Journal of Pathology* **Vol. 146, No. 1**, 3-15, 1995.

[44] Kroemer, Guido, and Beth Levine. 'Autophagic Cell Death: The Story of a Misnomer', *Nature Reviews Molecular Cell Biology* **Vol. 9, No. 12**, 1004-1010, 2008.

[45] Galluzzi L, et al. Molecular mechanisms of regulated necrosis. Semin Cell Dev Biol (2014),

[46] Holler, N., R. Zaru, O. Micheau, M. Thome, A. Attinger, S. Valitutti, J. L. Bodmer, P. Schneider, B. Seed, and J. Tschopp. 'Fas Triggers an Alternative, Caspase-8-Independent Cell Death Pathway Using the Kinase Rip as Effector Molecule', *Nature Immunology* **Vol. 1, No. 6**, 489-495, 2000.

[47] Degterev, Alexei, Zhihong Huang, Michael Boyce, Yaqiao Li, Prakash Jagtap, Noboru Mizushima, Gregory D. Cuny, Timothy J. Mitchison, Michael A. Moskowitz, and Junying Yuan. 'Chemical Inhibitor of Nonapoptotic Cell Death with Therapeutic Potential for Ischemic Brain Injury (Vol 1, Pg 112, 2005)', *Nature Chemical Biology* **Vol. 9, No. 3**, 192-192, 2013.

[48] Takahashi, N., L. Duprez, S. Grootjans, A. Cauwels, W. Nerinckx, J. B. DuHadaway, V. Goossens, R. Roelandt, F. Van Hauwermeiren, C. Libert, W. Declercq, N. Callewaert, G. C. Prendergast, A. Degterev, J. Yuan, and P. Vandenabeele. 'Necrostatin-1 Analogues: Critical Issues on the Specificity, Activity and in Vivo Use in Experimental Disease Models', *Cell Death & Disease* **Vol. 3**, 2012.

[49] Mroz, Pawel, Anastasia Yaroslavsky, Gitika B. Kharkwal, and Michael R. Hamblin. 'Cell Death Pathways in Photodynamic Therapy of Cancer', *Cancers* **Vol. 3, No. 2**, 2516-39, 2011.

[50] Kessel, D. 'Death pathways associated with photodynamic therapy', *Med. Laser. Appl.*, **Vol 21**, 219-224, 2006.

[51] Reiners, J.J.; Jr.; Agostinis, P.; Berg, K.; Oleinick, N.L.; Kessel, D. 'Assessing autophagy in the context of photodynamic therapy', *Autophagy* **Vol 6**, 7-18, 2010.

[52] Scherz-Shouval, R.; Shvets, E.; Fass, E.; Shorer, H.; Gil, L.; Elazar, Z. 'Reactive oxygen species are essential for autophagy and specifically regulate the activity of Atg4', *EMBO J.* **Vol 26**, 1749-1760, 2007.

[53] Sasnauskiene, A.; Kadziauskas, J.; Vezelyte, N.; Jonusiene, V.; Kirveliene, V. 'Apoptosis, autophagy and cell cycle arrest following photodamage to mitochondrial interior'. *Apoptosis* **Vol 14**, 276-286, 2009.

[54] Scherz-Shouval, R.; Elazar, Z. 'ROS, mitochondria and the regulation of autophagy', *Trends Cell. Biol*. **Vol 17**, 422-427, 2007.

[55] Kessel, D.; Oleinick, N.L. 'Initiation of autophagy by photodynamic therapy', *Methods Enzymol.* **Vol 453**, 1-16, 2009.

[56] Kessel, D.; Arroyo, A.S. 'Apoptotic and autophagic responses to Bcl-2 inhibition and photodamage', *Photochem. Photobiol. Sci*. **Vol 6**, 1290-1295, 2007.

[57] Kessel, D.; Reiners, J.J.; Jr. 'Apoptosis and autophagy after mitochondrial or endoplasmic reticulum photodamage', *Photochem. Photobiol*. Vol 83, 1024-1028, 2007.

[58] Stromhaug, P.E.; Berg, T.O.; Berg, K.; Seglen, P.O. 'A novel method for the study of autophagy: Destruction of hepatocytic lysosomes, but not autophagosomes, by the photosensitizing porphyrin tetra(4-sulphonatophenyl)porphine', *Biochem. J*., **Vol 321 (Pt 1)**, 217-225, 1997.

[59] Apel, A.; Herr, I.; Schwarz, H.; Rodemann, H.P.; Mayer, 'A. Blocked autophagy sensitizes resistant carcinoma cells to radiation therapy'. *Cancer Res*., **Vol 68**, 1485-1494, 2008.

[60] Oltvai, Z.N.; Millima, C.L.; Kosmeyer, S.J.; 'Bcl-2 heterodimerizes in vivo with the conserved homologue, Bax, that accelerates programmed cell death'. *Cell*, **Vol 74**, 609-619, 1993.

[61] Cory, S.; Adams, J.M. 'The Bcl2 family: Regulators of the cellular life-or-death switch', *Nat. Rev. Cancer*, **Vol 2**, 647-656, 2002.

[62] Ross, A.J.; Waymire,K.G.; Moss, J.E.; Parlow, A.F.; Skinner, M.K.; Russell, L.D.; MacGregor, G.R. 'Testicular degeneration in Bcl-w deficient mice', *Nature Genet.*, **Vol 18**, 251-256, 1998.

[63] Oleinick, N.L.; Morris, R.L.; Belichenko, I. 'The role of apoptosis in response to photodynamic therapy: What, where, why, and how'. *Photochem. Photobiol. Sci.*, **Vol 1**, 1-21, 2002.

[64] He, G.F.; Bian, M.L.; Zhao, Y.W.; Xiang, Q.; Li, H.Y.; Xiao, C. 'A study on the mechanism of 5-aminolevulinic acid photodynamic therapy in vitro and in vivo in cervical cancer', *Oncol. Rep*., **Vol 21**, 861-868, 2009.

[65] Chen, X.; Zhao, P.; Chen, F.; Li, L.; Luo, R. 'Effect and mechanism of 5-aminolevulinic acid-mediated photodynamic therapy in esophageal cancer. ', *Lasers Med. Sci*., **Vol 26**, 69-78, 2011.

[66] Amo, T.; Kawanishi, N.; Uchida, M.; Fujita, H.; Oyanagi, E.; Utsumi, T.; Ogino, T.; Inoue, K.; Shuin, T.; Utsumi, K.; Sasaki, J. 'Mechanism of cell death by 5-aminolevulinic acid-based photodynamic action and its enhancement by ferrochelatase inhibitors in human histiocytic lymphoma cell line U937', *Cell Biochem. Funct*., **Vol 27**, 503-515, 2009.

[67] Koval, J.; Mikes, J.; Jendzelovsky, R.; Kello, M.; Solar, P.; Fedorocko, P. 'Degradation of HER2 receptor through hypericin-mediated photodynamic therapy', *Photochem. Photobiol*., **Vol 86,** 200-205, 2010.

[68] Adams, J. M. & Cory, S. 'The Bcl-2 protein family: arbiters of cell survival', *Science*, **Vol 281**, 1322–1326, 1998.

[69] Antonsson, B. & Martinou, J. C. 'The Bcl-2 protein family', *Exp. Cell Res*. **Vol 256**, 50–57, 2000.

[70] Lavie, G.; Kaplinsky, C.; Toren, A.; Aizman, I.; Meruelo, D.; Mazur, Y.; Mandel, M. 'A photodynamic pathway to apoptosis and necrosis induced by dimethyl tetrahydroxyhelianthrone and hypericin in leukaemic cells: Possible relevance to photodynamic therapy', *Br. J. Cancer*, **Vol 79**, 423-432, 1999.

[71] Kessel, D.; Poretz, R.D. 'Sites of photodamage induced by photodynamic therapy with a chlorin e6 triacetoxymethyl ester (CAME) ', *Photochem. Photobiol.*, **Vol 71**, 94-96, 2000.

[72] Vercammen, D., R. Beyaert, G. Denecker, V. Goossens, G. Van Loo, W. Declercq, J. Grooten, W. Fiers, and P. Vandenabeele. 'Inhibition of Caspases Increases the Sensitivity of L929 Cells to Necrosis Mediated by Tumor Necrosis Factor', *Journal of Experimental Medicine* **Vol. 187, No. 9**, 1477-1485, 1998.

[73] Mellor, H., and P. J. Parker. 'The Extended Protein Kinase C Superfamily', *Biochemical Journal* **Vol. 332**, 281-292, 1998.

[74] Nishizuka, Y. 'Protein Kinases .5. Protein-Kinase-C and Lipid Signaling for Sustained Cellular-Responses', *Faseb Journal* **Vol. 9, No. 7**, 484-496, 1995.

[75] Dzurova, Lenka, Dana Petrovajova, Zuzana Nadova, Veronika Huntosova, Pavol Miskovsky, and Katarina Stroffekova. 'The Role of Anti-Apoptotic Protein Kinase Calpha in Response to Hypericin Photodynamic Therapy in U-87 Mg Cells', *Photodiagnosis and photodynamic therapy* **Vol. 11, No. 2**, 213-26, 2014.

[76] do Carmo, Analia, Joana Balca-Silva, Diana Matias, and Maria Celeste Lopes. 'Pkc Signaling in Glioblastoma', *Cancer Biology & Therapy* **Vol. 14, No. 4**, 287-294, 2013.

[77] http://www.rcsb.org/pdb/explore/explore.do?structureId=3GPE

[78] Torrecillas, A., S. Corbalan-Garcia, and J. C. Gomez-Fernandez. 'An Infrared Spectroscopic Study of the Secondary Structure of Protein Kinase C Alpha and Its Thermal Denaturation', *Biochemistry* **Vol. 43, No. 8**, 2332-2344, 2004.

[79] Whelan, R. D. H., and P. J. Parker. 'Loss of Protein Kinase C Function Induces an Apoptotic Response', *Oncogene* **Vol. 16, No. 15**, 1939-1944, 1998.

[80] Ruvolo, P. P., X. M. Deng, B. H. Carr, and W. S. May. 'A Functional Role for Mitochondrial Protein Kinase C Alpha in Bcl2 Phosphorylation and Suppression of Apoptosis', *Journal of Biological Chemistry* **Vol. 273, No. 39**, 25436-25442, 1998.

[81] Merino D, Bouillet P. 'The Bcl-2 family in autoimmune and degenerative disorders'. *Apoptosis* **Vol 14**, 570-583, 2009.

[82] Koc M, Nad'ova Z, Truksa J, Ehrlichova M, Kovar J. 'Iron deprivation induces apoptosis via mitochondrial changes related to Bax translocation' *Apoptosis* **Vol 10**, 381-393, 2005

[83] Ackermann EJ, Taylor JK, Narayana R, Bennett CF. 'The role of antiapoptotic Bcl-2 family members in endothelial apoptosis elucidated with antisense oligonucleotides'. *Journal of Biological Chemistry* **Vol 274**, 11245-11252, 1999.

[84] Blagosklonny MV, Giannakakou P, el-Deiry WS, et al. 'Raf-1/bcl-2 phosphorylation: a step from microtubule damage to cell death', *Cancer Res* Vol 57, 130-135, 1997.

[85] Voehringer DW. 'BCL-2 and glutathione: Alterations in cellular redox state that regulate apoptosis sensitivity', *Free Radical Biology and Medicine* **Vol 27**, 945-950, 1999.

[86] Franco R, Cidlowski JA. 'Apoptosis and glutathione: beyond an antioxidant', *Cell Death and Differentiation* **Vol 16**, 1303-1314, 2009.

[87] Circu ML, Aw TY. 'Glutathione and apoptosis', *Free Radical Research* Vol 42, 689-706, 2008.

[88] Wilkins HM, Marquardt K, Lash LH, Linseman DA. 'Bcl-2 is a novel interacting partner for the 2-oxoglutarate carrier and a key regulator of mitochondrial glutathione' F*ree Radical Biology and Medicine* Vol 52, 410-419, 2012.

[89] Kikkawa, U., H. Matsuzaki, and T. Yamamoto. 'Protein Kinase C Delta (Pkc Delta): Activation Mechanisms and Functions', *Journal of Biochemistry* **Vol. 132, No. 6**, 831-839, 2002.

[90] Basu, A., and D. Pal. 'Two Faces of Protein Kinase C Delta: The Contrasting Roles of Pkc Delta in Cell Survival and Cell Death', *The scientific world journal* **Vol. 10**, 2272-2284, 2010.

[91] Welman, Arkadiusz, John R. Griffiths, Anthony D. Whetton, and Caroline Dive. 'Protein Kinase C Delta Is Phosphorylated on Five Novel Ser/Thr Sites Following Inducible Overexpression in Human Colorectal Cancer Cells', *Protein Science* **Vol. 16, No. 12**, 2711-2715, 2007.

[92] Stempka, L., M. Schnolzer, S. Radke, G. Rincke, F. Marks, and M. Gschwendt. 'Requirements of Protein Kinase C Delta for Catalytic Function - Role of Glutamic Acid 500 and Autophosphorylation on Serine 643', *Journal of Biological Chemistry* **Vol. 274, No. 13**, 8886-8892, 1999.

[93] Le Good, J. A., W. H. Ziegler, D. B. Parekh, D. R. Alessi, P. Cohen, and P. J. Parker. 'Protein Kinase C Isotypes Controlled by Phosphoinositide 3-Kinase through the Protein Kinase Pdk1', *Science* **Vol. 281, No. 5385**, 2042-2045, 1998.

[94] Steinberg, S. F. 'Distinctive Activation Mechanisms and Functions for Protein Kinase C Delta', *Biochemical Journal* **Vol. 384**, 449-459, 2004.

[95] Berridge, M. J., and R. F. Irvine. 'Inositol Trisphosphate, a Novel 2nd Messenger in Cellular Signal Transduction', *Nature* **Vol. 312, No. 5992**, 315-321, 1984.

[96] Dekker, L. V., and P. J. Parker. 'Protein-Kinase-C - a Question of Specificity', *Trends in Biochemical Sciences* **Vol. 19, No. 2**, 73-77, 1994.

[97] Blass, M., I. Kronfeld, G. Kazimirsky, P. M. Blumberg, and C. Brodie. 'Tyrosine Phosphorylation of Protein Kinase C Delta Is Essential for Its Apoptotic Effect in Response to Etoposide', *Molecular and Cellular Biology* **Vol. 22, No. 1**, 182-195, 2002.

[98] Griffiths, G., Garrone, B., Deacon, E. M., Owen, P. J., Mead, G., Bradwell, A., Watters, D., and Lord, J. M. 'The polyether Bistratene A selectively activates protein kinase C-d in HL60 cells'. *Biochem. Biophys. Res Commun.* **222,** 802–808; 1996.

[99] Lu, Z. M., A. Hornia, Y. W. Jiang, Q. Zang, S. Ohno, and D. A. Foster. 'Tumor Promotion by Depleting Cells of Protein Kinase C Delta', *Molecular and Cellular Biology* **Vol. 17, No. 6**, 3418-3428, 1997.

[100] Basu, A., and G. R. Akkaraju. 'Regulation of Caspase Activation and Cis-Diamminedichloroplatinum(Ii)-Induced Cell Death by Protein Kinase C', *Biochemistry* **Vol. 38, No. 14**, 4245-4251, 1999.

[101] Koivunen, J., V. Aaltonen, and J. Peltonen. 'Protein Kinase C (Pkc) Family in Cancer Progression', *Cancer Letters* **Vol. 235, No. 1**, 1-10, 2006.

[102] Teicher, Beverly A. 'Protein Kinase C as a Therapeutic Target', *Clinical Cancer Research* **Vol. 12, No. 18**, 5336-5345, 2006.

[103] Moriya, S., A. Kazlauskas, K. Akimoto, S. Hirai, K. Mizuno, T. Takenawa, Y. Fukui, Y. Watanabe, S. Ozaki, and S. Ohno. 'Platelet-Derived Growth Factor Activates Protein Kinase C Epsilon through Redundant and Independent Signaling Pathways Involving Phospholipase C Gamma or Phosphatidylinositol 3-Kinase', *Proceedings of the National Academy of Sciences of the United States of America* **Vol. 93, No. 1**, 151-155, 1996.

[104] Pettitt, T. R., and M. J. O. Wakelam. 'Diacylglycerol Kinase Epsilon, but Not Zeta Selectively Removes Polyunsaturated Diacylglycerol, Inducing Altered Protein Kinase C Distribution in Vivo', *Journal of Biological Chemistry* **Vol. 274, No. 51**, 36181-36186, 1999.

[105] Sarkar, Susobhan, and V. Wee Yong. 'Reduction of Protein Kinase C Delta Attenuates Tenascin-C Stimulated Glioma Invasion in Three-Dimensional Matrix', *Carcinogenesis* **Vol. 31, No. 2**, 311-317, 2010.

[106] Dave, Kunjan R., Sanjoy K. Bhattacharya, Isabel Saul, R. Anthony DeFazio, Cameron Dezfulian, Hung Wen Lin, Ami P. Raval, and Miguel A. Perez-Pinzon. 'Activation of Protein Kinase C Delta Following Cerebral Ischemia Leads to Release of Cytochrome C from the Mitochondria Via Bad Pathway', *Plos One* **Vol. 6, No. 7**, 2011.

[107] Khor, Ee Cheng, Tamara Abel, Jennifer Tickner, Shek Man Chim, Cathy Wang, Taksum Cheng, Ng Benjamin, Ng Pei Ying, Dian Astari Teguh, Jacob Kenny, Xiaohong Yang, Honghui Chen, Keiichi I. Nakayama, Keiko Nakayama, Nathan Pavlos, Ming H. Zheng, and Jiake Xu. 'Loss of Protein Kinase C-Delta Protects against Lps-Induced Osteolysis Owing to an Intrinsic Defect in Osteoclastic Bone Resorption', *Plos One* **Vol. 8, No. 8**, 2013.

[108] Anantharam, V., M. Kitazawa, C. Latchoumycandane, A. Kanthasamy, and A. G. Kanthasamy. 'Blockade of Pkc Delta Proteolytic Activation by Loss of Function Mutants Rescues Mesencephalic Dopaminergic Neurons from Methylcyclopentadienyl Manganese Tricarbonyl (Mmt)-Induced Apoptotic Cell Death', *Protective Strategies for Neurodegenerative Diseases* **Vol. 1035**, 271-289, 2004.

[109] W. Zhang, L. Anker, R.E. Law, D.R. Hinton, R. Gopalak- rishna, Q. Pu, U. Gundimeda, M.H. Weiss, W.T. Couldwell, 'Enhancement of radiosensitivity in human malignant glioma cells by hypericin in vitro', *Clin. Cancer Res*. **Vol. 2**, 843– 846, 1996.

[110] W.T. Couldwell, R. Gopalakrishna, D.R. Hinton, S. He, M.H. Weiss, M.L.J. Apuzzo, R.E. Law. 'Hypericin: a potential anti- glioma therapy', *Neurosurgery* **Vol 35**, 705–710, 1994.

[111] http://www.rcsb.org/pdb/explore/explore.do?structureId=3UEJ

[112] Brannon-Peppas, L., and J. O. Blanchette. 'Nanoparticle and Targeted Systems for Cancer Therapy', *Advanced Drug Delivery Reviews* **Vol. 64**, 206-212, 2012.

[113] Cross, T., G. Griffiths, E. Deacon, R. Sallis, M. Gough, D. Watters, and J. M. Lord. 'Pkc-Delta Is an Apoptotic Lamin Kinase', *Oncogene* **Vol. 19, No. 19**, 2331-2337, 2000.

[114] Torchilin V. P., 'Passive and Active Drug Targeting: Drug Delivery to Tumors as an Example', *Handbook of Experimental Pharmacology*. **Vol. 197**, 3 – 53, 2010.

[115] Faraji, A. H., and P. Wipf. 'Nanoparticles in Cellular Drug Delivery', *Bioorganic & Medicinal Chemistry* **Vol. 17, No. 8**, 2950-2962, 2009.

[116] Voet D., Voet J.G. 'Biochemistry', 4th edition, New Jersey, USA: John Wiley & Sons, Inc., p. 449-461, ISBN 13 978-0470-91745-9, 2011.

[117] Jairam V., Uchida K., Narayanaswami V. 'Pathophysiology of Lipoprotein Oxidation, Lipoproteins-Role in Health and Diseases', Prof. Gerhard Kostner (Ed.), InTech, DOI: ISBN: 978-953-51-0773-6, p. 384, 2012.

[118] Zhang, Wen-Li, Xiao Gu, Hui Bai, Ru-Hui Yang, Chen-Dong Dong, and Jian-Ping Liu. 'Nanostructured Lipid Carriers Constituted from High-Density Lipoprotein Components for Delivery of a Lipophilic Cardiovascular Drug', *International Journal of Pharmaceutics* **Vol. 391, No. 1-2**, 313-321, 2010.

[119] Forti N., Diament J. 'High-density lipoproteins: metabolic, clinical, epidemiological and therapeutic intervention aspects. *Arq. Bras. Cardiol*.**Vol.87, No.5**, p. 671-679, 2006.

[120] Thaxton, C. Shad, Weston L. Daniel, David A. Giljohann, Audrey D. Thomas, and Chad A. Mirkin. 'Templated Spherical High Density Lipoprotein Nanoparticles', *Journal of the American Chemical Society* **Vol. 131, No. 4**, 1384-+, 2009.

[121] Segrest, J. P., M. K. Jones, H. De Loof, and N. Dashti. 'Structure of Apolipoprotein B-100 in Low Density Lipoproteins', *Journal of Lipid Research* **Vol. 42, No. 9**, 1346-1367, 2001.

[122] Buriankova, L., D. Buzova, D. Chorvat, F. Sureau, D. Brault, P. Miskovsky, and D. Jancura. 'Kinetics of Hypericin Association with Low-Density Lipoproteins', *Photochemistry and Photobiology* **Vol. 87, No. 1**, 56-63, 2011.

[123] Ng, Kenneth K., Jonathan F. Lovell, and Gang Zheng. 'Lipoprotein-Inspired Nanoparticles for Cancer Theranostics', *Accounts of Chemical Research* **Vol. 44, No. 10**, 1105-1113, 2011.

[124] Damiano, Marina G., R. Kannan Mutharasan, Sushant Tripathy, Kaylin M. McMahon, and C. Shad Thaxton. 'Templated High Density Lipoprotein Nanoparticles as Potential Therapies and for Molecular Delivery', *Advanced Drug Delivery Reviews* **Vol. 65, No. 5**, 649-662, 2013.

[125] Davis, Mark E., Zhuo Chen, and Dong M. Shin. 'Nanoparticle Therapeutics: An Emerging Treatment Modality for Cancer', *Nature Reviews Drug Discovery* **Vol. 7, No. 9**, 771-782, 2008.

[126] Lacko, A. G., M. Nair, S. Paranjape, S. Johnson, and W. J. McConathy. 'High Density Lipoprotein Complexes as Delivery Vehicles for Anticancer Drugs', *Anticancer Research* **Vol. 22, No. 4**, 2045-2049, 2002.

[127] Jori, G., and E. Reddi. 'The Role of Lipoproteins in the Delivery of Tumor-Targeting Photosensitizers', *International Journal of Biochemistry* **Vol. 25, No. 10**, 1369-1375, 1993.

[128] Hevonoja, T., M. O. Pentikainen, M. T. Hyvonen, P. T. Kovanen, and M. Ala-Korpela. 'Structure of Low Density Lipoprotein (Ldl) Particles: Basis for Understanding Molecular Changes in Modified Ldl', *Biochimica Et Biophysica Acta-Molecular and Cell Biology of Lipids* **Vol. 1488, No. 3**, 189-210, 2000.

[129] Vitols, S., B. Angelin, S. Ericsson, G. Gahrton, G. Juliusson, M. Masquelier, C. Paul, C. Peterson, M. Rudling, K. Soderbergreid, and U. Tidefelt. 'Uptake of Low-Density Lipoproteins by Human Leukemic-Cells Invivo - Relation to Plasma-Lipoprotein Levels and Possible Relevance for Selective Chemotherapy', *Proceedings of the National Academy of Sciences of the United States of America* **Vol. 87, No. 7**, 2598-2602, 1990.

[130] Wasan, Kishor M., Dion R. Brocks, Stephen D. Lee, Kristina Sachs-Barrable, and Sheila J. Thornton. 'Impact of Lipoproteins on the Biological Activity and Disposition of Hydrophobic Drugs: Implications for Drug Discovery', *Nature Reviews Drug Discovery* **Vol. 7, No. 1**, 84-99, 2008.

[131] Kascakova, S., M. Refregiers, D. Jancura, F. Sureau, J. C. Maurizot, and P. Miskovsky. 'Fluorescence Spectroscopic Study of Hypericin-Photosensitized Oxidation of Low-Density Lipoproteins', *Photochemistry and Photobiology* **Vol. 81, No. 6**, 1395-1403, 2005.

[132] Kascakova, S., Z. Nadova, A. Mateasik, J. Mikes, V. Huntosova, M. Refregiers, F. Sureau, J. C. Maurizot, P. Miskovsky, and D. Jancura. 'High Level of Low-Density Lipoprotein Receptors Enhance Hypericin Uptake by U-87 Mg Cells in the Presence of Ldl', *Photochemistry and Photobiology* **Vol. 84, No. 1**, 120-127, 2008.

[133] Huntosova, V., L. Alvarez, L. Bryndzova, Z. Nadova, D. Jancura, L. Buriankova, S. Bonneau, D. Brault, P. Miskovsky, and F. Sureau. 'Interaction Dynamics of Hypericin with Low-Density Lipoproteins and U87-Mg Cells', *International Journal of Pharmaceutics* **Vol. 389, No. 1-2**, 32-40, 2010.

[134] Huntosova, V., D. Buzova, D. Petrovajova, P. Kasak, Z. Nadova, D. Jancura, F. Sureau, and P. Miskovsky. 'Development of a New Ldl-Based Transport System for Hydrophobic/Amphiphilic Drug Delivery to Cancer Cells', *International Journal of Pharmaceutics* **Vol. 436, No. 1-2**, 463-471, 2012.

[135] Ng, Kenneth K., Jonathan F. Lovell, and Gang Zheng. 'Lipoprotein-Inspired Nanoparticles for Cancer Theranostics', *Accounts of Chemical Research***Vol. 44, No. 10**, 1105-1113, 2011.

[136] Song, Liping, Hui Li, Ulas Sunar, Juan Chen, Ian Corbin, Arjun G. Yodh, and Gang Zheng. 'Naphthalocyanine-Reconstituted Ldl Nanoparticles for in Vivo Cancer Imaging and Treatment', *International Journal of Nanomedicine***Vol. 2, No. 4**, 767-774, 2007.

[137] Nikanjam, Mina, Eleanor A. Blakely, Kathleen A. Bjornstad, Xiao Shu, Thomas F. Budinger, and Trudy M. Forte. 'Synthetic Nano-Low Density Lipoprotein as Targeted Drug Delivery Vehicle for Glioblastoma Multiforme', *International Journal of Pharmaceutics* **Vol. 328, No. 1**, 86-94, 2007.

[138] Brandt M. 'Introduction to Absorbance Spectroscopy', Copyright © 1999 – 2010 by Mark Brandt, Ph.D., http://www.rosehulman.edu/~brandt/Fluorescence/Absorbance_Spectroscopy.pdf.

[139] http://chemistry.tutorvista.com/analytical-chemistry/molecular-spectroscopy.html

[140] Lakowicz J. R. 'Principle of Fluorescence Spectroscopy', 3rd edition, Singapore: Springer Science+Business Media, LLC., 954p. ISBN 978- 0387- 31278-1, 2006.

[141] Mitchelson K. R. 'Perspectives in Bioanalysis', 1st edition, Elsevier Science, ISBN-13: 978-0444522238, 2007.

[142] BroussardJ. A., Rappaz B., Webb D. J, Brown C. M. 'Fluorescence Resonance Energy Transfer Microscopy as Demonstrated by Measuring the Activation of the Serine/Threonine Kinase Akt', *Nature Protocols***Vol. 8, No. 2**, 265-281, 2013.

[143] http://fluorescence-foundation.org/lectures%5Cchicago2011%5Clecture3.pdf

[144] Forster, T. '*Zwischenmolekulare Energiewanderung Und Fluoreszenz', *Annalen Der Physik* **Vol. 2, No. 1-2**, 55-75, 1948.

[145] Gonnella, Thomas P., Jennifer M. Keating, Jessica A. Kjemhus, Matthew J. Picklo, and Joseph P. Biggane. 'Fluorescence Lifetime Analysis and Effect of Magnesium Ions on Binding of Nadh to Human Aldehyde Dehydrogenase 1', *Chemico-Biological Interactions* **Vol. 202, No. 1-3**, 85-90, 2013.

[146] Marcu L., Frebch P. M. V., Elson D. S. 'Fluorescence Lifetime Spectroscopy and Imaging: Principles and Applications in Biomedical Diagnostics', 1st edition, USA: Taylor & Francis Group, ISBN-13: 978-1439861677, 2014.

[147] Jameson D. M. 'Introduction to Fluorescence', 1st edition, USA: Taylor & Francis Group, ISBN-13: 978-1439806043, 2014.

[148] Wilhelm S., Gröbler B., Gluch M., Heinz H. 'Confocal Laser Scanning Microscopy-Principles', Microscopy from Carl Zeiss

[149] Wulff S. 'Guide to Flow Cytometry', 2nd edition, USA: Dako, Carpinteria, 2006.

[150] Arzenšek D. 'Dynamic light scattering and application to proteins in solutions', seminar paper, 2010.

[151] Diaz O. L. 'Membrane activities of proapoptotic BAK and antiapoptotoic MCL-1, Dissertation thesis, 2013.

[152] https://www.lifetechnologies.com/order/catalog/product/D275?CID=search-product

[153] Chen, B., Y. Xu, T. Roskams, E. Delaey, P. Agostinis, J. R. Vandenheede, and P. de Witte. 'Efficacy of Antitumoral Photodynamic Therapy with Hypericin: Relationship between Biodistribution and Photodynamic Effects in the Rif-1 Mouse Tumor Model', *International Journal of Cancer* **Vol. 93, No. 2**, 275-282, 2001.

[154] Eriksson, Emma S. E., and Leif A. Eriksson. 'The Influence of Cholesterol on the Properties and Permeability of Hypericin Derivatives in Lipid Membranes', *Journal of Chemical Theory and Computation***Vol. 7, No. 3**, 560-574, 2011.

[155] Siboni, G., H. Weitman, D. Freeman, Y. Mazur, Z. Malik, and B. Ehrenberg. 'The Correlation between Hydrophilicity of Hypericins and Helianthrone: Internalization Mechanisms, Subcellular Distribution and Photodynamic Action in Colon Carcinoma Cells', *Photochemical & Photobiological Sciences* **Vol. 1, No. 7**, 483-491, 2002.

[156] Gbur, P., R. Dedic, D. Chorvat, P. Miskovsky, J. Hala, and D. Jancura. 'Time-Resolved Luminescence and Singlet Oxygen Formation after Illumination of the Hypericin-Low-Density Lipoprotein Complex', *Photochemistry and Photobiology***Vol. 85, No. 3**, 816-823, 2009.

[157] Jambeck, Joakim P. M., Emma S. E. Eriksson, Aatto Laaksonen, Alexander P. Lyubartsev, and Leif A. Eriksson. 'Molecular Dynamics Studies of Liposomes as Carriers for Photosensitizing Drugs: Development, Validation, and Simulations with a Coarse-Grained Model', Journal of Chemical Theory and Computation **Vol. 10, No. 1**, 5-13, 2014.

[158] Strejckova, Alena, Jana Stanicova, Daniel Jancura, Pavol Miskovsky, and Gregor Bano. 'Spatial Orientation and Electric-Field-Driven Transport of Hypericin inside of Bilayer Lipid Membranes', Journal of Physical Chemistry B **Vol. 117, No. 5**, 1280-1286, 2013.

[159] Jonas, A., Phillips, M.C., 'Lipoprotein structure', 5th edition, Vance, D.E., Vance, J.E. (Eds.), Biochemistry of lipids, lipoproteins and membranes, Elsevier Science, pp. 485-506.

[160] Jurgenliemk, G., and A. Nahrstedt. 'Dissolution, Solubility and Cooperativity of Phenolic Compounds from Hypericum Perforatum L. In Aqueous Systems', *Pharmazie* **Vol. 58, No. 3**, 200-203, 2003.

[161] Adhikary, Gautam, Yap Ching Chew, E. Albert Reece, and Richard L. Eckert. 'Pkc-Delta and -Eta, Mekk-1, Mek-6, Mek-3, and P38-Delta Are Essential Mediators of the Response of Normal Human Epidermal Keratinocytes to Differentiating Agents', Journal of Investigative Dermatology Vol. 130, No. 8, 2017-2030, 2010.

[162] Kocanova, S., T. Hornakova, J. Hritz, D. Jancura, D. Chorvat, A. Mateasik, J. Ulicny, M. Refregiers, J. C. Maurizot, and P. Miskovsky. 'Characterization of the Interaction of Hypericin with Protein Kinase C in U-87 Mg Human Glioma Cells', *Photochemistry and Photobiology***Vol. 82, No. 3**, 720-728, 2006.

[163] Petrovajova, D., D. Jancura, P. Miskovsky, D. Chorvat, A. Chorvatova, X. Ragas, M. Garcia-Diaz, S. Nonell, and Z. Nadova. 'Monitoring of Singlet Oxygen Luminescence and Mitochondrial Autofluorescence after Illumination of Hypericin/Mitochondria Complex: A Time-Resolved Study', *Laser Physics Letters***Vol. 10, No. 7**, 7, 2013.

[164] Buriankova L, Nadova Z, Jancura D, et al. 'Synchrotron based Fourier-transform infrared microspectroscopy as sensitive technique for the detection of early apoptosis in U-87 MG cells', *Laser Physics Letters*, **Vol 7**, 613-620, 2010.

[165] Finkel, T. 'Signal Transduction by Reactive Oxygen Species', *Journal of Cell Biology***Vol. 194, No. 1**, 7-15, 2011.

[166] Ruvolo, P. P., X. Deng, and W. S. May. 'Phosphorylation of Bcl2 and Regulation of Apoptosis', *Leukemia* **Vol. 15, No. 4**, 515-522, 2001.

[167] Esteve, J. M., J. Mompo, J. G. De La Asuncion, J. Sastre, M. Asensi, J. Boix, J. R. Vina, J. Vina, and F. V. Pallardo. 'Oxidative Damage to Mitochondrial Dna and Glutathione Oxidation in Apoptosis: Studies in Vivo and in Vitro', *Faseb Journal* **Vol. 13, No. 9**, 1055-1064, 1999.

[168] Wilkins, Heather M., Kristin Marquardt, Lawrence H. Lash, and Daniel A. Linseman. 'Bcl-2 Is a Novel Interacting Partner for the 2-Oxoglutarate Carrier and a Key Regulator of Mitochondrial Glutathione', *Free Radical Biology and Medicine* **Vol. 52, No. 2**, 410-419, 2012.

[169] Benderdour, M., G. Charron, B. Comte, R. Ayoub, D. Beaudry, S. Foisy, D. deBlois, and C. Des Rosiers. 'Decreased Cardiac Mitochondrial Nadp(+)-Isocitrate Dehydrogenase Activity and Expression: A Marker of Oxidative Stress in Hypertrophy Development', *American Journal of Physiology-Heart and Circulatory Physiology* **Vol. 287, No. 5**, H2122-H2131, 2004.

[170] Hockenbery, D. M., Z. N. Oltvai, X. M. Yin, C. L. Milliman, and S. J. Korsmeyer. 'Bcl-2 Functions in an Antioxidant Pathway to Prevent Apoptosis', *Cell* **Vol. 75, No. 2**, 241-251, 1993.

[171] Kane, D. J., T. A. Sarafian, R. Anton, H. Hahn, E. B. Gralla, J. S. Valentine, T. Ord, and D. E. Bredesen. 'Bcl-2 Inhibition of Neural Death - Decreased Generation of Reactive Oxygen Species', *Science* **Vol. 262, No. 5137**, 1274-1277, 1993.

[172] Voehringer, David W., and Raymond E. Meyn. 'Redox Aspects of Bcl-2 Function', *Antioxidants & Redox Signaling* **Vol. 2, No. 3**, 537-550, 2000.

[173] Hochman, A., H. Sternin, S. Gorodin, S. Korsmeyer, I. Ziv, E. Melamed, and D. Offen. 'Enhanced Oxidative Stress and Altered Antioxidants in Brains of Bcl-2-Deficient Mice', *Journal of Neurochemistry* **Vol. 71, No. 2**, 741-748, 1998.

[174] Marengo, Barbara, Chiara De Ciucis, Roberta Ricciarelli, Mario Passalacqua, Mariapaola Nitti, Jean-Marc Zingg, Umberto M. Marinari, Maria A. Pronzato, and Cinzia Domenicotti. 'Pkc Delta Sensitizes Neuroblastoma Cells to L-Buthionine-Sulfoximine and Etoposide Inducing Reactive Oxygen Species Overproduction and Dna Damage', *Plos One***Vol. 6, No. 2**, 2011.

[175] Hsiao, Po-Ni, Ming-Cheng Chang, Wen-Fang Cheng, Chi-An Chen, Han-Wei Lin, Chang-Yao HsiehB, and Wei-Zen Sun. 'Morphine Induces Apoptosis of Human Endothelial Cells through Nitric Oxide and Reactive Oxygen Species Pathways', *Toxicology* **Vol. 256, No. 1-2**, 83-91, 2009.

[176] Kroemer, G. 'The Proto-Oncogene Bcl-2 and Its Role in Regulating Apoptosis (Vol 3, Pg 614, 1997)', *Nature Medicine* **Vol. 3, No. 8**, 934-934, 1997.

[177] Youle, Richard J., and Andreas Strasser. 'The Bcl-2 Protein Family: Opposing Activities That Mediate Cell Death', *Nature Reviews Molecular Cell Biology* **Vol. 9, No. 1**, 47-59, 2008.

[178] Annis, M. G., J. A. Yethon, B. Leber, and D. W. Andrews. 'There Is More to Life and Death Than Mitochondria: Bcl-2 Proteins at the Endoplasmic Reticulum', *Biochimica Et Biophysica Acta-Molecular Cell Research* **Vol. 1644, No. 2-3**, 115-123, 2004.

[179] Buytaert, Esther, Geert Callewaert, Nico Hendrickx, Luca Scorrano, Dieter Hartmann, Ludwig Missiaen, Jackie R. Vandenheede, Ingeborg Heirman, Johan Grooten, and Patrizia Agostinis. 'Role of Endoplasmic Reticulum Depletion and Multidomain Proapoptotic Bax and Bak Proteins in Shaping Cell Death after Hypericin-Mediated Photodynamic Therapy', *Faseb Journal* **Vol. 20, No. 2**, 756-+, 2006.

[180] Hwang, S. I., D. H. Lundgren, V. Mayya, K. Rezaul, A. E. Cowan, J. K. Eng, and D. K. Han. 'Systematic Characterization of Nuclear Proteome During Apoptosis - a Quantitative Proteomic Study by Differential Extraction and Stable Isotope Labeling', *Molecular & Cellular Proteomics* **Vol. 5, No. 6**, 1131-1145, 2006.

[181] Gilmore, A. P., A. D. Metcalfe, L. H. Romer, and C. H. Streuli. 'Integrin-Mediated Survival Signals Regulate the Apoptotic Function of Bax through Its Conformation and Subcellular Localization', *Journal of Cell Biology* **Vol. 149, No. 2**, 431-445, 2000.

[182] Balogova, L., M. Maslanakova, P. Miskovsky, and K. Stroffekova. 'Relationship between Bax and Bak Distribution and Apoptosis Onset in U-87 Mg Cells Upon Hyppdt', *European Biophysics Journal with Biophysics Letters* **Vol. 42**, S45-S45, 2013.

[183] Mandavilli BS, Janes MS. (2010) Detection of intracellular glutathione using ThiolTracker violet stain and fluorescence microscopy. Current protocols in cytometry / editorial board, J Paul Robinson, managing editor [et al] Chapter 9:Unit 9.35-Unit 39.35.

[184] Huntosova, Veronika, Zuzana Nadova, Lenka Dzurova, Viera Jakusova, Franck Sureau, and Pavol Miskovsky. 'Cell Death Response of U87 Glioma Cells on Hypericin Photoactivation Is Mediated by Dynamics of Hypericin Subcellular Distribution and Its Aggregation in Cellular Organelles', *Photochemical & Photobiological Sciences* **Vol. 11, No. 9**, 1428-1436, 2012.

[185] Sitailo, L. A., S. S. Tibudan, and M. F. Denning. 'Bax Activation and Induction of Apoptosis in Human Keratinocytes by the Protein Kinase C Delta Catalytic Domain', *Journal of Investigative Dermatology* **Vol. 123, No. 3**, 434-443, 2004.

[186] Park, J. K., M. Y. Kang, Y. H. Kim, H. C. Jo, J. K. Shin, W. J. Choi, S. A. Lee, J. H. Lee, W. S. Choi, and W. Y. Paik. 'Pkc Delta in Preeclamptic Placentas Promotes Bax Dissociation from 14-3-3 Zeta through 14-3-3 Zeta Phosphorylation', *Placenta* **Vol. 29, No. 7**, 584-592, 2008.

ATTACHMENTS

International Journal of Pharmaceutics 475 (2014) 578–584

Contents lists available at ScienceDirect

International Journal of Pharmaceutics

journal homepage: www.elsevier.com/locate/ijpharm

Pharmaceutical nanotechnology

Kinetics of incorporation/redistribution of photosensitizer hypericin to/from high-density lipoproteins

Jaroslava Joniova [a], Luboslava Buriankova [a,b], Diana Buzova [a,c], Pavol Miskovsky [a,d], Daniel Jancura [a,d,*]

[a] Department of Biophysics, Faculty of Science, Safarik University, Kosice, Slovakia
[b] Department of Physics, Faculty of Mathematics and Physics, Charles University, Prague, Czech Republic
[c] Department of Adaptation Biotechnologies, Czech Globe, Drasov, Czech Republic
[d] Center for Interdisciplinary Biosciences, Faculty of Science, Safarik University, Kosice, Slovakia

ARTICLE INFO

Article history:
Received 11 June 2014
Received in revised form 12 September 2014
Accepted 13 September 2014
Available online 17 September 2014

Keywords:
Drug delivery
High- and low- density lipoproteins
Fluorescence
Aggregation
Hypericin

ABSTRACT

By means of fluorescence spectroscopy we have studied the kinetics of interaction of a photosensitizer hypericin (Hyp) with high-density lipoproteins (HDL). Hyp is incorporated into HDL molecules as monomer till ratio Hyp/HDL ~8:1 and above this ratio forms non-fluorescent aggregates. This number is different from that found in the case of Hyp incorporation into low-density lipoprotein (LDL) molecules (8:1 vs 30:1). The difference is mainly attributed to the smaller size of HDL in comparison with LDL molecule. Biphasic kinetics of Hyp association with HDL was observed. The rapid phase of incorporation is completed within seconds, while the slow one lasts several minutes. The kinetics of the association of Hyp molecules with free HDL, Hyp/HDL = 10:1 complex and the redistribution of Hyp from Hyp/HDL = 70:1 complex to free HDL molecules reveal a qualitative similar characteristics of these processes with those observed for the interaction of Hyp with LDL. However, the incorporation of Hyp into HDL in the "slow" phase is more rapid than to LDL and extend of Hyp penetration into lipoproteins in the fast phase is also much higher in the case of HDL. The lower concentration of cholesterol molecules in outer shell of HDL particles is probably the determining factor for the more rapid kinetics of Hyp incorporation to and redistribution from these molecules when comparing with LDL particles.

1. Introduction

In the recent years an important attention has been dedicated to the use of lipoproteins for targeted drug delivery (Zheng et al., 2005; Lacko et al., 2007; Glickson et al., 2008; Ng et al., 2011). This fact is based on the establishing of a direct relationship between the relative number of lipoprotein receptors in various tumors and the uptake of drugs by malignant cells (Brown and Goldstein, 1976; Vitols et al., 1990; Puussinen et al., 2000; Damiano et al., 2013). Of the lipoproteins the most important in terms of drug delivery are low-density lipoproteins (LDL) (Konan et al., 2002; Polo et al., 2002; Sherman et al., 2004; Zheng et al., 2005; Derycke and de Witte, 2004), however, the importance of high-density lipoproteins (HDL) is also recognized and in many cases seems to be even higher than LDL (Corbin et al., 2007; Davis et al., 2008; McConathy et al., 2008; Damiano et al., 2013). The capacity of both types of the lipoproteins, LDL as well as HDL, to bind some drugs and their functionality as drug carriers have been examined in several studies (Jori, 1996; Lacko et al., 2002; Oda et al., 2006; Corbin et al., 2007). It has been also shown that mixing of anticancer drugs with LDL or HDL before administration led to an increase of cytotoxic effects of the drugs in the comparison when the drugs are administered alone (Jori and Reddi 1993; Chowdhary et al., 2003; Davis et al., 2008; McConathy et al., 2008).

LDL are recognized by and internalized into the cells through specific membrane receptors that interact with the apolipoprotein B of the LDL particle (Hevonoja et al., 2000). Certain tumor cells and tumor vascular endothelial cells express the LDL receptors in higher number due to either their increased proliferation or increased membrane turnover (Brown and Goldstein, 1976; Vitols et al., 1990). HDL have been implicated in cholesterol delivery in some malignancies including breast cancer, ovarian cancer, adrenocortical tumors and prostate cancer. The mechanism for HDL mediated delivery appears to be SR-B1 receptor dependent (Damiano et al., 2013). It is known that

* Corresponding author at: Department of Biophysics, Faculty of Science, Safarik University, Jesenna 5, 041 54 Kosice, Slovakia. Tel.: +421 552342246.
E-mail addresses: daniel.jancura@upjs.sk, djancura@yahoo.com (D. Jancura).

http://dx.doi.org/10.1016/j.ijpharm.2014.09.025
0378-5173/

this receptor is broadly expressed among a variety of cancer cells (Rao et al., 2003). The above mentioned facts make LDL and HDL particles attractive natural occurring vehicles for drug delivery and targeting to cancer tissues.

Both types of the lipoproteins assume a globular shape with an average particle diameter 20–25 nm and 7–13 nm for LDL and HDL, respectively. These lipoproteins posses the outer surface layer, which consists of cholesterol and phospholipids molecules with a single apo B-100 protein wrapped around the surface of the LDL particle and apoA1, which is responsible for scaffolding, the size and shape of natural HDL, further the hydrophobic core composed of triacylglycerides and cholestrol esters, and an interfacial region between these two parts (Hevonoja et al., 2000; Prassl and Laggner, 2009; Jonas and Phillips, 2008). LDL and HDL have important advantages in comparison to other drug nano-delivery systems: (i) as natural molecules both lipoproteins escape recognition by mononuclear phagocytic system (MPS), which favors their long circulation time in the plasma, (ii) they are not immunogenic, (iii) their hydrophobic core and phospholipid shell favor binding of hydrophobic and amphiphilic drugs, respectively (Lacko et al., 2007; Glickson et al., 2008; Ng et al., 2011; Damiano et al., 2013). The importance of the study of the physicochemical properties of complexes of drugs with lipoproteins is confirmed by the fact that the US Food and Drug Administration (FDA) encouraged the inclusion of lipoprotein-drug interaction studies as part of any investigational new drug application that contains a hydrophobic compound (Wasan et al., 2008).

Our group has published in the recent years several articles about the properties of the complexes of LDL with photosensitizer hypericin (Hyp). Hyp (Fig. 1), (7,14-dione-1,3,4,6,8,13-hexahydroxy10,11-dimethyl-phenanthrol[1,10,9,8-*opqra*] perylene), is a natural photosensitizing pigment from plants of the genus *Hypericum*. This compound under light illumination causes antiproliferative and cytotoxic effects (necrosis as well as apoptosis) in many tumor cell lines. These properties, together with minimal dark toxicity, certain tumor selectivity, and high clearance rate from the host body, make Hyp a promising agent for photodynamic therapy (PDT) of cancer as well as for tumor photo-diagnosis (for reviews see Falk, 1999; Agostinis et al., 2002; Kiesslich et al., 2006; Karioti and Bilia, 2010). Chen et al. have shown that Hyp associates in human plasma predominatly with LDL and to a lesser extend with HDL and human serum albumin (HSA), however, binds dominantly to HDL in mouse plasma (Chen et al., 2001).

In our previous studies was shown that high Hyp/LDL ratios (>30:1) leads to a significant decrease of quantum yield of Hyp fluorescence (Kascakova et al., 2005). This decrease is caused by the formation of non-fluorescent Hyp aggregates inside LDL particles and by dynamic self-quenching of Hyp fluorescence (Mukherjee et al., 2008; Gbur et al., 2009). It was shown that only monomeric form of Hyp is able to produce the excited triplet state of Hyp in LDL, which in aerobic conditions leads to a singlet oxygen production (Gbur et al., 2009). Kinetics of Hyp association with free LDL molecules and Hyp/LDL complex have been also thoroughly studied and described (Huntosova et al., 2010; Buriankova et al., 2011). We have demonstrated the important role of the LDL receptor pathway for Hyp delivery into U-87 MG cells in the presence of LDL. A substantial increase of Hyp uptake was observed after over-expression of LDL receptors on the cell surface (Kascakova et al., 2008). It was also shown that overloading of LDL with Hyp (Hyp/LDL = 200:1) leads to a higher intracellular accumulation of Hyp molecules in comparison with the situation when the same quantity of Hyp is accumulated in LDL, but with a lower Hyp/LDL ratio (20:1). Moreover, Hyp/LDL ratio seems to affect the subcellular distribution of Hyp (Huntosova et al., 2010) and consequently the mechanism of photodynamically induced cell death.

To continue this study, we present a work in which a description of the association of Hyp with HDL particles is shown. The emphasis is given on the kinetics of Hyp incorporation into free HDL molecules, saturated Hyp/HDL = 10:1 complex, and the redistribution of Hyp from the complex Hyp/HDL = 70:1 to free lipoprotein particles. Similarly to our study of Hyp/LDL complexes (Kascakova et al., 2005; Buriankova et al., 2011), we have utilized the fluorescence spectroscopy approach and the fact that molecules of Hyp form non-fluorescent aggregates in aqueous solutions and the Hyp aggregates can be formed also in lipoprotein particles at high local Hyp concentrations (Kascakova et al., 2005; Lavie et al., 1995; Siboni et al., 2002). The differences between characteristics of Hyp association with LDL and HDL are also discussed.

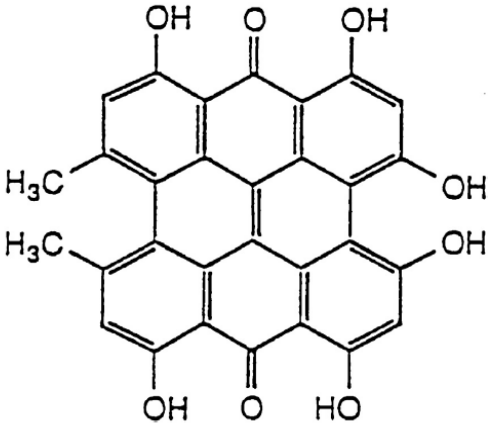

Fig. 1. Structure of hypericin.

2. Material and methods

2.1. Chemicals

Hypericin, ethylenediaminetetraacetic acid (EDTA), phosphate buffer saline (PBS) and dimethyl sulfoxide (DMSO) were obtained from Sigma–Aldrich. HDL (purity >95% of total lipoprotein content by electrophoresis) was purchased from Calbiochem (Darmstadt, Germany).

2.2. Preparation of Hyp and HDL solutions

The stock solution of Hyp was prepared by dissolving Hyp in 100% DMSO (c(Hyp) = 2 mM) and was kept in the dark at 4 °C. A stock solution of HDL (c(HDL) = 8.6 μM) was prepared in 150 mM NaCl solution at pH 7.4 in the presence of 0.1% EDTA. The Hyp–HDL solutions used in experiments were prepared by mixing of appropriate volumes of HDL and Hyp stock solutions in PBS at pH 7.4. The final concentration of DMSO in all Hyp–HDL solutions was under 1%. As revealed by UV–vis absorption and fluorescence spectroscopies, Hyp/HDL complexes are stable in PBS (pH 7.4) at room temperature (23 °C) for several days (5 days in this case).

2.3. Hyp incorporation into free HDL molecules

HDL solutions were mixed with Hyp as it is mentioned above. The concentration of HDL was kept at the constant value (10 nM). The final concentration of Hyp in Hyp/HDL complex varied from 10 nM to 700 nM (correspondingly Hyp/HDL ratio varied from 1:1 to 70:1).

2.4. Hyp incorporation into complex Hyp/HDL = 10:1

Firstly, the complex of Hyp/HDL = 10:1 (c(HDL) = 10 nM) was prepared. After 2 h of stabilization of the complex in the dark at the room temperature, the appropriate amount of Hyp stock solution (2 mM) was added to the Hyp/HDL complex to obtain various final Hyp/HDL ratios. HDL concentration was kept at constant value (10 nM) in all Hyp/HDL complexes and the final concentration ratios Hyp/HDL were from the range 16:1–70:1.

2.5. Transfer of Hyp molecules from Hyp/HDL = 70:1 complex to free HDL molecules

Initially, the complex Hyp/HDL = 70:1 was prepared. This complex was stabilized 2 h in the dark conditions at the room temperature. After this time period, the appropriate volume of free HDL molecules was added to the solution of Hyp/HDL = 70:1 complex, and several final ratios Hyp/HDL were obtained. Hyp concentration in all solutions was kept constant (700 nM) and the final Hyp/HDL ratios were in the range 60:1–1:1.

2.6. Fluorescence spectroscopy measurements:

Fluorescence spectra were recorded at room temperature by SHIMADZU RF-5301 spectrofluorimeter (Kyoto, Japan). The excitation wavelength was 515 nm and the emission was collected in the range 525–700 nm for all kinetic measurements. Spectra were collected at various time after mixing Hyp and HDL, Hyp and Hyp/HDL = 10:1, HDL and Hyp/HDL = 70:1 solutions at a room temperature, and were analyzed with Origin Pro program version 8.0.

3. Results and discussion

3.1. Incorporation of Hyp into HDL: a steady-state approach

The fluorescence emission spectra of Hyp in the presence of HDL resemble those in the presence of LDL (not shown). The spectral maximum is positioned at 599 nm (Kascakova et al., 2005) and the intensities are also almost identical in the presence of both types of the lipoproteins (at the same Hyp concentration and molar ratio Hyp/lipoprotein = 1:1).

The dependence of Hyp fluorescence intensity at its maximum on the molar ratio Hyp/HDL, 300 min after mixing of Hyp with HDL solutions (HDL concentration in the mixtures was 10 nM), is presented in Fig. 2. The intensity of Hyp fluorescence increases up to Hyp/HDL molar ratio 8:1 (c(Hyp) = 80 nM) and beyond this value a quenching of Hyp fluorescence is observed. At the molar ratio Hyp/HDL = 60:1, the fluorescence of Hyp almost disappears. This behavior can be explained similarly as in the case of Hyp association with LDL (Kascakova et al., 2005). Until Hyp/HDL = 8:1 ratio, the molecules of Hyp are present inside HDL particles as monomers, and at high Hyp/HDL molar ratios (>8:1), the formation of non-fluorescent Hyp aggregates inside HDL occurs. However, the values of molar ratio at which Hyp still exists in the lipoprotein particles in monomeric state are different, ca. 30:1 for Hyp/LDL and 8:1 for Hyp/HDL complex (Fig. 2). This difference should be mainly attributed to a smaller size of HDL in comparison with LDL particle (diameter in average of HDL and LDL particles is 11 nm and 22 nm, respectively).

The ratio of the values (30:1 and 8:1), which represent thresholds for the existence of the monomeric form of Hyp inside LDL and HDL molecules, respectively, equals approximately to 4. This observation leads to a speculation above the possible localization of the Hyp molecules inside lipoprotein particles. It is apparent that the square of the ratio of the diameters of LDL/HDL

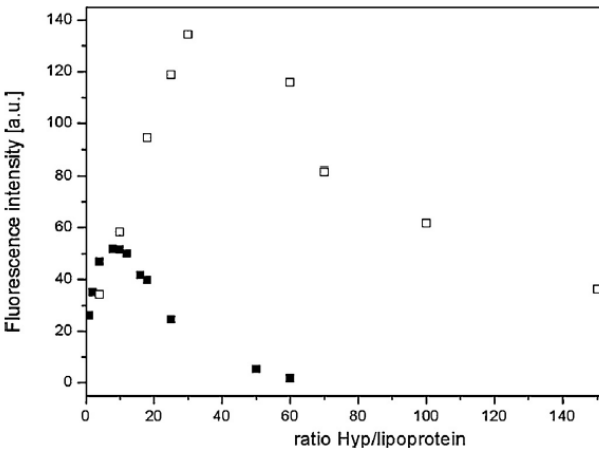

Fig. 2. Dependence of Hyp fluorescence intensity on concentration ratio Hyp/HDL (■) and Hyp/LDL (□) after 120 min of stabilization of the complexes (fluorescence maximum 599 nm, excitation line 515 nm). Concentration of HDL and LDL was kept constant during the measurements (10 nM).

is also approximately 4 $(22\,nm/11\,nm)^2$. It suggests that the molecules of monomeric Hyp are most probably distributed on the "like sphere surface", likely in phospholipid–cholesterol outer layer of LDL and HDL molecules. Further increase of Hyp concentration (above the ratio 8:1 and 30:1 for Hyp/HDL and Hyp/LDL, respectively) leads to a Hyp clustering in lipid membranes which has been previously proposed (Kascakova et al., 2005; Gbur et al., 2009) and also theoretically supported (Jämbeck et al., 2013). This clustering is mostly due to π-stacking interaction between aromatic cores of Hyp molecules. In this theoretical work (Jämbeck et al., 2013) it was moreover suggested that aggregates of Hyp can be formed and sticked on the liposome surface. Similar situation can occur in the case of Hyp interaction with HDL(LDL) molecules and Hyp aggregates are possibly also localized on the surface of the lipoprotein particles. Regarding Hyp localization in HDL (LDL) molecules it was proposed by several groups that Hyp is mainly localized close to the polar head groups of the outer layer of lipid structure (liposomes, biological membranes) (Losi, 1997; Weitman et al., 2001; Eriksson et al., 2009; Eriksson and Eriksson, 2011; Jämbeck et al., 2013; Strejckova et al., 2013). Concretely, UV–vis absorption, fluorescence and NMR experiments have shown that when Hyp is incorporated into a lipisomal phospholipid bilayer then it is preferentially located in the polar zone close to the lipid/water interface (Losi, 1997; Weitman et al., 2001). These observations are also supported by theoretical molecular dynamic studies which showed that molecules of Hyp are mainly found close to the polar headgroup region of the outer lipid layer of liposomes (Jämbeck et al., 2014). In principle, similar structures of the outer shell of HDL (LDL) molecules and liposomes suggest similar way of the localization of Hyp inside HDL (LDL) and liposome molecules. However, the presence of cholesterol in the outer shell of the lipoproteins molecules can move Hyp a more deeply inside the LDL or HDL particles, as it was proposed for Hyp localization in cholesterol enriched biological membranes (Eriksson and Eriksson, 2010). This proposition is in accordance with the earlier suggestion of Mukherjee et al. about partial localization of Hyp molecules also in the region between phospholipid–cholesterol outer shell and hydrophobic core of LDL particles (Mukherjee at al., 2008). The principal role of cholesterol for the selectivity of Hyp incorporation in biological membrane systems has been discussed also by Ho et al. (2009).

3.2. The kinetics of Hyp interaction with HDL particles

The time evolution of the fluorescence intensity of Hyp after mixing Hyp molecules with free HDL particles is shown in Fig. 3. It is evident that there exists 2 phases of the incorporation of Hyp into HDL molecules. The rapid phase of the incorporation is manifested by a non-zero fluorescence intensity of Hyp immediately (5–10 s) after mixing Hyp and HDL solutions (Fig. 3). The second, slow phase of the process, lasts several minutes. The fluorescence intensity of Hyp in Hyp/HDL (until molar ratio 8:1) complexes increases and reaches saturation ca. 10 min after mixing. For the complexes with higher Hyp/HDL ratios, an increase of Hyp fluorescence observed immediately after mixing is followed by its decrease. This decrease is caused, as it was already mentioned, by the creation of Hyp aggregates and self-quenching of Hyp fluorescence in HDL particles when continuous flow of Hyp molecules into HDL particles leads to a number of Hyp molecules per one HDL particle to be above 8. For the Hyp/HDL = 1:1 and 2:1 complexes, a major part of Hyp molecules is incorporated into HDL in the slow phase (Table 1). On the other hand, for the complexes with the molar ratios 6:1 and 8:1, the major part of Hyp (about 70%) is incorporated into HDL in the first, rapid phase (Fig. 3, Table 1). This behavior is slightly different than the properties of Hyp/LDL complex, where we have observed that most of Hyp molecules (ca. 65%) are associated with LDL in the slow phase of the incorporation process until the concentration ratio 30:1 (Buriankova et al., 2011). For the determination of the half-times of Hyp incorporation into HDL (until ratio Hyp/HDL = 8:1) we have fitted the experimental data by a mono-exponential function. However, we are aware that the process of Hyp incorporation into lipoproteins is complicated and mono-exponential fitting is only a rough approximation of the real situation. The obtained half-times for the internalization of Hyp molecules into HDL are summarized in Table 1. The comparison of these values with those characterizing a formation of Hyp/LDL complex reveals that the process of internalization of Hyp molecules into lipoproteins is more rapid in the presence of HDL than LDL. The half-times for Hyp incorporation into HDL is 2–7 min, depending on the final Hyp/HDL ratio, meanwhile the half-times for Hyp association with LDL is 14–26 min (Buriankova et al., 2011). The reason for this observation

Table 1
Half-times of the slow phase of Hyp incorporation into free HDL molecules. I_0 and I_{60} represent intensity of Hyp fluorescence immediately and 60 min after mixing Hyp and HDL solutions, respectively.

Hyp/HDL	τ (min)	I_0 (a.u)	I_{60} (a.u)	I_0/I_{60}
1	7	10	27	0.39
2	5	15	37	0.48
6	4	32	47	0.68
10	2	40	53	0.75

should be in a relative higher contain of cholesterol molecules in LDL (11%) in comparison with HDL (7%) (Jonas and Phillips, 2008). It was shown that Hyp displays slower diffusion in biological membranes enriched by cholesterol (Eriksson and Eriksson, 2011). This fact correlates with our present observation that Hyp molecules are more rapidly incorporated to and monomerized in the outer phospholipid–cholesterol shell of HDL than of LDL particles.

In conclusion of this part we would like to emphasize qualitatively similar properties of the kinetics of Hyp incorporation into HDL and LDL molecules. However, incorporation of Hyp into HDL is more rapid than to LDL and also the relative contribution of the fast phase vs slow phase of Hyp accumulation into HDL particles is higher than in the case of LDL. The concentration of cholesterol molecules in the outer shell of the lipoprotein particle is probably the determining factor for the kinetics of Hyp incorporation into lipoproteins.

3.3. Kinetics of Hyp incorporation to Hyp/HDL = 10:1 complex

The incorporation of Hyp molecules into the pre-formed Hyp/HDL complex (Hyp/HDL = 10:1) was also investigated. After 2 h of stabilization of Hyp/HDL = 10:1 complex, an appropriate amount of free Hyp molecules was added to the complex in order to increase the final molar ratio of Hyp/HDL. The time dependence of the intensity of Hyp fluorescence emission as a function of the final Hyp/HDL ratio is illustrated in Fig. 4. The increase of Hyp concentration leads to a drop in Hyp fluorescence intensity. This behavior was expected because the raise of the Hyp/HDL

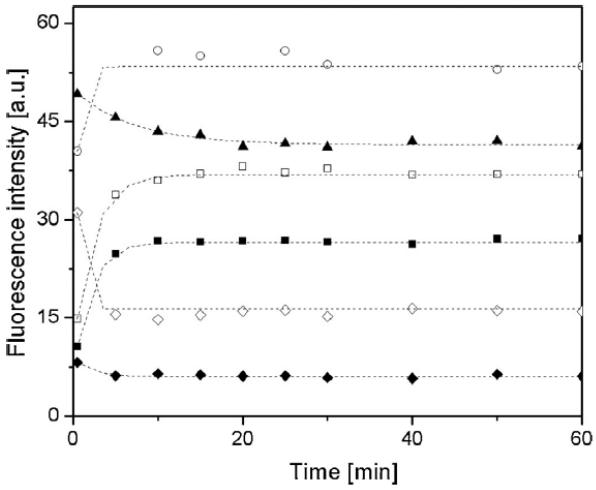

Fig. 3. Time dependence of fluorescence intensity of Hyp after mixing Hyp and HDL solutions: (■) Hyp/HDL = 1:1, (□) Hyp/HDL = 2:1, ○ Hyp/HDL = 6:1, (▲) Hyp/HDL = 20:1, (◇) Hyp/HDL = 35:1, (◆) Hyp/HDL = 60:1). Concentration of HDL was kept constant (10 nM). Fluorescence of Hyp was recorded at 599 nm, the excitation line was 515 nm.

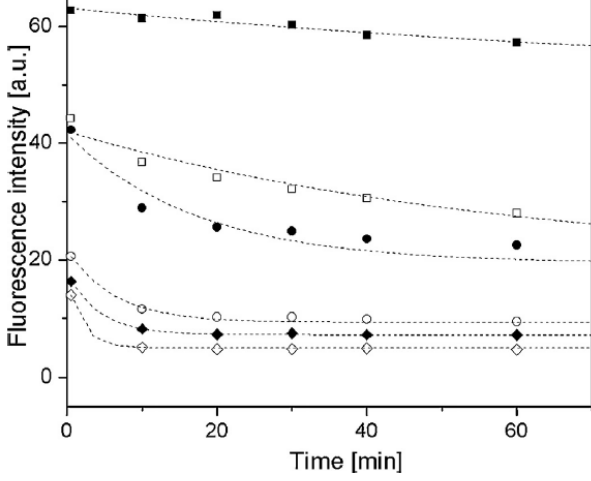

Fig. 4. Time evolution of fluorescence intensity of Hyp during accumulation of fre Hyp into Hyp/HDL = 10:1 complex. Final Hyp/HDL ratios: ((■) Hyp/HLDL = 12:1, (□ Hyp/HDL = 18:1, (●) Hyp/HDL = 22:1, (○) Hyp/HDL = 30:1, (◆) Hyp/HDL = 40:1, (◇ Hyp/HDL = 50:1). The initial complex Hyp/HDL = 10:1 was stabilized for 2 h befor starting the experiment. The concentration of HDL was constant in all experiment (10 nM). Fluorescence of Hyp recorded at 599 nm, excitation line 515 nm.

Table 2
Half-times of the slow phase of the incorporation of Hyp molecules into Hyp/HDL = 10:1 complex. I_0 and I_{60} represent intensities of Hyp fluorescence immediately and 60 min after mixing solutions of Hyp/HDL = 10:1 and free Hyp molecules, respectively. I_{max} is the intensity of Hyp fluorescence in Hyp/HDL = 10:1 complex.

Hyp/HDL	τ (min)	I_0 (a.u.)	I_{60} (a.u.)	$(I_{max} - I_0)/(I_{max} - I_{60})$
22	17	42	22	0.53
30	6	20	9	0.80
40	5	16	7	0.84
50	2	14	4	0.84

Table 3
Half-times of the slow phase of the redistribution of Hyp from Hyp/HDL = 70:1 complex to free HDL molecules. I_0 and I_{60} represent intensities of Hyp fluorescence immediately and 60 min after mixing solutions of Hyp/LDL = 70:1 complex and free HDL molecules, respectively. Concentration of Hyp was constant (10^{-6} M).

Ratio Hyp/HDL	τ (min)	I_0 (a.u.)	I_{60} (a.u.)	I_0/I_{60}
5	8	78	692	0.11
8	5	107	475	0.23
10	1	125	349	0.36

concentration ratio above 8:1 leads to the generation of non-fluorescent Hyp aggregates inside outer shell and/or on the surface of HDL molecules. The rapid decrease of the Hyp fluorescence immediately after mixing Hyp/HDL = 10:1 complex with free Hyp molecules (Fig. 4) suggests rapid accumulation of Hyp molecules into Hyp/HDL complex. The slow phase is almost negligible, mainly at the high (>30:1) final Hyp/HDL concentration ratios (Fig. 4 and Table 2). This observation suggests that further uptake of Hyp molecules by Hyp/HDL complex lead to a rapid formation of Hyp aggregates in/on HDL particles. The studied process is qualitatively similar to that one for Hyp incorporation into Hyp/LDL complex (Buriankova et al., 2011), however, the fast phase of this process is prevailing in the case of HDL. Again we attribute this observation to a more rapid permeability of Hyp molecules into HDL particles in comparison with LDL molecules which is caused by a lower content of cholesterol molecules in outer shell of HDL vs LDL.

3.4. Kinetics of Hyp redistribution from Hyp/HDL complexes

Similarly as for transport of Hyp molecules from saturated complex Hyp/LDL to free LDL molecules (Buriankova et al., 2011), we have studied in this work the translocation of Hyp molecules from saturated Hyp/HDL = 70:1 complex to free HDL particles. This investigation is possible due to the fact that this translocation leads to a lower number of Hyp molecules per one lipoprotein particle which leads to appearance of Hyp fluorescence. The increase of fluorescence signal corresponds to a monomerization of Hyp molecules which is a consequence of the translocation of these molecules from Hyp/HDL complex on free lipoprotein particles.

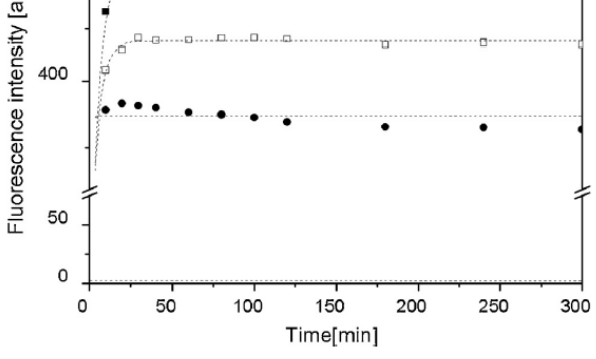

Fig. 5. Time dependence of fluorescence intensity of Hyp after mixing free HDL with Hyp/HDL = 70:1 complex. The initial complex Hyp/HDL = 70:1 was mixed after 2 h of stabilization with different amount of free HDL to obtain arious final Hyp/LDL molar ratios: Hyp/HDL = 5:1 (■), Hyp/HDL = 8:1 (□), Hyp/HDL = 10:1 (●), Hyp/HDL = 30:1 (■), Hyp/HDL = 50:1 (□), Hyp/HDL = 70:1 (◄). The concentration of Hyp was kept constant (10 μM). Fluorescence of Hyp recorded at 599 nm, excitation line 515 nm.

The kinetics of the redistribution of Hyp molecules from Hyp HDL = 70:1 complex to free HDL particles, represented by the time evolution of Hyp fluorescence spectra, are presented in Fig. 5. Th appropriate amounts of HDL were added to the stabilized comple Hyp/HDL = 70:1 (stabilization for 2 h at the room temperature) ar the evolution of Hyp fluorescence intensity at its maximu (599 nm) was registered. After adding HDL to the Hyp HDL = 70:1 complex, the increase of Hyp fluorescence for a Hyp/HDL final ratios was observed. The observed redistributio has two phases. First one is represented by the increase of Hy fluorescence immediately (ca. 5–10 s) after mixing HDL and Hyp HDL = 70:1 solutions and the second is expressed by the furth gradual fluorescence increase (Fig. 5). In accordance with th results obtained for the redistribution process of Hyp from Hyp LDL to free LDL, the contribution of the fast phase to the who process appears to be negligible (Fig. 5 and Table 3). The half-time of the slower phase of the process, depending on the final Hyp/HD ratio, are in the range 5–15 min. These values are lower than thos observed for the redistribution of Hyp from the complex Hyp/LD to free LDL (12–45 min). Lower rates for the Hyp translocation fro the complex with LDL to free LDL molecules in comparison wit those observed in the presence of HDL again suggests the role cholesterol in incorporation of Hyp to and releasing fro lipoprotein particles. The mechanism of redistribution of Hy molecules from Hyp/HDL (LDL) complex to free HDL (LDL) particle is not resolved yet. We think that both direct Hyp translocatio from saturated Hyp/HDL complex to free HDL molecules as well translocation through water phase are possible in this redistribu tion process. The partition coefficient of Hyp in octanol/wat mixture has been determined to be log P = 3.43 (Jürgenliemk an Nahrstedt, 2003). This value clearly suggests a strong preference Hyp to be incorporated in lipid structures in comparison wit aqueous phase. As it was previously mentioned, Hyp aggregate formed at high Hyp/HDL ratios can be sticked to the HDL (LD surface. Under collisions of Hyp/HDL complex with free HD particles, a part of Hyp molecules can be transferred directly these free particles. However, certain part of Hyp molecules exis as aggregates in aqueous phase. From this phase, molecules of Hy can be also incorporated into free HDL molecules. More thorough studies are necessary to be performed to definitely resolve th problem.

4. Conclusion

In this study we have shown that molecules of Hyp ar incorporated into HDL particles as monomers until molar rat Hyp/HDL ~8:1. At higher ratios Hyp forms non-fluorescen aggregates in/on these particles. The number of Hyp molecul which can exist in the fully monomeric state in the HDL particles different from that in the case of LDL molecules (8 vs 30). Th difference is mainly related to the smaller size of HDL molecule comparison with LDL molecule (11 nm vs 22 nm). The molecules monomeric Hyp are most probably distributed on the "like spher surface" region located in phospholipid–cholesterol outer lay

(close to the polar head-groups as well as in the interface between outer shell and lipoprotein core) of LDL and HDL molecules.

The kinetics of the association of Hyp molecules with free HDL particles, Hyp/HDL = 10:1 complex as well as the redistribution of Hyp molecules from over-loaded Hyp/HDL = 70:1 complex to free HDL molecules reveal a qualitative similar characteristics of these processes with those obtained for the association of Hyp with LDL (Buriankova et al., 2011)). However, some quantitative differences have been detected. The relative contribution of the rapid and the slow phase of Hyp incorporation into LDL and HDL are different. In the presence of LDL, the major part of Hyp is incorporated into lipoprotein particles in the slow phase (ca. 65%). On the other hand, in the presence of HDL this statement is valid only for the very low Hyp/HDL ratios (1:1 and 2:1), Higher Hyp/HDL ratios lead to a situation when most of Hyp molecules is incorporated into lipoprotein in the rapid phase. Moreover, the incorporation of Hyp into HDLn in the "slow" phase is more rapid than to LDL and extend of HDL penetration into lipoprotein particle in the fats phase is also much higher in the case of HDL. The lower concentration of cholesterol molecules in outer shell of HDL particles is probably the determining factor for the more rapid kinetics of Hyp incorporation to and redistribution from these molecules when comparing with LDL particles. This fact should be taken into account when one is elucidating mechanism of transport and delivery of hydrophobic or amphiphilic drugs in biological organisms.

In conclusion, the obtained data for the kinetics of Hyp association with HDL and LDL provide solid basis for the further investigation of natural lipoproteins molecules (or modified structures of these molecules) as suitable nano-carriers for efficient transport and delivery of hydrophobic and/or amphiphilic drugs to targeted tissues.

Acknowledgements

This work has been supported by the Slovak Research and Development Agency under the contract APVV-0242-11, the Agency of the Ministry of Education of Slovak Republic for the Structural funds of the European Union: Operational Program Research and Development (NanoBioSens (ITMS code: 26220220107), SEPO II (ITMS code: 26220120039), and CEVA II (ITMS code: 26220120040)), and the project CELIM (316310) funded by 7FP EU.

References

Agostinis, P., Vantieghem, A., Merlevede, W., de Witte, P., 2002. Hypericin in cancer treatment: more light on the way. Int. J. Biochem. Cell Biol. 34, 221–241.
Brown, M.S., Goldstein, J.L., 1976. Receptor-mediated control of cholesterol metabolism. Science 191, 150–154.
Buriankova, L., Buzova, D., Chorvat Jr., D., Sureau, F., Brault, D., Miskovsky, P., Jancura, D., 2011. Kinetics of hypericin association with low-density lipoproteins. Photochem. Photobiol. 87, 56–63.
Corbin, I.R., Chen, J., Cao, W., Lund-Katz, S., Zheng, G., 2007. Enhanced cancer targeted delivery using engineered high-density lipoproteinn based nano-carriers. J. Biomed. Nanotechnol. 3, 367–376.
Damiano, M.C., Mutharasan, R.K., Tripathy, S., McMahon, K.M., Thaxton, C.S., 2013. Templated high density lipoprotein nanoparticles as potential therapies and for molecular delivery. Adv. Drug Deliv. Rev. 65, 649–662.
Davis, M.E., Chen, Z., Shin, D.M., 2008. Nanoparticle therapeutics: an emerging treatment modality for cancer. Nat. Rev. Drug Discov. 7, 771–782.
Derycke, A.N.L., de Witte, P., 2004. Liposomes for photodynamic therapy. Adv. Drug Deliv. Rev. 56, 17–30.
Eriksson, E.S.E., Eriksson, L.A., 2011. The influence of cholesterol on the properties and permeability of hypericin derivatives in lipid membranes. J. Chem. Theory Comput. 7, 560–574.
Eriksson, E.S.E., dos Santos, D.J.V.A., Guedes, R.C., Eriksson, L.A., 2009. Properties and permeability of hypericin and brominated hypericin in lipid membranes. J. Chem. Theory Comput. 5, 3139–3149.
Falk, H., 1999. From the photosensitizer hypericin to the photoreceptor stentorin – the chemistry of phenanthroperylene quinones. Angew. Chem. (Int. Ed.) 38, 3116–3136.
Gbur, P., Dedic, R., Chorvat Jr., D., Miskovsky, P., Hala, J., Jancura, D., 2009 resolved luminescence and singlet oxygen formation after illumination hypericin-low-density lipoprotein complex. Photochem. Photobio 816–823.
Glickson, J.D., Lund-Katz, S., Zhou, R., Choi, H., Chen, J.W., Li, H., Corbin, I., Popo Cao, W., Song, L., Qi, C., Marotta, D., Nelson, D.S., Chen, J., Chance, B., Zhe 2008. Lipoprotein nanoplatform for targeted delivery of diagnosti therapeutic agents. Mol. Imaging 7, 101–110.
Hevonoja, T., Pentikainen, M.O., Hyvonen, M.T., Kovanen, P.T., Ala-Korpela, M. Structure of low density lipoprotein (LDL) particles: basis for understa molecular changes in modified LDL. Biochim. Biophys. Acta 1488, 189–
Ho, Y.F., Wu, M.H., Cheng, B.H., Chen, Y.W., Shih, M.C., 2009. Lipid-me preferential localization of hypericin in lipid membranes. Biochim. Bi Acta 1788, 1287–1295.
Huntosova, V., Alvarez, L., Bryndzova, L., Nadova, Z., Jancura, D., Burianko Bonneau, S., Brault, D., Miskovsky, P., Sureau, F., 2010. Interaction dynar hypericin with low-density lipoproteins and U-87 MG cells. Int. J. Pharm 32–40.
Chen, B., Xu, Y., Roskams, T., Delaey, E., Agostinis, P., Vandenheede, J.R., de W 2001. Efficacy of antitumoral photodynamic therapy with hypericin: re ship between biodistribution and photodynamic effects in the RIF-1 tumor model. Int. J. Cancer 93, 275–282.
Chowdhary, R.K., Sharif, I., Chansarkar, N., Dolé hán, D., Ratkay, L., Delar Meadows, H., 2003. Correlation of photosensitizer delivery to lipoprotei efficacy in tumor and arthritis mouse model: comparison of lipid base Pluronic P123 formulations. J. Pharm. Pharm. Sci. 6, 198–204.
Jämbeck, J.P.M., Eriksson, E.S.E., Laaksonen, A., Lyubartsev, A.P., Eriksson, L.A. Molecular dynamics studie sof liposomes as carriers for photosensitizing development validation, and simulations with a coarse-grained model. J. Theory Comput. 10, 5–13.
Jonas, A., Phillips, M.C., 2008. Lipoprotein structure, In: Vance, D.E., Vance, J.E. Biochemistry of Lipids, Lipoproteins and Membranes. 5th ed. Elsevier Sc pp. 485–506.
Jori, G., 1996. Tumour photosensitizers: approaches to enhance the selectivi efficiency of photodynamic therapy. J. Photochem. Photobiol. B 36, 87–
Jori, G., Reddi, E., 1993. The role of lipoproteins in the delivery of tumour-tar photosensitizers. Int. J. Biochem. 25, 1369–1375.
Jürgenliemk, G., Nahrstedt, A., 2003. Dissolution: solubility and cooperati phenolic compounds from *Hypericum perforatum* L. in aqueous sy Pharmazie 58, 200–203.
Karioti, A., Bilia, A.R., 2010. Hypericin as potential leads for new therapeutic Sci. 11, 562–594.
Kascakova, S., Refregiers, M., Jancura, D., Sureau, F., Maurizot, J.C., Miskov 2005. Fluorescence spectroscopic study of hypericin-photosensitized oxi of low-density lipoproteins. Photochem. Photobiol. 81, 1395–1403.
Kascakova, S., Nadova, Z., Mateasik, A., Mikes, J., Huntosova, V., Refregie Sureau, F., Maurizot, J.C., Miskovsky, P., Jancura, D., 2008. High level o density lipoproteins receptors enhance hypericin uptake by U-87 cells presence of LDL. Photochem. Photobiol. 84, 120–127.
Kiesslich, T., Krammer, B., Plaetzer, K., 2006. Cellular mechanisms and prosp applications of hypericin in photodynamic therapy. Curr. Med. Che 2189–2204.
Konan, Y.N., Gurny, R., Alleman, E., 2002. State of the art in the deliv photosensitizers for photodynamic therapy. J. Photochem. Photobiol. 89–106.
Lacko, A.G., Nair, M., Prokai, L., McConathy, W.J., 2007. Prospects and challen the development of lipoprotein-based formulations for anti-cancer drugs Deliv. 4, 665–675.
Lacko, A.G., Nair, M., Paranjape, S., Johnso, S., McConathy, W.J., 2002. High d lipoprotein complexes as delivery vehicles for anticancer drugs. Anticanc 22, 2045.
Lavie, G., Mazur, Y., Lavie, D., Prince, A.M., Pascual, D., Liebes, L., Levin, B., Me D., 1995. Hypericin as an inactivator of infectious viruses in blood compo Transfusion 35, 392–400.
Losi, A., 1997. Fluorescence and time-resolved photoacoustics of hypericin in in liposomes: dependence on pigment concentration and bilayer Photochem. Photobiol. 65, 791–801.
McConathy, W.J., Nair, M.P., Paranjape, S., Mooberry, L., Lacko, A.G., 2008. Eval of synthetic/reconstituted high-density lipoproteins as delivery vehic paclitaxel. Anticancer Drugs 19, 183–188.
Mukherjee, P., Adhikary, R., Halder, M., Petrich, J.W., Miskovsky, P., Accumulation and interaction of hypericin in low-density lipoprotei photophysical study. Photochem. Photobiol. 84, 706–712.
Ng, K.K., Lovell, J.F., Zheng, G., 2011. Lipoprotein-inspired nanoparticles for theranostics. Acc. Chem. Res. 44, 1105–1113.
Oda, M.N., Hargraeves, P.L., Beckstead, J.A., Redmond, K.A., van Antwerpen, R. R.O., 2006. Reconstituted high density lipoprotein antitumoral dru hepatoma cells. J. Lipid. Res. 47, 260–267.
Polo, L., Valduga, G., Jori, G., Reddi, E., 2002. Low-density lipoprotein receptors uptake of tumour photosensitizers by human and rat transformed fibro Int. J. Biochem. Cell Biol. 34, 10–23.
Prassl, R., Laggner, P., 2009. Molecular structure of low density lipoprotein: c status and future challenges. Eur. Biophys. J. Biophys. Lett. 38, 145–158
Puussinen, P.J., Karten, B., Wintersperger, A., Reicher, H., McLean, M., Ma Sattler, W., 2000. The human breast carcinoma cell lines HBL-100 ac exogenous cholesterol from high density lipoprotein via CLA-1 (CD3

LIMPII analoqous 1)-mediated selective cholesteryl ester uptake. Biochem. J. 349, 559–566.
Rao, R.M., Jo, Y., Leers-Sucheta, S., Bose, H.S., Miller, W.L., Azhar, S., Stcco, D.M., 2003. Differential regulation of steroid hormone bios&nthesis in R2C and MA-10 Leyding tumor cells: role of SR-B1 mediated selectivecholesteryl ester transport. Biol. Reprod. 68, 114–121.
Sherman, W.M., van Lier, J.E., Allen, C.M., 2004. Targeted photodynamic therapy via receptor mediated delivery systems. Adv. Drug Deliv. Rev. 56, 53–76.
Siboni, G., Weitman, H., Freeman, D., Mazur, Y., Malik, Z., Ehrenberg, B., 2002. The correlation between hydrophilicity of hypericins and helianthrone: internalization mechanisms, subcellular distribution and photodynamic action in colon carcinoma cells. Photochem. Photobiol. Sci. 1, 483–491.
Strejckova, A., Stanicova, J., Jancura, D., Miskovsky, P., Bano, G., 2013. Spatial orientation and electric-field-driven transport of hypericin inside of bilayer lipid membranes. J. Phys. Chem. B 117, 1280–1286.
Vitols, S., Angelin, B., Ericsson, S., Gahtron, G., Juliusson, G., Maquelier, M., Paul, C Peterson, C., Rudling, M., Sodergreid, K., Tidefelt, G., 1990. Uptake of low densit lipoproteins by human leukemic cells in vivo: relation to plasma lipoprotei levels and possible relevance for selective chemotherapy. Proc. Natl. Acad. Sc U. S. A. 87, 2598–2602.
Wasan, K.M., Brocks, D.R., Lee, S.D., Sachs-Barrable, K., Thornton, S.J., 2008. Impact lipoproteins on the biological activity and disposion of hydrophobic drug implications for drug discovery. Nat. Rev. Drug Discov. 7, 84–99.
Weitman, H., Roslaniec, M., Frimer, A.A., Afri, M., Freeman, D., Mazur, Y., Ehrenbe B., 2001. Solvatochromic effects in the electronic absorption and nuclea megnetic resonance spectra of hypericin in organic solvents and in lipi bilayers. Photochem. Photobiol. 73, 110–118.
Zheng, G., Chen, J., Li, H., Glickson, J.D., 2005. Rerouting lipoprotein nanoparticles t selected alternate receptors for the targeted delivery of cancer diagnostic an therapeutic agents. Proc. Natl. Acad. Sci. U. S. A. 102, 17757–17762.

Apoptosis
DOI 10.1007/s10495-014-1043-7

ORIGINAL PAPER

Effect of PKCα expression on Bcl-2 phosphorylation and cell death by hypericin

Jaroslava Joniova · Matus Misuth · Franck Sureau · Pavol Miskovsky · Zuzana Nadova

Abstract In order to explain the contribution of the protein kinase Cα (PKCα) in apoptosis induced by photo-activation of hypericin (Hyp), a small interfering RNA was used for post-transcriptional silencing of *pkcα* gene expression. We have evaluated the influence of Hyp photo-activation on cell death in non-transfected and transfected ($PKC\alpha^{-}$) human glioma cells (U-87 MG). No significant differences were detected in cell survival between non-transfected and transfected $PKC\alpha^{-}$ cells. However, the type of cell death was notably affected by silencing the *pkcα* gene. Photo-activation of Hyp strongly induced apoptosis in non-transfected cells, but the level of necrotic cells in transfected $PKC\alpha^{-}$ cells increased significantly. The differences in cell death after Hyp photo-activation are demonstrated by changes in: (i) reactive oxygen species production, (ii) Bcl-2 phosphorylation on Ser70 (pBcl-2(Ser70)), (iii) cellular distributions of pBcl-2(Ser70) and (iv) cellular distribution of endogenous anti-oxidant glutathione and its co-localization with mitochondria. In summary, we suggest that post-transcriptional silencing of the *pkcα* gene and the related decrease of PKCα level considerably affects the anti-apoptotic function and the anti-oxidant function of Bcl-2. This implies that PKCα, as Bcl-2 kinase, indirectly protects U-87 MG cells against oxidative stress and subsequent cell death.

Keywords Hypericin · PKCα · Bcl-2 · Apoptosis · Necrosis · Mitochondria · ROS · GSH

J. Joniova · M. Misuth · P. Miskovsky · Z. Nadova (✉)
Department of Biophysics, Faculty of Science, University of Pavol Jozef Safarik, Jesenna 5, 041 54 Kosice, Slovak Republic
e-mail: zuzana.nadova@upjs.sk

J. Joniova · F. Sureau
Laboratoire Jean Perrin LJP, CNRS/UPMC Univ Paris 06, FRE 3231, 75005 Paris, France

P. Miskovsky · Z. Nadova
Centre for Interdisciplinary Biosciences, University of Pavol Jozef Safarik, Kosice, Slovak Republic

Published online: 10 October 2014

Introduction

The protein kinase C (PKC) comprises a family of serine/threonine protein kinases which play a crucial role in transducing signals during proliferation, differentiation and apoptosis. The PKC family is divided into three groups: (i) classical (α, β_I, β_{II}, γ), (ii) novel (δ, ε, η, θ, μ) and (iii) a typical (ζ, ι/λ) isoforms. This division is based on differences in their structure and co-factor (Ca^{2+}, DAG) requirement. In general, atypical isoforms play a role in stress-signaling pathways, while classical PKC members such as PKCα support cell survival and proliferation. The protection of stressed cells by PKCα involves, at least in part, regulation of key anti-apoptotic protein Bcl-2 [1–3].

Because the level of intracellular ATP plays an important role in the decision of a cell between apoptosis and necrosis, mitochondria are the key organelles in this context [4]. Moreover, mitochondria are the place of the integration of pro and anti-apoptotic signals coming from extracellular or intracellular environments. A predominance of pro-apoptotic signals may result in mitochondrial membrane permeabilization and subsequent apoptosis. At the mitochondrial level, key players are members of Bcl-2 family proteins [5]. Pro-apoptotic proteins of the Bcl-2 family (e.g., Bax, Bak) can translocate from cytosol to mitochondria and participate in outer membrane destabilization. Anti-apoptotic family members (e.g., Bcl-2) protect the integrity of the outer mitochondrial membrane via

inhibitory interactions with pro-apoptotic Bax and Bak [6, 7].

In this context, Bcl-2 contains at least three sites that have been identified as phosphorylation sites in a flexible loop region (Thr69, Ser70 and Ser87). Phosphorylation that occurs at Ser70, the PKC phosphorylation site, is required for full anti-apoptotic function of Bcl-2 [8] and can affect the ability to associate with Bax [9].

Beyond its classical anti-apoptotic role, Bcl-2 is also known to have a critical anti-oxidant like function which has been linked experimentally to the regulation of cellular glutathione (GSH) content [10]. GSH is an endogenous antioxidant and key player averting mitochondrial oxidative stress and evading apoptosis [11, 12]. Synthesis of GSH occurs in cytoplasm, and originated GSH must be actively transported into mitochondria. The results obtained by Wilkins et al. suggest that Bcl-2 plays a central role in the regulation of mitochondrial GSH transport through its interaction with 2-oxoglutarate GSH carrier and maintenance of the mitochondrial glutathione pool [13].

It is well known that reactive oxygen species (ROS) mediates intracellular signaling cascades which induce the disintegration of mitochondrial membranes [14] following mitochondria-associated events resulting in apoptosis [15, 16]. Excessive production of ROS and massive oxidative stress is the principal consequence of photodynamic therapy, which combines a force of photo-active drug, appropriate light dose and molecular oxygen.

Hypericin (Hyp) is a naturally occurring photosensitizer, which under light illumination induces anti-proliferative and cytostatic effects on many tumor cell lines. Its photoactivity is characterized by high ROS formation, predominantly singlet oxygen production through the type II mechanism of photo-dynamic action [17, 18]. Specific accumulation of Hyp in tumor cells can also be used for photo-diagnosis of early epithelial cancer [19].

Our previous experimental and molecular modeling study demonstrated that Hyp and phorbol 12-myristate-13-acetate (PMA; PKC activator) might competitively bind to the regulatory C1B domain of PKC. Furthermore Hyp influenced intracellular localization of PKC reflecting its activity, and this influence differed from that observed for PMA [20]. We have also demonstrated that the majority of PKCα present in U-87 MG cells is already in a catalytically competent form phosphorylated at Thr638, and that it is a Bcl-2 kinase [21]. We have shown that in U-87 MG cells, Hyp localizes in subcellular compartments including ER and mitochondria [19]. Photo-activated Hyp affects mitochondrial functions [22] and induces predominantly apoptosis with the participation of Bcl-2 family proteins [19, 21, 23]. To follow up on our previous work and taking into account that in U-87 cells PKCα is Bcl-2 kinase, in the present study we aim to focus more closely on the modulation of PKCα expression and to find out the effects of such a modification on cell survival and cell death pathways after Hyp photo-activation.

Materials and methods

Chemicals

Phosphate saline buffer (PBS), Fetal bovine serum (FBS), Trypsin, 0.05 % (1X) with EDTA 4Na, Penicilin/streptomycin, Hypericin, Annexin-V-FITC, Propidium iodid (PI), CellROX® Deep Red Reagent, CellROX® Green Reagent, CellROX Orange Reagent®, MitoTracker® Orange-CMTMRos ThiolTracker™ Violet were purchased from Gibco-Invitrogen (France). MTT (3-[4, 5-dimethylthiazol-2-yl]-2, 5-diphenyltetrazolium bromide), Hoechst 33258, Triton™ X-100, proteinase K, Formaldehyde and Bovine serum albumin (BSA) were purchased from Sigma-Aldrich (USA). PKCα small interfering RNA (siRNA)(h) and Control siRNA (FITC Conjugate)-A were obtained from Santa Cruz Biotechnology (USA). PKCα[p Thr638] Antibody (E195) was obtained from Novus (USA). PKCδ Antibody (ab47473) was purchased from Abcam (United Kingdom). Rabbit mono-clonal antibody Phospho-Bcl-2 (Ser70) (5H2) against human Bcl-2 phosphorylated on Ser70 was purchased from Cell Signaling Technology (USA). Rabbit poly-clonal antibody against human β-actin was purchased from Sigma-Aldrich (USA). Alexa Fluor® 488 F(ab′)2 fragment of goat anti-rabbit IgG (H+L) and Alexa Fluor® 546 F(ab')$_2$ Fragment of Goat Anti-Rabbit IgG (H+L) were purchased from Gibco-Invitrogen (France). Goat polyclonal secondary antibody against rabbit IgG-H&L (FITC) was purchased from Abcam (United Kingdom).

Cell culture

U-87 MG human glioma cells (Cell Lines Services, Germany) were routinely maintained in Dulbeccós modified Eagle medium (D-MEM) (Gibco-Invitrogen, France) containing L-glutamine (862 mg L^{-1}), sodium pyruvate (110 mg L^{-1}), glucose (4,500 mg L^{-1}), streptomycin (50 μg ml^{-1}), penicillin (50 μg ml^{-1}) and supplemented with 10 % FBS or lipid-free serum substitute 2 % Ultroser G (Pall Life Sciences, France), in the presence of 5 % CO_2 humidified atmosphere at 37 °C [24].

si-RNA transfection protocol

Cells (2×10^5 cells) were seeded onto 35 mm culture dishes (Corning, USA) in 2 ml antibiotic free D-MEM supplemented with 10 % FBS and were incubated at 37 °C

in a CO_2 incubator until they were 60–80 % confluent. For each transfection, 5 µl of siRNA duplex (solution A) was diluted in 100 µl siRNA Transfection Medium and 5 µl of siRNA Transfection Reagent (solution B) was also diluted in 100 µl siRNA Transfection Medium. The siRNA duplex solution (solution A) was added to the Transfection Reagent solution (solution B), and the mixture was incubated for 45 min at room temperature. Meanwhile, cells were washed once with 2 ml of siRNA Transfection Medium. After 45 min of mixture incubation 0.8 ml of siRNA Transfection Medium was added to each tube containing siRNA Transfection Reagent mixture (Solution A + Solution B). The solution was mixed gently and was overlaid to the washed cells and incubated 5 h in the CO_2 incubator. 1 ml of DMEM containing 20 % FBS and 2 % of antibiotics was added to cells without removing the transfection mixture. Cells were incubated for an additional 18 h and were treated according to PDT protocol. The effectiveness of transfection was assessed by confocal microscopy after indirect immunofluorescence staining of PKCα and subsequently verified by western blot analysis. Control siRNA (FITC Conjugate)-A was used as a negative control to avoid false positive results according to manufacturer's recommendation.

Hypericin photo-activation

Cells were incubated for 1 h in dark condition in culture medium containing 2 % Ultroser G and Hyp. The final concentration of Hyp was either 1×10^{-7} or 5×10^{-7} M. For all experiments, the final content of DMSO was less than 0.1 %. After incubation with Hyp, the medium was removed and normal D-MEM containing 10 % FBS was added. Cells were irradiated by monochromatic homemade diode illuminator at 590 nm wavelength and light dose of 4 J/cm^2 [20, 23]. Cellular response was observed 0, 5 and 24 h after irradiation.

Cell survival experiments

Cells were harvested by low-speed centrifugation and seeded at 1×10^4 cells/100 µl of 2 % UG medium per well of 96-well plates. Cell survival was monitored immediately and within 24 h after Hyp photo-activation employing the MTT method [21]. The absorbance of samples was measured at 570 nm (GloMax™-Multi+Detection System with Instinct Software, USA).

DNA fragmentation

Irradiated cells (10^6 cells per sample) were harvested by low-speed centrifugation and lysed in 400 µl of lysis buffer (10 mM Tris, 1 ml EDTA, 0.2 % Triton-X-100) for 5 min at 4 °C. Lysates were centrifuged at 13,000 g for 15 min at 4 °C. DNA in the supernatant was precipitated overnight at −20 °C by the addition of 700 µl of 96 % ethanol and 120 µl of 5 M NaCl. The samples were centrifugated again at 13,000 g for 15 min at 4 °C. The pellet was washed twice with 200 µl of 70 % ethanol and dried at the room temperature. The dried pellet was dissolved in 20 µl of TE buffer (10 mM Tris, 1 mM EDTA) at 65 °C. After cooling to room temperature, 2 µl of RNAse (100 U/ml of PBS) and 2 µl of proteinase K (2 mg/ml) were added and samples were incubated for 10 min at the room temperature. Samples were run on a 2 % agarose gel (Invitrogen). DNA was visualized under UV light [25].

Flow cytometric analysis of apoptosis/necrosis

Cells (approximately 0.5×10^6 cells per sample) were harvested by low-speed centrifugation, resuspended in 100 µl Annexin-binding buffer (Invitrogen, USA) and incubated with 5 µl AnnexinV-FITC for 15 min at room temperature. After the incubation, 400 µl of Annexin-binding buffer was added to each sample. PI was added to each sample to distinguish the necrotic cells. Analysis was performed using a MACSQuant®Analyzer (Miltenyi, GER). Fluorescence was excited with an Argon laser 488 nm and the emission of AnnexinV- FITC was detected in B1 channel (525 ± 50 nm), fluorescence of Hyp was detected in B2 channel (585 ± 40 nm) and fluorescence of PI was detected in B3 channel (655–730 nm). The obtained data were analyzed by MACSQuantify™ Software (Miltenyi, GER).

Flow cytometric analysis of ROS production

Cells were harvested by low-speed centrifugation and resuspended in PBS (approximately 0.5×10^6 cells per sample) and 5×10^{-6} M CellROX® Deep Red reagent was added. After 30 min incubation at room temperature, samples were measured using a MACSQuant® Analyzer (Miltenyi, GER). Fluorescence was excited with an Argon laser 488 nm and emission of CellROX® Deep Red was collected in B3 channel (655 nm-730 nm). The data were analyzed by MACSQuantify™ Software (Miltenyi, GER).

Flow cytometric analysis of pBcl-2(Ser70)

Cells (1×10^6 cell per sample) were harvested by low-speed centrifugation, resuspended in PBS fixed with 3.7 % formaldehyde at room temperature for 10 min and immediately chilled on ice for 1 min. Cells were washed, centrifuged, gently resuspended in ice-cold 90 % methanol and incubated 30 min on ice. 2 ml of incubation buffer (0.5 % BSA in PBS) was added to each aliquot

(approximately 1×10^5 cell per aliquot) and two-times centrifugation was followed. After centrifugation, cells were resuspended in 100 µl of incubation buffer and blocked for 10 min at room temperature. Rabbit mAb (5H2) (Cell Signaling Technology, USA) against human Bcl-2 phosphorylated on Ser70 was used as the primary antibody (1:300, 1 h at room temperature). Consequently, 2 ml of incubation buffer was added to each sample and unconjugated antibody was removed by centrifugation. Fluorochrome-conjugated anti-rabbit AlexaFluor546 (Gibco-Invotrogen, France) was added and cells were incubated for 30 min at room temperature. Then 2 ml of incubation buffer was added to each sample and unconjugated antibody was removed by centrifugation. Cells were resuspended in 0.5 ml of PBS and analyzed using MACSQuant® Analyzer (Miltenyi, GER). Flouorescence was excited with an Argon laser 488 nm and emission of AlexaFluor546 was collected in B2 channel. The data were analyzed by MACSQuantify™ Software (Miltenyi, GER).

Confocal microscopy

Cells (2×10^5 cells) were seeded onto 35 mm culture dishes with integral No. 0 glass cover slip bottoms (MatTek, USA). Cells were incubated with 5×10^{-6} M CellROX® Green or Orange Reagent for 15 min, Hoechst 33258 for 30 min at room temperature, 4×10^{-7} M MitoTracker® Orange [21] and/or with 0.2×10^{-7} M ThiolTracker™ Violet [26] for 10 min at 37 °C. For followed indirect immunofluorescence staining the cells were washed three times with 0.2 % BSA/PBS and fixed with 3.7 % formaldehyde for 15 min. Fixed cells were permeabilized with 0.2 % Triton X-100 for 5 min at room temperature and washed three times with 0.2 % BSA/PBS. Cells were incubated for 1 h in PBS containing 1 % BSA, 10 % goat serum, 0.4 mM Mg^{2+} and 0.2 mM Ca^{2+} at 37 °C to block unspecific labeling. After three washes with 0.2 % BSA/PBS, cells were incubated with specific primary antibodies (Ab) (against PKCα, PKCδ, pBcl-2(Ser70)) overnight at 4 °C. Then cells were washed out three times with 0.2 % BSA-PBS followed by 1 h incubation with appropriate secondary Ab AlexaFluor488 or AlexaFluor546 at 37 °C and washed three times with 0.2 % BSA/PBS to remove unbound secondary Ab and were placed in 0.2 % BSA/PBS. Samples were measured by LSM700 confocal microscope (Zeiss Germany) in using 488 and 555 nm excitations and 63 × oil objective (NA = 1.46). Fluorescence signals were analyzed by the Zen 2011 software (Zeiss, Germany). Co-localization analysis [21] of fluorescence images was performed by means of the ZEN 2011 image processing.

Co-localization analysis

Co-localization analysis was performed on fluorescence images obtained above using the ZEN 2011 image processing. Mander's coefficients, defined as follow, were used for co-localization analysis:

$$M = (R_i.G_i)/\sqrt{\left[\sum R_i^2 \sum G_i^2\right]} \quad (1)$$

$$M_1 = \sum (R_i.G_i)/\sum R_i^2 \quad (2)$$

$$M_2 = \sum (R_i.G_i)/\sum G_i^2 \quad (3)$$

where R_i and G_i are the signal intensity of the pixel number "i" obtained for the red and the green channel, respectively. M-values are thus ranging from 0 to 1. Absolute co-localization corresponds to $M = 1$. The M_1 correlation coefficient, displays how well the red pixels co-localize with some green ones, and the M_2 correlation coefficient displays how well the green pixels co-localize with some red ones. Overlap coefficient does not depend on the relative strengths of each channel, but can be affected by the background signal [27].

Whole cell lysate preparation

Cells (approximately 5×10^5 cells pre sample) were harvested by low-speed centrifugation and were washed twice with PBS. The cell pellet was lysed in 500 µl of RIPA lysis buffer (150 mM NaCl, 1 % Triton X-100, 0.5 % sodium deoxycholate, 0.1 %SDS, 50 mM TRIS) for 5 min on ice. The crude cell lysate was homogenized by using insulin needle and centrifuged [21]. The supernatant was collected into a new Eppendorf tube and protein content was determined by BCA protein assay kit (Thermo Scientific, Rockford, IL, USA) according to manufacturer's recommendation.

Western blot analysis

Protein samples (120 µg) were diluted in 2 x Laemmli solution (10 % SDS, 1 M Tris–HCl, water, 0.02 % bromphenol blue) and incubated for 5 min at 95 °C in a dry bath to prevent protein denaturation during electrophoresis. SDS-PAGE was performed. Samples were run at a voltage of 75 V for 30 min for transition through 4 % polyacrylamide stacking gel, and 100 V for 70 min for passage samples through 10 % polyacrylamide resolving gel, employing Mini-PROTEAN Tetra Cell, (Bio-Rad, USA). Proteins separated by SDS-PAGE were blotted onto 0.45 µm nitrocellulose membrane from Bio-RAD (USA) for 30 min at a constant voltage of 75 V using Trans-Blot SD, Semi-Dry Electrophoretic Transfer Cell (Bio-Rad, USA).

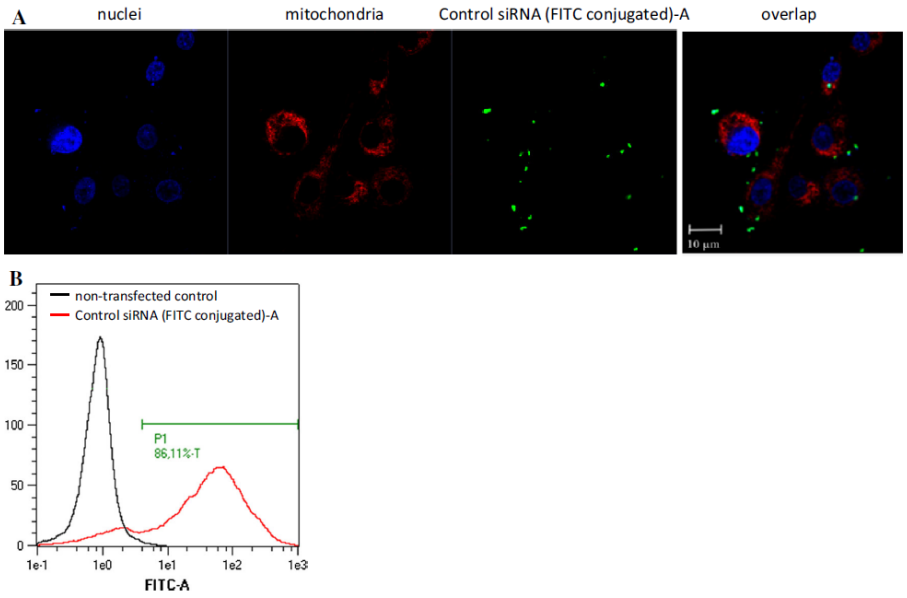

Fig. 1 Detection of siRNA transfection efficiency in U87-MG cells **a** Confocal fluorescence image of nuclei (*blue*) and mitochondria (*red*) of U87-MG cells entered by FITC-conjugated scrambled siRNA Control-A (*green*). Scrambled siRNA was transfected into U87-MG cells and nuclei (Hoechst 33258) and mitochondria (MitoTracker Orange) were stained after 5 h. **b** Flow cytometry histograms of control non-transfected cells (*black line*) and cells entered by FITC-conjugated scrambled siRNA Control-A (*red line*)

Western Breeze Chromogenic Immunodetection System (Invitrogen, USA) was used for immunodetection of selected proteins. The membrane was blocked by manufacturer blocking solution for 30 min and then washed with distilled water two times for 5 min. The washed membrane was incubated overnight at 4 °C with primary antibody. Rabbit poly-clonal antibody (pTHR638) (1:10,000) against human PKCα and rabbit poly-clonal antibody (1:500) against human β-actin were used as primary antibody.

After the incubation the membrane was washed with manufacturer antibody washing buffer and incubated with secondary antibody solution for 30 min. Then the membrane was washed with antibody washing solution and incubated with Chromogenic substrate until purple bands developed on the membrane. Results were evaluated with ImageJ Software on the basis of comparison of optical density of each band.

Results

Transfection efficiency

To determine the transfection efficiency, Control siRNA (FITC Conjugate)-A was used. This control contains a scrambled sequence that does not lead to specific degradation of any known cellular RNA and represents a negative control to avoid false positive results. Figure 1a shows confocal fluorescence images of cells transfected with scrambled siRNA. siRNA entered the cells, and green fluorescence originated from Control siRNA (FITC Conjugate)-A was detected in the cytoplasm. Based on nuclear (blue fluorescence originated from Hoechst 33258) and mitochondrial (red fluorescence originated from MitoTracker Orange®) morphology, no significant changes have been detected. The effect of scrambled Control siRNA-A on key investigated parameters (such as cell viability, ROS production and Bcl-2 phosphorylation) is described further within the corresponding paragraphs. Figure 1b shows histograms of non-transfected control cells (black line) and cells transfected with Control siRNA (FITC Conjugate)-A (red line) obtained by flow cytometry. Flow cytometry clearly demonstrates that after 5 h transfection efficiency was about 87 %.

PKCα gene silencing

To silence the *pkcα* gene, U-87 MG cells were treated according to siRNA transfection protocol. Confocal fluorescence microscopy along with western blot analysis were used to confirm *pkcα* gene silencing. Figure 2a shows confocal fluorescence image of non-transfected and

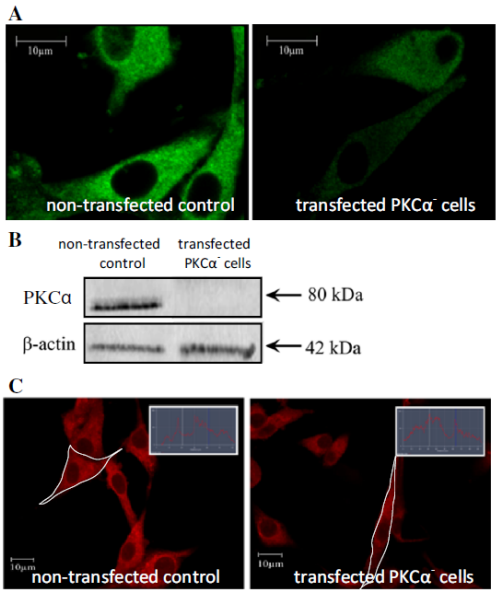

Fig. 2 Effectivity and specificity of siRNA PKCα(h) transfection. **a** Distribution of PKCα in human U87-MG cells. The figure shows confocal fluorescence image of U87-MG non-transfected control cells (*left*) and cells transfected with siRNA PKCα(h) (*right*) both stained with primary Ab against PKCα (E195, Novus, USA) for visualization of distribution of PKCα. **b** Western blot analysis of endogenous expression of PKCα in non-transfected (PKCα) and transfected (PKCα^{-}) U87-MG cells. Cell lysates were prepared according to the Whole cell lysate preparation protocol described in Materials and methods and were subjected to SDS-PAGE and Western blot analysis. The membranes were probed withAb (E195, Novus, USA), which specifically recognized the catalytically competent form of PKCα phosphorylated at Thr638 (PKC, (pThr638)). As protein reference control, anti β-actin antibody (Abcam, GB) was used. **c** Distribution of PKCδ in human U87-MG cells. The figure shows confocal fluorescence image of U87-MG non-transfected control cells (*left*) and cells transfected with siRNA PKCα(h) (*right*) both stained with primary Ab against PKCδ (ab47473, Abcam) for visualization of distribution of PKCδ. In all cases images were taken with the same measuring parameters (brightness, contrast and laser power). The scale bar represents 10 μm. *Inset*: Fluorescence intensity profile of marked cells obtained by using ZEN 2010 software (Zeiss, Germany)

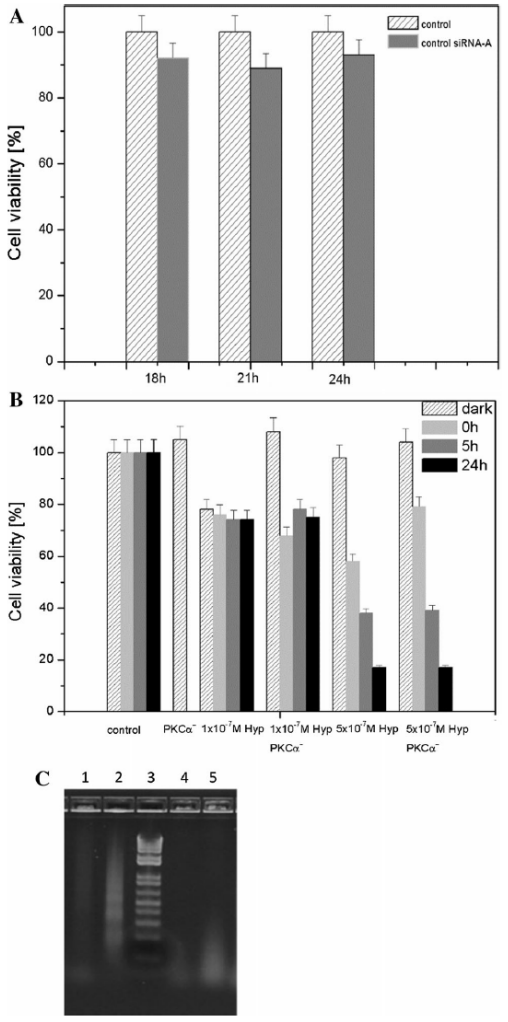

Fig. 3 Cell survival and DNA fragmentation after Hyp photo-activation. **a** Cell viability test and the effect of scrambled siRNA Control-A (negative control) on cell survival. **b** Cell viability test of non-treated and siRNA PKCα(h) treated U87-MG cells before and after Hyp photo-activation. Viability of non-transfected U87-MG cells and cells transfected with siRNAPKCα(h) after Hyp photo-activation was determined by the MTT test. The cells were plated into 96-well tissue culture plates at a density of 10,000 cells per well and were cultivated until an optimal population density was reached. Cells were incubated with Hyp, and Hyp photo-activation protocol was used as described in Materials and methods. Results of adherent cell numbers from three independent experiments are expressed relative to control (100 %) and represent mean values. **c** DNA fragmentation after Hyp photo-activation in non-transfected and transfected PKCα^{-} cells. Non-transfected cells treated with (*1*) 1×10^{-7} Hyp, (*2*) 5×10^{-7} Hyp, (*3*) DNA Ladder, transfected PKCα^{-} cells treated with (*4*) 1×10^{-7} Hyp, (*5*) 5×10^{-7} Hyp

transfected PKCα^{-} cells. One can see that the fluorescence intensity of cells transfected with siRNA is much lower than the fluorescence intensity of the control cells. This result was verified by western blot analysis (Fig. 2b) where the optical density of transfected PKCα^{-} cells was 6.37 % in comparison with non-transfected cells for which optical density was 93.62 %. It proves that *pkcα* gene silencing carried through siRNA efficiently decreased the amount of PKCα protein in transfected U-87 MG cells. The specificity of siRNA PKCα(h) transfection was verified by confocal

microscopy (Fig. 2c). Non-transfected and transfected PKCα⁻ cells were stained by indirect immunofluorescence, and PKCδ (as a representative member of PKCs) was visualized. Fluorescence intensity of the measured cells (marked with white line) are comparable (Fig. 2c) and indicate that silencing of *pkcα* gene expression is specific and the expression of PKCδ is not affected. The specificity of pkcα silencing observed in our work was confirmed also by other groups [28].

Cell survival after Hyp photo-activation

For better elucidation of the significance of PKCα in apoptosis induced by photo-activated Hyp, cell survival was assessed after silencing *pkcα* gene transcription. We have assumed that silencing of anti-apoptotic PKCα by using of siRNA would result in more effective treatment with a lower concentration of Hyp and would thus significantly reduce the amount of surviving cells. To be sure that transfection has no influence on the cell survival, the colorimetric MTT assay with scrambled Control siRNA-A (Fig. 3a) was performed. It shows that scrambled Control siRNA-A has no influence on cell viability. We have observed that decreased transcription of the *pkcα* gene has a negligible effect on the U-87 MG cell survival (Fig. 3b): Cell viability assessed 0, 5 and 24 h after 1×10^{-7}M Hyp photo-activation decreased by about 30 % and appeared to be similar when compared with transfected PKCα⁻ cells. 5×10^{-7} M Hyp is of course more effective in comparison with 1×10^{-7} M, and percentages of living cells decrease with time after irradiation. However, similar decreases of cell survival were observed both for transfected PKCα⁻ and non-transfected cells after Hyp photo-activation. Thus, the effect of Hyp photo-activation in combination with *pkcα* gene silencing on cell survival did not fulfill expected differences between transfected PKCα⁻ and non-transfected cells.

Figure 2c shows DNA fragmentation in non-transfected and transfected PKCα⁻ cells after Hyp photo-activation where the DNA ladder is clearly visible in non-transfected cells, but in transfected PKCα⁻ cells DNA fragmentation was not observed.

Apoptosis versus necrosis after Hyp photo-activation

The balance between photo-induced apoptotic and necrotic cell death was determined by flow cytometry after dual staining with Annexin V-FITC and PI (Fig. 4a). For both Hyp concentrations, we can clearly observe a decreased level of apoptosis and an increased level of necrosis in transfected U-87 MG cells (Fig. 4a, rows 3, 5) when compared with non-transfected cells (Fig. 4a, rows 2, 4) and cells transfected with scrambled siRNA. For cells treated with 5×10^{-7}M Hyp, increased necrosis can be observed in transfected PKCα- cells immediately after irradiation. Figure 4b presents histograms representing the relative level of necrosis and apoptosis 24 h after photo-activation for non-transfected and transfected cells either treated with 1×10^{-7} or 5×10^{-7} M.

Reactive oxygen species production

Based on detected changes in the type of cell death, we assessed the level of reactive oxygen species production related to Hyp photo-activation. Cells were stained with CellROX reagents (Green, Orange and/or Deep Red), and confocal microscopy and flow cytometry analysis was immediately performed. CellROX reagents are non-fluorescent dyes in a reduced state that exhibit bright fluorescence upon oxidation by ROS. As shown in Fig. 5a, fluorescence related to increased ROS production can be observed after Hyp photo-activation for both transfected PKCα⁻ cells and non-transfected cells. One can see that Hyp photo-activation leads to an increase of ROS production inside tested cells, and the level of ROS production is more pronounced in transfected PKCα- cells. To determine the effect of *pkcα* gene silencing and Hyp photo-activation on nuclear morphology, cells were stained with Hoechst 33258, a blue-fluorescent dye used for fluorescence detection of the compacted state of the chromatin. From Fig. 5a one can see that the nuclear morphology of both controls (non-transfected cells vs Control siRNA-A transfected cells) is comparable, without observed increase of chromatin condensation. Apoptotic nuclei are more visible after Hyp photo-activation in non-transfected cells. On the contrary, no significant chromatin condensation of nuclei in transfected PKCα- cells has been observed. However, flow cytometric quantitative analysis of ROS production 5 h after Hyp photo-activation shows significant differences between transfected PKCα⁻ and non-transfected cells. In all cases, ROS production appears to be related to the initial concentration of Hyp and slightly decreased as a function of post-irradiation time, but it is also clearly higher in transfected cells when compared to non-transfected ones (Fig. 4b).

Bcl-2 phosphorylation on serine70 (pBcl-2(Ser70))

Taking into account that 5×10^{-7}M Hyp is an effective concentration of photo-sensitizer, experiments focused on the role of Bcl-2 protein in cell death induction were carried out with this concentration of Hyp. Bcl-2 phosphorylation on Ser70 was first assessed by flow cytometry 2 h after Hyp photo-activation. Data analysis (Fig. 6a) showed a slight decrease in the level of Bcl-2 protein phosphorylated at Ser70 after Hyp photo-activation (black line)

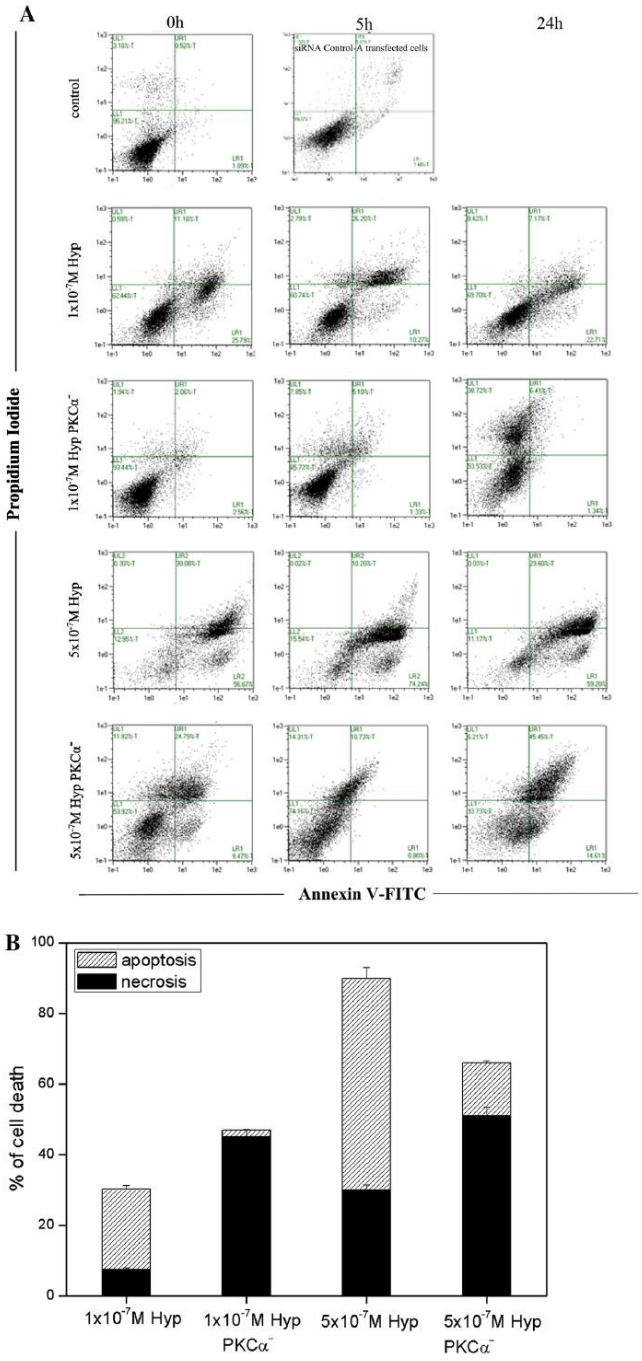

Fig. 4 Determination of the cell death (apoptosis/necrosis) induced by photo-activated Hyp within 24 h after cell irradiation. **a** Representative flow-cytometric dot plot analysis of apoptosis/necrosis after Annexin V-FITC/PI staining in non-transfected cells and cells transfected with siRNA PKCα(h) obtained 0, 5 or 24 after Hyp photo-activation. Three major populations of cells can be observed in the cytotoxicity assay: Annexin V^-/PI^- cells are defined as live cells, Annexin V^+/PI^- cells as apoptotic cells and PI+ as dead cells (late apoptotic or necrotic). **b** *Histograms* showing the comparison ratio of apoptosis and necrosis (live cells are not considered) in the cells non-treated and treated with siRNA PKCα(h) 24 h after Hyp photo-activation. Values are mean ± SD of three independent experiments

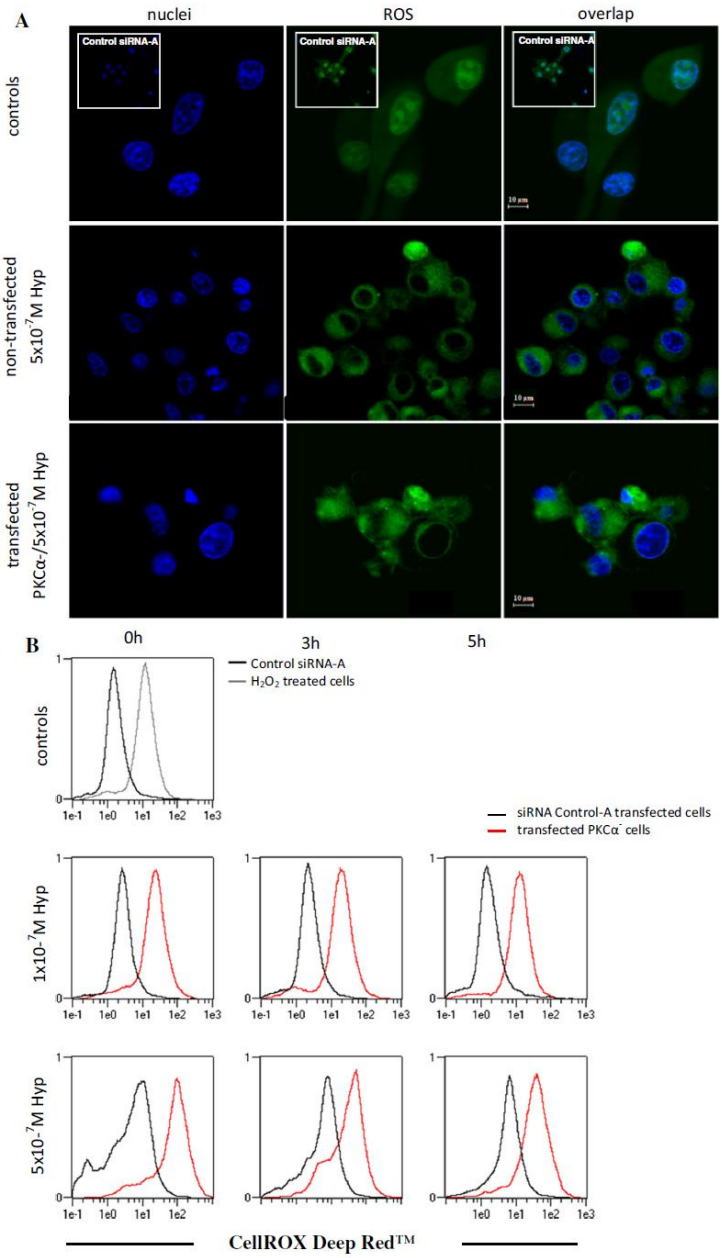

Fig. 5 ROS production after Hyp photo-activation. **a** CellROX (*green*) and Hoechst 33258 (*blue fluorescence*) confocal fluorescence images displaying production of ROS and nuclear morphology (*blue*) in the non-transfected cells (*first row*) and cells transfected with siRNA PKCα(h) (*second row*) incubated with Hyp measured within 1 h after Hyp photo-activation. The *scale bar* represents 10 µm. *Inset:* Effect of negative control (scrambled siRNA Control-A) on ROS production and nuclear morphology. **b** Histograms of ROS production obtained by flow cytometry after CellROX DeepRed™ staining in non-transfected cells and cells transfected with siRNA PKCα(h) 0, 1, and 3 h after Hyp photo-activation

compared with control cells (grey line). A consequence of *pkcα* gene silencing followed by Hyp photo-activation is an additional decrease of Bcl-2 phosphorylation (red line). This result was verified by western blot analysis (Fig. 6b). It proves that *pkcα* gene silencing decreases phosphorylation of Bcl-2 protein at Ser70.

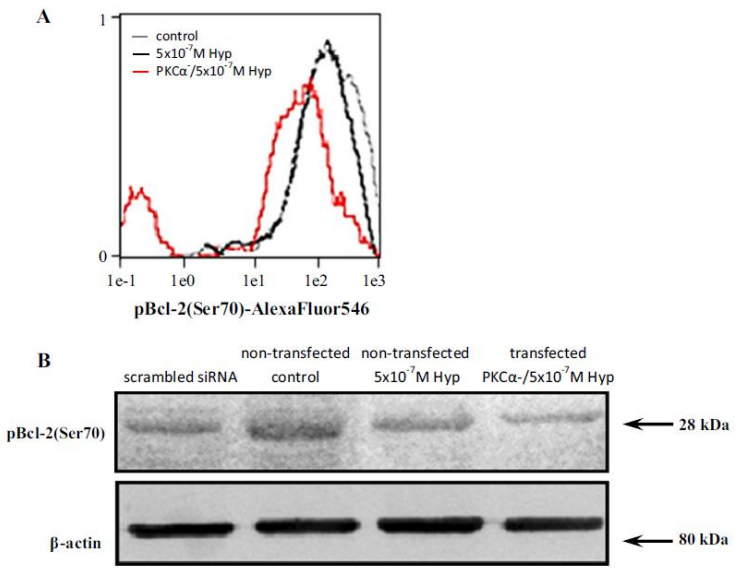

Fig. 6 Level of Bcl-2 phosphorylation on Ser70 after Hyp photo-activation. a Flow cytometry histogram of Bcl-2 phosphorylation on Ser70 after indirect immuno-fluorescence staining with rabbit mAb (5H2) (Cell Signaling Technology, USA) against human pBcl-2(Ser70). Level of Bcl-2 phosphorylation on Ser70 after Hyp photo-activation is obtained for control cells (*grey line*), non-transfected cells (*black line*) and cells transfected with siRNA PKCα(h) (*red line*). **b** Western blot analysis of endogenous expression of pBcl-2(Ser70) in non-transfected (PKCα) and transfected (PKCα$^-$) U87-MG cells. Cell lysates were prepared according to the Whole cell lysate preparation protocol described in Materials and methods and were subjected to SDS-PAGE and Western blot analysis. The membranes were probed with Ab (ab47473, Abcam, UK), which specifically recognized Bcl-2 phosphorylated at Ser70. As protein reference control, anti β-actin antibody (Abcam, UK) was used

Fluorescence imaging of pBcl-2(Ser70), mitochondria and GSH

Mitochondrial localization of pBcl-2(Ser70) and GSH was studied by fluorescence imaging 2 h after Hyp photo-activation as a function of *pkcα* gene silencing. Figure 7 and corresponding Table 1 represent the results of co-localization analysis. Co-localization analysis was performed on fluorescence images by ZEN2010 Software (Zeiss, Germany) and co-localized pixels are presented as yellow points in the Fig. 7. Confocal microscopy showed (Fig. 7a) that the pBcl-2(Ser70) is distributed through whole cells in control conditions. However, after Hyp photo-activation, strong re-localization of pBcl-2(Ser70) to mitochondria occurred in both, non-transfected and transfected PKCα$^-$ cells. There is evidence of co-localization between pBcl-2(Ser70) and mitochondria, but the information from the image is just qualitative. Co-localization coefficients calculated for better understanding and quantification of co-localization are presented in Table 1, where M_1 coefficient displays co-localization of the red pixels with green ones, and the M_2 coefficient displays co-localization of the green pixels with red ones. Quantitative results of the co-localization analysis (Table 1) describe (i) the presence of pBcl-2(Ser70) in mitochondria, (ii) co-localization of and (iii) the presence of GSH in mitochondria. This means that we have observed a slight decrease of co-localization of pBcl-2(Ser70) and mitochondria 2 h after Hyp photo-activation (M_2 = 0.91) compared with control cells (M_2 = 0.99). A substantial decrease of co-localization between pBcl-2(Ser70) and mitochondria (M_2 = 0.75) was detected in transfected PKCα$^-$ cells after Hyp photo-activation. Figure 7b shows confocal images of cells stained with ThiolTracker™ Violet (green fluorescence) and primary antibody against pBcl-2(Ser70) (red fluorescence). Under control conditions GSH (green) is distributed throughout the cells. Co-localization between pBcl-2(Ser70) and GSH was calculated from only the cytoplasmic region of measured cells, while the fluorescence signal from the nucleus was disregarded. Under control conditions, co-localization images show that GSH is co-localized with pBcl-2(Ser70) (M_2 = 0.99). Decreased co-localization was observed after Hyp photo-activation (M_2 = 0.88) in non-transfected cells compared to the control. A considerable decrease of the co-localization was related to *pkcα* gene silencing (M_2 = 0.73) in transfected PKCα$^-$cells exposed to photo- activation of Hyp.

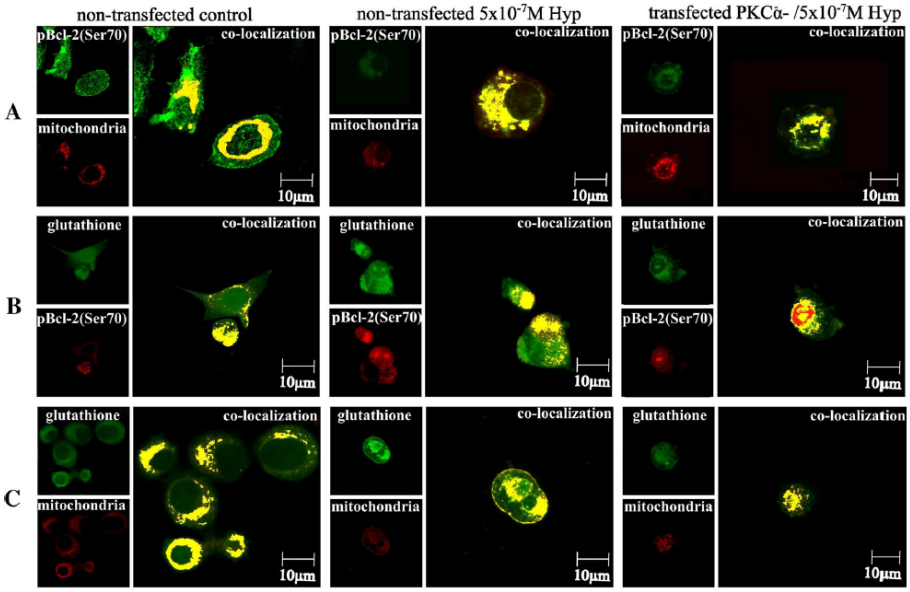

Fig. 7 Cellular distributionand co-localization of pBcl-2(Ser70), GSH and mitochondria after Hyp photo-activation. **a** Cellular distribution of pBcl-2(Ser70) and mitochondria. **b** Cellular distribution of glutathione and pBcl-2(Ser70). **c** Cellular distribution of glutathione and mitochondria in control cells (*left*), non-transfected (*middle*) and PKCα^{-} cells transfected with siRNA PKCα after Hyp photo-activation (*right*). The distribution of pBcl-2(Ser70), glutathione and mitochondria was detected by confocal microscopy following vital cell staining with ThiolTracker™ Violet and MitoTracker Orange®) and indirect immunofluorescence staining with 5H2 antibody against Bcl-2 phosphorylated on Ser70

Table 1 Co-localization analysis of pBcl-2(Ser70) in mitochondria, pBcl-2(Ser70) and GSH, and the presence of GSH in mitochondria

	pBcl-2(Ser70) MitoTracker®Orange			ThiolTracker™Violet pBcl-2 (Ser70)			ThiolTracker™Violet_MitoTracker®Orange		
	Overlap	M_1	M_2	Overlap	M_1	M_2	Overlap	M_1	M_2
Control	0.83	0.62	0.99	0.77	0.17	0.99	0.75	0.37	0.96
5×10^{-7} M Hyp	0.77	0.51	**0.91**	0.68	0.65	**0.88**	0.65	0.34	**0.98**
5×10^{-7} M Hyp/PKCα^{-}	0.63	0.55	**0.75**	0.65	0.41	**0.73**	0.87	0.65	**0.88**

Bold values are used to make a visible significant decrease of co-localization between observed fluorescent probes as describe M_2 coefficients

Co-localization analysis was performed on the obtained fluorescence images using the ZEN 2011 image processing (Zeiss, Germany). Co-localization coefficients M_1; M_2 represents a relative number of co-localized pixels in channel 1 or 2 as compared to the total number of pixels about thresholds (min. value 0: no co-localization, max value 1: all pixels co-localized). Co-localization was calculated only from the cytoplasmic region of measured cells, while fluorescence signal from the nucleus was disregarded

Finally, we investigated co-localization between GSH (green fluorescence) and mitochondria (red fluorescence). Figure 6c shows confocal images of cells stained with ThiolTracker™ Violet and MitoTracker® Red FM. Under control conditions some portion of GSH was strongly associated with mitochondria ($M_2 = 0.96$). After Hyp photo-activation, redistribution of GSH to cellular membranes was detected, and the association of GSH with mitochondria was still evident ($M_2 = 0.98$). In transfected PKCα^{-} cells co-localization coefficients suggested that photo-activation of Hyp after *pkcα* gene silencing ($M_2 = 0.88$) affects and decreases the presence of GSH in mitochondria.

Discussion

Various types of tumors including glioblastomas, breast and prostate tumors have high expression levels of anti-apoptotic protein PKCα. Several studies have tried to investigate the role of PKCα in cell survival. It has been

suggested that PKCα is involved in tumor development and plays a role in promoting cell survival [28, 29]. We have previously studied the role of PKCα in U87-MG cells after Hyp photo-activation [21]. For a better understanding of the role of PKCα in cell death induced by Hyp photo-activation, the effect of *pkcα* gene silencing in the U-87 MG cell line was studied. We focused on better understanding the impact and consequence of such silencing on cell survival and cell death. Previous results [21, 23] indicate that cells undergo apoptosis after Hyp photo-activation (Fig. 2b). Thus, we can expect that silencing of this protein by using of siRNA would have an effect on Hyp photo-induced cell death. We hypothesized that the level of apoptosis could occur more easily and that this modulation of PKCα expression would result in more effective treatment with a lower concentration of Hyp and consequently would reduce surviving cells. Surprisingly, the combination of PKCα silencing and Hyp photo-activation did not result in a greater impact on cell viability (Fig. 1b). On the other hand, after Hyp photo-activation a significant difference between transfected PKCα^{-} cells was detected when compared with non-transfected cells. Cells with a blocked *pkcα* gene underwent necrosis prior to apoptosis which was present in the non-transfected cells (Fig. 4b). This behavior can be explained by much higher formation of ROS in the transfected PKCα^{-} cells (Fig. 5b). As has already been shown, the level of ROS formation plays an important homeostatic role regulating signal transduction involved in proliferation and cell survival. Moreover, when ROS formation is deregulated and surpasses antioxidant defenses, oxidative stress takes place, and when oxidative stress exceeds the capacity of the cell to repair biomolecule oxidation (nucleic acids, lipids and proteins), irreversible oxidative damage occurs [14, 15, 30]. Thus, the predominance of necrosis prior to apoptosis in transfected cells can be considered to be related to such an ROS increase.

The Bcl-2 family of proteins are important regulators of programmed cell death pathways with individual members that can suppress (e.g., Bcl-2, Bcl-XL) or promote (e.g., Bax, Bad) apoptosis [7, 31, 32]. Occurrence of necrosis in the transfected PKCα^{-} cells is connected to much higher decrease of the phosphorylation of Bcl-2 after Hyp photo-activation (Fig. 6) because in the cells, phosphorylation of Bcl-2 occurs in order to protect cells from apoptosis [32]. Recent studies have shown that agonist-activated phosphorylation of Bcl-2 at Ser70 (single site phosphorylation is required for Bcl-2′s full and potent anti-apoptotic function [32]. Thus the observed decrease of Bcl-2 phosphorylation after siRNA gene silencing and Hyp photo-activation could explain the decreased amount of apoptotic cells. However, the question why we observed such an important increase of ROS production and subsequent necrosis in transfected PKCα^{-}cells after Hyp photo-activation remains to be answered. Our hypothesis is that the increased oxidative stress generated during photo-dynamic action of Hyp in transfected cells as well as during cell death development could be a key factor for the observed shift from apoptosis to necrosis. It was reported previously that mitochondria, ROS, GSH and Bcl-2 are closely related [33, 34]. Indeed, GSH is considered a key endogenous anti-oxidant to combat ROS produced by the electron transport chain in mitochondria. Moreover, it has already been shown that intracellular GSH plays a crucial role in determining the mode of death in isolated rat hepatocytes [35]. The role of Bcl-2 in GSH transport into mitochondria is well described in the work of Wilkins et al. [13]. We have previously reported changes in the mitochondrial NAD(P)H content and possible alteration in the mitochondrial metabolic state after Hyp photo-activation [22]. The observed rise of mitochondrial NAD(P)H fluorescence could be explained in relation to enzymatic elimination of mitochondrial oxidative stress with participation of GSH [36]. It was shown that an anti-oxidant like protein Bcl-2 over expression leads to an increase of cellular GSH [37–39]. In contrast, Bcl-2 knockout mice had reduced level of GSH in brain tissue and were more sensitive to neuronal cell death induced by mitochondrial oxidative stress [40]. In the context of anti-oxidative protection of mitochondria against oxidative stress, we have investigated the co-localization of GSH with Bcl-2 and mitochondria. Bcl-2 is localized in the outer mitochondrial membrane, and GSH is within the mitochondrial matrix where its anti-oxidative functions are linked to other enzymatic systems of the mitochondria [36]. PKCα post-transcriptional gene silencing decreases GSH presence in mitochondria and lower co-localization between pBcl-2(Ser70) and GSH (Fig. 6). Our results indicate that pBcl-2(Ser70) is involved in the maintenance of mitochondrial GSH level in U-87 MG cells. Consequently, the observed necrosis after Hyp photo-activation seems to be a result of insufficient elimination of ROS by free radical scavenging systems, such as mitochondrial GSH, as a consequence of decreased phosphorylation of Bcl-2 in the background of post-transcriptional silencing of *pkcα* gene.

Acknowledgments This work was supported by: the FP7 EU project CELIM 316310, the project of the Slovak Res. and Dev. Agency APVV-0242-11, the project of the Agency of the Ministry of Education of Slovak (Republic for the Structural funds of the European Union: Doktorand (ITMS code: 26110230013) and KVARK (ITMS code: 26110230084) and by the International Program for Scientific Cooperation (PICS N°5398) from the CNRS. This work forms a part of the co-tutoring doctoral study of J. J. (P. J. Safarik University and UPMC).

Conflict of interest The authors declare that they have no conflict of interest.

References

1. Mellor H, Parker PJ (1998) The extended protein kinase C superfamily. Biochem J 332:281–292
2. Nishizuka Y (1995) Protein kinases.5. Protein-kinase-C and lipid signaling for sustained cellular-responses. Faseb Journal 9: 484–496
3. Jiffar T, Kurinna S, Suck G et al (2004) PKC alpha mediates chemoresistance in acute lymphoblastic leukemia through effects on Bcl2 phosphorylation. Leukemia 18:505–512
4. Nikoletopoulou V, Markaki M, Palikaras K, Tavernarakis N (2013) Crosstalk between apoptosis, necrosis and autophagy. Biochimica Et Biophysica Acta-Molecular Cell Research 1833:3448–3459
5. Merino D, Bouillet P (2009) The Bcl-2 family in autoimmune and degenerative disorders. Apoptosis 14:570–583
6. Koc M, Nad'ova Z, Truksa J, Ehrlichova M, Kovar J (2005) Iron deprivation induces apoptosis via mitochondrial changes related to Bax translocation. Apoptosis 10:381–393
7. Ackermann EJ, Taylor JK, Narayana R, Bennett CF (1999) The role of antiapoptotic Bcl-2 family members in endothelial apoptosis elucidated with antisense oligonucleotides. J Biol Chem 274:11245–11252
8. Ruvolo PP, Deng XM, Carr BH, May WS (1998) A functional role for mitochondrial protein kinase C alpha in Bcl2 phosphorylation and suppression of apoptosis. J Biol Chem 273: 25436–25442
9. Blagosklonny MV, Giannakakou P, el-Deiry WS et al (1997) Raf-1/bcl-2 phosphorylation: a step from microtubule damage to cell death. Cancer Res 57:130–135
10. Voehringer DW (1999) BCL-2 and glutathione: alterations in cellular redox state that regulate apoptosis sensitivity. Free Radic Biol Med 27:945–950
11. Franco R, Cidlowski JA (2009) Apoptosis and glutathione: beyond an antioxidant. Cell Death Differ 16:1303–1314
12. Circu ML, Aw TY (2008) Glutathione and apoptosis. Free Radical Res 42:689–706
13. Wilkins HM, Marquardt K, Lash LH, Linseman DA (2012) Bcl-2 is a novel interacting partner for the 2-oxoglutarate carrier and a key regulator of mitochondrial glutathione. Free Radic Biol Med 52:410–419
14. Malik F, Kumar A, Bhushan S et al (2007) Reactive oxygen species generation and mitochondrial dysfunction in the apoptotic cell death of human myeloid leukemia HL-60 cells by a dietary compound with a ferin A with concomitant protection by N-acetyl cysteine. Apoptosis 12:2115–2133
15. Papa L, Gomes E, Rockwell P (2007) Reactive oxygen species induced by proteasome inhibition in neuronal cells mediate mitochondrial dysfunction and a caspase-independent cell death. Apoptosis 12:1389–1405
16. Shen S, Zhang Y, Zhang R, Gong X (2013) Sarsasapogenin induces apoptosis via the reactive oxygen species-mediated mitochondrial pathway and ER stress pathway in HeLa cells. Biochem Biophys Res Commun 441:519–524
17. Miskovsky P (2002) Hypericin - A new antiviral and antitumor photosensitizer: mechanism of action and interaction with biological macromolecules. Curr Drug Targets 3:55–84
18. Kocanova S, Buytaert E, Matroule JY et al (2007) Induction of heme-oxygenase 1 requires the p38(MAPK) and PI3K pathways and suppresses apoptotic cell death following hypericin-mediated photodynamic therapy. Apoptosis 12:731–741
19. Huntosova V, Alvarez L, Bryndzova L et al (2010) Interaction dynamics of hypericin with low-density lipoproteins and U87-MG cells. Int J Pharm 389:32–40
20. Kocanova S, Hornakova T, Hritz J et al (2006) Characterization of the interaction of hypericin with protein kinase c in U-87 MG human glioma cells. Photochem Photobiol 82:720–728
21. Dzurova L, Petrovajova D, Nadova Z, Huntosova V, Miskovsky P, Stroffekova K (2014) The role of anti-apoptotic protein kinase Calpha in response to hypericin photodynamic therapy in U-87 MG cells. Photodiagn Photodyn Ther 11:213–226
22. Petrovajova D, Jancura D, Miskovsky P et al (2013) Monitoring of singlet oxygen luminescence and mitochondrial autofluorescence after illumination of hypericin/mitochondria complex: a time-resolved study. Laser Phys Lett 10:7
23. Buriankova L, Nadova Z, Jancura D et al (2010) Synchrotron based Fourier-transform infrared microspectroscopy as sensitive technique for the detection of early apoptosis in U-87 MG cells. Laser Phys Lett 7:613–620
24. Kascakova S, Nadova Z, Mateasik A et al (2008) High level of low-density lipoprotein receptors enhance hypericin uptake by U-87 MG cells in the presence of LDL. Photochem Photobiol 84:120–127
25. Ehrlichova M, Koc M, Truksa J, Naldova Z, Vaclavikova R, Kovarr J (2005) Cell death induced by taxanes in breast cancer cells: cytochrome c is released in resistant but not in sensitive cells. Anticancer Res 25:4215–4224
26. Mandavilli BS, Janes MS. (2010) Detection of intracellular glutathione using ThiolTracker violet stain and fluorescence microscopy. Curr Protoc cytom Chapter 9:Unit 9.35–Unit 39.35
27. Huntosova V, Nadova Z, Dzurova L, Jakusova V, Sureau F, Miskovsky P (2012) Cell death response of U87 glioma cells on hypericin photoactivation is mediated by dynamics of hypericin subcellular distribution and its aggregation in cellular organelles. Photochem Photobiol Sci 11:1428–1436
28. Adhikary G, Chew YC, Reece EA, Eckert RL (2010) PKC-delta and -eta, MEKK-1, MEK-6, MEK-3, and p38-delta Are Essential Mediators of the Response of Normal Human Epidermal Keratinocytes to Differentiating Agents. J Invest Dermatol 130: 2017–2030
29. Lahn M, Kohler G, Sundell K et al (2004) Protein kinase C alpha expression in breast and ovarian cancer. Oncology 67:1–10
30. Finkel T (2011) Signal transduction by reactive oxygen species. J Cell Biol 194:7–15
31. Lindsay J, Esposti MD, Gilmore AP (2011) Bcl-2 proteins and mitochondria-Specificity in membrane targeting for death. Biochim Biophys Acta 1813:532–539
32. Ruvolo PP, Deng X, May WS (2001) Phosphorylation of Bcl2 and regulation of apoptosis. Leukemia 15:515–522
33. Esteve JM, Mompo J, De La Asuncion JG et al (1999) Oxidative damage to mitochondrial DNA and glutathione oxidation in apoptosis: studies in vivo and in vitro. Faseb J 13:1055–1064
34. Zimmermann AK, Loucks FA, Schroeder EK, Bouchard RJ, Tyler KL, Linseman DA (2007) Glutathione binding to the Bcl-2 homology-3 domain groove - A molecular basis for Bcl-2 antioxidant function at mitochondria. J Biol Chem 282:29296–29304
35. Vairetti M, Ferrigno A, Bertone R, Richelmi P, Berte F, Freitas I (2005) Apoptosis vs. necrosis: glutathione-mediated cell death during rewarming of rat hepatocytes. Biochim Biophys Acta 1740:367–374
36. Benderdour M, Charron G, Comte B et al (2004) Decreased cardiac mitochondrial NADP(+)-isocitrate dehydrogenase activity and expression: a marker of oxidative stress in hypertrophy development. Am J Physiol Heart Circ Physiol 287:H2122–H2131
37. Hockenbery DM, Oltvai ZN, Yin XM, Milliman CL, Korsmeyer SJ (1993) Bcl-2 functions in an antioxidant pathway to prevent apoptosis. Cell 75:241–251

38. Kane DJ, Sarafian TA, Anton R et al (1993) Bcl-2 inhibition of neural death - decreased generation of reactive oxygen species. Science 262:1274–1277
39. Voehringer DW, Meyn RE (2000) Redox Aspects of Bcl-2 Function. Antioxid Redox Signal 2:537–550
40. Hochman A, Sternin H, Gorodin S et al (1998) Enhanced oxidative stress and altered antioxidants in brains of Bcl-2-deficient mice. J Neurochem 71:741–748

Incorporation of photosenzitizer hypericin into synthetic lipid-based nano-particles for drug delivery and large unilamellar vesicles with different content of cholesterol

Jaroslava Joniova*[a,b], Ludmila Blascakova[a], Daniel Jancura[a,c], Zuzana Nadova[a,c], Franck Sureau[b] and Pavol Miskovsky[a,c]

[a]Department of Biophysics, University of P.J. Safarik, Kosice, Slovak Republic

[b]Laboratoire Jean Perrin, Université Pierre et Marie Curie, Paris, France

[c]Center for Interdisciplinary Biosciences, University of P.J. Safarik, Kosice, Slovak Republic

Abstract

Low-density lipoproteins (LDL) and high-density lipoproteins (HDL) are attractive natural occurring vehicles for drug delivery and targeting to cancer tissues. The capacity of both types of the lipoproteins to bind hydrophobic drugs and their functionality as drug carriers have been examined in several studies and it has been also shown that mixing of anticancer drugs with LDL or HDL before administration led to an increase of cytotoxic effects of the drugs in the comparison when the drugs were administered alone. However, a difficult isolation of the lipoproteins in large quantity from a biological organism as well as a variability of the composition and size of these molecules makes practical application of LDL and HDL as drug delivery systems quite complicated. Synthetic LDL and HDL and large unilamellar vesicles (LUV) are potentially suitable candidates to substitute the native lipoproteins for targeted and effective drug delivery. In this work, we have studied process of an association of potent photosensitizer hypericin (Hyp) with synthetic lipid-based nano-particles (sLNP) and large unilamellar vesicles (LUV) containing various amount of cholesterol. Cholesterol is one of the main components of both LDL and HDL particles and its presence in biological membranes is known to be a determining factor for membrane properties. It was found that the behavior of Hyp incorporation into sLNP particles with diameter ca ~ 90 nm is qualitatively very similar to that of Hyp incorporation into LDL (diameter ca. 22 nm) and these particles are able to enter U-87 MG cells by endocytosis. The presence of cholesterol in LUV influences the capacity of these vesicles to incorporate Hyp into their structure.

Key words

drug delivery, low-density lipoproteins, synthetic lipid-based nano-particles, photodynamic therapy, hypericin, cholesterol

* jaroslava.joniova@gmail.com

Biosensing and Nanomedicine VII, edited by Hooman Mohseni, Massoud H. Agahi, Manijeh Razeghi,
Proc. of SPIE Vol. 9166, 916604 · © 2014 SPIE · CCC code: 0277-786X/14/$18 · doi: 10.1117/12.2060672

1. INTRODUCTION

The main hurdles associated with the conventional cancer chemotherapy include limited accessibility of drug to tumor tissues which therefore requires a higher drug dose leading to intolerable cytotoxicity and nonspecific targeting [1]. Thus, to mitigate the difficulty associated with conventional chemotherapy, there is a need for developing a drug delivery system that could optimize the pharmaceutical action of drugs while reducing toxic side effects.

In the recent years an important attention has been dedicated to the use of native plasma lipoproteins for targeted drug delivery to cancer cells [2-5]. This fact is based on the establishing of a direct relationship between the high relative number of lipoprotein receptors in various tumor cell lines and the elevated uptake of drugs by these cells [6-10]. Native plasma lipoproteins have important advantages in comparison to other drug nano-delivery systems: i) as natural molecules, the lipoproteins escape recognition by mononuclear phagocytic system (MPS), which favors their long circulation time in the plasma, ii) they are not immunogenic, iii) their hydrophobic core and phospholipid shell favor binding of hydrophobic and amphiphilic drugs, respectively [2-5, 10]. Of the lipoproteins, the most important in terms of drug delivery are low-density lipoproteins (LDL) [2, 11, 13], however, the importance of high-density lipoproteins (HDL) is also recognized and in many cases seems to be even higher than LDL [10, 14-17]. The capacity of both types of the lipoproteins, LDL as well as HDL, to bind some drugs and their functionality as drug carriers have been examined in several studies [14, 18-23]. It has been also shown that mixing of anticancer drugs with LDL or HDL before administration led to an increase of cytotoxic effects of the drugs in the comparison when the drugs are administered alone [9, 16, 17, 24, 25].

LDL are recognized and internalized into the cells through specific membrane receptors that interact with the apo-lipoprotein B of the LDL particle [26][1]. Certain tumor cells and tumor vascular endothelial cells express the LDL receptors in higher number due to either their increased proliferation or increased membrane turnover [6, 7]. HDL have been implicated in cholesterol delivery in some malignancies including breast cancer, ovarian cancer, adrenocortical tumors and prostate cancer. The mechanism for HDL mediated delivery appears to be SR-B1 receptor dependent [10]. It is known that this receptor is broadly expressed among a variety of cancer cells [9]. The above mentioned facts make LDL and HDL particles attractive natural occurring vehicles for drug delivery and targeting to cancer tissues.

Both types of the lipoproteins particles assume a globular shape with an average particle diameter 20-25 nm and 7-13 nm for LDL and HDL, respectively. These lipoproteins possess the outer surface layer, which consists of cholesterol and phospholipids molecules with a single apo B-100 protein wrapped around the surface of the LDL particle and apoA1 protein, which is responsible for scaffolding, the size and shape of natural HDL, further the hydrophobic core composed of triacylglycerides and cholesterol esters, and an interfacial region between these two parts [26-28].

Our group has published in the recent years several articles about the properties of the complexes of LDL with photosensitizer hypericin (Hyp) [21, 29-34]. Hyp (Figure 1), (7,14-dione-1,3,4,6,8,13-hexahydroxy 10,11-dimethyl-

phenanthrol [1,10,9,8- opqra] perylene), is a natural photosensitizing pigment from plants of the genus Hypericum. This compound under light illumination causes anti-proliferative and cytotoxic effects (necrosis as well as apoptosis) in many tumor cell lines. These properties, together with minimal dark toxicity, certain tumor selectivity and high clearance rate from the host body, make Hyp a promising agent for photodynamic therapy (PDT) of cancer as well as for tumor photo-diagnosis [35-39].

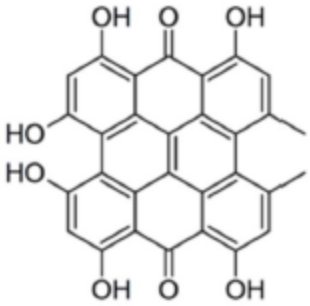

Figure 1. Two-dimensional structure of Hypericin.

We have shown that high Hyp/LDL ratios (>30:1) leads to a significant decrease of quantum yield of Hyp fluorescence [21]. This decrease is caused by the formation of non-fluorescent Hyp aggregates inside LDL particles and by dynamic self-quenching of Hyp fluorescence [29-33]. It was shown that only monomeric form of Hyp is able to produce the excited triplet state of Hyp in LDL, which in aerobic conditions leads to a singlet oxygen production [33]. The kinetics of association of Hyp with free LDL molecules and Hyp/LDL complex has been also thoroughly studied and described [30-32]. We have demonstrated the important role of the LDL receptor pathway for Hyp delivery into U-87 MG cells in the presence of LDL. A substantial increase of Hyp uptake was observed after over-expression of LDL receptors on the cell surface [34]. It was also shown that overloading of LDL with Hyp (Hyp/LDL = 200:1) leads to a higher intracellular accumulation of Hyp molecules in comparison with the situation when the same quantity of Hyp is accumulated in LDL, but with a lower Hyp/LDL ratio (20:1). Moreover, Hyp/LDL ratio seems to affect the subcellular distribution of Hyp and consequently the mechanism of photodynamically induced cell death [30, 31].

Despite the advantages of LDL and HDL as carriers for hydrophobic/amphiphilic drugs, the clinical application of native lipoproteins as drug delivery systems is complicated by relatively expensive and pretentious procedures required for their isolation, variability in the composition and size of these nanoparticles, non-adequate supply of the lipoproteins and safety concerns [3]. Consequently, alternative strategies have been developed via artificially prepared lipoproteins for the purpose of targeted drug delivery [40-46]. These strategies are summarized in the review published by Lacko et al. [3]. In the present work we have utilized the procedure for lipoprotein construction developed by Nikanjam et al. [40]. This group has prepared synthetic LDL (sLDL) particles by combining a synthetic peptide containing a lipid binding motif

and the LDL receptor binding domain of apoB-100 with a lipid based nano-platform containing phosphatidyl choline (PC), triolein (TO) and cholesteryloleate (CO).

The purpose of this work is to characterize binding properties of Hyp to synthetic lipid-based nano-particles (sLNP) and compare them with those observed in the case of the formation of Hyp-LDL complex. In addition to the study of interaction of Hyp with sLNP, we have also investigated the effect of cholesterol on Hyp incorporation into lipid structures. It has been recently proposed that the presence of cholesterol in biological membranes can significantly influence the localization and extend of accumulation of Hyp inside these structures [47-49]. Utilizing large unilamellar vesicles (LUV) with various cholesterol content we confirm the hypothesis that cholesterol influences extend of Hyp incorporation into lipid structures. Similarly to our study of Hyp-LDL complexes [21, 32], we have utilized the fluorescence spectroscopy approach and the fact that molecules of Hyp form non-fluorescent aggregates in aqueous solutions and that Hyp aggregates can be formed also in lipid media at high local Hyp concentrations [21, 50, 51].

2. MATERIAL AND METHODS

2.1. Chemicals

Phosphate saline buffer (PBS) and hypericin were purchased from Gibco-Invitrogen (France). Chloroform, methanol, ethanol, triolein (TO) and cholesteryl oleate (CO), Butylated hydroxytoulene (BHT) and 3,3'-dioctadecyloxacarbocyanine perchlorate (DiOC18(3)) were purchased from Sigma Aldrich. Egg yolk phosphatidyl choline (PC) was obrained from Avanti Polar Lipids (USA). LDL was purchased from Calbiochem (United Kingdom). Egg yolk phosphatidyl choline (PC) and 1,2-dioleoyl-*sn*-glycero-3-phosphocholine (DOPC) were obtained from Avanti Polar Lipids (USA).

2.2. Preparation of sLNP

Synthesis of sLNP was performed according to Nikanjam et al. [40]. Concretely, the emulsion of PC, TO and CO was mixed in a molar ratio 3:2:1 and dried under N2. Tris-saline buffer (20mM Tris, pH 7.2) was introduced into the dried lipids and the solution was then vortexed for 1 min on the high settings. BHT (20μM) was added and the solution was sonicated for 1h on ice. Sonicated particles were spun 20 min at 4000 rpm to remove particulates. The lipid emulsion was heated up to 55°C and extruded using an Avanti Polar Lipids extruder 5 times through 0.2 μm, 0.1 μm and 0.05 μm filter. The final emulsion was filter sterilized using a 0.22 μm filter.

2.3. Formation of LUV and LUV enriched with cholesterol

Large unilamellar vesicles (LUV) were prepared by extrusion method. Stock solution of DOPC was prepared by dissolving DOPC ([DOPC] = 5.10^{-2}M) in a mixture of chloroform and methanol (1:1, v/v). 100 μl of DOPC solution was added to the round bottom glass tube and the solution was evaporated under the stream of N_2 forming a thin film of lipids

visible at the bottom of the glass tube. 1 ml of PBS was then added to the lipid film (making the final concentration of lipids = 5.10^{-3} M), and the mixture was vortexed for 1 minute at the highest settings. The emulsion was then extruded using Avanti Polar Lipids extruder with 100 nm filter. The particles were extruded 8-10 times each. The LUV enriched with cholesterol (LUV-Chol) were prepared similarly as LUV without cholesterol. Stock solution of DOPC ([DOPC] = 5.10^{-2}M) was mixed with stock solution of cholesterol ([cholesterol] = 5.10^{-2}M) dissolved in chloroform in different ratios 8:2, 7:3 and 5:5. The mixture was positioned on the bottom of glass tube and the same procedure as for LUV preparation was consequently applied.

2.4. Preparation of Hyp complexes with sLNP and LUV

The stock solution of Hyp was prepared by dissolving Hyp in 100% DMSO. Molar concentration of Hyp was determined by absorption spectra using extinction coefficient for Hyp as 44 000 cm-1 M-1 at 600 nm. The sLNP-Hyp or LUV-Hyp complexes used in experiments were obtained by mixing of appropriate volumes of sNLP or LUV and Hyp in PBS at pH=7.4. The final quantity of DMSO in all sNLP-Hyp or LUV-Hyp complexes was under 0.5%.

2.5. sLNP stained with $DiOC_{18}(3)$

DiOC18(3) was dissolved in acetone with a concentration of 10-3M. DiOC18(3) was added to the mixture of PC:TO:CO = 3:2:1 in chloroform : methanol (1:1, v/v) (a final concentration of DiOC18(3) was 0.1%). Next steps in the preparation of SLNP- DiOC18(3) complexes were the same as was described for the formation of sLNP.

2.6. Dynamic light scattering measurements

Dynamic light scattering for size characterizations of sNLP was performed by Malvern Instruments Zetasizer Nano-ZS instrument (Malvern, Worcs. UK) equipped with a 4 mW He–Ne laser (633 nm) operating at 90° angle and a temperature of 20°C. A concentration of sNLP solution in PBS used for measurements was 10-8M.

2.7. Cell culture

U-87 MG human glioma cells (Cell Lines Services, Germany) were routinely maintained in Dulbecco´s modified Eagle medium (D-MEM)(Gibco-Invitrogen, France) containing L - glutamine (862 mg.l-1), sodium pyruvate (110 mg.l-1), glucose (4500 mg.l-1), streptomycin (50 µg.ml-1), penicilin (50 µg.ml-1) and supplemented with 10% FBS (Pall Life Sciences, France), in the presence of 5% CO2 humidified atmosphere at 37°C.

2.8. Fluorescence spectroscopy measurements

Fluorescence spectra were recorded at room temperature (22°C) using SHIMADZU RF-5301 spectrofluorimeter (Kyoto, Japan). The excitation wavelength was 560 nm and the emission was collected in the range 530-700 nm in all measurements. Spectra were recorded 120 min after mixing solutions of Hyp and sLNP or LUV in an appropriate ratio. The spectra were analyzed by OriginPro program version 8.0.

2.9. Fluorescence microscopy experiments

sLNP were stained with DiOC18(3) as it is described above. U87-MG cells were first incubated in 10% FBS and seeded onto 35 mm culture dishes with integral No.0 glass cover slip bottoms (MatTek, USA) and were incubated until they were 60-80% confluent. Subsequently, the cells were incubated with sLNP-DiOC18(3) complex and fluorescence microscopy was used for determining the localization of DiOC18(3) inside the cells. Optiphot-2 epifluorescence microscope equipped with a Nipkow Wheel coaxial–confocal attachment (Technical Instrument, CA, USA) was used for the measurements. Fluorescence images were taken by using water-immersion objective (Zeiss Neofluar, X63, N.A. 1.2), TE cooled CCD Micromax camera (Princeton Instruments, NJ, USA) and standard filters system: FITC filter set (λexc = 450–490 nm, λem = 520–570 nm). Exposure time was set to 5 s. Image processing was performed by ImageJ software.

3. RESULTS AND DISCUSSION

3.1. Characterization of sLNP

sLNP were prepared according to modified Nikanjam et al. protocol for preparation of sLDL particles (see Material and methods) [40]. Synthetic peptide was left out from the preparation process because sLDL with synthetic peptide were not able to incorporate Hyp into their structure (data not shown). The diameter of constructed sLNP determined by dynamic light scattering was 89 nm (Figure 2A). This value was confirmed also by electron-cryo microscopy (Figure 2B, left) which attributed to these particles the size ~ 90 nm.

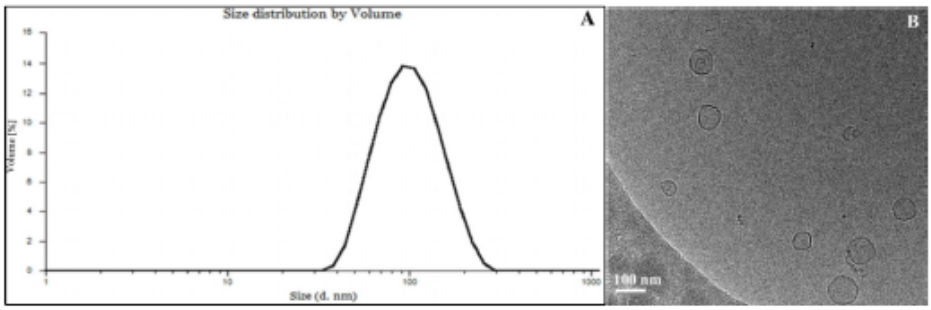

Figure 2. (A) Size distribution of sLNP determined by dynamic light scattering. For the measurements the size of sLNP the total concentration of lipid was 10^{-8}M. (B) Cryo-electron microscopy image of sLNP.

3.2. Inxorporation of Hyp into sLNP

The fluorescence emission spectra of Hyp in the presence of sLNP resemble those in the presence of LDL (spectra not shown). The spectral maximum is at 599 nm [21] and the intensities are almost identical to those found for LDL (at the same Hyp concentrations).

The dependence of Hyp fluorescence intensity maxima on the concentration of Hyp, 120 minutes after mixing of Hyp with sLNP solutions, is presented in Figure 3.

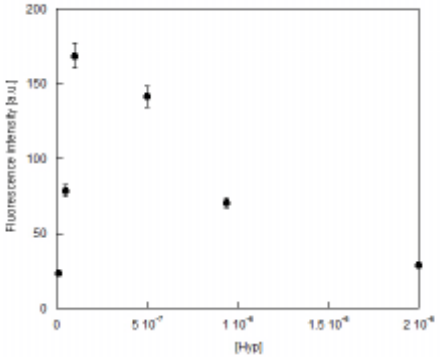

Figure 3. Dependence of Hyp fluorescence intensity in the presence of sLNP on Hyp concentration after 120 min of stabilization of the complexes (fluorescence maximum 599 nm, excitation line 560 nm). Concentration of sLNP was kept constant during the measurements.

The intensity of Hyp fluorescence increases up to Hyp concentration 1.10^{-7}M and beyond this value a quenching of Hyp fluorescence is observed. At Hyp concentrations > 2.10^{-6}M, the fluorescence of Hyp almost disappears. This behavior can be explained similarly as in the case of Hyp association with LDL [21]. Until Hyp concentration 1.10^{-7}M, the molecules of Hyp are present inside sLNP particles as monomers, and at higher Hyp concentrations the formation of non-fluorescent Hyp aggregates inside sLNP occurs. It was proposed that a high local concentration of Hyp leads to a Hyp clustering in lipid media [21, 33] and this hypothesis was also theoretically supported by Jämbeck et al. [49].

In conclusion of this part it should be noted that the behavior of Hyp incorporation into sLNP particles with diameter ca ~ 90 nm is qualitatively very similar to that of Hyp incorporation into natural LDL (diameter ca. 22 nm) [21, 30, 32].

3.3. Uptake of sLNP by U87-MG cells

In order to demonstrate that sLNP are able to enter cells, we have stained these particles with DiOC18(3) and incubated them with U-87 MG cells. The green fluorescent lipophilic carbocyanine DiOC18(3) is widely used as a lipophilic tracer. It is weakly fluorescent in water, but highly fluorescent when incorporated into membranes. Once applied to cells, the dye diffuses laterally within the plasma membrane [52]. 60 min after incubation of sLNP with U-87 MG cells, the cells were analyzed by fluorescence microscopy. Fluorescence of DiOC18(3) serves as a marker for entering process of sLNP into U-87 MG cells and provides clear evidence that sLNP are able to enter cells (Figure 4). The point-like structure of DiOC18(3) fluorescence inside U-87 MG cells suggests that sLNP particles enter these cells most probably by the endocytosis process.

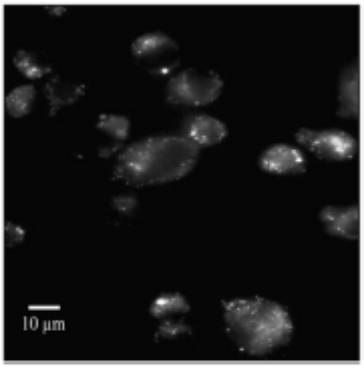

Figure 4. Fluorescence microscopy image of U-87 MG cells incubated with sLNP stained with DiO18(3). Cells were incubated with sLNP-DiO18(3) complex for 1 hour and consequently the fluorescence intensity and sub-cellular distribution of sLNP was observed.

3.4. Influence of cholesterol on extend of Hyp incorporation into LUV

Similarly as in the case of Hyp interaction with sLNP, the fluorescence measurements revealed that in the presence of LUV the fluorescence intensity linearly increase until certain Hyp concentration (in this case 4.10-7M) and beyond this concentration the quenching of Hyp fluorescence is observed (Figure 5). At high Hyp concentrations > 4.10-6M, the fluorescence almost disappears. It is obvious that this behavior is common for all known Hyp-lipid structure studies [21, 30-32, 50, 51]. It means that Hyp can penetrate into lipid structures from aqueous environment and is monomerized in the lipid media. However, an entrance of more Hyp molecules leads to a high local concentration of Hyp resulting in a formation of Hyp aggregates or self-quenching of Hyp fluorescence [21, 31, 32].

The effect of cholesterol on characteristics of Hyp incorporation into LUV is presented on Figure 5.

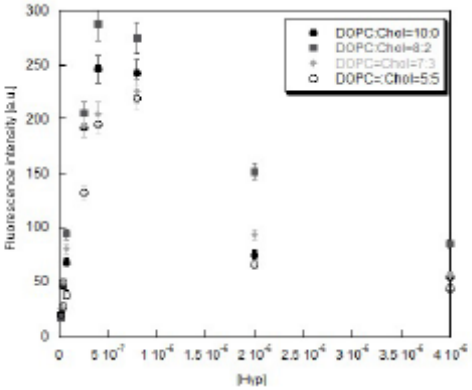

Figure 5. Dependence of Hyp fluorescence intensity in the presence of LUV with various content of cholesterol on Hyp concentration after 120 min of stabilization of the complexes (fluorescence maximum 599 nm, excitation 560 nm). Concentration of LUV+cholesterol complexes was kept constant during the measurements.

The maximum fluorescence intensity is observed when Hyp is incorporated into LUV:cholesterol = 8:2 mixture. It means that at this molar ratio, Hyp molecules are incorporated in LUV as monomers most effectively. Further increase of cholesterol concentration leads to a decrease of the amount of Hyp molecules which can be incorporated into LUV-cholesterol as monomers. Ho et al. have proposed that the major element for attracting Hyp in DPPC/cholesterol LUV is cholesterol, in other words, cholesterol attracts Hyp more effectively than other components of LUV [47]. As a consequence of this possibility, Hyp exhibits preferential binding towards cholesterol rich domains in LUV. The lower level of Hyp monomerization in the presence of higher cholesterol concentration in LUV should be explained as follows. The presence of cholesterol in LUV leads to a higher local Hyp concentration around cholesterol rich domains which leads to a formation of non-fluorescent Hyp aggregates around these domains at lower total Hyp concentration than in the case when cholesterol is not present in LUV.

The role of cholesterol in Hyp, and other hydrophobic drugs, accumulation inside cell lipid structures as well as in lipid-based drug transport system requires further study. A clarification of this topic would substantially contribute to construction of effective transport system for targeted and effective delivery of hydrophobic/amphiphilic drugs.

4. CONCLUSION

This work shows that sLNP can serve as a transport system for hydrophobic/amphiphilic drugs which was confirmed by the accumulation of Hyp molecules inside these particles and uptake of sLNP by U-87 MG cells through process of endocytosis. This ability of sLNP should be taken into account when this type of drug delivery system will be applied in clinical practice. However, the presence of a specific ligand towards receptors expressed on a cancer cell surface is required to be present on the surface of sLNP to achieve a selective targeted delivery of drugs to cancer cells. We have also shown that the presence of cholesterol in LUV leads probably to a higher local Hyp concentration around cholesterol rich domains. As consequence of this fact, a formation of non-fluorescent Hyp aggregates around these domains is reached at lower total Hyp concentration than in the case when cholesterol is not present in LUV.

Acknowledgements

This work has been supported by the Slovak Research and Development Agency under the contract APVV-0242-11, the Agency of the Ministry of Education of Slovak Republic for the Structural funds of the European Union: Operational program Education (Doctorand (ITMS code: 26110230013) and KVARK (ITMS code: 26110230084)), International Program for Scientific Cooperation (PICS N°5398) from the CNRS, Operational program Research and Development (SEPO II (ITMS code:26220120039) and CEVA II (ITMS code: 26220120040)), and the project CELIM 316310 funded by7FP EU.

REFERENCES

[1] Parhi P., Mohanty C. Sahoo S.K. 'Nanotechnology based combinational drug delivery: an emerging approach for cancer therapy', Drug Discovery Today 17, 1044-1052, (2012).

[2] Zheng, G., Chen, J., Li, H., Glickson, J.D. 'Rerouting lipoprotein nanoparticles to selected alternate receptors for the targeted delivery of cancer diagnostic and therapeutic agents', Proc. Natl. Acad. Sci. USA 102, 17757-17762, (2005).

[3] Lacko, A.G., Nair, M., Prokai, L., McConathy, W.J. 'Prospects and challenges of the development of lipoprotein-based formulations for anti-cancer drugs', Drug Deliv. 4, 665-675, (2007).

[4] Glickson, J.D., Lund-Katz, S., Zhou, R., Choi, H., Chen, J.W., Li, H., Corbin, I., Popov, A.V., Cao, W., Song, L., Qi, C., Marotta, D., Nelson, D.S., Chen, J., Chance, B., Zheng, G. 'Lipoprotein nanoplatform for targeted delivery of diagnostic and therapeutic agents', Mol. Imaging 7, 101-110, (2008).

[5] Ng, K.K., Lovell, J.F., Zheng, G. 'Lipoprotein-inspired nanoparticles for cancer theranostics', Accounts Chem, Res. 44, 1105-1113, (2011).

[6] Brown, M.S., Goldstein, J.L., 'Receptor-mediated control of cholesterol metabolism', Science 191, 150-154, (1976).

[7] Vitols, S., Angelin, B., Ericsson, S., Gahtron, G., Juliusson, G., Maquelier, M., Paul, C., Peterson, C., Rudling, M., Sodergreid, K., Tidefelt, G. 'Uptake of low density lipoproteins by human leukemic cells in vivo: relation to plasma lipoprotein levels and possible relevance for selective chemotherapy', Proc. Natl. Acad. Sci. USA 87, 2598-2602, (1990).

[8] Puussinen, P.J., Karten, B., Wintersperger, A., Reicher, H., McLean, M., Malle, E., Sattler, W. 'The human breast carcinoma cell lines HBL-100 acquires exogenous cholesterol from high density lipoprotein via CLA-1 (CD36 and LIMPII analoqous 1)-mediated selective cholesteryl ester uptake', Biochem. J. 349, 559-566, 2000.

[9] Mooberry, L.K., Nair, M, Paranjape, S., McConazhy, W.J., Lacko, A.G. 'Receptor mediated uptake of paclitaxel from a synthetic high density lipoprotein nanocarrier', J. Drug Target. 18, 53-58, (2010).

[10] Damiano, M.C., Mutharasan, R.K., Tripathy, S., McMahon, K.M., Thaxton, C.S. 'Templated high density lipoprotein nanoparticles as potential therapies and for molecular delivery', Adv. Drug Del. Rev. 65, 649-662, (2013).

[11] Konan, Y.N., Gurny, R., Alleman, E. 'State of the art in the delivery of photosensitizers for photodynamic therapy', J. Photochem. Photobiol. B 66, 89-106, (2002).

[12] Polo, L., Valduga, G., Jori, G., Reddi, E. 'Low-density lipoprotein receptors in the uptake of tumour photosensitizers by human and rat transformed fibroblasts', Int. J. Biochem. Cell Biol. 34, 10-23, (2002).

[13] Sherman, W.M., van Lier, J.E., Allen, C.M. 'Targeted photodynamic therapy via receptor mediated delivery systems', Adv. Drug Deliver. Rev. 56, 53-76, (2004).

[14] Corbin, I.R., Chen, J., Cao, W., Lund-Katz, S., Zheng, G. 'Enhanced cancer targeted delivery using engineered hgh-density lipoproteinn based nanocarriers', J. Biomed. Nanotechnol. 3, 367-376, (2007).

[15] McKenney.J.M. 'Effect of drugs on high-density lipoprotein', J.Clin. Lipid. 1, 74-87, (2007).

[16] Davis, M.E., Chen, Z., Shin, D.M. 'Nanoparticle therapeutics: an emerging treatment modality for cancer', Nat. Rev. Drug Discov. 7, 771-782, (2008).

[17] McConathy, W.J., Nair, M.P., Paranjape, S., Mooberry, L., Lacko A.G. 'Evaluation of synthetic/reconstituted high-density lipoproteins as delivery vehicles for paclitaxel', Anticancer Drugs 19, 183-188, (2008).

[18] Jori, G. 'Tumour photosensitizers: approaches to enhance the selectivity and efficiency of photodynamic therapy', J. Photochem. Photobiol. B 36, 87-93, (1996).

[19] Reddi, E. 'Role of delivery vehicles for photosensitizers in the photodynamic therapy of tumors', J. Photochem. Photobiol. B 37, 189-195, (1997).

[20] Lacko, A.G., Nair, M., Paranjape, S., Johnso, S., McConathy, W.J. 'High density lipoprotein complexes as delivery vehicles for anticancer drugs', Anticancer Res. 22, 2045, (2002).

[21] Kascakova, S., Refregiers, M., Jancura, D., Sureau, F., Maurizot, J.C., Miskovsky, P. 'Fluorescence spectroscopic study of hypericin-photosensitized oxidation of low-density lipoproteins', Photochem. Photobiol. 81, 1395-1403, (2005).

[22] Oda, M.N., Hargraeves, P.L., Beckstead, A., Redmond, A., van Antwerpen, R., Ryan, R.O. 'Reconstituted high density lipoprotein antitumoral drug into hepatoma cells', J. Lipid Res. 47, 260, (2006).

[23] Maziere, J.C., Moliere, P., Santus, R. 'The role of the low density lipoproteid receptor pathway in the delivery of lipophilic photosensitizers in the photodynamic therapy of tumors', J. Photochem. Photobiol. B 8, 351-360, (1991).
[24] Jori, G., Reddi, E. 'The role of lipoproteins in the delivery of tumour-targeting photosensitizers', Int. J. Biochem. 25, 1369-1375, (1993).
[25] Chowdhary, R.K., Sharif, I., Chansarkar, N., Doléhán, D., Ratkay, L., Delaney, S., Meadows, H. 'Correlation of photosensitizer delivery to lipoproteins and efficacy in tumor and arthritis mouse model: comparison of lipid based and Pluronic P123 formulations', J. Pharm. Pharm. Sci. 6, 198-204, (2003).
[26] Hevonoja, T., Pentikainen, M.O., Hyvonen, M.T., Kovanen, P.T., Ala-Korpela, M. 'Structure of low density lipoprotein (LDL) particles: Basis for understanding molecular changes in modified LDL', Biochim. Biophys. Acta 1488, 189-210, (2000).
[27] Prassl, R., Laggner, P. 'Molecular structure of low density lipoprotein: current status and future challenges', Eur. Biophys. J. Biophys. Lett. 38, 145-158, (2009).
[28] Jonas, A., Phillips, M.C. 'Lipoprotein structure' in Vance, D.E., Vance, J.E. (Eds.), Biochemistry of lipids, lipoproteins and membranes (5th Edition), Elsevier Science, pp. 485-506, (2008).
[29] Miskovsky, P. 'Hypericin-a new antiviral and antitumor photosensitizer: Mechanism of action and interaction with biological macromolecules', Current Drug Targets 3, 55-84, (2002).
[30] Huntosova, V., Alvarez, L., Bryndzova, L., Nadova, Z., Jancura, D., Buriankova, L., Bonneau, S., Brault, D., Miskovsky, P., Sureau, F. 'Interaction dynamics of hypericin with low-density lipoproteins and U-87 MG cells', Int. J. Pharm. 389, 32-40, (2010).
[31] Huntosova, V., Buzova, D., Petrovajova, D., Kasak, P., Nadova, Z., Jancura, D., Sureau, F., Miskovsky, P, 'Development of a new LDL-based transport system for hydrophobic/amphiphilic drug delivery to cncer cells', Int. J. Pharm. 436, 463-471, (2012).
[32] Buriankova, L., Buzova, D., Chorvat, D. jr., Sureau, F., Brault, D., Miskovsky, P., Jancura, D. 'Kinetics of hypericin association with low-density lipoproteins', Photochem. Photobiol. 87, 56–63, (2011).
[33] Gbur, P., Dedic, R., Chorvat jr., D., Miskovsky, P., Hala, J., Jancura, D. 'Time resolved luminescence and singlet oxygen formation after illumination of the hypericin-low-density lipoprotein complex', Photochem. Photobiol. 85, 816-823, (2009).
[34] Kascakova, S., Nadova, Z., Mateasik, A., Mikes, J., Huntosova, V., Refregiers, M., Sureau, F., Maurizot, J.C., Miskovsky, P., Jancura, D. 'High level of low-density lipoproteins receptors enhance hypericin uptake by U-87 cells in the presence of LDL', Photochem. Photobiol. 84, 120-127, (2008).
[35] Strejckova, A., Stanicova, J., Jancura, D., Miskovsky, P., Bano, G. 'Spatial orientation and electric-field-driven transport of hypericin inside of bilayer lipid membranes', J.Phys. Chem. B 117, 1280-1286, (2013).
[36] Falk, H. 'From the photosensitizer hypericin to the photoreceptor stentorin - The chemistry of phenanthroperylene quinones', Angew. Chem. (Int. Ed.) 38, 3116-3136, (1999).
[37] Agostinis, P., Vantieghem, A., Merlevede, W., de Witte, P. 'Hypericin in cancer treatment: More light on the way', Int. J. Biochem. Cell Biol.34, 221-241, (2002).
[38] Olivo, M., Fu, C.Y., Raghavan, V., Lau, W.K.O. 'New frontier in hypericin-mediated diagnosis of cancer with current optical technologies', Annals Biochem. Engn. 40, 460-473, (2012).
[39] Karioti, A., Bilia, A.R. 'Hypericin as potential leads for new therapeutics', Molecular Sciences 11, 562-594, (2010).
[40] Nikanjam, Mina, Eleanor A. Blakely, Kathleen A. Bjornstad, Xiao Shu, Thomas F. Budinger, and Trudy M. Forte. 'Synthetic Nano-Low Density Lipoprotein as Targeted Drug Delivery Vehicle for Glioblastoma Multiforme', International Journal of Pharmaceutics 328, 86-94, (2007).
[41] Baillie, G., M. D. Owens, and G. W. Halbert. 'A Synthetic Low Density Lipoprotein Particle Capable of Supporting U937 Proliferation in Vitro', J. Lipid Res. 43, 69-73, (2002).
[42] Favero, Giovani M., Raul C. Maranhao, Durvanei A. Maria, Debora Levy, and Sergio P. Bydlowski. 'Synthetic Nanoemulsion Resembling a Protein-Free Model of 7-Ketocholesterol Containing Low Density Lipoprotein: In Vitro and in Vivo Studies', Biol. Res. 43, 439-444, (2010).
[43] Hayavi, Sima, George Baillie, Moira D. Owens, and Gavin W. Halbert. 'Receptor Dependent Cellular Uptake of Synthetic Low Density Lipoprotein by Mammalian Cells in Serum-Free Tissue Culture', J. Pharm. Pharmacol. 58, 1337-1342, (2006).
[44] Luthi, Andrea J., Pinal C. Patel, Caroline H. Ko, R. Kannan Mutharasan, Chad A. Mirkin, and C. Shad Thaxton. 'Nanotechnology for Synthetic High-Density Lipoproteins', Trends Mol. Med. 16, 553-560, (2010).

[45] Nikanjarn, Mina, Andrew R. Gibbs, Anthony Hunt, Thomas F. Budinger, and Trudy M. Forte. 'Synthetic Nano-Ldl with Paclitaxel Oleate as a Targeted Drug Delivery Vehicle for Glioblastoma Multiforme', J. Controlled Release 124, 163-171, 2007.
[46] Rensen, P. C. N., R. L. A. de Vrueh, J. Kuiper, M. K. Bijsterbosch, E. A. L. Biessen, and T. J. C. van Berkel. 'Recombinant Lipoproteins: Lipoprotein-Like Lipid Particles for Drug Targeting', Advanced Drug Delivery Reviews 47, 251-276, 2001.

[47] Ho, Yunn-Fang, Ming-Huang Wu, Bor-Hen Cheng, Yar-Wen Chen, and Ming-Chih Shih. 'Lipid-Mediated Preferential Localization of Hypericin in Lipid Membranes', Biochim. Biophys. Acta-Biomembranes 1788, 1287-1295, 2009.
[48] Eriksson, Emma S. E., and Leif A. Eriksson. 'The Influence of Cholesterol on the Properties and Permeability of Hypericin Derivatives in Lipid Membranes', J. Chem. Theory Comp. 7, 560-574, 2011.

[49] Jämbeck, J.P.M., Eriksson, E.S.E., Laaksonen, A., Lyubartsev, A.P., Eriksson, L.A. 'Molecular dynamics studie sof liposomes as carriers for photosensitizing druha: development, validation, and simulations with a coarse-grained model', J. Chem. Theory Comput., 10, 5-13, 2014.
[50] Lavie, G., Mazur, Y., Lavie, D., Prince, A.M., Pascual, D., Liebes, L., Levin, B., Meruelo, D. 'Hypericin as an inactivator of infectious viruses in blood components', Transfusion 35, 392-400, 1995.
[51] Siboni, G., Weitman, H., Freeman, D., Mazur, Y., Malik, Z., Ehrenberg, B. 'The correlation between hydrophilicity of hypericins and helianthrone.: Internalization mechanisms, subcellular distribution and photodynamic action in colon carcinoma cells', Photochem. Photobiol. Sci. 1, 483-491, 2002.

[52] https://www.lifetechnologies.com/order/catalog/product/D275?CID=search-product

Towards increased selectivity of drug delivery to cancer cells: Development of a LDL-based nanodelivery system for hydrophobic photosensitizers

Diana Buzova*[a], Veronika Huntosova[a, b], Peter Kasak[c], Dana Petrovajova[a], Jaroslava Joniova[a,b], Lenka Dzurova[a], Zuzana Nadova[a], Franck Sureau[b], Pavol Miskovsky[a,d] and Daniel Jancura[a]
[a]Department of Biophysics, University of Pavol Jozef Safarik, Kosice, Slovak Republic
[b]Laboratoire Jean Perrin, CNRS-FRE 3231, Pierre & Marie Curie University, Paris, France
[c]Polymer Institute of the Slovak Academy of the Sciences, Bratislava, Slovak Republic
[d]International Laser Center, Bratislava, Slovak Republic

ABSTRACT

Low-density lipoproteins (LDL), a natural *in vivo* carrier of cholesterol in the vascular system, play a key role in the delivery of hydrophobic photosensitizers (pts) to tumor cells in photodynamic therapy (PDT) of cancer. To make this delivery system even more efficient, we have constructed a nano-delivery system by coating of LDL surface by polyethylene glycol (PEG) and dextran. Fluorescence spectroscopy and confocal fluorescence imaging were used to characterize redistribution of hypericin (Hyp), a natural potent pts, loaded in LDL/PEG and LDL/dextran complexes to free LDL molecules as well as to monitor cellular uptake of Hyp by U87-MG cells. It was shown than the redistribution process of Hyp between LDL molecules is significantly suppressed by dextran coating of LDL surface. On the other hand, PEG does not significantly influence this process. The modification of LDL molecules by the polymers does not inhibit their recognition by cellular LDL receptors. U-87 MG cellular uptake of Hyp loaded in LDL/PEG and LDL/dextran complexes appears to be similar to that one observed for Hyp transported by unmodified LDL particles. It is proposed that by polymers modified LDL molecules could be used as a basis for construction of a drug transport system for targeted delivery of hydrophobic drugs to cancer cells expressing high level of LDL receptors.

Keywords:
Drug delivery, low-density lipoproteins, polyethylene glycol, dextran, hypericin, glioma cells, fluorescence, photodynamic therapy

1. INTRODUCTION

The selective killing of tumor cells without significant damage of the cells of healthy tissues belongs between the main goals of all cancer therapies. One of promising and innovative modalities for the targeted cancer therapy is photodynamic therapy (PDT). This procedure is utilized for a treatment of small localized tumors or as an adjuvant therapy to surgery for more advanced tumors. PDT is based on the concept that tumor destruction occurs when a photoactive drug, photosensitier (pts), is administered into a body and this is followed at a given interval of time by light illumination of a selected tumor area [see reviews 1-4].

In clinical practice, the accumulation of pts in tumor tissue is based on "passive targeting" mainly due to the higher permeability of the tumor microvasculature („leaky vasculature"), which is typical for most malignant tissues. An increasing of the efficacy of the PDT treatment will therefore require considerable increase and preferential selective accumulation of pts in tumor cells. The research in this field is rapidly developing and the main concept is based on a construction of targeted drug vehicles consisting of nano-sized particles loaded with pts, connected to ligands that specifically bind to receptors that are over-expressed on tumor cells [5-14].

* diana.buzova@gmail.com

Biosensing and Nanomedicine V, edited by Hooman Mohseni, Massoud H. Agahi, Manijeh Razeghi,
Proc. of SPIE Vol. 8460, 84600U · © 2012 SPIE · CCC code: 0277-786/12/$18 · doi: 10.1117/12.981831

In the recent years more attention has been focused on the clinical use of lipoproteins following the establishing of a direct relationship between the relative number of lipoprotein receptors in various tumors and the uptake of pts by malignant cells. Of the lipoproteins, the most important in terms of drug delivery are the low-density lipoproteins (LDLs) [11-14]. The capacity of LDL to bind some pts and their functionality as drug carriers have been examined in several studies [14-17]. LDLs are recognized by and internalized into the cells through specific membrane receptors that interact with the apolipoprotein B of the LDL particle [18, 19]. The tumor cells and tumor vascular endothelial cells express the LDL receptor in higher number due to either their increased proliferation or increased membrane turnover [18, 19]. This makes LDL particles extremely attractive vehicles for drug delivery and targeting.

LDL particles assume a globular shape with an average particle diameter 22 nm having three different regions. The outer surface layer, which consits of phospholipids molecules with a single apo B-100 protein wrapped around the surface of the LDL particle, the hydrophobic core of LDL which is composed of triacylglycerides and cholestrol esters, and an interfacial region between these two parts [20, 21]. LDL have important advantages in comparison to other nano-delivery systems: i) as natural molecules, LDL escape recognition by mononuclear phagocytic system (MPS) which favors their long circulation time in the plasma, ii) they are not immunogenic, iii) their hydrophobic core and phospholipid shell favor binding of hydrophobic and amphiphilic drugs, respectively. The importance of the study of the physico-chemical properties of complexes of pts with lipoproteins is confirmed by the fact, that the US Food and Drug Administration (FDA) encouraged the inclusion of lipoprotein-drug interaction studies as part of any investigational new drug application that contains a hydrophobic compound [22].

Our group has published several articles in the recent years about the properties of the complex of LDL with photosensitizer hypericin (Hyp). Hyp (Fig. 1), (7,14-dione-1,3,4,6,8,13-hexahydroxy 10,11-dimethyl-phenanthrol [1,10,9,8- *opqra*] perylene), is a natural photosensitizing pigment from plants of the genus *Hypericum*. Hyp under light illumination causes anti-proliferative and cytotoxic effects (necrosis as well as apoptosis) in many tumor cell lines. These properties together with minimal dark toxicity, tumor selectivity and high clearance rate from the host body, make Hyp a promising agent for PDT of cancer as well as for tumor photo-diagnosis [23-25].

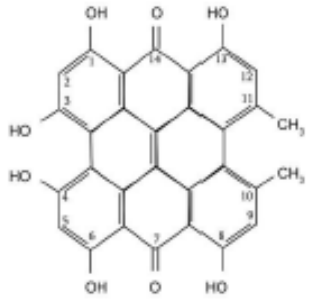

Figure 1. Structure of hypericin.

In our studies was shown that high Hyp / LDL ratios (>30/1) leads to a significant decrease of quantum yield of Hyp fluorescence [26]. This decrease is caused by the formation of non-fluorescent Hyp aggregates inside LDL particles and by dynamic self-quenching of Hyp fluorescence [27, 28]. We have demonstrated the important role of the LDL receptor pathway for Hyp delivery into U-87 MG cells in the presence of LDL: a substantial increase of Hyp uptake was observed after overexpression of LDL receptors on the cell surface [29]. It was also shown that overloading of LDL with Hyp (Hyp / LDL = 200/1) leads to a higher intracellular accumulation of Hyp molecules in comparison with the situation when the same quantity of Hyp is accumulated in LDL, but with a lower Hyp/LDL ratio (20/1). Moreover, Hyp/LDL ratio seems to affect the subcellular distribution of Hyp and consequently the mechanism of photodynamically induced cell death [30].

The main goal of this work is to improve the effectivity and stability of LDL-based drug delivery nanosystem by coating of LDL surface by polymers, polyethylene glycol (PEG) and dextran (Fig. 2).

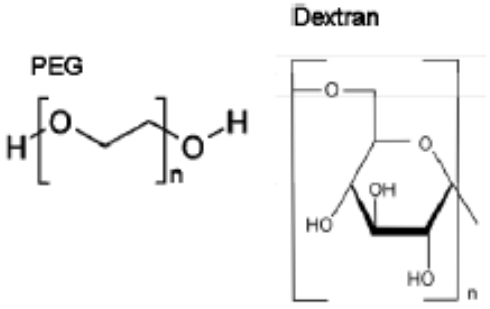

Figure 2. Structure of PEG and dextran.

PEG is the most popular hydrophilic polymer for the surface modification of drug carriers, or for the composing the corona of therapeutic micelles. It has proven to be an efficient steric protector of various biologically active molecules and particular delivery systems. This polymer is inexpensive, has low toxicity, the lack of immunogenicity, antigenicity and toxicity, high solubility in water and organic solvents, high flexibility of the chain and has been approved for applications by drug regulatory agencies [31-34]. Dextran is a family of natural polysaccharides that is widely used as polymeric carrier in novel drug delivery systems. It is proposed that dextran prodrugs are very useful systems for achieving controlled drug release and drug targeting. Various dextran-antitumor drug conjugates enhances the effectiveness and improve the cytotoxic effects of chemotherapeuic agents [35].

In this work, PEG and dextran serve as elements which modify surface of LDL particles. This modification should reduce the interaction of LDL with other serum constituents in order to prevent the redistribution of Hyp over-loaded in LDL to the other free lipoproteins. Further, we would like to show that LDL surface modification by PEG and dextran does not influence the LDL recognition by LDL receptors of U-87 MG cancer cells as well as the cellular uptake of Hyp incorporated in LDL. This approach could lead to a construction of effective and selective delivery system of hydrophobic drugs to cancer cells.

2. MATERIALS AND METHODS

2.1 Chemicals

Dextran T1, (1000 g/mol) was purchased from PHARMA COSMOS (Denmark); PEGylated phospholipids, PEG_{1000}-PE and PEG_{5000}-PE were purchased from Avanti Lipids (USA); LDL from human plasma was purchased from CALBIOCHEM (Germany); LDLb (BODIPY® FL stained LDL) from human plasma, Hyp and PBS were purchased from Invitrogen (France); DMSO was purchased from Sigma-Aldrich (France); DMEM with GlutaMAXTM, L-glucose (4500 mg/L) and sodium pyruvate (110 mg/L), penicillin/streptomycin and FBS were purchased from GIBCO® (France); Ultroser®G was purchased from Pall Corporation (France).

2.2 Preparation of PEG/LDL and dextran/LDL complexes

100 µl of LDL solution (40 nM) in PBS (pH 7.4) was prepared. Dextran powder was diluted in PBS (pH 7.4) at 37°C and PEG_{1000}-PE (PEG_{5000}-PE) were diluted in 100% DMSO at 20°C. Such prepared dextran and PEG-PE solutions were carefully (100 µl by 100 µl) added to LDL solution and gently mixed. 1 ml of final 2.8 µM dextran/4 nM LDL (concentration ratio of dextran/LDL is 700/1) solution and 4 µM PEG-PE/4 nM LDL (concentration ratio of PEG-PE/LDL is 1000/1) solution was kept at room temperature during 1 hour stabilization. Dialysis using a permeable membrane with molecular weight cut-off below 3500 g/mol (Spectra/Por® 6, #132592, Spectrum Laboratories, Inc., CA, USA) against PBS (pH 7.4) for 16 hours at 4 °C was applied to ensure removal of non-complexed PEG and dextran molecules. For confocal microscopy experiments LDL was replaced by green fluorescence BODIPY® FL labeled LDL_b.

2.3 Preparation of Hyp/LDL-dextran and Hyp/LDL-PEG dextran complexes

Before the coating of LDL by PEG or dextran, Hyp-LDL complex was prepared. 0.8 µl of the stock solution of Hyp in DMSO (0.5 mM Hyp) was added to 100 µl of LDL (40 nM) in PBS solution (pH=7.4). The solution was then gently stirred and stabilized overnight at 8°C in the dark. After stabilization of the Hyp-LDL complex, PEG and dextran coated Hyp/LDL complexes were prepared in dark conditions as described above. The final mixtures (1 ml) with the concentration ratio of Hyp-LDL/dextran as 100/1/700 and Hyp-LDL/PEG as 100/1/1000 were obtained. Dialysis using a permeable membrane with molecular weight cut-off below 3500 g/mol (Spectra/Por® 6, #132592, Spectrum Laboratories, Inc., CA, USA) against PBS solution at pH 7.4 for 16 hours at 4 °C was applied to ensure removal of non-complexed PEG, dextran and Hyp molecules.

2.4 Dynamic light scattering

Dynamic light scattering for size characterizations of LDL, LDL/PEG and LDL/dextran nano-delivery systems was performed by Malvern Instruments Zetasizer Nano-ZS instrument (Malvern, Worcs. UK) equipped with a 4mW He–Ne laser (633 nm) operating at 90° angle and a temperature of 20°C. 0.5 nM solutions of LDL, dextran coated LDL (dextran/LDL ratio is 700/1) and PEG-PE coated LDL (PEG-PE/LDL ratio is 1000/1) were prepared in PBS as previously described. The esperiments were performed on 5 different preparations of the LDL-dextran and LDL-PEG-PE complexes.

2.5 Kinetics of the transfer of Hyp from Hyp/LDL, Hyp/LDL-PEG and Hyp/LDL-dextran complexes to free LDL molecules molecules

Initially, the complexes Hyp/LDL, Hyp/LDL-PEG and Hyp/LDL-dextran were prepared as described above. Next, the appropriate volumes of stock solution of free LDL molecules were added to the solution of the above mentioned complexes Hyp. The Hyp concentration in all solutions was kept constant (10^{-6}M) and final Hyp/LDL ratio was 3:1.

2.6 Fluorescence spectroscopy

Fluorescence spectra were recorded at room temperature by SHIMADZU RF-5301 spectrofluorimeter (Kyoto, Japan). The excitation wavelength was 515 nm, and the emission was collected in the range 525-700 nm for all kinetic measurements. Spectra were acquired at various time after the mixing of LDL with Hyp/LDL, Hyp/LDL-PEG and Hyp/LDL-dextran solutions, and analyzed by Origin Pro program version 8.0.

2.7 Cell culture

The U87-MG human glioma cells were grown in Dulbecco's modified Eagle's medium (DMEM) containing L-glutamine (862 mg L^{-1}), sodium pyruvate (110 mg L^{-1}), glucose (4500 mg L^{-1}), streptomycin (50 µg mL^{-1}), penicillin (50 µg mL^{-1}) and supplemented with 10% fetal bovine serum (FBS) or serum substitute 2% Ultroser G, in the presence of 5% CO_2 humified atmosphere at 37°C. In all experiments DMSO concentration was under 0.5%. For all experiments, U-87 MG cells were incubated in dark conditions.

2.8 Cellular samples preparations

U-87 MG cells were first incubated in DMEM with 2% Ultroser®G (lipid free substitute of FBS). After 24 hours, cells were washed, suspended by trypsin/EDTA and 10^5 cells were then seeded on a cover glass placed into a 3.5cm Petri dishes with 2 ml DMEM + 2% Ultroser®G. Incubation of cells with Hyp: Culture medium was replaced by 1ml of a 0.4µM Hyp solution (PBS pH 7.4, 2% Ultroser®G, DMSO<0.01%). After 1hour incubation, cells were washed and observed by fluorescence microscopy. Incubation of cells with Hyp-LDL complex: Culture medium was replaced by 1 ml of a Hyp-LDL complex solution (Hyp/LDL ratio 100/1, 0.4µM Hyp, PBS pH 7.4, 2% Ultroser®G, DMSO<0.01%). After 1 hour incubation, cells were washed and observed by fluorescence microscopy. Incubation of cells with Hyp/LDL-dextran and Hyp/LDL-PEG complexes: Culture medium was replaced by 1 ml of Hyp-LDL/dextran and Hyp-LDL/PEG complexes solution (Hyp-LDL/dextran ratio 100/1/700, Hyp-LDL/PEG-PE ratio 100/1/1000, 0.4µM Hyp, PBS pH 7.4, 2% Ultroser®G, DMSO<0.01%). After 1hour incubation, cells were washed and observed by fluorescence microscopy. In the case of Hyp-LDL/dextran complex we have utilized BODIPY® FL labeled LDL_b.

2.9 Fluorescence cellular imaging

U-87 MG cells were observed by inverted confocal fluorescence microscope Nikon Eclipse TE300 with a 100x objective (Plan Fluor Ph3 DLL Oil 1.3 NA, 0.2mm working distance). Mercury lamp and appropriate filters for fluorescence of

BODIPY®FL (LDL_b): HQ-FITC 480/40 λ_{exc} (460-500) nm, DM 505, BA 535/50 λ_{em} (510- 560) nm; and of Hyp: DAPI 360/20 λ_{exc} (340-380) nm, DM 400, BA 652/75 λ_{em} (615-690) nm; were used. Fluorescence images were collected by CCD camera (Photometrics CoolSnap HQ 1392 x 1040 pixels, 12 bits, analog-numeric converter 10 or 20 MHz). Data acquisition, processing and analysis were performed with Metamorph software (Roper Scientific, France) and Image J software.

3. RESULTS AND DISCUSSION

3.1 Characterization of LDL/PEG and LDL/dextran complexes

The hydrodynamic diameters of LDL/PEG and LDL/dextran complexes were determined by dynamic light scattering method (Fig. 3). The obtained results show that the mean diameter of LDL/PEG complexes is increasing with the increase of molecular weight of PEG (LDL alone = 22.3 nm, LDL/PEG_{1000} = 27.4 nm, and LDL/PEG_{5000}=32.4 nm). Surprisingly, a slightly lower diameter of LDL/dextran complex in comparison with LDL alone was observed (LDL/dextran = 21.2 nm). At this time we have no reasonable explanation for this observation. The presence of PEG and dextran on the surface of LDL particles does not lead to the formation of aggregates (Fig. 3) (less than 1 % of LDL is present in the aggregated form in the presence of dextran and 15 % in the presence of PEG-PE). This enable us to use LDL/PEG or LDL/dextran complexes for the study of Hyp transfer from LDL-polymer complex to free LDL molecules. The stability of the LDL/PEG and LDL/dextran complexes were followed for 5 days at 20° C and no changes in the particle size or size distribution were observed during this time period (not shown).

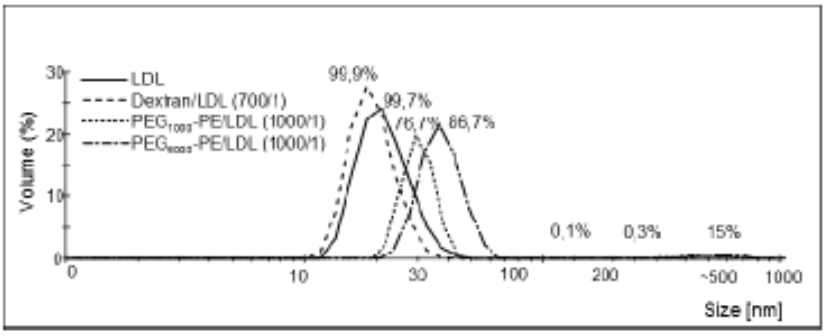

Figure 3. Size distribution of LDL particles determined by dynamic light scattering: LDL alone, dextran/LDL, PEG_{1000}-PE/LDL and PEG_{5000}-PE/LDL.

3.2 Interaction of hypericin with LDL/PEG and LDL/dextran complexes

Hyp in aqueous solutions, as well as in LDL at high concentration ratios (>30/1), forms non-fluorescent aggregates that are also characterized by distinct UV-VIS absorption spectra comparing to those of its monomer form (Fig.4) [26, 27, 28,30, 36].

To evaluate the influence of PEG and dextran on solubility of Hyp in aqueous solutions, we investigated fluorescence property of Hyp in the presence of these polymers.

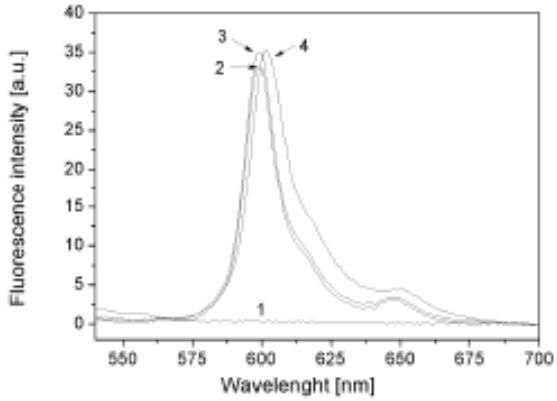

Figure 4. Fluorescence emision spectra (excitation wavelenght 515 nm) of hypericin, c(Hyp)=10^{-6}M, in different solvent conditions: (1) in aqueous solutions; (2) in the presence of LDL, c(LDL)=10^{-6}M; (3) in the presence of PEG_{1000}-PE/LDL=1000/1, c(LDL)=10^{-6}M); (4) in 100% DMSO)

The fluorescence intensity of Hyp as a function of PEG concentration for polymers with different molecular weights is presented in Fig. 5. The intensity increases with the rise of PEG concentration, which means that PEG alone enables transformation of Hyp from aggregated to its monomeric fluorescent form. It is observed that PEGs with molecular weight under 1000 g/mol has only slight influence on the monomerization of Hyp aggregates. However, PEGs with high molecular weights (> 2000 g/mol) enable aqueous solubilizition of Hyp and can partially dissociate Hyp aggregates into monomeric state. This property of PEG signify that the presence of PEG molecules on the surface of LDL particles can interfere with the process of Hyp solubilzation in LDL and consequently with the evaluation of the redistrution of Hyp from the complex Hyp/LDL-PEG to free LDL molecules.

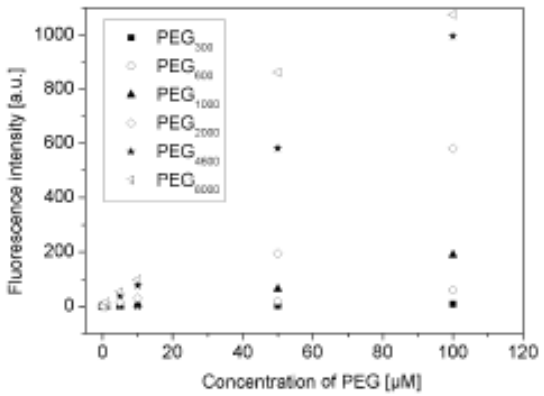

Figure 5. Dependence of the fluorescence intensity of hypericin (c=2x10^{-6}M) at its maximum maximum – 599 nm, on PEG concentration for different molecular weights of PEG polymer. Excitation line was 515 nm.

The presence of dextran does not have impact on the fluorescence and UV-VIS absorption spectra of Hyp in aqueous solution (not shown). Thus dextran, which is used in this study to coat surface of LDL molecules, does not directly interfere with the monomer-aggregate equilibrium of Hyp.

3.3 Redistribution of Hyp from the Hyp-LDL complexes to free LDL molecules

In our previous works we have demonstrated that Hyp can be released from the Hyp-LDL complex and incorporated into neighbouring lipid structures (LDL and cytoplasmatic cell membranes) [30, 36]. The redistribution of Hyp from the complex with LDL (Hyp/LDL concentration ratio > 100/1) to free LDL has been described by biexponential kinetics [36]. Similar situation was observed for the Hyp redistribution pattern from saturated LDL to cells [30]. In this case, the fast component corresponds to direct trans-membrane diffusion of Hyp monomers into cells from overloaded Hyp/LDL complexes (Hyp/LDL>100/1), while the slow one corresponds to the endocytosis process of LDL particles mediated by LDL-receptors on the cell surface [30].

In the present study, the redistribution of Hyp from Hyp-LDL, Hyp-LDL/dextran and Hyp-LDL/PEG complexes to free LDL was investigated by fluorescence spectroscopy. Hyp fluorescence at 600 nm was used to monitor the monomerization of Hyp aggregates caused by Hyp transfer to free LDL molecules (Fig. 6). The redistributive process of Hyp was followed during 420 min after addition of 1.3×10^{-7} M free LDL solution to the initial Hyp/LDL=100/1, Hyp/LDL-dextran and Hyp/LDL-PEG complexes. The corresponding final Hyp/LDL ratio is 3/1 (in this case all Hyp molecules in LDL are in the monomer form). The increase of Hyp fluorescence intensity with time reflects the monomerization process after Hyp transfer to free LDLs. The influence of PEG and dextran molecules on Hyp redistribution process is show on figure 6. The dextran coating leads to approximately 40 % reduction of the final Hyp fluorescence intensity. On the other hand, PEG coating of LDL has not substantial impact on the kinetics as well as amplitude of Hyp transfer from the Hyp/LDL-PEG complex to free LDL in comparison with the transfer from Hyp/LDL complex. In this case even higher fluorescence amplitude is observed which corresponds to higher redistribution from Hyp-LDL/PEG to free LDL than in the case of Hyp transfer from non-coated LDL particles. These results provide an evidence that dextran coating effectively prevents the transfer of an important fraction of Hyp molecules from the initial Hyp-LDL/dextran complex towards free LDL particles.

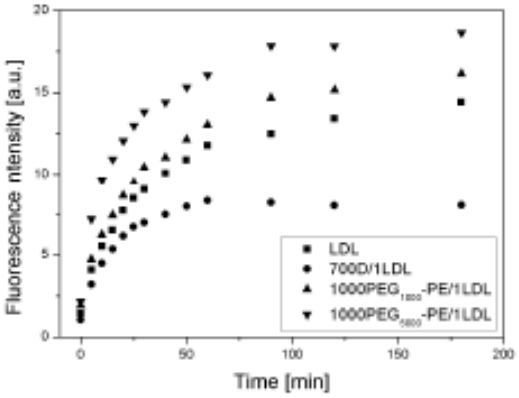

Figure 6. Kinetics of Hyp redistribution from Hyp/LDL = 100/1, Hyp/LDL/dextran = 100/1/700, Hyp/LDL/PEG_{1000}-PEG = 100/1/1000 and Hyp/LDL/PEG_{5000}-PEG = 100/1/1000 toward free LDL molecules as observed by fluorescence spectroscopy. Final concentration ratio of 3:1 corresponds to the addition of $1.3.10^{-7}$ M of free LDL. Fluorescence of Hyp at 599 nm, excitation line was 515 nm.

We can conclude that coating of LDL by dextran can substantially decrease sponataneous redistribution of Hyp molecules from the Hyp-LDL/dextran complex to other serum (lipo)proteins in plasma (LDL in this study). A quite surprisingly, PEG does not have such profound effect, which can be explained by the fact that PEG alone is able to

solubilize Hyp and the molecules of Hyp can be localized as monomers in the outer shell of the LDL/PEG complex. This position of Hyp molecules on the surface of LDL/PEG complex is not consistent with the required decrease of the transfer of Hyp from the complex to other surum (lipo)proteins.

Finally, we propose that Hyp will not dissociate from „shielded" Hyp-LDL/dextrane conjugate in the circulatory plasma what increase possibility for the higher uptake of the complex by cells with a high expression of LDL receptors e.g. several cancer cell lines. This approach would contribute to the higher effectivity of drug targeting in cancer therapy.

3.4 Delivery of Hyp to U-87 MG cells by LDL/PEG and LDL/dextran complexes

LDL-receptors recognize LDL due to the binding domain of the apoprotein B (apoB) in LDL structure (Brown et al., 1976; Vitols et al., 1992). Possible structural modification of this domain as a result of PEG or dextran interaction with LDL could induce some inhibition of the LDL endocytosis process. To verify whether LDL coated by PEG or dextran can still enter into cells by the endocytosis pathway, LDL/PEG and LDL/dextran complexes were loaded with Hyp and consequently added to the medium containing U87-MG cells. In the case of Hyp-LDL/dextran complex, we have used fluorescent BODIPY®FL labeled LDL_b to monitor localization of LDL inside the cells. One hour after incubation, U-87 MG cells were analyzed by fluorescence imaging microscopy. Fluorescence of BODIPY®FL serves as a marker for endocytosis process of LDL_b while Hyp fluorescence is used as a marker of its cellular uptake. As shown on Fig. 7, confocal fluorescence microscopy provides clear evidence that both LDL_b and Hyp are able to enter cells also in the situation when the surface of LDL is coated by PEG or dextran. The cellular uptake of Hyp appears to be higher in cells incubated with free Hyp when compared with cells incubated with Hyp-LDL_b=100/1, Hyp-LDL/PEG =100/1/1000 and Hyp-LDL_b/dextran=100/1/700 complexes. However, as demonstrated and discussed in our previous work, fluorescence intensity does not always reflects the real concentration of Hyp inside cells. It should be considered that for cells incubated with Hyp-LDL_b complex, Hyp molecules which are not directly release from LDL toward cellular membrane, enters cells via the endocytosis pathway along with LDL and are thus partially under their nonfluorescent aggregates form [30]. On the other hand, in the case of free Hyp, all molecules enter cells by transmembrane diffusion and are thus present under their monomer - fluorescent state. To conclude, we have shown that process of LDL endocytosis is not inhibited by the PEG or dextran coating of the LDL surface and complex LDL/PEG or LDL/dextran can serve as a suitable delivery system for hydrophobic pts Hyp to cancer cells.

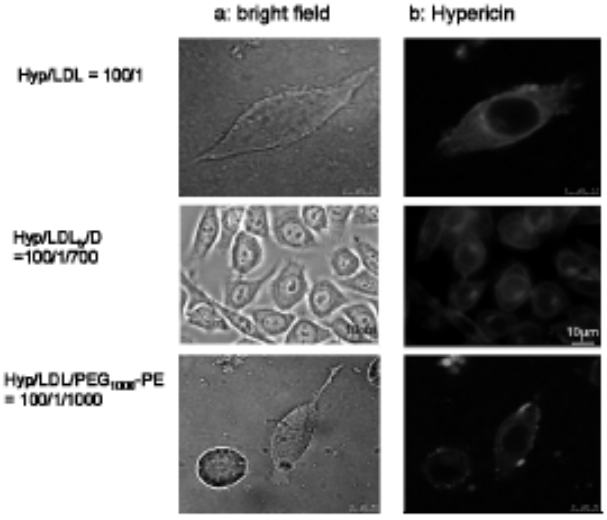

Figure 7. Sub-cellular distribution of LDLb and Hyp in U-87MG cells after incubation with Hyp/LDL = 100/1, Hyp/LDLb/D=100/1/700 and Hyp/LDL/PEG1000-PE = 100/1/1000: bright field imaging (a) and fluorescence imaging of Hyp (b) as observed one hour after incubation by confocal fluorescence microscopy.

4. CONCLUSION

The present study demonstrates a new concept of drug delivery system based on LDL particles. Surface coating of LDL particles by dextran leads to a decrease of Hyp redistribution from Hyp-LDL/polymer complex to free LDL molecules in comparison with Hyp transfer from Hyp-LDL complex to free LDL. It is also shown that the PEG or dextran coating does not influence the recognition of ApoB by LDL receptors expressed in U-87 MG cancer cells. We propose that LDL particles modified by dextran could be potentially used for targeted delivery of hydrophobic drugs to cancer cells expressing higher level of LDL receptors. To confirm a possible pharmaceutical application of this new delivery system, further experiments are needed with the aim to reach detailed structural characterization and higher structural stability of LDL particles coated by dextran (or PEG).

Acknowledgements:
This work was supported by the Slovak Research and Development Agency contracts No. APVV-0 242-11, LPP-0072-07, the Scientific Grant Agency of the Ministry of Education of Slovak Republic (grant VEGA-0164-09) and by the International Scientific Cooperation Program (PICS contract N°5398) from the French National Scientific Research Center (CNRS), and by the Agency of the Ministry of Education of the Slovak Republic for the Structural funds of the European Union, Operational program Research and Development (Contracts: Doctorand, ITMS code: 26110230013 (50%) and NanoBioSens ITMS code: 26220220107 (50%).

REFERENCES

[1] Castano, A., Demidova, T. and Hamblin, M.R., "Mechanisms in photodynamic therapy: part two-cellular signaling, cell metabolism and modes of cell death," Photodiagnosis and Photodynamic Therapy 2, 1-23 (2005).
[2] Dougherty, T.J., Gomer, C.J., Henderson, B.W., Jodi, G., Kessel, D., Korbelik, M., Moan, J. and Peng, Q., "Photodynamic therapy," J. Natl. Can. Inst. 90, 889-905 (1998).
[3] Moan, J. and Peng, Q., "An outline of the hundred- year history of PDT," Anticancer Research 23, 3591-3600 (2003).
[4] MacDonald, I.J. and Dougherty, T.J., "Basic principles of photodynamic therapy,"J.Porphyrins and Phthalocyanines 5, 105-129 (2001).
[5] Solban, N., Rizvi, I. and Hasan, T., "Targeted photodynamic therapy," Lasers in Surgery and Medicine 38, 522-531 (2006).
[6] Chen, B., Pogue, W. and Hasan, T., "Liposomal delivery of photosensitising agents," Expert. Opin. Drug Del. 2, 477-487 (2005).
[7] Kreuter, J., "Nanoparticulate systems for brain delivery of drugs," Adv. Drug Deliv. Rev. 47, 65-81 (2001).
[8] Rensen, P.C., de Vrueh, R.L., Kuiper, J. et al., "Recombinantlipoproteins: lipoprotein-like lipid particles for drug targeting," Adv. Drug Del. Rev. 47, 251-276 (2001).
[9] Konan, Y.N., Gurny, R. and Alleman, E., "State of the art in the delivery of photosensitizers for photodynamic therapy," J. Photochem. Photobiol. B: Biol. 66, 89-106 (2002).
[10] Derycke, A.S. and de Witte, P.A., "Liposomes for photodynamic therapy," Adv. Drug Del. Rev. 56, 17-30 (2004).
[11] Sherman, W.M., van Lier, J.E. and Allen, C.M., "Targeted photodynamic therapy via receptor mediated delivery systems," Adv. Drug Del. Rev. 56, 53-76 (2004).
[12] Jori, G., "Tumour photosensitizers: approaches to enhance the selectivity and efficiency of photodynamic therapy," J. Photochem. Photobiol. B: Biol. 36, 87-93 (1996).
[13] Reddi, E., "Role of delivery vehicles for photosensitizers in the photodynamic therapy of tumours," J. Photochem. Photobiol. B: Biol. 37, 189-195 (1997).
[14] Polo, L., Valduga, G., Jori, G. and Reddi, E., "Low-density lipoprotein receptors in the uptake of tumour photosensitizers by human and rat transformed fibroblasts," Int. J. Biochem and Cell Biol. 34, 10-23 (2002).
[15] Bonneau, S., Vever-Bizet, Ch., Morliere, P., Maziere, J.C. and Brault, D., "Equilibrium and kinetic studies of the interactions of a porphyrin with low-density lipoproteins," Biophys. Journal 83, 3470-3481 (2002).
[16] Jin, H., Lowell, L.E., Chen, J., Ng, K., Cao, W., Ding, L., Zhang, Z. and Zheng, G., "Cytosolic delivery of LDL nanoparticle cargo using photochemical internalization," Photochem. Photobiol. Sci. 10, 810-816 (2011).

[17] Zheng, G., Chen, J., Li, H. and Glickson, J.D., "Rerouting lipoprotein nanoparticles to selected alternate receptors for the targeted delivery of cancer diagnostic and therapeutic agents," PNAS 102, 17757-17762 (2005).
[18] Brown, M.S. and Goldstein, J.L., "Receptor-mediated control of cholesterol metabolism," Science 191, 150-154 (1976).
[19] Vitols, S., Peterson, C., Larsson, O., Holm, P. and Aberg, B., "Elevated uptake of low density lipoproteins by human lung cancer tissue in vivo," Cancer Res.52, 6244-6247 (1992).
[20] Hevonoja, T., Petikainen, M.O., Hyvonen, M.T., Kovanen, P.T. and Ala-Korpela, M., "Structute of low density lipoprotein (LDL) particles: basis for understanding molecular changes in modified LDL," Biochim. Biophys. Acta 1488, 189-210 (2000).
[21] Prassl, R., Laggner, P., "Molecular structure of low density lipoprotein: current status and future challenges," Eur. Bioph. J. 38, 145-158 (2009).
[22] Wasan, K.M., Brocks, D.R., Lee S.D., Sachs-Barrable, K. and Thornton, T.J., "Impact of lipoproteins on the biological activity and disposition of hydrophobic drugs: implications for drug discovery," Nature Reviews-Drug Discovery 7, 84-99 (2008).
[23] Miskovsky, P., "Hypericin- a new antiviral and antitumor photosensitizer: mechanism of action and interaction with biological macromolecules." Current Drug Targets 3, 55-84 (2002).
[24] Kiesslich, T., Krammer, B. and Plaetzer, K., "Cellular mechanisms and prospective applications of hypericin in photodynamic therapy," Curr. Med. Chem. 13, 2189-2204 (2006).
[25] Kober, M., Pohl, K. and Efferth, T., "Molecular mechanisms underlying St. John's wort drug interactions," Curr. Drug Metab. 9, 1027-1037 (2008).
[26] Kascakova, S., Refregiers, M., Jancura, D., Sureau, F., Maurizot, J.C. and Miskovsky, P., "Fluorescence spectroscopic study of hypericin-photosensitized oxidation of low-density lipoproteins," Photochem. Photobiol. 81, 1395–1403 (2005).
[27] Mukherjee, P., Adhikary, R., Halder, M., Petrich, J.W. and Miskovsky, P., "Accumulation and interaction of hypericin in low-density lipoproteins – A photophysical study," Photochem. Photobiol. 84, 706–712 (2008).
[28] Gbur, P., Dedic, R., Chorvat, Jr. D., Miskovsky, P., Hala, J. and Jancura, D., "Time resolved luminescence and singlet oxygen formation after illumination of the hypericin-low-density lipoprotein complex," Photochem. Photobiol. 85, 816–823 (2009).
[29] Kascakova, S., Nadova, Z., Mateasik, A., Mikes, J., Huntosova, V., Refregiers, M., Sureau, F., Maurizot, J.C., Miskovsky, P. and Jancura, D., "High level of low-density lipoproteins receptors enhance hypericin uptake by U-87 cells in the presence of LDL," Photochem. Photobiol. 84, 120–127 (2008).
[30] Huntosova, V., Alvarez, L., Bryndzova, L., Nadova, Z., Jancura, D., Buriankova, L., Bonneau, S., Brault, D, Miskovsky, P. and Sureau, F., "Interaction dynamics of hypericin with low-density lipoproteins and U-87 MG cells," Int. J. Pharm. 389, 32–40 (2010).
[31] Bailon, P. and Won, Ch.Y., "PEG - modified biopharmaceuticals," Expert Opinion on Drug Delivery 6, 1-16 (2009).
[32] Wattendorf, U. and Hans, P.M., "PEGylation as a tool for the biomedical engineering of surface modified microparticles, " J. Pharm. Sci. 97, 4655–4669, (2008).
[33] Fishburn, C.S., "The Pharmacology of PEGylation: balancing PD with PK to generate novel therapeutics," J. Pharm. Sci. 97, 4167–4183 (2008).
[34] Lukyanov, A.N. and Torchilin, V.P., "Micelles from lipid derivatives of water-soluble polymers as delivery systems for poorly soluble drugs," Adv. Drug Del Rev. 56, 1273-1289(2004).
[35] Varshosaz, J., "Dextran conjugates in drug delivery," Expert Opinion on Drug Delivery 5, 509-523 (2012).
[36] Buriankova, L., Buzova, D., Chorvat, Jr. D., Sureau, F., Brault, D., Miskovsky, P. and Jancura, D., "Kinetics of hypericin association with low-density lipoproteins, " Photochem. Photobiol. 87, 56-63 (2011).